UNIVERSIDADE ESTADUAL PAULISTA
"JÚLIO DE MESQUITA FILHO"
Câmpus de São José do Rio Preto

Mariana Bastos dos Santos

Híbridos Chalcona-Inibidores de Histona Desacetilase como Agentes Antiproliferativos: Síntese e Avaliação em Células de Mama e em Histona Desacetilases

São José do Rio Preto
2019

Mariana Bastos dos Santos

Híbridos Chalcona-Inibidores de Histona Desacetilase como Agentes Antiproliferativos: Síntese e Avaliação em Células de Mama e em Histona Desacetilases

Tese apresentada como parte dos requisitos para obtenção do título de Doutora em Química, junto ao Programa de Pós-Graduação em Química, do Instituto de Biociências, Letras e Ciências Exatas da Universidade Estadual Paulista "Júlio de Mesquita Filho", Câmpus de São José do Rio Preto.

Financiadora: FAPESP – Proc. 2016/00580-5

Orientador: Prof. Dr. Luis Octavio Regasini
Coorientadora: Profa. Dra. Debora Aparecida Pires de Campos Zuccari

São José do Rio Preto
2019

S237h

Santos, Mariana Bastos dos

Híbridos chalcona-inibidores de Histona Desacetilase como agentes antiproliferativos : Síntese e avaliação em células de mama e em Histona Desacetilases / Mariana Bastos dos Santos. -- São José do Rio Preto, 2019

159 f. : il., tabs.

Tese (doutorado) - Universidade Estadual Paulista (Unesp), Instituto de Biociências Letras e Ciências Exatas, São José do Rio Preto

Orientador: Luis Octavio Regasini

Coorientadora: Debora Aparecida Pires de Campos Zuccari

1. Chalcona. 2. Câncer de mama. 3. HDAC. 4. Inibidor de HDAC. 5. Híbridos moleculares. I. Título.

Sistema de geração automática de fichas catalográficas da Unesp. Biblioteca do Instituto de Biociências Letras e Ciências Exatas, São José do Rio Preto. Dados fornecidos pelo autor(a).

Essa ficha não pode ser modificada.

Mariana Bastos dos Santos

Híbridos Chalcona-Inibidores de Histona Desacetilase como Agentes Antiproliferativos: Síntese e Avaliação em Células de Mama e em Histona Desacetilases

Tese apresentada como parte dos requisitos para obtenção do título de Doutora em Química, junto ao Programa de Pós-Graduação em Química, do Instituto de Biociências, Letras e Ciências Exatas da Universidade Estadual Paulista "Júlio de Mesquita Filho", Câmpus de São José do Rio Preto.

Financiadora: FAPESP – Proc.: 2016/00580-5

Comissão Examinadora

Prof. Dr. Luis Octavio Regasini
UNESP - Câmpus de São José do Rio Preto - Ibilce
Orientador

Profa. Dra. Maria Luiza Zeraik
UEL - Universidade Estadual de Londrina

Prof. Dr. Jean Leandro dos Santos
UNESP - Câmpus de Araraquara - Faculdade de Ciências Farmacêuticas

Prof. Dr. Marcio José Tiera
UNESP - Câmpus de São José do Rio Preto - Ibilce

Profa. Dra. Iêda Aparecida Pastre Fertonani
UNESP - Câmpus de São José do Rio Preto - Ibilce

São José do Rio Preto
25 de julho de 2019

Este trabalho foi desenvolvido no Laboratório de Antibióticos e Quimioterápicos (LAQ) do Departamento de Química e Ciências Ambientais do Instituto de Biociências, Letras e Ciências Exatas, Unesp, Câmpus São José do Rio Preto, no Laboratório de Investigação Molecular no Câncer (LIMC) do Departamento de Biologia Molecular, da Faculdade de Medicina de São José do Rio Preto - Famerp. Contando com parceria do Laboratório de Genética Molecular e Bioinformática da Unidade de Biotecnologia da Universidade de Ribeirão Preto - UNAERP e do Laboratório de Pesquisa e Desenvolvimento de Fármacos - Lapdesf da Faculdade de Ciências Farmacêuticas da Unesp de Araraquara.

Fomento: Bolsa de doutorado – FAPESP nº 2016/00580-5

Dedico aos meus pais, Antonio Paulo e Maria Elisa, ao meu irmão Gustavo, ao meu companheiro Osvaldo, e às minhas avós Adélia e Iraci, com carinho.

AGRADECIMENTOS

À Deus pela vida, conquistas e força em todos os momentos da realização desse trabalho.

À minha família, em especial à minha mãe Maria Elisa e meu pai Antonio Paulo, por sempre me incentivarem, pelo exemplo de conduta que são para mim, pelo apoio incondicional, pelo amor que me manteve firme em meu propósito. Ao meu irmão Gustavo, que sempre me incentivou, apoiou e caminhou comigo. Ao Osvaldo pelo incentivo, amizade, cumplicidade, compreensão, paciência, e apoio incondicionais. Às minhas avós Adélia e Iraci por me ensinarem diariamente o que é ser forte e ter a doçura de viver com amor. Todos vocês foram imprescindíveis para que eu chegasse até aqui, vocês são o meu porto, eu amo vocês! Obrigada por tudo.

Ao meu orientador Prof. Dr. Luis Octavio, por confiar a mim a realização deste trabalho, pela orientação, ensinamentos, disponibilidade de tempo e do laboratório, pela parceria ao longo desses seis anos. À minha coorientadora Profa. Dra. Débora Zuccari, por ter me recebido tão bem, por sempre me ajudar, e por ter colocado seu laboratório à minha disposição, pela confiança, parceria e ensinamentos.

À Dra. Bruna Jardim-Perassi por ter me ensinado a fazer os experimentos de citotoxidade e por ter me acompanhado, à Me. Jéssica Oliveira por ter me acompanhado e me auxiliado no cultivo das células, pela paciência e parceria.

Ao Prof. Dr. Mozart Marins pela parceria ao longo desses anos, por ter nos ajudado em diversos experimentos biológicos, pela grande contribuição, pelas conversas, conselhos e ensinamentos. À Me Daiane Anselmo pela amizade, parceria e ajuda com a realização dos experimentos de Western Blot e citometria de fluxo em Ribeirão Preto.

À todos que passaram pelo atual Laboratório de Antibióticos e Quimioterápicos (LAQ) e antigo Laboratório de Química Verde e Medicinal (LQVM) durante esses seis anos, em especial à Me Beatriz Carvalho Marques, Me. Gabriela Miranda Ayusso, Ricardo André Zucato Bertani, que me ajudaram muito, e me ensinaram muito mais do que imaginam; também à Me. Mayara Aparecida Rocha Garcia, Me. Daiane Bertholin Anselmo, Me. Carlos Roberto Polaquini, Me. Ana Carolina Nazaré, Caroline Sprengel Lima, Me Guilherme Torrezan, à todos vocês pela ajuda, amizade, companheirismo, conversas, desabafos, e pelos desafios que enfrentamos juntos, muito obrigada!

Ao Prof. Dr. Terry Van Raay da Universidade de Guelph - Canadá, que sempre foi muito receptivo e muito nos auxiliou. À Dra. Flávia Lopes, pois também sempre foi muito pronta, e me ajudou em tudo que precisei.

Ao Prof. Dr. Jean dos Santos por ter me recebido em seu laboratório, pelas discussões, pelo grande auxílio e realização dos experimentos de modelagem molecular. À Me Aline Pavan que me auxiliou no laboratório, me ensinou e realizou os experimentos de modelagem molecular comigo.

À Profa. Dra. Eleni Gomes por ter cedido o equipamento de HPLC e ao Me. Diego Alves Monteiro por realizar as análises de cromatografia.

Aos técnicos dos equipamentos de Ressonância Magnética Nuclear, Dr. Fábio Rogério de Moraes, do Centro de Inovação Biomolecular; Dr. Nivaldo Boralle e Dra. Lucinéia Vizzotto Marconcini de Araraquara. Aos técnicos do laboratório didático, Eliani Nobuco Ikeguchi Ohira, Claudinei Antonio Nobile, Daniela Corrêa de Oliveira Lisboa e Jucilene Conceição de Souza que sempre prontos e me auxiliaram em alguns experimentos. Ao André Luis Domingues que sempre pronto nos ajuda muito. À todos os professores e funcionários da Unesp - Ibilce - São José do Rio Preto.

Às minhas amigas Me. Isabela Constantino, Me. Anna Carolina Alves, Carla Tukamoto, Bruna Borges, Nathália Bongiorno, e à todos amigos que também me ajudaram, por estarem sempre comigo, me incentivarem e fazerem com que tudo fosse mais leve.

À Fundação de Amparo à Pesquisa do Estado de São Paulo (FAPESP) pela bolsa e suporte financeiro (Processo FAPESP: 2016/00580-5), sem os quais a realização deste trabalho não seria possível. À Coordenação de Aperfeiçoamento de Pessoal de Nível Superior (CAPES) - Código de Financiamento 001, pela bolsa durante o mestrado e auxílios ao laboratório.

"[...] A cola se dissolve
e todo seu conteúdo [...]
jorra sobre o tapete,
qual mito desmontado.
Amanhã recomeço."

Carlos Drummond de Andrade (1998)

"Não entendo.
Isso é tão vasto que ultrapassa qualquer entender.
Entender é sempre limitado.
Mas não entender pode não ter fronteiras.
Sinto que sou muito mais completa quando não entendo.
Não entender, do modo como falo, é um dom. [...]
Só que de vez em quando vem a inquietação: quero entender um pouco.
Não demais: mas pelo menos entender que não entendo."
Clarice Lispector (1999)

RESUMO

Câncer de mama é o câncer que mais acomete mulheres no mundo. Os tratamentos atuais têm demonstrado resistência e taxas de reincidência, de acordo com cada subtipo da doença, portanto a busca por novas substâncias capazes de atuar contra essas neoplasias se torna premente. No presente trabalho objetivou-se a síntese de chalconas, híbridos chalconas-inibidores de Histona Desacetilases (HDAC) e análogos, bem como a avaliação biológica dessas substâncias para o câncer de mama por ensaios celulares, moleculares e enzimáticos. No segundo capítulo discorre-se da síntese de 20 aminochalconas pela condensação de Claisen-Schmidt com rendimentos variando de 30 a 96 %. Essas substâncias foram avaliadas contra as linhagens de células de câncer de mama MCF-7 e MDA-MB-231. As cinco substâncias mais ativas contra cada linhagem tiveram seus valores de CI_{50} determinados, destacando-se as substâncias **11** ((*E*)-2-flúor-4'-aminochalcona) e **17** ((*E*)-3-piridil-4'-aminochalcona), que foram as mais ativas contra ambas linhagens com valores de CI_{50} de 13,2 ± 3,5 e 15,7 ± 5,9 μmol L^{-1} respectivamente, contra MCF-7, e de 33,9 ± 7,1 e 34,7 ± 5,2 μmol L^{-1} respectivamente, contra MDA-MB-231. Essas chalconas induziram a morte celular por apoptose em ambas linhagens, e aumentaram a expressão da proteína pró-apoptótica p53 na linhagem MCF-7. As chalconas **11** e **17** foram ainda capazes inibir a proliferação celular mesmo em condições de acidose, demonstrando serem substâncias promissoras para o tratamento de câncer de mama. No capítulo III foi planejada e realizada a síntese de dois novos híbridos chalcona-inibidor de HDAC, utilizando subunidades de chalconas, dos fármacos belinostato e entinostato, bem como, de análogos sulfonamídicos, com rendimentos variando de 14 a 83 %. Essas substâncias foram testadas contra cinco isoformas de HDAC (HDAC1, 2, 4, 6 e 11) a 10 μmol L^{-1}. A substância **23a** foi o híbrido mais potente, e seu análogo **27c** a substância mais potente triada, exibindo valores de CI_{50} de 3,6 e 0,15 μmol L^{-1}, respectivamente, contra HDAC2. O análogo sulfonamídico **27c** foi tão potente quanto o inibidor de HDAC, ácido hidroxâmico suberoilanilida (SAHA). O híbrido **23a** demonstrou ser classe I-seletivo, enquanto **27c** foi ativa contra as classes I e II. As substâncias **23a** e **27c** tiveram a atividade antiproliferativa contra células de câncer de mama (MCF-7 e MDA-MB-231) avaliadas e exibiram valores de CI_{50} que variaram de 9,10 ± 2,5 a 10,51 ± 1,0 μmol L^{-1}. Portanto, o trabalho realizado conduziu a substâncias potentes inibidoras de HDAC e antiproliferativas contra o câncer de mama.

Palavras-chave: chalconas, câncer de mama, p53, inibidor de HDAC, híbridos

ABSTRACT

Breast cancer is the type of cancer more incident in women worldwide. Current treatments have demonstrated resistance and recurrence rate, according to each subtype of disease, therefore the search for new compounds capable to act against these neoplasms becomes urgent. In the present work it was aimed the synthesis of chalcones, chalcone-HDAC inhibitors hybrids and analogues, as well as, biological evaluation of these compounds to breast cancer by cellular, molecular and enzymatic assays. In the second chapter is discussed the synthesis of 20 aminochalcones by Claisen-Schmidt condensation in yields ranging from 30 to 96 %. These compounds were evaluated against breast cancer cell lines MCF-7 and MDA-MB-231. The five most active compounds against each line had their IC_{50} values determined, highlighting **11** ((*E*)-2-fluoro-4'-aminochalcone) and **17** ((*E*)-3-pyridil-4'-aminochalcone) were the most active compounds against both cell lines with IC_{50} value of 13.2 ± 3.5 and 15.7 ± 5.9 μmol L^{-1} respectively, against MCF-7, and of 33,9 ± 7,1 and 34.7 ± 5.2 μmol L^{-1} against MDA-MB-231. These chalcones induced apoptosis death on both lines, and upregulated the p53 pro-apoptotic protein expression on MCF-7 cells. Chalcones **11** and **17** were capable to inhibit cell proliferation even in acidosis condition, demonstrating to be promising compounds to breast cancer treatment. In the chapter III it was designed and synthesized two new chalcone-HDAC inhibitor hybrids, using chalcones, belinostat and entinostat subunits, as well as sulfonamidic analogues, in yields ranging from 14 to 83 %. These compounds were tested against five HDAC isoforms (HDAC1, 2, 4, 6 and 11) at 10 μmol L^{-1}. Compound **23a** was the most potent hybrid, and analogue **27c** was the most potent compound, showing IC_{50} values of 3.6 e 0.15 μmol L^{-1}, respectively, against HDAC2. Sulfonamidic analogue **27c** was as potent as the HDAC inhibitor suberanilohydroxamic acid (SAHA). Hybrid **23a** demonstrated to be class I-selective, and **27c** was active against class I and II. Compounds **23a** and **27c** had their antiproliferative activity against breast cancer cells (MCF-7 and MDA-MB-231) evaluated and exhibited IC_{50} values ranging from 9.10 ± 2.5 to 10.51 ± 1.0 μmol L^{-1}. Therefore, the work has led to potent HDAC-inhibitors compounds and antiproliferative against breast cancer.

Keywords: chalcones, breast cancer, p53, HDAC-inhibitor, hybrids

LISTA DE FIGURAS

Capítulo I

Capítulo II

Capítulo III

LISTA DE TABELAS

Capítulo II

Capítulo III

LISTA DE ESQUEMAS

Capítulo II

Capítulo III

LISTA DE ABREVIATURAS E SIGLAS

br s - *broad singlet* - singleto largo

CI_{50} - (IC_{50}) concentração capaz de inibir 50% de viabilidade celular

d - dubleto

DCM - diclorometano

dd - duplo dubleto

ddd - duplo duplo dubleto

DMEM - *Dulbecco's Modified Eagle's Medium*

DMF - *N*,*N*-dimetilformamida

DMSO-d_6 - dimetilsulfóxido hexadeuterado

DNA - ácido desoxirribonucléico

EDAC - cloridrato de *N*-(3-dimetilaminopropil)-*N'*-etilcarbodiimida

ER - *Estrogen Receptor* - Receptor de estrógeno

HAT - histona acetil-transferase

HDAC - histona desacetilase

HER2 - *human epidermal growth factor 2*

Hex - hexano

HMBC - *Heteronuclear Multiple Bond Coherence*

HOBt - 1-hidroxibenzotriazol

HSQC - *Heteronuclear Single Quantum Coherence*

J - constante de acoplamento

m - multipleto

MCF-7 - Michigan Cancer Foundation 7 - linhagem de câncer de mama receptor de estrógeno positivo

MDA-MB-231 - M.D. Anderson - Metastasis Breast Cancer - linhagem de câncer de mama triplo negativa

MeOH - metanol

MES - ácido 4-morfolinoetanossulfônico

miR - micro RNA

MTT - *3-(4,5-Dimethyl-2-thiazolyl)-2,5-diphenyl-2H-tetrazolium bromide* - brometo de [3-(4,5-dimetiltiazol-2-il)-2,5-difeniltetrazólio]

OPD - o-*phenylenediamine* - *o*-fenilenodiamina

pHe - pH do meio extracelular

pHi - pH do meio intracelular

PR - *Progesterone Receptor* - Receptor de progesterona

RMN - Ressonância Magnética Nuclear

s - singleto

SAHA - ácido hidroxâmico suberoilanilida, vorinostato

t - tripleto

ta - temperatura ambiente

TNBC - *triple negative breast cancer*

TSA - tricostatina A

UV-vis - ultravioleta-visível

δ - deslocamento químico

δ_C - deslocamento químico de ^{13}C

δ_H - deslocamento químico de ^{1}H

SUMÁRIO

Capítulo I

1. Capítulo I

1.1. INTRODUÇÃO E REVISÃO BIBLIOGRÁFICA

1.1.1. Câncer e Câncer de mama

Câncer é o conjunto de doenças também denominadas neoplasias, as quais são caracterizadas por um crescimento celular invasivo e descontrolado. A carcinogênese ocorre em células que sofrem distúrbios homeostáticos. Os agentes carcinogênicos podem ser físicos, químicos e biológicos, estando correlacionados principalmente a mudanças moleculares, incluindo alterações nos ácidos nucléicos e proteínas (SARKAR et al., 2013).

As neoplasias podem ser classificadas segundo sua origem embrionária, histológica bem como do estágio clínico de desenvolvimento (HASSANPOUR & DEHGHANI, 2017). Os tratamentos convencionais para os diversos tipos de câncer são definidos pelas classificações das doenças e envolvem cirurgias, terapias hormonais, terapias antiangiogênicas, radioterapia, imunoterapia e quimioterapia clássica com agentes citotóxicos/antiproliferativos (BARNES et al., 2017).

De acordo com a Organização Mundial da Saúde, o câncer é a principal causa de morte no mundo, sendo responsável por 9,6 milhões em 2018. Nesse mesmo ano, entre os 18,1 milhões de novos casos, os tipos de câncer mais diagnosticados foram de pulmão e mama (BRAY et al., 2018). No Brasil, estima-se uma incidência de 324 mil novos casos de câncer em mulheres e 310 mil em homens entre os anos de 2018 e 2019 (INCA, 2017).

O câncer de mama é a neoplasia que mais acomete as mulheres em todo o mundo, sendo estimado como responsável por 626.679 mortes entre os 2,08 milhões de casos no ano de 2018 (BRAY et al., 2018). Em 2018 estimou-se a ocorrência de 59.700 novos casos de câncer de mama feminina no Brasil (INCA, 2017).

O câncer de mama compreende um grupo de doenças com características morfológicas e de comportamentos clínicos diferentes (GOLDHIRSCH et al., 2011). A presença de receptores de membranas nas células malignas permite classificar essa neoplasia em três subtipos: (*i*) HR positivo (*hormone receptor*): apresentam células com expressão dos receptores de estrógeno (ER) ou receptores de progesterona (PR); (*ii*) HER2 (*human epidermal growth factor 2*): apresentam células com receptores tipo 2 do fator de crescimento epidérmico humano; (*iii*) TNBC (*triple negative breast cancer*) as células que não possuem os receptores HER2, ER ou PR (EISNER & LUOH, 2011).

A carcinogêse de mama envolve estágios fisiológicos que resultam em células malignas invasivas, os estágios da doença são classificados em três principais: iniciação, progressão e metástase (GATENBY et al., 2007).

O tratamento para o câncer de mama é sistêmico e se baseia nos seus subtipos, incluindo a quimioterapia adjuvante, a qual abrange taxanos como paclitaxel e docetaxel (Figura 1, p. 24), vinorelbina e eribulina, fármacos que são utilizados atualmente, principalmente para o tipo TNBC. Para o subtipo ER a terapia se baseia principalmente no uso de moduladores de receptores de estrógeno, como tamoxifeno, e inibidores de aromatase, como o anastrozol (Figura 1, p. 24), que antagonizam os receptores de estrógeno, esse tipo de ação farmacológica pode culminar em resistência endócrina. Para o tipo HER2, o tratamento envolve a administração de trastuzumab, um anticorpo monoclonal, como agente adjuvante (GOLDHIRSCH et al., 2011).

O subtipo de câncer de mama TNBC é o de difícil tratamento, pois não há terapia molecular dirigida, culminando na maioria das ocorrências de mortes de pacientes até o quinto ano após início do tratamento, e com recorrência da doença entre o primeiro e terceiro ano (FEDELE; ORLANDO; CINIERI, 2017). Sulaiman e coautores demonstraram que para o subtipo TNBC invasivo a co-supressão de proteínas histona desacetilases (HDAC) e Wingless/Integrate (Wnt) permite que as células-tronco tumorais (CTT) do tipo TNBC sejam convertidas a apenas células tumorais TNBC, demonstrando assim que essa pode ser uma abordagem molecular efetiva no tratamento desse subtipo de neoplasia de mama (SULAIMAN et al., 2016; GARMPS et al., 2017). Essa abordagem é corroborada pelo fato de que nas linhagens de câncer de mama subtipo TNBC ocorre aumento da expressão das HDAC 1–3 e 5–8, mais exacerbada do que nas linhagens receptor de estrógeno positivo, de forma inversamente proporcional à expressão dos receptores ER e PR (SULAIMAN et al., 2018).

Nesse contexto, Tate e coautores (2012) demonstraram ação do inibidor de histona desacetilase (HDAC) panobinostato: a) na hiperacetilação das histonas H3 e H4 de células TNBC; b) citotoxicidade contra células TNBC das linhagens MDA-MB-157 e 231 em ensaios de viabilidade celular; e c) atividade *in vivo*, demonstrando capacidade de diminuição do volume tumoral de 3 a 4 vezes sem apresentar toxicidade em camundongos (TATE et al., 2012).

Figura 1. Fármacos utilizados para o tratamento do câncer de mama

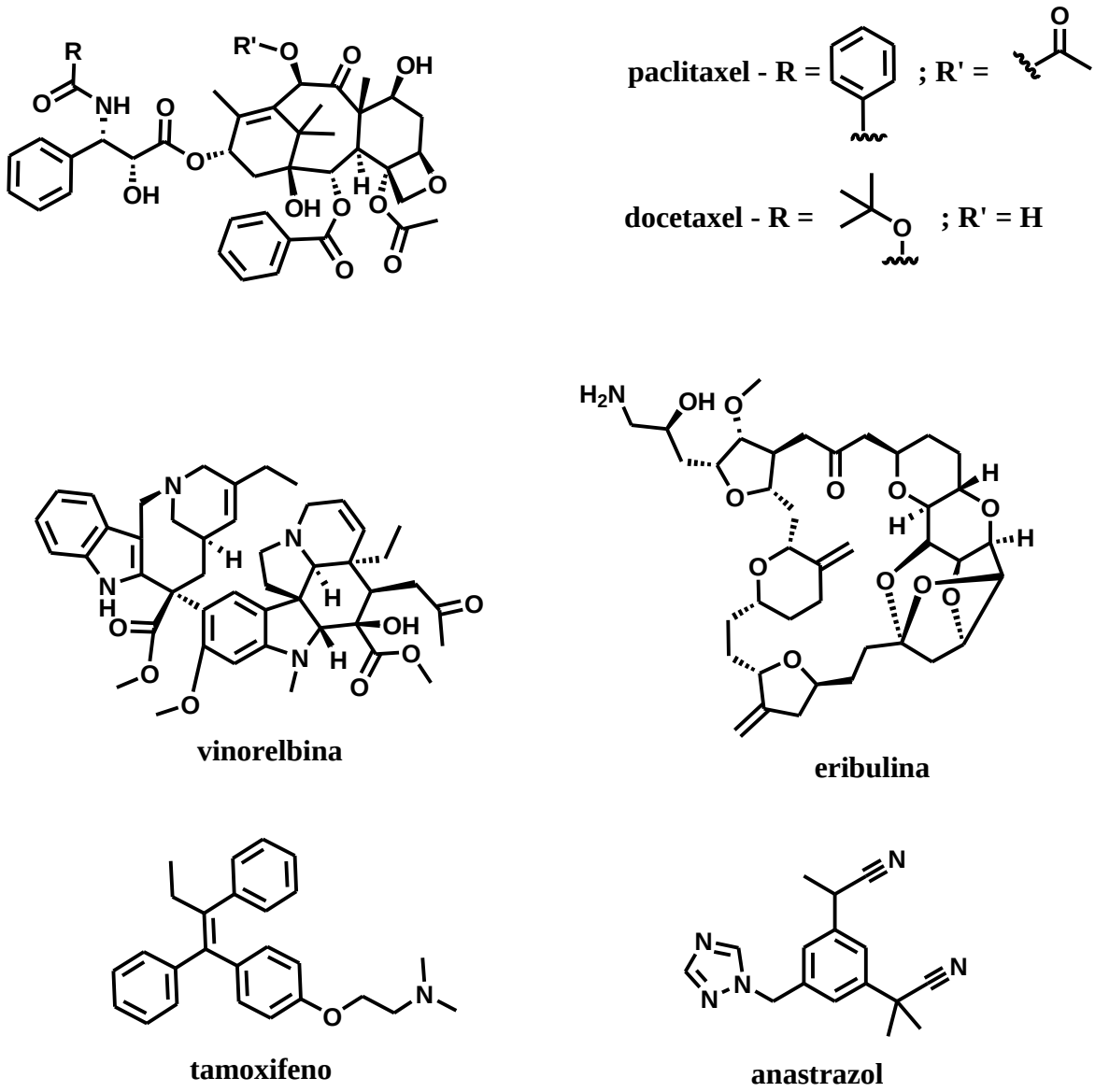

FONTE: autora

1.1.2. Microambiente Tumoral e Acidose no Câncer de Mama

O surgimento e desenvolvimento dos tumores, conhecido como tumorigênese, é um processo complexo e dinâmico, e pode ser dividido em três estágios principais: iniciação, progressão e metástase. Esses estágios estão diretamente correlacionados com o microambiente tumoral, o qual é composto por matriz extracelular e células estromais (WANG et al., 2017).

Nas células tumorigênicas, como forma de adaptação a pouca demanda de nutrientes e de manutenção das elevadas taxas de proliferação, ocorre o efeito Warburg. Este consiste no metabolismo distinto de glicose entre as células tumorigênicas e não-

tumorigênicas, de forma que as tumorigênicas metabolizam prioritariamente *via* fermentativa com produção de lactato, do que *via* fosforilação oxidativa mitocondrial (VANDER HEIDEN; CANTLEY; THOMPSON, 2009). Consequentemente, no microambiente tumoral, a produção de lactato e de prótons promove a diminuição do pH extracelular (pHe), uma vez que o lactato e os hidrogênios são secretados (XU et al., 2013; DAMAGHI; WOJTKOWIAK; GILLIES, 2013).

Em tecidos não-tumorais, os valores de pH intracelular (pHi) tendem a ser similares ou mais baixos do que do meio extracelular (pHe). Nas células tumorais, o pHi é mais alto (7,3 – 7,5) do que o pHe (6,8 – 7,3) (MCINTYRE & HARRIS, 2016; DAMAGHI; WOJTKOWIAK; GILLIES, 2013; HASHIM et al., 2011). O mecanismo de controle do pHi das células pode envolver tampões e várias proteínas, incluindo anidrases carbônicas, que são responsáveis pelo transporte de CO_2, e prótons, contribuindo para a secreção de lactato para o meio extracelular. Destaca-se que as anidrase carbônicas estão superexpressas nas células tumorigênicas (XU et al., 2013).

A mudança de pH na massa tumoral em relação aos tecidos normais caracteriza o processo de acidose no microambiente tumoral, um dos estados fisiológicos prévios à metástase tumoral no câncer de mama (GATENBY et al., 2007; HASHIM et al., 2011).

1.1.3. Fator de Transcrição p53 e sua Relação com Câncer de Mama

Fatores de transcrição são proteínas que se ligam ao DNA de eucariotos durante o processo de transcrição, permitindo a interação entre uma enzima RNA-polimerase e o material genético, são proteínas que regulam a quantidade de RNA mensageiro produzida pela célula (LATCHMAN, 1997).

A p53 é uma proteína tetramérica que possui 393 resíduos de aminoácidos em cada subunidade e apresenta um domínio de ligação ao DNA (JOERGER & FERSHT, 2010). Fisiologicamente, é um fator de transcrição que regula diretamente a transcrição de genes de RNA-polimerase II, e indiretamente, a expressão de outros tipos de RNA-polimerases. Para desenvolver sua função biológica, p53 pode recrutar enzimas modificadoras de histona tais como as HDAC, enzimas remodelantes de cromatina e subunidades de complexos mediadores. É uma proteína com efeito supressor de tumores, podendo induzir a senescência celular, parada do ciclo celular, bem como apoptose, tendo sua expressão diminuída em diversos tipos de câncer (BECKERMAN & PRIVES, 2010).

O gene *TP53* codifica a p53, e pode sofrer mutações em diversos tipos de câncer. Contudo, no câncer de mama essa mutação é menos acentuada ocorrendo em apenas em 30 % dos casos, sendo correlacionada diretamente com os subtipos da doença. Nos subtipos de câncer de mama que expressam os receptores de estrógeno (ER), ocorre a expressão de p53 selvagem. Nos subtipos que não expressam receptor de estrógeno (subtipos HER2 ou TNBC), a p53 ocorre na sua forma mutada (BERTHEAU et al., 2013).

No câncer de mama receptor de estrógeno positivo (ER), a expressão de p53 tem sido correlacionada a um fenótipo de senescência dos genes *TP53*, e consequente aumento da proliferação, devido ao efeito antagônico que os receptores de estrógeno podem ter na indução de apoptose *via* p53. Esse efeito tem sido correlacionado à resistência ao tratamento realizado com fármacos indutores de apoptose, como a doxorrubicina (SAYEED et al., 2007; BERTHEAU et al., 2013). No entanto, Bailey e coautores demonstraram que a inibição total dos receptores de estrógeno pelo fármaco antagonista fulvestranto, associada aos indutores de apoptose *via* p53 culminam em quimioterapia eficaz (BAILEY et al., 2012).

1.1.4. Fator de Transcrição Sp1 e sua Relação com Câncer de Mama

A proteína de especificidade 1 - Sp1 (*Specificity Protein* 1) pertence à família multigene Sp. Fisiologicamente, é um fator de transcrição ubíquo e apresenta 785 aminoácidos. Destes aminoácidos, 164 são serina ou treonina, sendo sítios reativos a acetilações, glicosilações e fosforilações, as quais regulam sua estabilidade e ação. Em sua estrutura ocorre um domínio de ligação ao DNA formado por dedos de zinco, o qual se liga a regiões do DNA conhecidas como caixas GC. Essa proteína pode ter ação ativadora ou repressora do processo transcricional (DENIAUD et al., 2009, BEISHLINE & AZIZKHAN-CLIFFORRD, 2015).

Sp1 está correlacionada a diversos processos celulares, tais como: proliferação, diferenciação e apoptose. A superexpressão de Sp1 é relatada em diversos tipos de câncer, incluindo o câncer de mama. Beishline e coautores indicam que Sp1 como um alvo nos processos de carcinogênese pode não ser adequado, pois a mesma está correlacionada a diversos processos celulares complexos, e demonstraram a necessidade de validação da mesma como alvo terapêutico. Ainda assim, Sp1 é caracterizada como um marcador para diversos tipos de câncer (BEISHLINE& AZIZKHAN-CLIFFORRD, 2015).

Wang e coautores relataram a expressão de Sp1 no câncer de mama, como um marcador relacionado a prognóstico negativo, e estágio clínico da doença, bem como, indicaram a participação de Sp1 em processos de invasão e metástase do câncer de mama (WANG et al., 2007). Além disso Sp1 tem sido reportado por se ligar a uma extremidade da proteína histona desacetilase 2 (HDAC2), promovendo o silenciamento transcricional do gene *hTERT* que codifica a enzima telomerase, uma das enzimas correlacionadas à carcinogênse (WON; YIM; KIM, 2002)

1.1.5. Histonas Desacetilases (HDAC)

As histonas são proteínas globulares e nucleares, as quais interagem por ligações iônicas com os grupos fosfato do DNA, por meio de seus resíduos de lisina, constituindo assim os nucleossomos da cromatina (ECKSCHLAGER et al., 2017).

Processos epigenéticos correspondem às mudanças de caráter reversível na cromatina, principalmente nas histonas, não promovendo alteração na estrutura da sequência do DNA. As cadeias laterais dos resíduos de lisina histônicos são suscetíveis a diversas reações regulatórias dos processos epigenéticos, tais como: acetilação, metilação e fosforilação (DELCUVE; KHAN; DAVIE, 2012). A acetilação das histonas está correlacionada à ativação da transcrição de genes, enquanto que a desacetilação, à condensação da cromatina e à repressão da transcrição. As enzimas responsáveis pela acetilação e desacetilação das histonas são as Histona-Acetil-Transferases (HAT), e Histona-Desacetilases (HDAC), respectivamente (CECCACCI & MINUCCI, 2016).

As proteínas HDAC são subdividas em quatro classes, de acordo com sua dependência de cofator e similaridade na sequência de aminoácidos, bem como em duas famílias: tradicional e sirtuinas (SETO, 2014). As classes de HDAC são: (classe I) HDAC 1, 2, 3 e 8; (classe IIa) HDAC 4, 5, 7; (classe IIb) HDAC 6 e 10; e (classe IV) HDAC 11. As classes I, IIa, IIb e IV são zinco-dependentes para atividade hidrolítica. A classe I é presente no núcleo e as classes IIa, IIb e IV podem ser encontradas no núcleo ou citoplasma. A classe III de HDAC é composta pela família de proteínas sirtuínas (SIRT 1–7) que são dependentes de nicotinamida adenina dinucleotídeo (NAD), sendo encontradas no núcleo, citoplasma e nas mitocôndrias. No entanto, o interesse pelas sirtuínas ainda é pouco explorado (DAMASKOS et al., 2017; HABERLAND; MONTGOMERY; OLSON, 2009).

A superexpressão de HDAC das classes I, II e IV tem sido correlacionada com doenças como: câncer e disfunções neurodegenerativas (FALKENBERG & JOHNSTONE, 2014). A superexpressão da HDAC 2 (classe I) tem sido reportada na doença de Alzheimer, tendo sua ação na supressão de genes responsáveis pela função cognitiva e de neuroplasticidade, enquanto que HDAC (classe IIa) têm sua relevância na doença de Parkinson, e a HDAC 6 (classe IIb) na regulação do humor (CHUANG et al., 2009).

Em diversos tipos de câncer tais como: linfoma cutâneo de células T, carcinomas colorretal, hepatocelular, de próstata e de mama, as HDACs são superexpressas e correlacionadas ao processo de carcinogênese (WEICHERT, 2009).

A abordagem epigenética no tratamento antineoplásico envolve a inibição das HDAC, visando a manutenção das histonas acetiladas, permitindo a expressão de genes que conduzam à apoptose das células malignas. Sendo, portanto consideradas alvos para o tratamento antineoplásico (CECCACCI & MINUCCI, 2016).

No câncer de mama ocorre superexpressão da atividade das HDACs. Shan e colaboradores (2017) demonstraram que ocorre superexpressão do gene *HDAC2* em células de câncer de mama, enquanto que Ververis e colaboradores demonstraram superexpressão da classe I (SHAN et al., 2017; VERVERIS & KARAGIANNIS, 2012). Muller descreveu que as HDACs 2 e 3 são altamente expressas nos subgrupos de câncer de mama, e destacou a superexpressão das HDACs da classe I (MULLER et al., 2013).

1.1.6. Inibidores de Histona-Desacetilases

Os inibidores de HDAC compõem uma classe promissora de antineoplásicos. Em 2006, o vorinostato ou SAHA (ácido hidroxâmico suberoilanilida, Figura 2, p. 29) foi o primeiro inibidor de HDAC aprovado pela *Food and Drug Administration* (FDA), para tratamento de linfoma cutâneo de células T. É um fármaco administrado por via oral, e inibe as HDACs 1 e 3 (BEHERA; JAYAPRAKASH; SINHA, 2015).

Mottamal e coautores (2015) demonstraram que as regiões farmacofóricas de inibidores de HDACs das classes I, II e IV, tais como o vorinostato (SAHA, Figura 2, p. 29), são compostas pelas subunidades: **A** (representada em azul) uma região com capacidade quelatogênica responsável pela interação com o zinco; **B** (representada em vermelho) um espaçador hidrofóbico; e **C** (representada em preto) uma região de superfície de domínio, que promove o bloqueio estérico para o substrato ao sítio catalítico (MOTTAMAL et al., 2015).

Figura 2. Subunidades farmacofóricas do vorinostato (SAHA)

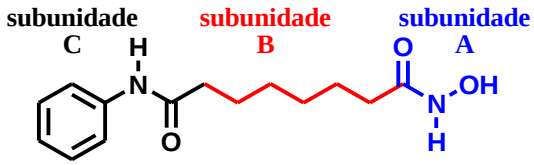

FONTE: autora

A romidepsina (Figura 3, p. 30), foi aprovada em 2009 para tratamento de linfoma cutâneo de células T, devido a sua ação inibitória sobre as HDACs 1 e 2. Em 2014, foi aprovado o belinostato (Figura 3, p. 30) para tratamento de linfoma de células T periférico, por via intravenosa, um inibidor das HDACs 3 e 4. O panobinostato (Figura 3, p. 30) inibe as HDACs 3 e 4, e foi aprovado em 2015 para tratamento de mieloma múltiplo por administração por via oral (FDA, 2017).

Os inibidores de HDAC (Figura 3, p. 30) podem ser classificados de acordo com sua estrutura química em; **(*i*) hidroxamatos**: vorinostato (SAHA), belinostato, panobinostato; **(*ii*) peptídeos cíclicos**: romidepsin; **(*iii*) ácidos graxos**: ácido valpróico e **(*iv*) benzamidas**: entinostato, **20Y** (BEHERA; JAYAPRAKASH; SINHA, 2015; SHARMA et al., 2015; LAUFFER et al., 2013).

Figura 3. Inibidores de Histona Desacetilases

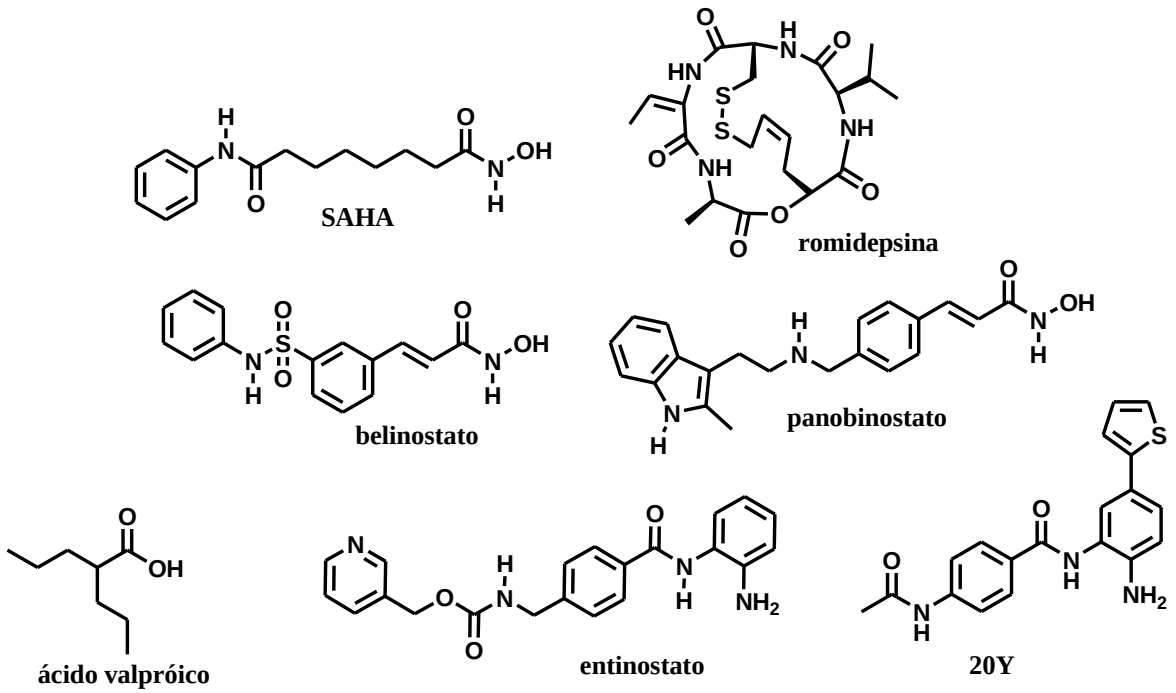

FONTE: autora

Benzamidas vem sendo considerada uma classe preferêncial frente aos ácidos hidroxâmicos, quando avaliados quanto à estabilidade metabólica (BEHERA JAYAPRAKASH; SINHA, 2015) O inibidor de HDAC pertencente à classe das benzamidas, entinostato, encontra-se em estudos clínicos de fase III para tratamento de câncer de mama do tipo HR, localmente avançado ou em estágio metastático, como alternativa para a resistência endócrina aos tratamentos hormonais (YERUVA et al., 2018). Lauffer, e coautores desenvolveram uma nova benzamida, a substância **20Y**, com potente inibição contra HDAC2 e com tempo de meia vida maior do que o entinostato (LAUFFER et al., 2013).

Os inibidores de HDAC também são classificados de acordo com sua atuação inibitória, inibidores pan-HDAC são substâncias capazes de inibirem as classes I, II e IV de HDAC, ou seja, substâncias não-seletivas para isoformas de HDAC zinco-dependentes (BEHERA; JAYAPRAKASH; SINHA, 2015). A maioria dos ácidos hidroxâmicos são inibidores pan-HDAC, enquanto que inibidores benzamídicos são seletivos para as classes I ou II (CECCACCI & MINUCCI, 2016; KHAN et al., 2008).

1.1.7. Chalconas

Chalconas são substâncias compostas por duas fenilas (anéis A e B), unidas por uma ponte cetônica α,β-insaturada (Figura 4, p. 31). São substâncias exploradas e privilegiadas pela Química Medicinal por serem de síntese simples e apresentarem um amplo espectro de bioatividades, tais como: antifúngica (WANG et al., 2016), antibacteriana (MARLIYANA; SYAH; MUJAHIDIN, 2017), antiviral (GAN et al., 2017), antioxidante (LAHSASNI; AL KORBI; ALJABER, 2014; ZHUANG et al., 2017).

Figura 4. Núcleo chalcônico

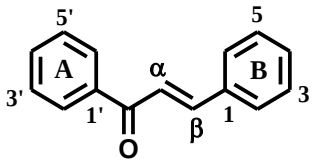

FONTE: autora

A atividade citotóxica das chalconas vem sendo investigada devido à capacidade de atuação em diversos alvos moleculares relacionados à carcinogenese, tais como: proteassoma, p53, 5α-redutase, aromatases, sirtuína-1 e *via* Wnt/β-catenina (MAHAPATRA; BHARTI; ASATI, 2015; IFTIKHAR et al., 2017).

Mai e co-autores (2014) demonstraram que a 2'-aminochalcona (Figura 5, p. 32) exibiu atividade contra linhagens de câncer, entre elas a linhagem de mama, receptor de estrógeno positivo (MCF-7), com valor de CI_{50} de 5,42 μmol L^{-1}. Adicionalmente, a 2'-aminochalcona demonstrou atividade pró-apoptótica, atuando sobre as caspases 3 e 8 (MAI et al., 2014).

Tseng e coautores (2013) demonstraram que a chalcona quinolínica (Figura 5, p.32) foi tóxica contra linhagem de mama MDA-MB-231, com valor de CI_{50} de 0,41 μmol L^{-1}, bem como não se mostrou tóxica para a linhagem de células não-tumorigênicas de mama H184B5F5/M10, sendo indutora de apoptose, via ativação de caspase-3 (TSENG et al., 2013).

A 4'-aminochalcona (Figura 5, p. 32) foi ativa contra as linhagens de células de carcinoma de ovário humano ES-2 e Hey-A8, segundo Su e co-autores (2017), demonstrando supressão do gene *C-MYC*, um oncogene envolvido na regulação do ciclo celular, diferenciação, metabolismo, crescimento celular, apoptose (SU et al., 2017).

Mokale e coautores (2015) reportaram que a chalcona pirrolidínica (Figura 5, p. 32) foi efetiva contra a linhagem MCF-7, devido ao estudo por modelagem molecular de possíveis interações com receptores de estrógeno (MOKALE et al., 2015).

A chalcona tetrahidroxilada foi reportada por Kahyo e colaboradores (2008), como inibidora da atividade de sirtuína-1 sobre p53, promovendo aumento de p53 acetilada endógena, suprimindo assim a proliferação celular (KAHYO et al., 2008).

Figura 5. Chalconas citotóxicas

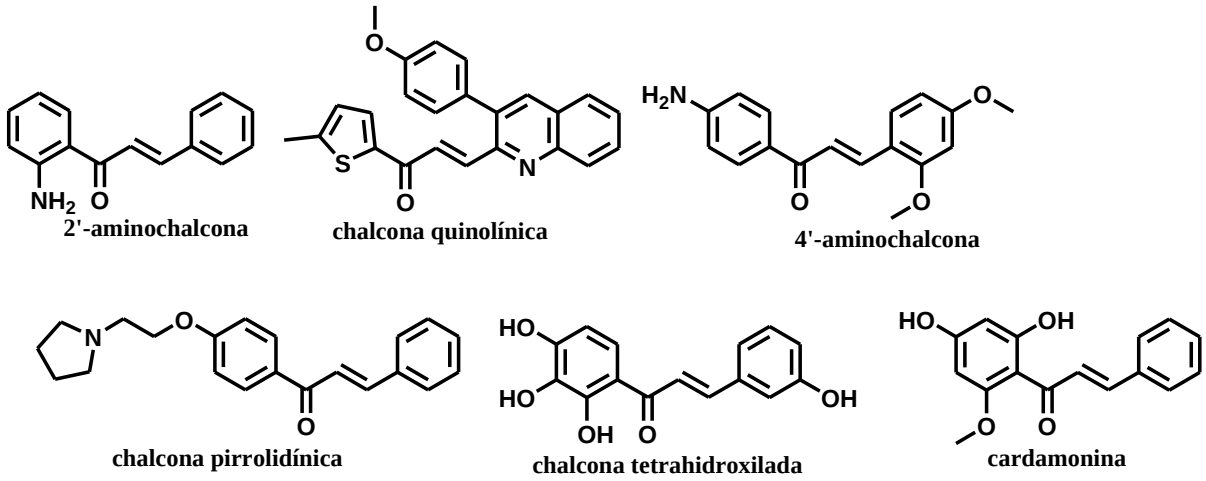

FONTE: autora

Cho e colaboradores (2009) reportaram que a cardamonina (Figura 5, p. 32), foi capaz de inibir a pigmentação de melanócitos devido ao bloqueio da via Wnt/β-catenina e degradação da β-catenina (CHO et al., 2009). Shrivastava e coautores (2017) demonstraram que a cardamonina foi tóxica para MDA-MB-231, devido à inibição específica da sinalização canônica via Wnt3a, sendo capaz de inibir a transição epitélio-mesenquimal (SHRIVASTAVA et al., 2017).

1.1.8. Hibridação Molecular

A hibridação molecular é uma ferramenta da química medicinal empregada no planejamento de substâncias farmacologicamente ativas. Consiste na união de subunidades estruturais de duas ou mais substâncias bioativas, para obtenção de um híbrido, com características farmacocinéticas e farmacodinâmicas otimizadas em relação às substâncias parentais (FRAGA, 2009).

A hibridação molecular tem sido utilizada para o desenvolvimento de novos fármacos, principamente antineoplásicos. Lai e coautores (2010) empregaram a hibridação molecular entre subunidades farmacofóricas do erlotinibe, um inibidor de fator de crescimento epidérmico (EGFR) e HER2, com uma subunidade do inibidor de HDAC, vorinostato (**SAHA**), permitindo a obtenção do híbrido CUDC-101 (Figura 6, p. 33). O híbrido apresentou atividade citotóxica potente contra mais de 15 tipos de células de câncer, incluindo linhagens de mama, sendo mais potente do que seus precursores **SAHA** e erlotinib, e com capacidade de inibição multi-alvos: HDAC, EGFR e HER2 (LAI et al., 2010). CUDC-101 é um atual candidato a fármaco, em estudos clínicos de fase I para tratamento das neoplasias da cabeça e pescoço, gástricas, fígado e mama.

Figura 6. Planejamento do Híbrido CUDC-101

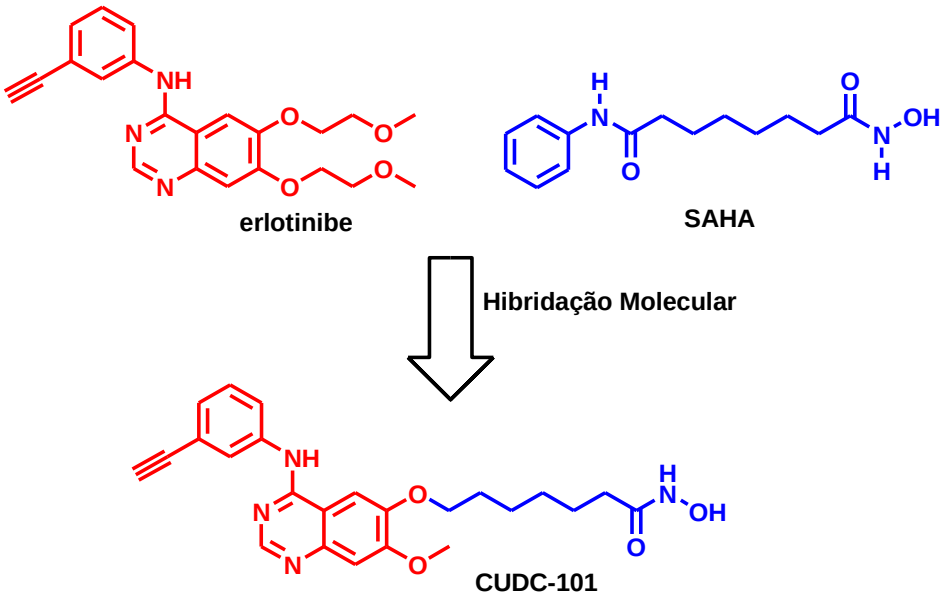

FONTE: autora

Gryder e coautores (2013) empregaram a hibridação molecular entre o tamoxifeno, um fármaco antagonista de receptores alfa de estrógeno (ER-α), e o SAHA, um inibidor de HDAC, permitindo a obtenção de um híbrido SAHA-tamoxifeno (Figura 7, p. 34) com atividade antiproliferativa em células de mama semelhante ao do SAHA, e com capacidade de inibição de ER-α semelhante ao do tamoxifeno (GRYDER et al., 2013). Desse modo, a hibridação molecular utilizando inibidores de HDAC para tratamento do câncer de mama tem se mostrado como uma abordagem efetiva.

Figura 7. Planejamento do híbrido **SAHA**-tamoxifeno

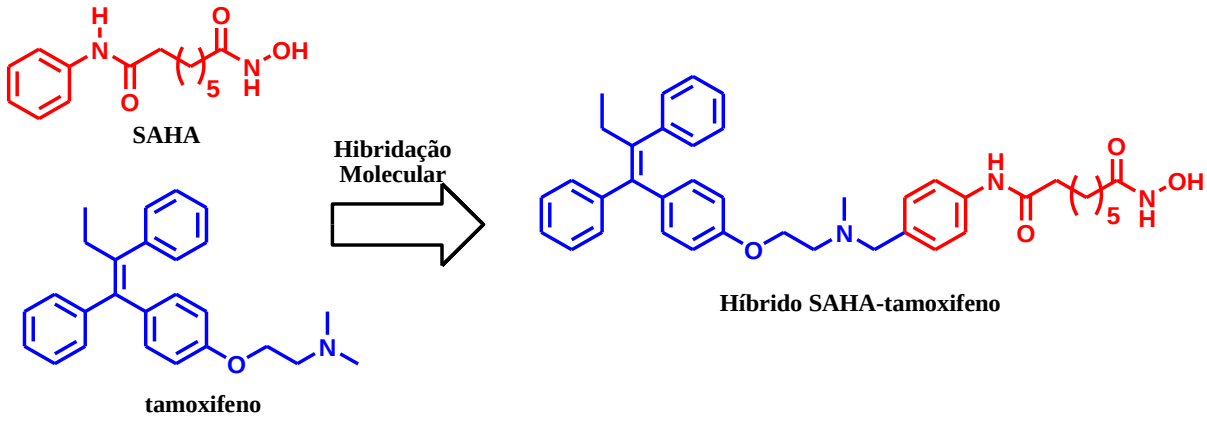

FONTE: autora

Abou-Zied e colaboradores empregaram a hibridação entre chalconas e xantinas com estruturas baseadas na teofilina (Figura 8, p. 34), para desenvolvimento de uma série de híbridos, os quais tiveram atividade antiproliferativa potente e pró-apoptótica contra células de câncer, incluindo células de câncer de mama (MCF-7), bem como demonstraram atividade inibitória de EGFR (ABOU-ZIED et al., 2019).

Figura 8. Planejamento do híbrido teofilina-chalcona

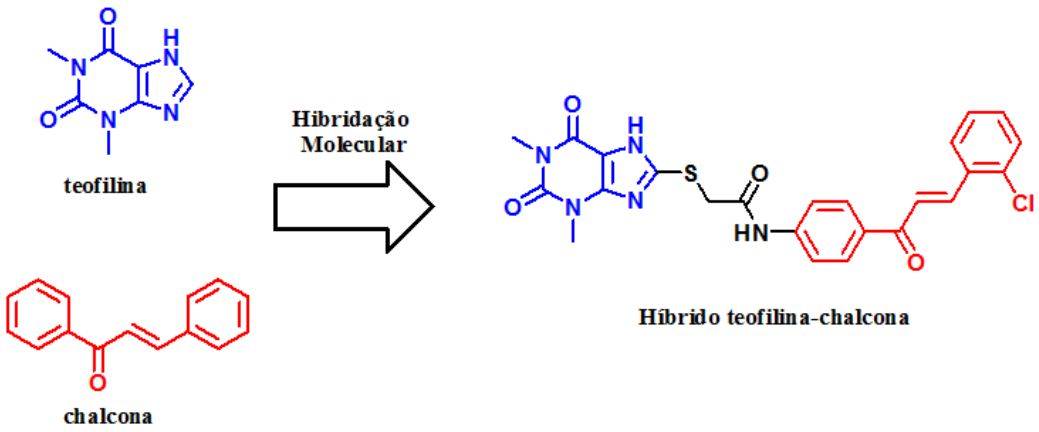

FONTE: autora

1.2. OBJETIVOS

Objetivos Gerais

Síntese e avaliação farmacológica de chalconas, híbridos chalcona-inibidores de Histona Desacetilases e análogos para o câncer de mama, utilizando ensaios celulares, moleculares e enzimáticos.

Objetivos Específicos

a) Síntese de uma série de aminochalconas com anel fenílico B substituído por grupos eletrodoadores/eletroatratores, hidrofóbicos/hidrofílicos, e anéis B não-fenílicos;

b) Avaliação da atividade antiproliferativa das aminochalconas por ensaio de viabilidade celular utilizando MTT contra as linhagens de câncer de mama, MCF-7 e MDA-MB-231, determinação dos valores de CI_{50} em pH 7,4 das substâncias mais ativas, e avaliação em microambiente ácido (pH 6,7);

c) Determinação do tipo de morte celular por citometria de fluxo que as aminochalconas mais potentes induziram nas células MCF-7 e MDA-MB-231;

d) Investigação do efeito das aminochalconas na expressão das proteínas p53 e Sp1 da linhagem MCF-7;

e) Síntese de híbridos chalcona-inibidores de HDAC, e de sulfonamidas;

f) Avaliação da atividade inibitória enzimática dos híbridos e seus análogos contra cinco isoformas de HDACs (HDAC1, 2, 4, 6 e 11);

g) Determinação do valor de CI_{50} do híbrido e análogos contra HDAC2;

h) Avaliação da atividade antiproliferativa do híbrido e análogos mais potentes contra células MCF-7 e MDA-MB-231;

i) Estudo por modelagem molecular do modo de interação dos híbridos e análogos com a HDAC2.

1.3. REFERÊNCIAS

ABOU-ZIED, H. A. et al. EGFR inhibitors and apoptotic inducers: Design, synthesis, anticancer activity and docking studies of novel xanthine derivatives carrying chalcone moiety as hybrid molecules. **Bioorganic Chemistry**, v. 89, p. 102997, 2019.

ANDRADE, C. D. DE. **A rosa do povo**. Rio de Janeiro, RJ: Editora Record, 1998.

BAILEY, S. T. et al. Estrogen receptor prevents p53-dependent apoptosis in breast cancer. **Proceedings of the National Academy of Sciences**, v. 109, n. 44, p. 18060–18065, 2012.

BARNES, T. A. et al. Efficacy, safety, tolerability and price of newly approved drugs in solid tumors. **Cancer Treatment Reviews**, v. 56, p. 1–7, 2017.

BECKERMAN, R.; PRIVES, C. Transcriptional Regulation by P53. **Cold Spring Harbor Perspectives in Biology**, v. 2, n. 8, p. a000935–a000935, 2010.

BEHERA, J.; JAYAPRAKASH, V.; SINHA, B. N. Histone Deacetylase Inhibitors: A Review on Class-I Specific Inhibition. **Mini-Reviews in Medicinal Chemistry**, v. 15, n. 9, p. 731–750, 2015.

BEISHLINE, K.; AZIZKHAN-CLIFFORD, J. Sp1 and the 'hallmarks of cancer'. **FEBS Journal**, v. 282, n. 2, p. 224–258, 2015.

BERTHEAU, P. et al. p53 in breast cancer subtypes and new insights into response to chemotherapy. **The Breast**, v. 22, p. S27–S29, 2013.

BRAY, F. et al. Global cancer statistics 2018: GLOBOCAN estimates of incidence and mortality worldwide for 36 cancers in 185 countries. **CA: A Cancer Journal for Clinicians**, v. 68, n. 6, p. 394–424, 2018.

CECCACCI, E.; MINUCCI, S. Inhibition of histone deacetylases in cancer therapy: lessons from leukaemia. **British Journal of Cancer**, v. 114, n. 6, p. 605–611, 2016.

CHO, M. et al. Cardamonin suppresses melanogenesis by inhibition of Wnt/β-catenin signaling. **Biochemical and Biophysical Research Communications**, v. 390, n. 3, p. 500–505, 2009.

CHUANG, D.-M. et al. Multiple roles of HDAC inhibition in neurodegenerative conditions. **Trends in Neurosciences**, v. 32, n. 11, p. 591–601, 2009.

DAMAGHI, M.; WOJTKOWIAK, J. W.; GILLIES, R. J. pH sensing and regulation in cancer. **Frontiers in Physiology**, v. 4, 2013.

DAMASKOS, C. et al. Histone Deacetylase Inhibitors: An Attractive Therapeutic Strategy Against Breast Cancer. **Anticancer Research**, v. 37, n. 1, p. 35–46, 2017.

DELCUVE, G. P.; KHAN, D. H.; DAVIE, J. R. Roles of histone deacetylases in epigenetic regulation: emerging paradigms from studies with inhibitors. **Clinical Epigenetics**, v. 4, n. 1, p. 5, 2012.

DENIAUD, E. et al. Overexpression of Transcription Factor Sp1 Leads to Gene Expression Perturbations and Cell Cycle Inhibition. **PLoS ONE**, v. 4, n. 9, p. e7035, 2009.

ECKSCHLAGER, T. et al. Histone Deacetylase Inhibitors as Anticancer Drugs. **International Journal of Molecular Sciences**, v. 18, n. 7, p. 1414, 2017.

EISNER, A.; LUOH, S.-W. Breast Cancer Medications and Vision: Effects of Treatments for Early-stage Disease. **Current Eye Research**, v. 36, n. 10, p. 867–885, 2011.

FALKENBERG, K. J.; JOHNSTONE, R. W. Histone deacetylases and their inhibitors in cancer, neurological diseases and immune disorders. **Nature Reviews Drug Discovery**, v. 13, n. 9, p. 673–691, 2014.

FEDELE, P.; ORLANDO, L.; CINIERI, S. Targeting triple negative breast cancer with histone deacetylase inhibitors. **Expert Opinion on Investigational Drugs**, v. 26, n. 11, p. 1199–1206, 2017.

FONSECA, B. F. et al. Derricin and Derricidin Inhibit Wnt/β-Catenin Signaling and Suppress Colon Cancer Cell Growth In Vitro. **PLOS ONE**, v. 10, n. 3, p. e0120919, 2015.

FRAGA, C. A. M. Drug hybridization strategies: before or after lead identification? **Expert Opinion on Drug Discovery**, v. 4, n. 6, p. 605–609, 2009.

GARMPIS, N.; et al. Histone Deacetylases as New Therapeutic Targets in Triple-negative Breast Cancer: Progress and Promises. **Cancer Genomics & Proteomics**, v. 14, n. 5, 2017.

GAN, X. et al. Design, Synthesis, and Antiviral Activity of Novel Chalcone Derivatives Containing a Purine Moiety. **Chinese Journal of Chemistry**, v. 35, n. 5, p. 665–672, 2017.

GATENBY, R. A. et al. Cellular adaptations to hypoxia and acidosis during somatic evolution of breast cancer. **British Journal of Cancer**, v. 97, n. 5, p. 646–653, 2007.

GOLDHIRSCH, A. et al. Strategies for subtypes—dealing with the diversity of breast cancer: highlights of the St Gallen International Expert Consensus on the Primary Therapy of Early Breast Cancer 2011. **Annals of Oncology**, v. 22, n. 8, p. 1736–1747, 2011.

GRYDER, B. E. et al. Histone Deacetylase Inhibitors Equipped with Estrogen Receptor Modulation Activity. **Journal of Medicinal Chemistry**, v. 56, n. 14, p. 5782–5796, 2013.

HABERLAND, M.; MONTGOMERY, R. L.; OLSON, E. N. The many roles of histone deacetylases in development and physiology: implications for disease and therapy. **Nature Reviews Genetics**, v. 10, n. 1, p. 32–42, 2009.

HASHIM, A. I. et al. Imaging pH and metastasis. **NMR in Biomedicine**, p. 582–591, 2011.

HASSANPOUR, S. H.; DEHGHANI, M. Review of cancer from perspective of molecular. **Journal of Cancer Research and Practice**, v. 4, n. 4, p. 127–129, 2017.

IFTIKHAR, S. et al. Synthesis and evaluation of modified chalcone based p53 stabilizing agents. **Bioorganic & Medicinal Chemistry Letters**, v. 27, n. 17, p. 4101–4106, 2017.

JOERGER, A. C.; FERSHT, A. R. The Tumor Suppressor p53: From Structures to Drug Discovery. **Cold Spring Harbor Perspectives in Biology**, v. 2, n. 6, p. a000919–a000919, 2010.

KAHYO, T. et al. A Novel Chalcone Polyphenol Inhibits the Deacetylase Activity of SIRT1 and Cell Growth in HEK293T Cells. **Journal of Pharmacological Sciences**, v. 108, n. 3, p. 364–371, 2008.

KHAN, N. et al. Determination of the class and isoform selectivity of small-molecule histone deacetylase inhibitors. **Biochemical Journal**, v. 409, n. 2, p. 581–589, 2008.

KIM, N. H. et al. p53 and MicroRNA-34 Are Suppressors of Canonical Wnt Signaling. **Science Signaling**, v. 4, n. 197, p. ra71-ra71, 2011.

LAHSASNI, S.; AL KORBI, F.; ALJABER, N. A.-A. Synthesis, characterization and evaluation of antioxidant activities of some novel chalcones analogues. **Chemistry Central Journal**, v. 8, n. 1, p. 32, 2014.

LAI, C.-J. et al. CUDC-101, a Multitargeted Inhibitor of Histone Deacetylase, Epidermal Growth Factor Receptor, and Human Epidermal Growth Factor Receptor 2, Exerts Potent Anticancer Activity. **Cancer Research**, v. 70, n. 9, p. 3647–3656, 2010.

LATCHMAN, D. S. Transcription factors: An overview. **The International Journal of Biochemistry & Cell Biology**, v. 29, n. 12, p. 1305–1312, 1997.

LAUFFER, B. E. L. et al. Histone Deacetylase (HDAC) Inhibitor Kinetic Rate Constants Correlate with Cellular Histone Acetylation but Not Transcription and Cell Viability. **Journal of Biological Chemistry**, v. 288, n. 37, p. 26926–26943, 2013.

LISPECTOR, C. **A descoberta do mundo: crônicas**. Rio de Janeiro, RJ: Ed. Rocco, 1999.

MAHAPATRA, D. K.; BHARTI, S. K.; ASATI, V. Anti-cancer chalcones: Structural and molecular target perspectives. **European Journal of Medicinal Chemistry**, v. 98, p. 69–114, 2015.

MAI, C. W. et al. Chalcones with electron-withdrawing and electron-donating substituents: Anticancer activity against TRAIL resistant cancer cells, structure–activity relationship analysis and regulation of apoptotic proteins. **European Journal of Medicinal Chemistry**, v. 77, p. 378–387, 2014.

MARLIYANA, S. D.; SYAH, Y. M.; MUJAHIDIN, D.-. In vitro Antibacterial Activity of Chalcone Derivatives from *Kaempferia pandurata* Rhizomes Against Clinical Isolate Bacteria. **ALCHEMY Jurnal Penelitian Kimia**, v. 13, n. 1, p. 41, 2017.

MCINTYRE, A.; HARRIS, A. L. The Role of pH Regulation in Cancer Progression. In: CRAMER, T.; A. SCHMITT, C. (Eds.). . **Metabolism in Cancer**. Cham: Springer International Publishing, 2016. v. 207, p. 93–134, 2016.

MOKALE, S. N. et al. Synthesis, in-vitro screening, and docking analysis of novel pyrrolidine and piperidine-substituted ethoxy chalcone as anticancer agents. **Medicinal Chemistry Research**, v. 24, n. 5, p. 1842–1856, 2015.

MOTTAMAL, M. et al. Histone Deacetylase Inhibitors in Clinical Studies as Templates for New Anticancer Agents. **Molecules**, v. 20, n. 3, p. 3898–3941, 2 mar. 2015.

MÜLLER, B. M. et al. Differential expression of histone deacetylases HDAC1, 2 and 3 in human breast cancer - overexpression of HDAC2 and HDAC3 is associated with clinicopathological indicators of disease progression. **BMC Cancer**, v. 13, n. 1, p. 215, dez. 2013.

SARKAR, S. et al. Cancer Development, Progression, and Therapy: An Epigenetic Overview. **International Journal of Molecular Sciences**, v. 14, n. 10, p. 21087–21113, 2013.

SAYEED, A. et al. Estrogen Receptor Inhibits p53-Mediated Transcriptional Repression: Implications for the Regulation of Apoptosis. **Cancer Research**, v. 67, n. 16, p. 7746–7755, 2007.

SETO, E.; YOSHIDA, M. Erasers of Histone Acetylation: The Histone Deacetylase Enzymes. **Cold Spring Harbor Perspectives in Biology**, v. 6, n. 4, p. a018713–a018713, 2014.

SHAN, W. et al. HDAC2 overexpression correlates with aggressive clinicopathological features and DNA-damage response pathway of breast cancer. **American Journal of Cancer Research**, v. 7, n. 5, p. 1213–1226, 2017.

SHARMA, R. et al. A Review on Mechanisms of Anti Tumor Activity of Chalcones. **Anti-Cancer Agents in Medicinal Chemistry**, v. 16, n. 2, p. 200–211, 2015.

SHRIVASTAVA, S. et al. Cardamonin, a chalcone, inhibits human triple negative breast cancer cell invasiveness by downregulation of Wnt/β-catenin signaling cascades and reversal of epithelial-mesenchymal transition: CD inhibits human triple negative breast cancer cell. **BioFactors**, v. 43, n. 2, p. 152–169, 2017.

SU, Y. et al. Methoxyphenyl chalcone sensitizes aggressive epithelial cancer to cisplatin through apoptosis induction and cancer stem cell eradication. **Tumor Biology**, v. 39, n. 5, p. 101042831769168, 2017.

SULAIMAN, A. et al. Both bulk and cancer stem cell subpopulations in triple-negative breast cancer are susceptible to Wnt, HDAC, and ERα coinhibition. **FEBS Letters**, v. 590, n. 24, p. 4606–4616, 2016.

SULAIMAN, A. et al. Co-inhibition of mTORC1, HDAC and ESR1α retards the growth of triple-negative breast cancer and suppresses cancer stem cells. **Cell Death & Disease**, v. 9, n. 8, ago. 2018.

TATE, C. R. et al. Targeting triple-negative breast cancer cells with the histone deacetylase inhibitor panobinostat. **Breast Cancer Research**, v. 14, n. 3, 2012.

TSENG, C.-H. et al. Synthesis and antiproliferative evaluation of 3-phenylquinolinylchalcone derivatives against non-small cell lung cancers and breast cancers. **European Journal of Medicinal Chemistry**, v. 59, p. 274–282, 2013.

VANDER HEIDEN, M. G.; CANTLEY, L. C.; THOMPSON, C. B. Understanding the Warburg Effect: The Metabolic Requirements of Cell Proliferation. **Science**, v. 324, n. 5930, p. 1029–1033, 2009.

VERVERIS, K.; KARAGIANNIS, T. C. An atlas of histone deacetylase expression in breast cancer: fluorescence methodology for comparative semi-quantitative analysis. **American Journal of Translational Research**, v. 4, n. 1, p. 24–43, 2012.

WANG, M. et al. Role of tumor microenvironment in tumorigenesis. **Journal of Cancer**, v. 8, n. 5, p. 761–773, 2017.

WANG, X.-B. et al. [Expression and prognostic value of transcriptional factor sp1 in breast cancer]. **Ai Zheng = Aizheng = Chinese Journal of Cancer**, v. 26, n. 9, p. 996–1000, 2007.

WEICHERT, W. HDAC expression and clinical prognosis in human malignancies. **Cancer Letters**, v. 280, n. 2, p. 168–176, 2009.

WON, J.; YIM, J.; KIM, T. K. Sp1 and Sp3 Recruit Histone Deacetylase to Repress Transcription of Human Telomerase Reverse Transcriptase (hTERT) Promoter in Normal Human Somatic Cells. **Journal of Biological Chemistry**, v. 277, n. 41, p. 38230–38238, 2002.

XU, K. et al. Elucidation of How Cancer Cells Avoid Acidosis through Comparative Transcriptomic Data Analysis. **PLoS ONE**, v. 8, n. 8, p. e71177, 2013.

YERUVA, S. L. H. et al. E2112: randomized phase iii trial of endocrine therapy plus entinostat/placebo in patients with hormone receptor-positive advanced breast cancer. **npj Breast Cancer**, v. 4, n. 1, 2018.

ZHUANG, C. et al. Chalcone: A Privileged Structure in Medicinal Chemistry. **Chemical Reviews**, v. 117, n. 12, p. 7762–7810, 2017.

Capítulo II

2. Capítulo II - Artigo Publicado na Revista *Journal of Enzyme Inhibition and Medicinal Chemistry* em abril de 2019

JOURNAL OF ENZYME INHIBITION AND MEDICINAL CHEMISTRY
2019, VOL. 34, NO. 1, 1093–1099
https://doi.org/10.1080/14756366.2019.1615485

SHORT COMMUNICATION

Antiproliferative activity and p53 upregulation effects of chalcones on human breast cancer cells

Mariana Bastos dos Santos[a], Daiane Bertholin Anselmo[a], Jéssica Gisleine de Oliveira[b], Bruna V. Jardim-Perassi[b], Diego Alves Monteiro[c], Gabriel Silva[d], Eleni Gomes[c], Ana Lucia Fachin[d], Mozart Marins[d], Débora Aparecida Pires de Campos Zuccari[b] and Luis Octavio Regasini[a]

[a]Department of Chemistry and Environmental Chemistry, Institute of Biosciences, Humanities and Exact Sciences (IBILCE), São Paulo State University (UNESP), São Paulo, Brazil; [b]Department of Molecular Biology, Medicine College of São José do Rio Preto (FAMERP), São Paulo, Brazil; [c]Department of Biology, Institute of Biosciences, Humanities and Exact Sciences (IBILCE), São Paulo State University (UNESP), São Paulo, Brazil; [d]Biotechnology Unit, University of Ribeirão Preto (UNAERP), São Paulo, Brazil

ABSTRACT

Chalcones are valuable structures for drug discovery due to their broad bioactivity spectrum. In this study, we evaluated 20 synthetic chalcones against estrogen-receptor-positive breast cancer cells (MCF-7 line) and triple-negative breast cancer (TNBC) cells (MDA-MB-231 line). Antiproliferative screening by MTT assay resulted in two most active compounds: 2-fluoro-4′-aminochalcone (**11**) and 3-pyridyl-4′-aminochalcone (**17**). Their IC_{50} values ranged from 13.2 to 34.7 μM against both cell lines. Selected chalcones are weak basic compounds and maintained their antiproliferative activity under acidosis conditions (pH 6.7), indicating their resistance to ion-trapping effect. The mode of breast cancer cells death was investigated and chalcones **11** and **17** were able to induce apoptosis rather than necrosis in both lines. Antiproliferative target investigations with MCF-7 cells suggested **11** and **17** upregulated p53 protein expression and did not affect Sp1 protein expression. Future studies on chalcones **11** and **17** can define their *in vivo* therapeutic potential.

ARTICLE HISTORY
Received 21 March 2019
Accepted 28 April 2019

KEYWORDS
Chalcones; cancer; p53; antiproliferative; apoptosis

Journal of Enzyme Inhibition and Medicinal Chemistry

Antiproliferative activity and p53 upregulation effects of chalcones on human breast cancer cells

Mariana Bastos dos Santos[a], Daiane Bertholin Anselmo[a], Jéssica Gisleine de Oliveira[b], Bruna V. Jardim-Perassi[b], Diego Alves Monteiro[c], Gabriel Silva[d], Eleni Gomes[c], Ana Lucia Fachin[d], Mozart Marins[d], Débora Aparecida Pires de Campos Zuccari[b], Luis Octavio Regasini[a,*]

[a] *Department of Chemistry and Environmental Sciences, Institute of Biosciences, Humanities and Exact Sciences (IBILCE), São Paulo State University (UNESP), São José do Rio Preto, São Paulo, Brazil;*

[b] *Department of Molecular Biology, Medicine College of São José do Rio Preto (FAMERP), São José do Rio Preto, São Paulo, Brazil;*

[c] *Department of Biology, Institute of Biosciences, Humanities and Exact Sciences (IBILCE), São Paulo State University (UNESP), São José do Rio Preto, São Paulo, Brazil;*

[d]*Biotechnology Unit, University of Ribeirão Preto (UNAERP), Ribeirão Preto, São Paulo, Brazil*

***luis.regasini@unesp.br (L.O.R.); Tel.: +55-17-3221-2362.**

ABSTRACT

Chalcones are valuable structures for drug discovery due to their broad bioactivity spectrum. In this study, we evaluated 20 synthetic chalcones against estrogen-receptor-positive breast cancer cells (MCF-7 line) and triple-negative breast cancer cells (MDA-MB-231 line). Antiproliferative screening by MTT assay resulted in two most active compounds: 2-fluoro-4'-aminochalcone (**11**) and 3-pyridyl-4'-aminochalcone (**17**). Their IC_{50} values ranged from 13.2 μmol L^{-1} to 34.7 μmol L^{-1} against both cell lines. Selected chalcones are weak basic compounds and maintained their antiproliferative activity under acidosis conditions (pH 6.7), indicating their resistance to ion-trapping effect. The mode of breast cancer cells death was investigated and chalcones **11** and **17** were able to induce apoptosis rather than necrosis in both lines. Antiproliferative target investigations with MCF-7 cells suggested **11** and **17** upregulated p53 protein expression and did not affect Sp1 protein expression. Future studies on chalcones **11** and **17** can define their *in vivo* therapeutic potential.

KEYWORDS: chalcones, cancer, p53, antiproliferative, apoptosis.

2.1. INTRODUCTION

Breast cancer is the most common type of cancer that affects women around the world, corresponding to 25 % of cases. It is also the main cause of cancer death among women [1–3]. Its classification is based on presence of cellular receptors: (i) Hormone-Receptor (HR), with Estrogen (ER) and/or Progesterone-Receptors (PR); (ii) Human Epidermal Growth Factor-2 receptor (HER2); and (iii) Triple-Negative Breast Cancer (TNBC), which does not express ER, PR or HER2 receptors [4–6]. Chemotherapy choices for breast cancer are made according to its classification aiming to reach specific targets. ER-positive cancer treatments include estrogen-receptor modulators, such as tamoxifen or aromatase inhibitors. HER2-positive cancer is treated with monoclonal antibodies, such as trastuzumab, which is administered alongside tyrosine-kinase inhibitors [7,8,9]. TNBC cancer treatment is focused on cytotoxic agents, such as taxanes or doxorubicin. This cancer has poor response to chemotherapy, particularly at metastatic sites, with survival rates below 2 years. Altogether, TNBC cancer has been considered the most severe and difficult to treat due to a lack of targeted therapy [10–12].

Chalcones are valuable structures for drug discovery due to their broad bioactivity spectrum, as well as their versatile and simple synthesis. Their structures, bearing two benzene rings (A and B), are linked by an enone bridge. They have demonstrated antiproliferative activity against cancer cells, including breast cancer [13–15]. Mai and co-authors described chalcone was effective against ER-positive breast cancer cells (MCF-7 line) targeting 20 apoptotic markers[16]. Iftikhar et al. reported that chalcone bearing chlorine at position 2 was effective against breast cancer cells (CAL-51 line) and induced accumulation of p53 protein [17]. Silva and co-authors (2018) described unsubstituted chalcone increased p53 protein activity in osteosarcoma cells (U2OS line) through induction of heat shock protein DNAJB1 [18].

In our ongoing search for anticancer compounds with structures based on chalcone framework, we evaluated antiproliferative activity of 20 chalcones against ER-positive cells (MCF-7 line) and TNBC (MDA-MB-231 line). The two most active chalcones (11 and 17) were selected to antiproliferative evaluation under acidosis conditions (pH 6.7) and pro-apoptotic activity in MCF-7 and MDA-MB-231 lines. In addition, we investigated tumor molecular targets of 11 and 17 in MCF-7 line, which were able to upregulate p53 protein expression.

2.2. MATERIALS AND METHODS

Chemical procedure for synthesis of chalcones 1–20

Reagents and solvents were purchased from Merck®. Series of 20 chalcones was synthesized by Claisen-Schmidt aldol condensation reaction, according to protocol described by Santos and co-authors, with minor modifications [19,20]. Reactions were carried out at room temperature using 3.0 mmol of 4'-aminoacetophenone and 3.0 mmol of aldehydes, which were dissolved in ethanol (30 mL). Sodium hydroxide in ethanol (1.0 mol/L) was added as catalyst solution. Reagents conversion was monitored using thin layer chromatography. Crude product was poured onto ice (from distilled and deionized water) and filtered. All compounds were purified over silica gel chromatography column eluted with mixture of hexane and ethyl acetate (3:2). Melting points were determined in TecnoponPFM-II® apparatus and were uncorrected. Structure of compounds was confirmed by ^{1}H and ^{13}C Nuclear Magnetic Resonance (NMR) spectra analyses. Spectral data were obtained in Bruker Avance III® (14 Tesla, 600 MHz) using deuterated dimethyl sulfoxide (DMSO-d_6) as solvent. Chalcones had their UV-vis spectra and chromatograms obtained in High Performance Liquid Chromatography with Diode Array Detector (HPLC-DAD) Agilent Technologies® 1220 Infinity equipment coupled with a photodiode array system (1260 - Infinity®) and Agilent Zorbax Eclipse Plus C-18® column (250 mm × 4.6 mm, 5 μm), using methanol:water (3:1) as mobile phase (1.0 mL/min).

Antiproliferative activity of chalcones 1–20

Human breast cancer cell lines MCF-7 (HTB-22) and MDA-MB-231 (HTB-26) were purchased from American Type Culture Collection (ATCC). Both cell lines were cultured in DMEM (Gibco®) supplemented with 10 % fetal bovine serum (FBS - LGC®), penicillin-streptomycin (100 μg/mL, Merck®). Both cell lines were incubated at 37 °C under humidified atmosphere with 5% CO_2 (Thermo Fischer Scientific® Incubator).

Antiproliferative activity of chalcones **1**–**20** was evaluated by MTT assay [21–23]. Cells were seeded in 96-well plate, with initial cell density of 1×10^4 and 2.5×10^4 cells/well of MCF-7 and MDA-MB-23, respectively. Cells were cultured with DMEM supplemented with 10 % FBS and compounds at 20 μmol L^{-1} for 48 h at 37 °C under 5 % CO_2 humidified atmosphere. Cells were incubated with MTT (Sigma Aldrich®) solution (1 mg/mL) for 40 min. Formazan crystals were solubilized in dimethylsulfoxide (DMSO, Sigma Aldrich®), and absorbance rates were measured at 562 nm in ThermoPlate® TP

Reader. Chalcones **1**, **6**, **8**, **9**, **11**, **17**, **19** and **20** had the highest antiproliferative activity and were assayed against both cell lines at seven concentrations, ranging from 1.25 to 80 μmol L^{-1} for IC_{50} values determination.

Antiproliferative activity of selected chalcones 11 and 17 under acidosis

Cell viability was evaluated under acidosis conditions by MTT assay, using 4-morpholine-ethanesulfonic acid to produce a pH value of 6.7 [24,25]. Cells were treated with selected chalcones **11** and **17** at their respective IC_{50} values. All procedures were performed in triplicate and three independent experiments.

Pro-apoptotic activity of selected chalcones 11 and 17

Pro-apoptotic activity of selected chalcones **11** and **17** was evaluated using FITC Annexin V Apoptosis Detection Kit I (BD Pharmingen®) by flow cytometry[26]. MCF-7 and MDA-MB-231 cells were seeded and cultivated in 6-well plates (6.5×10^5 cells/well), for 24 h, and treated with 40 μmol L^{-1} selected chalcones in DMEM containing 10% FBS for 48 h. As negative control 0.1 % DMSO was used. Adherent and floating cells were collected, submitted to centrifugation, and washed with PBS (Sigma Aldrich®). Apoptotic cells were determined by flow cytometry in BD FACSCalibur® Flow Cytometer (BD Biosciences®), after double staining (annexin V/propidium iodide) using FITC Annexin V Apoptosis Detection kit I (BD Pharmigen®) according to instructions of manufacturer. All procedures were performed in triplicate and in three independent experiments.

Effect of selected chalcones 11 and 17 on Sp1 and p53 proteins expressions

Protein expression was assessed using Western Blot assay. Breast cancer cells (MCF-7) were seeded in 6-well plates at 7.5×10^5 cells/well, treated with selected chalcones **11** and **17** at 10 and 20 μmol L^{-1} or with negative control (0.1 % DMSO) for 24 h [26]. Cells were suspended in PBS solution, collected in RadioImmunoPrecipitation Assay buffer – (RIPA buffer at 4 °C), supplemented with proteinase inhibitors, sonicated for lysis, and submitted to centrifugation (14000 rpm, 4 °C, 20 minutes, Eppendorf®). Protein total concentration was obtained using PierceTM BCA Protein Assay reagent (Thermo Scientific®). Total proteins (30 μg) in sodium dodecyl sulfate (SDS) buffer were warmed at 95 °C, cooled at 4 °C and submitted to sodium dodecyl sulfate–polyacrylamide gel electrophoresis SDS-PAGE (12 %, 100 V, 360 mA) for 90 min at room temperature, and

were transferred to nitrocellulose membrane (PALL Corporation®). Membranes were blocked using TBST buffer (25 mM Tris, 3 mM KCl, 0.14 M NaCl, 0.05 % Tween 20) containing 5 % non-fat milk at room temperature for 1 h, followed by overnight incubation at 4 °C, with primary antibodies to Sp1 (MilliPore®), p53 and β-actin (Santa Cruz Biotechnology®). Subsequently, membranes were washed with TBST (3 ×) and incubated with peroxidase-conjugated secondary antibodies diluted in TBST buffer-5% non-fat milk (1:5000) at room temperature and washed several times with TBST buffer. Proteins were detected through chemiluminescence using Enhanced Chemiluminescent (ECL®) Western Blotting Detection reagent (Amersham Biosciences®) in LAS 500 luminescence analyzer (GE Healthcare®) [26]. Bands intensity in image was quantified using ImageJ® software.

Statistical analysis

Statistical analyses were carried out using one-way ANOVA multiple comparison tests followed by Tukey's HSD test [19,27]. Statistical significance difference was considered if $p < 0.05$.

2.3. RESULTS AND DISCUSSION

Chemistry

Chalcones **1**–**20** were synthesized by Claisen Schmidt reaction with yields of 30–93% after chromatography purification. Series of compounds has chalcones with amino at position 4' (ring A) and benzene ring B substituted by electron-withdrawing (EWG) and electron-donating groups (EDG). Also, aryl analogues with benzene ring B replaced for furan, thiophene, pyridine, and naphthyl rings were synthesized (Scheme 1).

All NMR parameters, including hydrogen and carbon chemical shifts (δ_H and δ_C in ppm), integrations, multiplicities, and coupling constants (J in Hz), corresponded to proposed structures of chalcones **1**–**20**. Two main signals in ^{1}H NMR spectra were diagnosed: (i) a pair of doublets with J ranging from 15 to 16 Hz (7.43–8.10 ppm), attributed to methyne hydrogens of *trans* carbon-carbon double bonds and (ii) broad singlets between 6.18 and 6.27 ppm related to geminal hydrogens of amino group. In ^{13}C NMR spectra, signals in 185.9–186.1 confirmed ketone carbonyls, which are shifted to downfield due to conjugation with carbon-carbon double bonds. UV-Vis had λ_{max} at 298-378 nm, which were related to a pivotal chromophore of chalcone framework (conjugation between ring B and enone bridge). High Performance Liquid Chromatography with Diode

Array Detector (HPLC-DAD) analyses of peak areas integrations indicated chalcones purity of 94.0–99.9 %. All chromatograms and spectra are presented in supplemental data (Figure S1–S62).

Antiproliferative activity of chalcones 1–20

Preliminary antiproliferative activity of chalcones **1**–**20** was evaluated by MTT assay for 48 h against MCF-7 (ER) and MDA-MB-231 (TNBC) lines. Percentages of metabolically viable cells (%MVC) are summarized in Table 1. Series of compounds demonstrated active (*e.g.*, **20**) and inactive (*e.g.*, **3**) chalcones, suggesting molecular variations were relevant for antiproliferative screening against both cell lines. Experiments at 20 μmol L^{-1} allowed us to derive preliminary structural features related to antiproliferative activity [28–30].

In previous studies conducted by our group, chalcone with unsubstituted rings A and B had potent antiproliferative and pro-apoptotic activities [18]. However, its low solubility in water enables limited additional pharmacological assays, mainly *in vivo* experiments. Therefore, we designed a series of analogues with amino group at position 4' on ring A, which had higher solubility in water compared to unsubstituted chalcone[16]. We evaluated chalcone with amino at position 4' and unsubstituted ring B (**1**), which was inactive against MCF-7 (%MVC = 97.3 ± 6.0) and active against MDA-MB-231 (%MVC = 80.6 ± 4.0). Such result encouraged us to prepare further analogues with substitutions on ring B. Mai and co-authors reported EWG on ring B of chalcones improved antiproliferative activity against a broad panel of cancer cells [16]. We assayed analogues substituted by nitro (**2**), trifluoromethyl (**3**), cyano (**4**) and halogens (**5**–**12**). 3-Chloro-4'-aminochalcone (**9**) and 2-fluoro-4'-aminochalcone (**11**) were the two most active compounds against MCF-7 line, with %MVC rates of 52.5 ± 6.7 and 50.3 ± 7.8, respectively. 3-Fluoro-4'-aminochalcone (**8**) was the most potent against MDA-MB-231 line, with %MVC of 73.3 ± 5.4. In summary, comparison among %MVC values of chalcones with EWG on ring B and 1 suggested more electronegative halogens corroborated to antiproliferative activity. 4-Methyl-4'-aminochalcone (**13**) and 4-methoxy-4'-aminochalcone (**14**) were less active than halogenated-chalcones (**5**–**15**), corroborating negative effect of EDG toward bioactivity. We hypothesized rings containing six π electrons, similarly to phenyl ring of 1, could conduce to bioactive analogues [31]. 2-Furyl-4'-aminochalcone (**15**) and 2-thiophenyl-4'-aminochalcone (**16**) were inactive compounds.

Pyridylchalcones **17** and **18** were strongly active against MCF-7 line, with %MVC rates of 51.8 ± 2.5 and 61.3 ± 3.4, respectively. We also investigated effect of additional benzene ring toward bioactivity, evaluating naphthylchalcone **19** and biphenylchalcone **20**, which have ten and twelve π electrons on ring B, respectively. Both chalcones presented strong antiproliferative activity against MCF-7 line, with %MVC rates of 53.4 ± 4.3 and 44.2 ±3.3, respectively. Despite effect against both lines, MCF-7 line (ER) was more sensitive to chalcones than MDA-MB-231 line (TNBC) (Table 1).

The five most antiproliferative compounds against MCF-7 were **9**, **11**, **17**, **19** and **20** (%MVC values lower than 60). Against MDA-MB-231, the five most potent ones were **1**, **6**, **8**, **11** and **17** (%MVC values lower than 85). These seven compounds were selected to determine IC_{50} values for both cell lines (Table 1). Chalcones **1**, **6** and **8** were inactive against MCF-7 (IC_{50} > 100 µM) and active against MDA-MB-231, with IC_{50} values of 60.3, 69.0 and 74.1 µmol L^{-1}, respectively. Chalcones **19** and **20** were active against MCF-7 with IC_{50} values of 14.3 and 22.7 µmol L^{-1}, respectively and inactive against MDA-MB-231 (IC_{50} > 100 µmol L^{-1}). Chalcones **11** and **17** were active against both cell lines, displaying IC_{50} values of 13.2–34.2 µmol L^{-1} and were selected for additional bioassays.

Antiproliferative activity of selected chalcones 11 and 17 under acidosis

In normal cells, intracellular and extracellular pH values are 7.2 and 7.4, respectively. On the other hand, in breast tumor cells, intracellular and extracellular pH values are 7.1–7.4 and 6.5–7.1, respectively [24,32]. This extracellular acidosis has been related to Warburg effect, in which tumor cells are in intense anaerobic metabolism, producing and exporting acid compounds through transporters. The biological central interest in acidosis is due to clear relationship with invasiveness and metastasis potential [24,33]. Tumor cells in acidic extracellular microenvironment can block membrane permeation of weak basic compounds, leading to ion-trapping effect. This phenomenon is caused by protonation of basic functionalities, converting neutral into cationic compounds. Cationic form exhibits reduced passive permeation through membrane phospholipids when compared to neutral form. Doxorubicin is antineoplastic and weak basic drug and has demonstrated low efficacy in acidosis microenvironment due to ion-trapping effect [34].

Chalcones **11** and **17** were submitted to antiproliferative assays under acid microenvironment (at pH 6.7) against both breast cancer cell lines (Figures 1a and 1b). In experiments with MCF-7 line, both chalcones maintained their antiproliferative effect,

showing ion-trapping resistance. In MDA-MB-231 line, chalcone **17** maintained similar %MVC rate at both pH values. Interestingly, chalcone **11** was five times more active at pH 6.7 (acidosis) than at 7.4, with %MVC of 14.4 and 73.7, respectively.

Pro-apoptotic activity of selected chalcones 11 and 17

Antiproliferative compounds can induce tumor cell death by several mechanisms [35]. Among these, apoptosis and necrosis are the most common and studied ones. Apoptosis events have been induced by chalcones toward different cancer cell lines [36,37]. In order to investigate antiproliferative effect mechanism of selected chalcones **11** and **17** toward MCF-7 and MDA-MB-231 lines, annexin V/PI staining and flow cytometry were used to detect whether cells were dying due to apoptosis or necrosis events (Figure 2).

Chalcones **11** and **17** induced 50.8% and 46.1% apoptotic events in MCF-7 line, 5- and 4-fold increases compared to cell treated with 0.1% DMSO, respectively. In MDA-MB-231 line, chalcones **11** and **17** caused death through apoptosis in 42.4% and 36.3% of cells, respectively. Additionally, selected chalcones induced apoptosis rather than necrosis.

Chalcones are known to induce apoptosis in several cancer cells, being able to up regulate more than 15 pro-apoptotic markers expression, such as Bad, Bax, Bid, Bim, CD40, Fas, IGFBP-5, IGFBP-6, p21, sTNF-R116. Hsu and Bortolloto and their respective collaborators have demonstrated pro-apoptotic activity of unsubstituted chalcone against MCF-7 breast cancer cells [38,39]. These authors have described intrinsic apoptotic pathway induced by unsubstituted chalcone, with inhibition of Bcl-2 and induction of Bax apoptotic markers.

Effect of selected chalcones 11 and 17 on Sp1 and p53 proteins expression

MCF-7 and MDA-MB-231 lines have demonstrated wild and mutant p53 protein, respectively [40]. Thus, we selected MCF-7 to conduct molecular target experiments. Western Blot assay was performed to evaluate effect of chalcones **11** and **17** on p53 and Sp1 proteins in MCF-7 line for 24 h at 10 and 20 μmol L^{-1} (Figure 3).

Sp1 protein is transcription factor involved in cell proliferation and differentiation. In breast cancers, it acts on invasion and metastasis processes [41, 42], and has been classified as marker for poor prognosis [43]. Chalcones **11** and **17** were not able to modulate Sp1 protein expression, at either concentration, presenting similar effect to DMSO 0.1% (negative control).

p53 protein is tumor suppressor and its mutated status has been related to several types of cancers. Expression of p53 in breast cancer cells varies according to its classification [44, 45]. ER-positive and ER-negative cancer types have wild-type p53 and mutated protein forms, respectively [46]. Activation and stabilization of wild-type p53 induces cell-cycle arrest and cell death through apoptosis, reducing cancer progression. This cell pathway has been recognized as attractive target to simple and low-weight-molecular compounds with promising antineoplastic potential. Chalcones **11** and **17** induced 5-fold upregulation of p53 expression in MCF-7 cells (Figure 3), indicating these compounds are able to activate and stabilize p53 protein expression. This result is the first evaluation of low-molecular-weight compounds against breast cancer cells. In this context, methoxychalcones and naphthylchalcones have been described as agents of p53 activation and stabilization in prostate cancer and osteosarcoma cell lines, respectively [26,47].

2.4. CONCLUSIONS

In summary, we reported activity of series of 20 chalcones against two types of breast cancer cells, ER-positive (MCF-7 line) and TNBC (MDA-MB-231 line). Preliminary investigations suggested halogens on ring B and additional benzene rings play central role in antiproliferative activity. Basic chalcones **11** and **17** were antiproliferative agents under acidosis (at pH 6.7), displaying resistance to ion-trapping effect. These compounds induced apoptosis rather than necrosis in both cells, upregulating p53 expression in ER-positive cells (MCF-7 line).

ACKNOWLEDGMENTS

M. B. S. thanks FAPESP for her research fellowship # 2016/00580-5. Authors acknowledge Center of Biomolecular Innovation (FAPESP Grant # 2009/53989-4) and National Institute of Science and Technology – Biodiversity and Natural Products INCT-BioNat (Grants FAPESP # 2014/50926-0 and CNPq # 465637/2014-0).

Disclosure Statement

No potential conflict of interest was reported by authors.

FUNDING

The authors gratefully acknowledge financial support from Coordination for Improvement of Higher Education Personnel (CAPES, Coordenação de Aperfeiçoamento de Pessoal de Nível Superior, Finance Code 001), Brazilian Council for Scientific and Technological Development (CNPq, Conselho Nacional de Desenvolvimento Científico e Tecnológico, Grants # 471129/2013-5, 306251/2016-7 and 429322/2018-6); São Paulo Research Foundation (FAPESP, Fundação de Amparo a Pesquisa do Estado de São Paulo, Grants # 2014/18330-0 and 2018/15083-2).

2.5. REFERENCES

1. Torre LA, Siegel RL, Ward EM, Jemal A. Global Cancer Incidence and Mortality Rates and Trends–An Update. Cancer Epidem Biomar. 2016;25(1):16–27.

2. Ferlay J, Soerjomataram I, Dikshit R, Eser S, Mathers C, Rebelo M, Parkin DM, Forman D, Bray F. Cancer Incidence and Mortality Worldwide: Sources, Methods and Major Patterns in GLOBOCAN 2012: Globocan 2012. Int J Cancer. 2015;136(5):E359–E386.

3. Sledge GW, Mamounas EP, Hortobagyi GN, Burstein HJ, Goodwin PJ, Wolff AC. Past, Present, and Future Challenges in Breast Cancer Treatment. J Clin Oncol. 2014;32(19):1979–1986.

4. Tate CR, Rhodes LV, Segar HC, Driver JL, Pounder FN, Burow ME, Collins-Burow BM. Targeting Triple-Negative Breast Cancer Cells with the Histone Deacetylase Inhibitor Panobinostat. Breast Cancer Res. 2012;14(3).

5. Rakha EA, Ellis IO. Triple-Negative/Basal-like Breast Cancer: Review. Pathology. 2009;41(1):40–47.

6. Eliyatkin N, Yalcin E, Zengel B, Aktaş S, Vardar E. Molecular Classification of Breast Carcinoma: From Traditional, Old-Fashioned Way to A New Age, and A New Way. J. Breast Health. 2015;11(2):59–66.

7. Goldhirsch A, Wood WC, Coates AS, Gelber RD, Thürlimann B, Senn H-J. Panel members. Strategies for Subtypes—Dealing with the Diversity of Breast Cancer: Highlights of the St Gallen International Expert Consensus on the Primary Therapy of Early Breast Cancer 2011. Ann Oncol. 2011;22(8):1736–1747.

8. Damaskos C, Valsami S, Kontos M, Spartalis E, Kalampokas T, Kalampokas E, Athanasiou A, Moris D, Daskalopoulou A, Davakis S, et al. Histone Deacetylase Inhibitors: An Attractive Therapeutic Strategy Against Breast Cancer. Anticancer Res. 2017;37(1):35–46.

9. Soheilifar MH, Taheri RA, Zolfaghari Emameh R, Moshtaghian A, Kooshki H, Motie MR. Molecular Landscape in Alveolar Soft Part Sarcoma: Implications for Molecular Targeted Therapy. Biomed Pharmacother. 2018;103:889–896.

10. Sulaiman A, Sulaiman B, Khouri L, McGarry S, Nessim C, Arnaout A, Li X, Addison C, Dimitroulakos J, Wang L. Both Bulk and Cancer Stem Cell Subpopulations in Triple-Negative Breast Cancer Are Susceptible to Wnt, HDAC, and ERα Coinhibition. FEBS Lett. 2016;590(24):4606–4616.

11. Sulaiman A, McGarry S, Lam KM, El-Sahli S, Chambers J, Kaczmarek S, Li L., Addison C, Dimitroulakos J, Arnaout A, et al. Co-Inhibition of MTORC1, HDAC and ESR1α Retards the Growth of Triple-Negative Breast Cancer and Suppresses Cancer Stem Cells. Cell Death Dis. 2018;9(8).

12. Yao H, He G, Yan S, Chen C, Song L, Rosol TJ, Deng X. Triple-Negative Breast Cancer: Is There a Treatment on the Horizon? Oncotarget. 2017;8(1).

13. Nazir S, Ansari FL, Hussain T, Mazhar K, Muazzam AG, Qasmi Z-H, Makhmoor T, Noureen H, Mirza B. Brine Shrimp Lethality Assay ‘an Effective Prescreen’: Microwave-Assisted Synthesis, BSL Toxicity and 3DQSAR Studies-Based Designing, Docking and Antitumor Evaluation of Potent Chalcones. Pharm Biol. 2013;51(9):1091–1103.

14. Reddy Kotha R, G Kulkarni R, Garige AK, Goud Nerella S, Garlapati A. Synthesis and Cytotoxic Activity of New Chalcones and Their Flavonol Derivatives. Med Chem. 2017;7(11).

15. Das M, Manna K. Chalcone Scaffold in Anticancer Armamentarium: A Molecular Insight J Toxicol. 2016;2016:1–14.

16. Mai CW, Yaeghoobi M, Abd-Rahman N, Kang YB, Pichika MR. Chalcones with Electron-Withdrawing and Electron-Donating Substituents: Anticancer Activity against TRAIL Resistant Cancer Cells, Structure–Activity Relationship Analysis and Regulation of Apoptotic Proteins. Eur J Med Chem. 2014;77:378–387.

17. Iftikhar S, Khan S, Bilal A, Manzoor S, Abdullah M, Emwas A-H, Sioud S, Gao X, Chotana GA, Faisal A, et al. Synthesis and Evaluation of Modified Chalcone Based P53 Stabilizing Agents. Bioorg Med Chem Lett. 2017;27(17):4101–4106.

18. Silva G, Marins M, Chaichanasak N, Yoon Y, Fachin AL, Pinhanelli VC, Regasini LO, Santos MB, Ayusso GM, Marques BC, et al. Trans-Chalcone Increases P53 Activity via DNAJB1/HSP40 Induction and CRM1 Inhibition. PLOS ONE. 2018;13(8):e0202263.

19. Santos MB, Pinhanelli VC, Garcia MAR, Silva G, Baek SJ, França SC, Fachin AL, Marins M, Regasini LO. Antiproliferative and Pro-Apoptotic Activities of 2′- and 4′-Aminochalcones against Tumor Canine Cells. Eur J Med Chem. 2017;138:884–889.

20. Konduri SD, Medisetty R, Liu W, Kaipparettu BA, Srivastava P, Brauch H, Fritz P, Swetzig WM, Gardner AE, Khan SA, et al. Mechanisms of Estrogen Receptor Antagonism toward P53 and Its Implications in Breast Cancer Therapeutic Response and Stem Cell Regulation. P Natl Acad Sci. 2010;107(34):15081–15086.

21. Mosmann T. Rapid Colorimetric Assay for Cellular Growth and Survival: Application to Proliferation and Cytotoxicity Assays. J Immunol Methods. 1983;65(1–2):55–63.

22. Silva G, Fachin A, Beleboni R, França S, Marins M. In Vitro Action of Flavonoids in the Canine Malignant Histiocytic Cell Line DH82. Molecules 2013;18(12):15448–15463.

23. Faraji F, Karjoo Z, Moghaddam MV, Heidari S, Emameh RZ, Falak R. Challenges related to the immunogenicity of parenteral recombinant proteins: Underlying mechanisms and new approaches to overcome it. Int Rev Immunol. 2018;37(6):301–315.

24. Gupta SC, Singh R, Pochampally R, Watabe K, Mo Y-Y. Acidosis Promotes Invasiveness of Breast Cancer Cells through ROS-AKT-NFκβ Pathway. Oncotarget. 2014;5(23).

25. Sonehara N, Lacerda J, Jardim-Perassi B, de Paula R, Moschetta-Pinheiro M, Souza Y, de Andrade J, Zuccari D. Melatonin Regulates Tumor Aggressiveness under Acidosis Condition in Breast Cancer Cell Lines. Oncol Lett. 2018;17:1635–1645.

26. Seba V, Silva G, Santos M, Baek S, França S, Fachin A, Regasini L, Marins M. Chalcone Derivatives 4′-Amino-1-Naphthyl-Chalcone (D14) and 4′-Amino-4-Methyl-1-Naphthyl-Chalcone (D15) Suppress Migration and Invasion of Osteosarcoma Cells Mediated by P53 Regulating EMT-Related Genes. Int J Mol Sci. 2018;19(9):2838.

27. Thompson HW, Mera R, Prasad C. The Analysis of Variance (ANOVA). Nutr Neurosci. 1999;2(1):43–55.

28. Ullah A, Ansari FL, Ihsan-ul-Haq, Nazir S, Mirza B. Combinatorial Synthesis, Lead Identification, and Antitumor Study of a Chalcone-Based Positional-Scanning Library. Chem Biodivers. 2007;4(2):203–214.

29. Jain U, Bhatia R, Rao A, Singh R, Saxena A, Sehar I. Design and Development of Halogenated Chalcone Derivatives as Potential Anticancer Agents. Tropical J Pharm Res. 2014;13(1):73.

30. Singh RK, Lange TS, Kim KK, Singh AP, Vorsa N, Brard L. Isothiocyanate NB7M causes selective cytotoxicity, pro-apoptotic signalling and cell-cycle regression in ovarian cancer cells. Brit J Cancer. 2008;99(11):1823–1831.

31. Brown N. Bioisosteres and Scaffold Hopping in Medicinal Chemistry. Mol Inform. 2014;33(6–7):458–462.

32. Hashim AI, Zhang X, Wojtkowiak JW, Martinez GV, Gillies RJ. Imaging PH and Metastasis. NMR Biomed. 2011;24(6):582–591.

33. Gatenby RA, Smallbone K, Maini PK, Rose F, Averill J, Nagle RB, Worrall L, Gillies RJ. Cellular Adaptations to Hypoxia and Acidosis during Somatic Evolution of Breast Cancer. Brit J Cancer. 2007;97(5):646–653.

34. Wojtkowiak JW, Verduzco D, Schramm KJ, Gillies RJ. Drug Resistance and Cellular Adaptation to Tumor Acidic PH Microenvironment. Mol Pharm. 2011;8(6):2032–2038.

35. Galluzzi L, Vitale I, Aaronson SA, Abrams JM, Adam D, Agostinis P, Alnemri ES, Altucci L, Amelio I, Andrews DW, et al. Molecular Mechanisms of Cell Death: Recommendations of the Nomenclature Committee on Cell Death 2018. Cell Death Differ. 2018;25(3):486–541.

36. Ramirez-Tagle R, Escobar C, Romero V, Montorfano I, Armisén R, Borgna V, Jeldes E, Pizarro L, Simon F, Echeverria C. Chalcone-Induced Apoptosis through Caspase-Dependent Intrinsic Pathways in Human Hepatocellular Carcinoma Cells. Int J Mol Sci. 2016;17(2):260.

37. Zhang S, Li T, Zhang L, Wang X, Dong H, Li L, Fu D, Li Y, Zi X, Liu H-M, et al. A Novel Chalcone Derivative S17 Induces Apoptosis through ROS Dependent DR5 Up-Regulation in Gastric Cancer Cells. Sci Rep-UK. 2017;7(1).

38. Hsu YL, Kuo PL, Tzeng WS, Lin CC. Chalcone inhibits the proliferation of human breast cancer cell by blocking cell cycle progression and inducing apoptosis. Food and Chemical Toxicology. 2006;44(5):704–713.

39. Bortolotto LFB, Barbosa FR, Silva G, Bitencourt TA, Beleboni RO, Baek SJ, Marins M, Fachin AL. Cytotoxicity of trans-chalcone and licochalcone A against breast cancer cells is due to apoptosis induction and cell cycle arrest. Biomedicine & Pharmacotherapy. 2017;85:425–433. doi:10.1016/j.biopha.2016.11.047

40. Muller PAJ, Vousden KH. Mutant P53 in Cancer: New Functions and Therapeutic Opportunities. Cancer Cell. 2014;25(3):304–317.

41. Wang XB, Peng W, Yi Z, Zhu S, Ghan Q. Expression and Prognostic Value of Transcriptional Factor Sp1 in Breast Cancer. Chin J Cancer. 2007;26(6):996–1000.

42. Vizcaíno C, Mansilla S, Portugal, J. Sp1 Transcription Factor: A Long-Standing Target in Cancer Chemotherapy. Pharmacol Therapeut. 2015;152:111–124.

43. Beishline K, Azizkhan-Clifford J. Sp1 and the 'Hallmarks of Cancer.' FEBS J. 2015;282(2):224–258.

44. Moll UM, Wolff S, Speidel D, Deppert W. Transcription-Independent pro-Apoptotic Functions of P53. Curr Opin Cell Biol. 2005;17(6):631–636.

45. Bailey ST, Shin H, Westerling T, Liu XS, Brown M. Estrogen Receptor Prevents P53-Dependent Apoptosis in Breast Cancer. P Natl Acad Sci. 2012;109(44):18060–18065.

46. Sayeed A, Konduri SD, Liu W, Bansal S, Li F, Das GM. Estrogen Receptor Inhibits P53-Mediated Transcriptional Repression: Implications for the Regulation of Apoptosis. Cancer Res. 2007;67(16):7746–7755.

47. Zhang Y, Srinivasan B, Xing C, Lu J. A New Chalcone Derivative (E)-3-(4-Methoxyphenyl)-2-Methyl- 1-(3,4,5-Trimethoxyphenyl)Prop-2-En-1-One Suppresses Prostate Cancer Involving P53-Mediated Cell Cycle Arrests and Apoptosis. Anticancer Res. 2012;32:3689–3698.

Scheme 1. Claisen-Schmidt reaction for synthesis of chalcones **1–20**

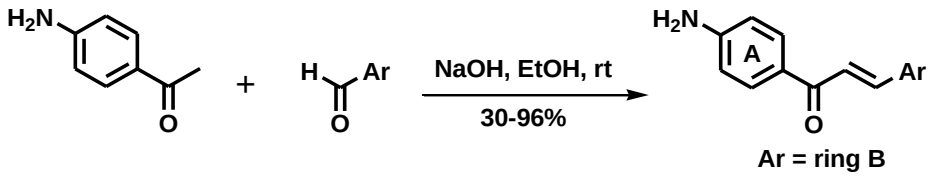

Figure 1. Percentage of metabolically viable cells (%MVC) under acidosis. a) treatments with selected chalcones **11** and **17** against MCF-7 line; b) treatments with selected chalcones **11** and **17** against MDA-MB-231 line. Different letters in the graph indicate statistical difference with significance $p < 0.05$ in Tukey's multiple comparisons test. DMSO 0.1% was used as a vehicle control.

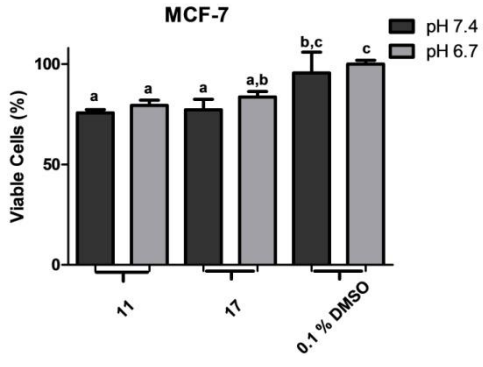

(a)

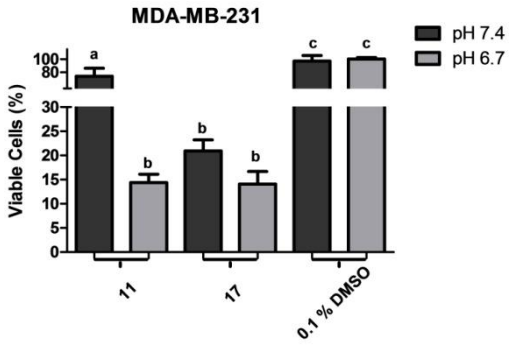

(**b**)

Figure 2. Pro-apoptotic activity of selected chalcones **11** and **17** toward MCF-7 (a) and MDA-MB-231 (b) cells. Different letters indicate statistical difference with significance $p < 0.05$ in Tukey's multiple comparisons test. DMSO 0.1% was used as a vehicle control.

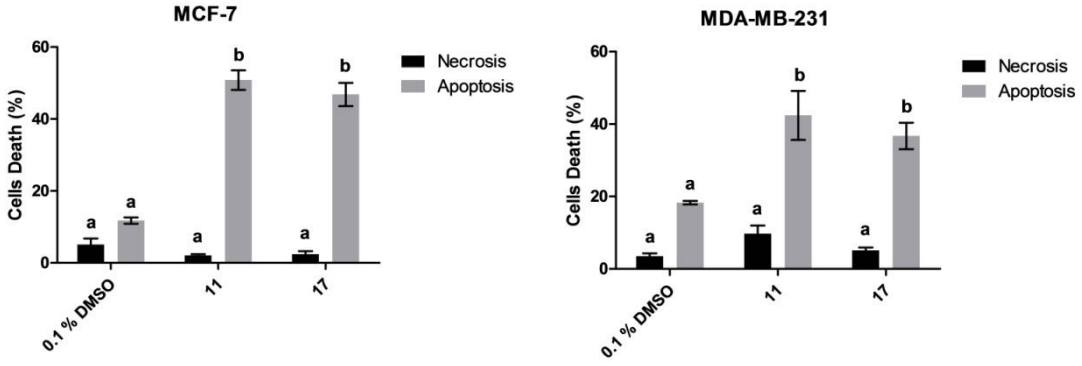

(**a**) (**b**)

Figure 3. Effect of selected chalcones **11** and **17** on Sp1 and p53 proteins expression in MCF-7 cell line

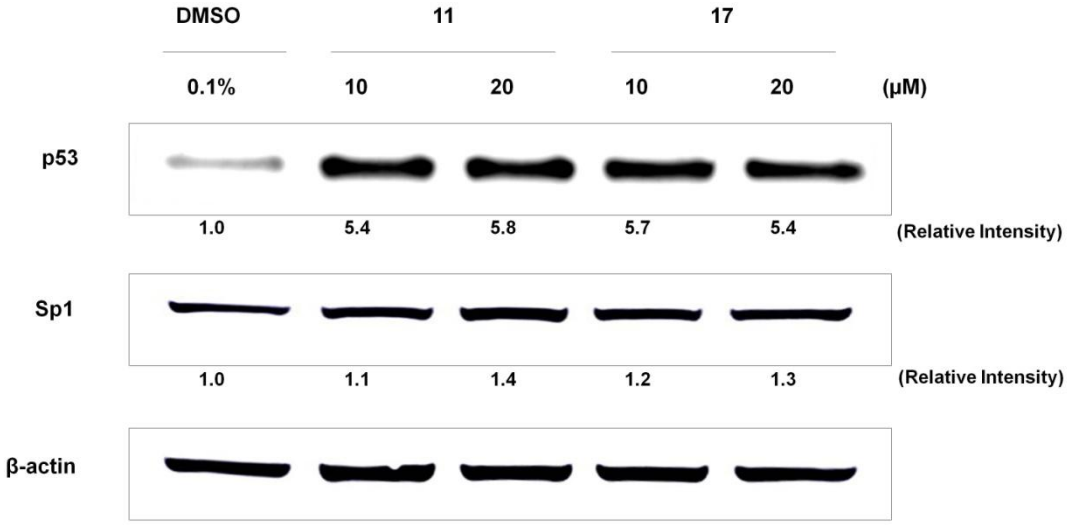

Table 1. Percentage of metabolically viable cells (%MVC) treated with chalcones **1**–**20** (at 20 μmol L^{-1}) and IC_{50} values (in μmol L^{-1}) of selected chalcones

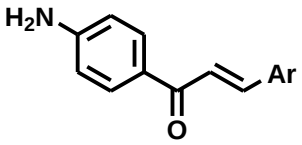

Cpd.	Ar	MCF-7 (ER)		MDA-MB-231 (TNBC)	
		%MVC	IC_{50}	%MVC	IC_{50}
1	phenyl	97.3 ± 6.0	>100	82.6 ± 4.0	60.3 ± 2.9 [c]
2	4-nitrophenyl	97.3 ± 4.9	nd	104.1 ± 3.8	nd
3	4-trifluoromethylphenyl	98.3 ± 6.6	nd	100.7 ± 6.7	nd
4	4-cyanophenyl	98.2 ± 2.1	nd	99.7 ± 6.3	nd
5	4-fluorophenyl	93.3 ± 5.7	nd	92.8 ± 4.6	nd
6	4-chlorophenyl	74.6 ± 5.2	>100	81.4 ± 7.3	69.0 ± 8.5 [c]
7	4-bromophenyl	70.1 ± 1.5	nd	97.1 ± 5.5	nd
8	3-fluorophenyl	72.8 ± 5.1	>100	73.3 ± 5.4	74.1 ± 1.2 [c]
9	3-chlorophenyl	52.5 ± 6.7	34.2 ± 6.4[a]	97.7 ± 4.8	>100
10	3-bromophenyl	68.3 ± 4.8	nd	100.1 ± 4.4	nd
11	2-fluorophenyl	50.3 ± 7.8	13.2 ± 3.5[a,b]	84.6 ± 3.2	34.7 ± 5.2 [d]
12	2-chlorophenyl	69.0 ± 6.4	nd	88.7 ± 3.6	nd
13	4-methylphenyl	88.7 ± 4.2	nd	100.2 ± 5.3	nd
14	4-methoxyphenyl	87.9 ± 7.5	nd	95.9 ± 6.4	nd
15	2-furyl	104.5 ± 3.6	nd	100.1 ± 7.1	nd
16	2-thiophenyl	99.4 ± 5.7	nd	95.6 ± 5.3	nd
17	3-pyridyl	51.8 ± 2.5	15.7 ± 5.9[a,b]	75.7 ± 6.3	33.9 ± 7.1 [d]
18	4-pyridyl	61.3 ± 3.4	nd	108.7 ± 2.4	nd
19	1-naphthyl	53.4 ± 4.3	14.3 ± 2.9[a,b]	88.9 ± 1.7	>100
20	1,4-biphenyl	44.2 ± 3.3	22.7 ± 6.0[a,b]	95.9 ± 11.2	>100
dox	–	nd	0.61 ± 0.2 [b]	nd	1.03 ± 0.3 [e]

[a–e] Different letters indicate different values with statistical significance $p < 0.05$ in Tukey's multiple comparisons test. dox = doxorubicin (reference antineoplastic drug). nd - not determined. Cpd = compound.

Supplemental Data

Antiproliferative activity and p53 upregulation effects of chalcones on human breast cancer cells

Mariana Bastos dos Santos[1], Daiane Bertholin Anselmo[1], Jéssica Gisleine de Oliveira[2], Bruna V. Jardim-Perassi[2], Diego Alves Monteiro[3], Gabriel Silva[4], Eleni Gomes[3], Ana Lúcia Fachin[4], Mozart Marins[4], Débora Aparecida Pires de Campos Zuccari[2], Luis Octavio Regasini[1,*].

[1]Department of Chemistry and Environmental Sciences, Institute of Biosciences, Humanities and Exact Sciences (IBILCE), São Paulo State University (UNESP), 15054-000, São José do Rio Preto, São Paulo, Brazil.

[2]Department of Molecular Biology, Medicine College of São José do Rio Preto (FAMERP), 15090-000, São José do Rio Preto, São Paulo, Brazil.

[3]Department of Biology, Institute of Biosciences, Humanities and Exact Sciences (IBILCE), São Paulo State University (UNESP), 15054-000, São José do Rio Preto, São Paulo, Brazil.

[4]Biotechnology Unit, University of Ribeirão Preto (UNAERP), 14096-900, Ribeirão Preto, São Paulo, Brazil.

***Correspondence**: *luis.regasini@unesp.br (L.O.R.), Tel. +55-17-3221-2362.

1. SPECTROSCOPY DATA ANALYSES

1.1. (*E*)-4'-aminochalcone (1)

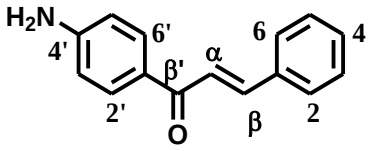

Yellow solid.

Purity: 99.3 %

UV-Vis: λ_{max} 306 and 364 nm.

Melting point, ^{1}H and ^{13}C NMR were represented in the supplementary materials of our previous work [1], and ^{1}H and ^{13}C NMR values were compared to other descriptions [2,3].

1.2. (*E*)-4-nitro-4'-aminochalcone (2)

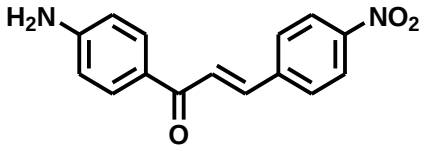

Orange solid.

Purity: 97.4 %

UV-Vis: λ_{max} 310 and 381 nm

Melting point, ^{1}H and ^{13}C NMR were represented in the supplementary materials of our previous work [1], and ^{1}H and ^{13}C NMR values were compared to other descriptions [2-4].

1.3. (*E*)-4-trifluoromethyl-4'-aminochalcone (3)

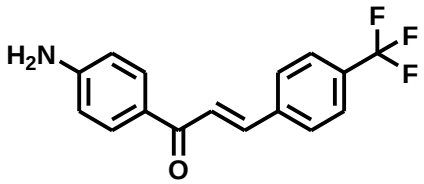

Yellow solid.

Yield: 96 %

Purity: 99.1 %

Melting Point: 129–130 °C

UV-Vis: λ_{max} 294 and 370 nm

^{1}H NMR (600 MHz, DMSO-d_6) δ_H: 8.07 (d, *J* = 8.3 Hz, H-3 and H-5), 8.01 (d, *J* = 15.6 Hz, H-β), 7.95 (d, *J* = 8.7 Hz, H-2' and H-6'), 7.79 (d, *J* = 8.3 Hz, H-2 and H-6), 7.66 (d, *J*

= 15.6 Hz, H-α), 6.63 (d, *J* = 8.7 Hz, H-3' and H-5'), 6.23 (br s, 4'-N$\underline{H}_2$). **^{13}C NMR (150 MHz, DMSO-d_6) δ_C:** 186.0 (C-β'), 154.6 (C-4'), 139.9 (C-β), 139.7 (C-1), 131.8 (C-2' and C-6'), 130.0 ($J_{C,F}$ = 31.7 Hz, C-4) 129.5 (C-2 and C-6), 127.9 (C-1'), 126.1 (d, $J_{C,F}$ = 3.4 Hz, C-3 and C-5), 125.7 (C-α),124.6 ($J_{C,F}$ = 271.9 Hz, 4-CF_3) 113.2 (C-3' and C-5'). These ^{1}H and ^{13}C NMR values were compared to other descriptions [5].

1.4. (*E*)-4-cyano-4'-aminochalcone (4)

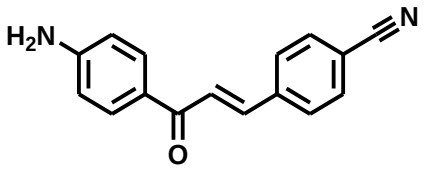

Yellow solid.

Yield: 95 %

Purity: 94.5 %

Melting Point: 202–204 °C

UV-Vis: λ_{max} 298 and 376 nm

^{1}H NMR (600 MHz, DMSO-d_6) δ_H: 8.05 (d, *J* = 8.7 Hz, H-2' and H-6'), 8.03 (d. *J* = 15,8 Hz, H-β), 7.95 (d, *J* = 8.6 Hz, H-3 and H-5), 7.91 (d, *J* = 8.6 Hz, H-2 and H-6), 7.64 (d, *J* = 15.8 Hz, H-α), 6.63 (d, *J* = 8.7 Hz, H-3' and H-5'), 6.24 (br s, 4'-N$\underline{H}_2$). **^{13}C NMR (150 MHz, DMSO-d_6) δ_C:** 186.0 (C-β'), 154.7 (C-4'), 140.3 (C-β), 139.7 (C-1), 133.1 (C-3 and C-5), 131.9 (C-2' and C-6'), 129.6 (C-2 and C-6), 126.3 (C-1'), 125.5 (C-α), 119.2 (4-CN), 113.2 (C-3' and C-5'), 112.2 (C-4). These ^{1}H and ^{13}C NMR values were compared to other descriptions [6,7].

1.5. (*E*)-4-fluoro-4'-aminochalcone (5)

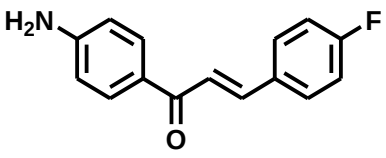

Yellow solid.

Purity: 94.1 %

UV-Vis: λ_{max} 310 and 363 nm

Melting point, ^{1}H and ^{13}C NMR were represented in the supplementary materials of our previous work [1], and ^{1}H and ^{13}C NMR values were compared to other descriptions [8].

1.6. (*E*)-4-chloro-4'-aminochalcone (6)

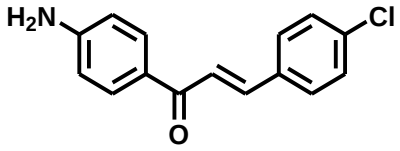

Yellow solid.

Purity: 97.9 %

UV-Vis: λ_{max} 310 and 367 nm

Melting point, ^{1}H and ^{13}C NMR were represented in the supplementary materials of our previous work [1], and ^{1}H and ^{13}C NMR values were compared to other descriptions [2,4,8,9].

1.7. (*E*)-4-bromo-4'-aminochalcone (7)

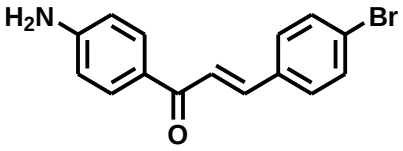

Yellow solid.

Yield: 75 %

Purity: 99.1 %

Melting Point: 149–150 °C

UV-Vis: λ_{max} 312 and 366 nm

^{1}H NMR (600 MHz, DMSO-d_6) δ_H: 7.93 (d, *J* = 8.8 Hz, H-2' and H-6'), 7.91 (d, *J* = 15.6 Hz, H-β), 7.81 (d, *J* = 8.5 Hz, H-2 and H-6), 7.64 (d, *J* = 8.5 Hz, H-3 and H-5), 7.58 (d, *J* = 15.6 Hz, H-α), 6.62 (d, *J* = 8.8 Hz, H-3' and H-5'), 6.18 (br s, 4'-N<u>H₂</u>). **^{13}C NMR (150 MHz, DMSO-d_6) δ_C:** 186.1 (C-β'), 154.5 (C-4'), 140.5 (C-β), 135.0 (C-1), 132.2 (C-3 and C-5), 131.7 (C-2' and C-6'), 130.9 (C-2 and C-6), 125.7 (C-1'), 123.7 (C-α), 113.2 (C-3' and C-5'). These ^{1}H and ^{13}C NMR values were compared to other descriptions [10].

1.8. (*E*)-3-fluoro-4'-aminochalcone (8)[8,11]

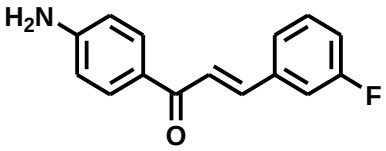

Yellow solid.

Yield: 30 %

Purity: 99.3 %

Melting Point: 126–127 °C

UV-Vis: λ_{max} 297 and 367 nm

^{1}H NMR (600 MHz, DMSO-d_6) δ_H: 7.96 (d, *J* = 8.7 Hz, H-2' and H-6'), 7.94 (d, *J* = 15.6 Hz, H-β), 7.81 (dd, *J* = 8.0 and 2.1 Hz, H-5), 7.65 (d, *J* = 8.0 Hz, H-6), 7.61 (d, *J* = 15.6 Hz, H-α), 7.48 (ddd, *J* = 8.0, 6.2 and 1.8 Hz, H-4), 7.25 (ddd, *J* = 8.4, 2.6 and 1.8 Hz, H-2), 6.63 (d, *J* = 8.8 Hz, H-3' and H-5'), 6.20 (br s, 4'-N$\underline{H_2}$). **^{13}C NMR (150 MHz, DMSO-d_6) δ_C:** 186.1 (C-β'), 163.0 (C-3, d, $J_{C,F}$ = 243.6), 154.5 (C-4'), 140.4 (C-β), 138.2 (C-1, d, $J_{C,F}$ = 8.0 Hz), 131.7 (C-2' and C-6'), 131.2 (C-5, d, *J* = 8.5 Hz), 125.7 (C-1'), 125.6 (C-6), 124.4 (C-α), 117.1 (C-4, d, $J_{C,F}$ = 21.5 Hz), 114.8 (C-2, d, $J_{C,F}$ = 21.9 Hz), 113.2 (C-3' and C-5'). These ^{1}H and ^{13}C NMR values were compared to other descriptions [8,11].

1.9. (*E*)-3-chloro-4'-aminochalcone (9)

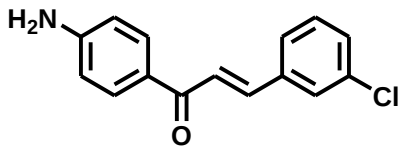

Yellow solid.

Yield: 44 %

Purity: 92.2 %

Melting Point: 140–141 °C

UV-Vis: λ_{max} 297 and 368 nm

^{1}H NMR (600 MHz, DMSO-d_6) δ_H: 8.03 (s, H-2), 7.96 (d, *J* = 8.7 Hz, H-2' and H-6'), 7.96 (d, *J* = 15.6 Hz, H-β), 7.80 – 7.73 (m, H-5), 7.59 (d, *J* = 15.6 Hz, H-α), 7.47 – 7.46 (m, H-4 and H-6), 6.63 (d, *J* = 8.7 Hz, H-3' and H-5'), 6.20 (br s, 4'-N$\underline{H_2}$). **^{13}C NMR (150 MHz, DMSO-d_6) δ_C:** 186.1 (C-β'), 154.5 (C-4'), 140.2 (C-β), 137.9 (C-1), 134.2 (C-3), 131.8 (C-2' and C-6'), 131.1 (C-5), 130.0 (C-4), 128.1 (C-1'), 128.0 (C-2), 125.6 (C-6), 124.5 (C-α), 113.2 (C-3' and C-5'). These ^{1}H and ^{13}C NMR values were compared to other descriptions [4,8].

1.10. (*E*)-3-bromo-4'-aminochalcone (10)

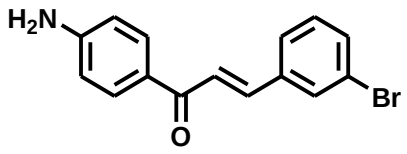

Yellow solid.

Yield: 76 %

Purity: 95.1 %

Melting Point: 165–166 °C

UV-Vis: λ_{max} 297 and 368 nm

^{1}H NMR (600 MHz, DMSO-*d*$_6$) δ_H: 8.17 (s, H-2), 7.96 (d, *J* = 8.5 Hz, H-2' and H-6'), 7.96 (d, *J* = 15.9 Hz, H-β), 7.81 (d, *J* = 7.8 Hz, H-6), 7.60 (d, *J* = 8.6 Hz, H-4), 7.57 (d, *J* = 15.9 Hz, H-α), 7.39 (dd, *J* = 8.6 and 7.8 Hz, H-5), 6.63 (d, *J* = 8.5 Hz, H-3' and H-5'), 6.20 (br s, 4'-N$\underline{H_2}$). **^{13}C NMR (150 MHz, DMSO-*d*$_6$) δ_C:** 186.1 (C-β'), 154.5 (C-4'), 140.1 (C-β), 138.2 (C-1), 132.9 (C-4), 131.8 (C-2' and C-6'), 131.3 (C-5), 130.9 (C-2), 128.4 (C-1'), 125.6 (C-6), 124.5 (C-3), 122.8 (C-α), 113.2 (C-3' and C-5'). These ^{1}H and ^{13}C NMR values were compared to other descriptions [12].

1.11. (*E*)-2-fluoro-4'-aminochalcone (11)

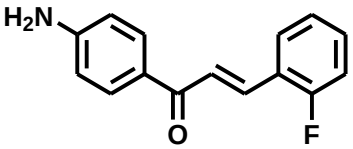

Yellow solid.

Yield: 39 %

Purity: 97.6 %

Melting Point: 116–117 °C

UV-Vis: λ_{max} 298 and 366 nm

^{1}H NMR (600 MHz, DMSO-*d*$_6$) δ_H: 8.08 (dd, *J* = 7.7 and 1.3 Hz, H-6), 7.92 (d, *J* = 8.7 Hz, H-2' and H-6'), 7.92 (d, *J* = 15.7 Hz, H-β), 7.73 (d, *J* = 15.7 Hz, H-α), 7.52 – 7.44 (m, H-4), 7.33 – 7.39 (m, H-3 and H-5), 6.63 (d, *J* = 8.7 Hz, H-3' and H-5'), 6.22 (br s, 4'-NH_2). **^{13}C NMR (150 MHz, DMSO-*d*$_6$) δ_C:** 186.0 (C-β'), 161.2 (C-2, d, *J* = 250.6 Hz), 154.6 (C-4'), 133.0 (C-β), 132.4 (C-4, d, $J_{C,F}$ = 8.6 Hz), 131.7 (C-2' and C-6'), 129.3 (C-1'), 125.4 (C-1, d, $J_{C,F}$ = 16.2 Hz), 125.3 (C-α) 125.0 (C-5), 123.2 (C-6, d, $J_{C,F}$ = 11.4 Hz), 116.5 (C-3, d, $J_{C,F}$ = 21.8 Hz), 113.2 (C-3' and C-5'). These ^{1}H and ^{13}C NMR values were compared to other descriptions [8,11].

1.12. (*E*)-2-chloro-4'-aminochalcone (12)

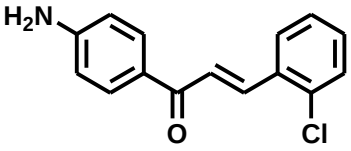

Yellow solid.

Yield: 43 %

Purity: 92.5 %

Melting Point: 135–136 °C

UV-Vis: λ_{max} 297 and 368 nm

^{1}H NMR (600 MHz, DMSO-d_6) δ: 8.18 (dd, *J* = 7.1 and 2.3 Hz, H-6), 7.95 (d, *J* = 8.6 Hz, H-2' and H-6'), 7.94 (d, *J* = 15.2 Hz, H-β), 7.94 (dd, *J* = 9.7 and 7,1 Hz. H-5), 7.57 – 7.54 (m, H-4), 7.44 (dd, *J* = 6.6 and 3.1 Hz, H-3), 7.43 (d, *J* = 15.2 Hz, H-α), 6.64 (d, *J* = 8.6 Hz, H-3' and H-5'), 6.23 (br s, 4'-N$\underline{H}_2$). **^{13}C NMR (150 MHz, DMSO-d_6) δ:** 185.9 (C-β'), 154.6 (C-4'), 136.5 (C-β), 134.5 (C-1), 133.3 (C-4), 131.8 (C-2' and C-6'), 131.8 (C-2), 130.4 (C-3), 128.8 (C-1'), 128.1 (C-6), 125.7 (C-α), 125.5 (C-5), 113.2 (C-3' and C-5'). These ^{1}H and ^{13}C NMR values were compared to other descriptions [4].

1.13. (*E*)-4-methyl-4'-aminochalcone (13)

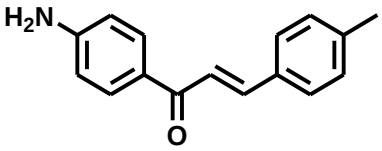

Light yellow solid.

Purity: 99.2 %

UV-Vis: λ_{max} 364 nm

Melting point, ^{1}H and ^{13}C NMR were represented in the supplementary materials of our previous work [1], and ^{1}H and ^{13}C NMR values were compared to other descriptions [2,8].

1.14. (*E*)-4-methoxy-4'-aminochalcone (14)

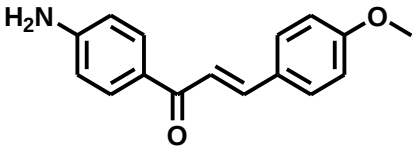

Light yellow solid.

Purity: 99.7 %

UV-Vis: λ_{max} 369 nm

Melting point, ^{1}H and ^{13}C NMR were represented in the supplementary materials of our previous work [1], and ^{1}H and ^{13}C NMR values were compared to other descriptions [3,8].

1.15. (*E*)-2-furyl-4'-aminochalcone (15)

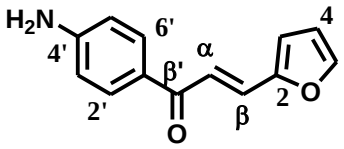

Orange solid.

Purity: 99.8 %

UV-Vis: λ_{max} 372 nm

Melting point, ^{1}H and ^{13}C NMR were represented in the supplementary materials of our previous work [1], and ^{1}H and ^{13}C NMR values were compared to other descriptions [8,13].

1.16. (*E*)-2-thiophenyl-4'-aminochalcone (16)

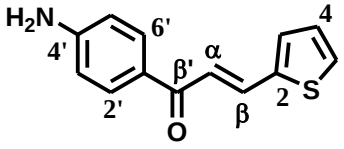

Yellow solid.

UV-Vis: λ_{max} 262 and 373 nm

Purity: 97.1 %

Melting point, ^{1}H and ^{13}C NMR were represented in the supplementary materials of our previous work [1], and ^{1}H and ^{13}C NMR values were compared to other descriptions [8].

1.17. (*E*)-3-pyridyl-4'-aminochalcone (17)

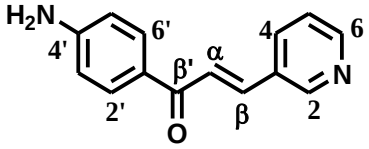

Light orange solid.

Yield: 63 %

Purity: 90.6 %

Melting Point: 179–180 °C

UV-Vis: λ_{max} 296 and 367 nm

^{1}H NMR (600 MHz, DMSO-d_6) δ_H: 8.98 (d, *J* = 1.3 Hz, H-6), 8.59 (dd, *J* = 1.2 and 4.0, H-2), 8.32 (d, *J* = 7.9 Hz, H-4), 8.02 (d, *J* = 15.7 Hz, H-β), 7.96 (d, *J* = 8.6 Hz, H-2' and H-6'), 7.64 (d, *J* = 15.7 Hz, H-α), 7.47 (dd, *J* = 7.8 and 7.8 Hz, H-5), 6.63 (d, *J* = 8.6 Hz, H-3' and H-5'), 6.21 (br s, 4'-N$\underline{H}_2$). **^{13}C NMR (150 MHz, DMSO-d_6) δ_C:** 186.0 (C-β'), 154.6 (C-4'), 150.9 (C-2), 150.5 (C-6), 138.4 (C-β), 135.2 (C-4), 131.8 (C-2' and C-6'), 131.4 (C-4), 125.5 (C-1'), 124.8 (C-α), 124.3 (C-5). 113.2 (C-3' and C-5'). These ^{1}H and ^{13}C NMR values were compared to other descriptions [8,14].

1.18. (*E*)-4-pyridyl-4'-aminochalcone (18)

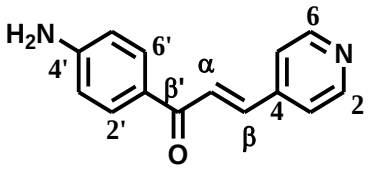

Yellow solid.

Yield: 65 %

Purity: 91.2 %

Melting Point: 166–167 °C

UV-Vis: λ_{max} 296 and 367 nm

^{1}H NMR (600 MHz, DMSO-d_6) δ_H: 8.64 (d, *J* = 6.0 Hz, H-6), 8.10 (d, *J* = 15.6 Hz, H-β), 7.95 (d, *J* = 8.7 Hz, H-2' and H-6'), 7.80 (d, *J* = 6.1 Hz, H-3), 7.56 (d, *J* = 15.6 Hz, H-α), 6.63 (d, *J* = 8.8 Hz, H-3' and H-5'), 6.27 (br s, 4'-N$\underline{H}_2$). **^{13}C NMR (150 MHz, DMSO-d_6) δ_C:** 185.9 (C-β'), 154.7 (C-4'), 150.7 (C-2 and C-6), 142.8 (C-β), 139.0 (C-4), 131.9 (C-2' and C-6'), 127.3 (C-α), 125.3 (C-1'), 122.8 (C-3 and C-5), 113.2 (C-3' and C-5'). These ^{1}H and ^{13}C NMR values were compared to other descriptions [8,14].

1.19. (*E*)-1-naphthyl-4'-aminochalcone (19)

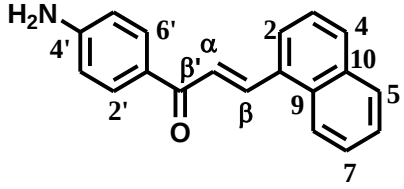

Yellow solid.

Purity: 99.9 %

UV-Vis: λ_{max} 378 nm

Melting point, ^{1}H and ^{13}C NMR were represented in the supplementary materials of our previous work [1], and ^{1}H and ^{13}C NMR values were compared to other descriptions [8,14].

1.20. (*E*)-4-pyridyl-4'-aminochalcone (20)

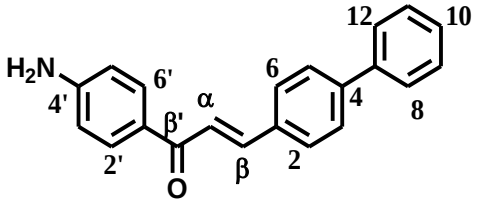

Light yellow solid.

Yield: 41 %

Purity: 99.0 %

Melting Point: 189–190 °C

UV-Vis: λ_{max} 369 nm

^{1}H NMR (600 MHz, DMSO-d_6) δ_H: 7.96 (d, *J* = 8.7 Hz, H-2' and H-6'), 7.94 (d, *J* = 8.0 Hz, H-3 and H-5), 7.93 (d, *J* = 15.5 Hz, H-β), 7.76 (d, *J* = 8.0 Hz, H-2 and H-6), 7.75 (dd, *J* = 8.0 and 1.1 Hz, H-8 and H-12), 7.67 (d, *J* = 15.5 Hz, H-α), 7.50 (dd, *J* = 7.7 and 7.4 Hz, H-9 and H-11), 7.41 (ddd, *J* = 7.4, 7.4 and 1.1 Hz, H-10), 6.63 (d, *J* = 8.7 Hz, H-3' and H-5'), 6.19 (br s, 4'-N$\underline{H}_2$). **^{13}C NMR (150 MHz, DMSO-d_6) δ_C:** 186.3 (C-β'), 154.4 (C-4'), 141.9 (C-β), 141.4 (C-7), 139.8 (C-4), 134.8 (C-1), 131.6 (C-2' and C-6'), 129.7 (C-9 and C-11), 129.5 (C-8 and C-12), 128.4 (C-1'), 127.5 (C-3 and C-5), 127.2 (C-2 and C-6), 125.8 (C-10), 122.9 (C-α), 113.2 (C-3' and C-5'). These ^{1}H and ^{13}C NMR values were compared to other descriptions [3].

Figure S.1. UV-vis spectrum of chalcone **1** from HPLC-DAD experiment

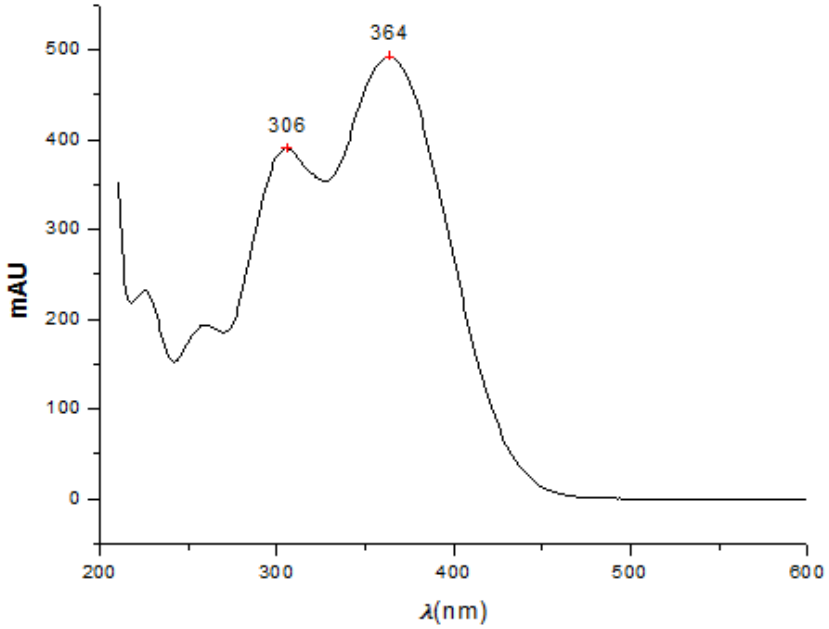

Figure S.2. HPLC-DAD chromatogram of chalcone **1**, MeOH:H_2O (3:1)

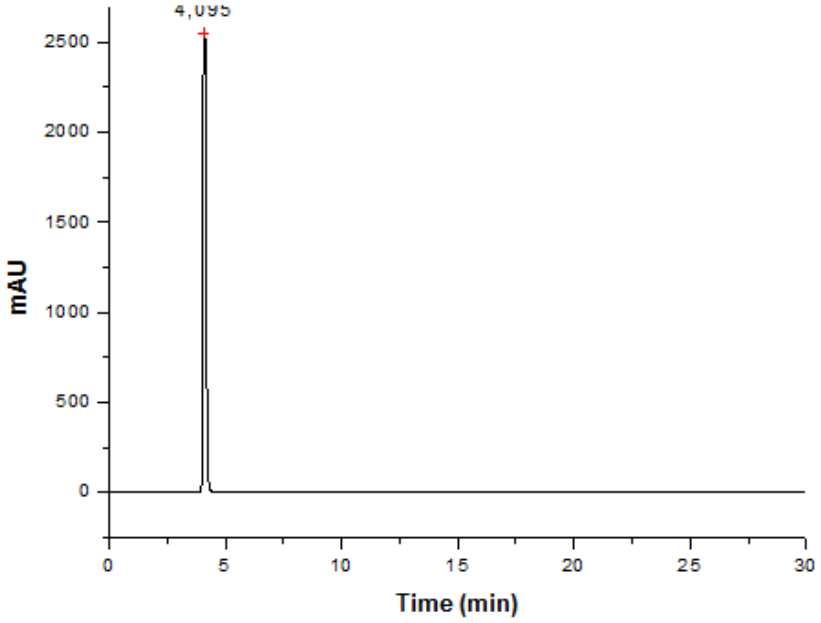

Figure S.3. UV-vis spectrum of chalcone **2** from HPLC-DAD experiment

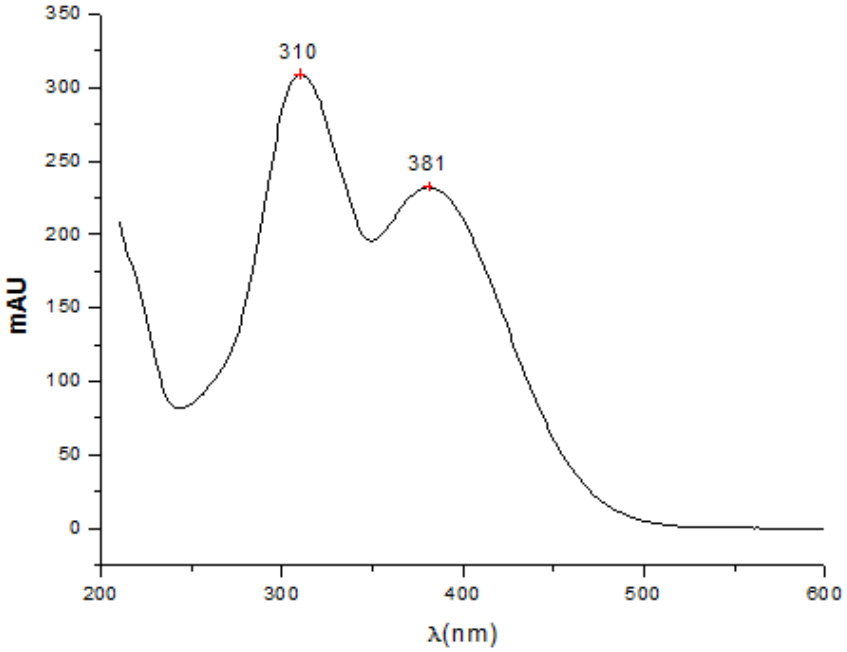

Figure S.4. HPLC-DAD chromatogram of chalcone **2**, MeOH:H_2O (3:1)

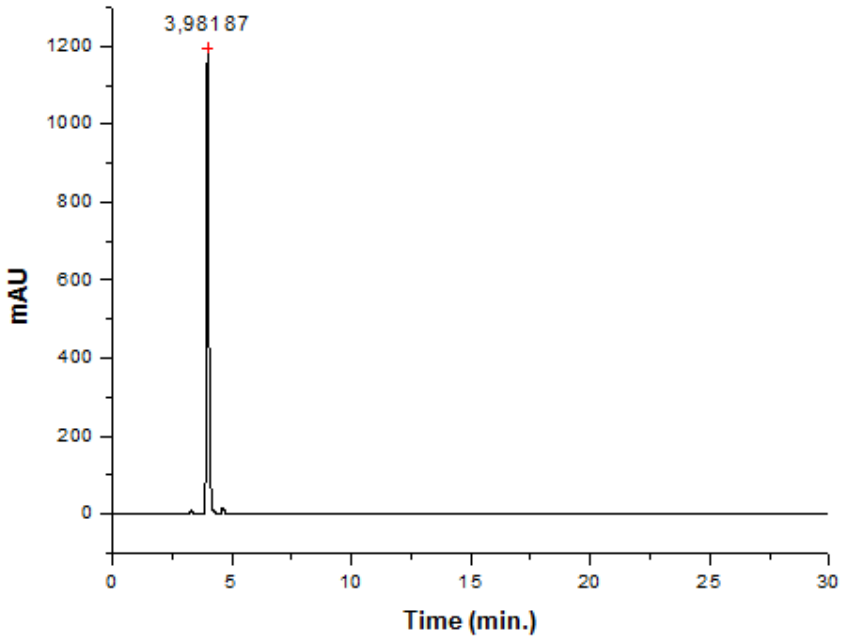

Figure S.5. ^{1}H NMR spectrum (DMSO-d_6, 600 MHz) of chalcone **3**

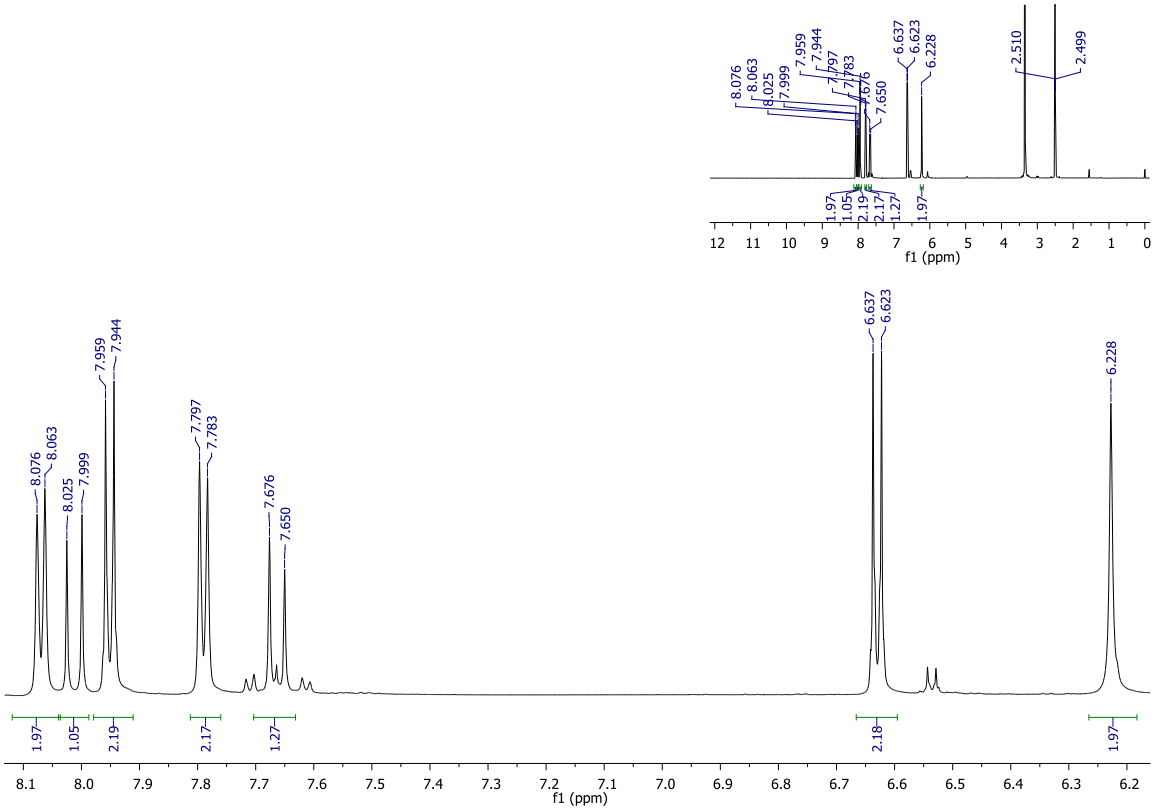

Figure S.6. ^{13}C NMR spectrum (DMSO-d_6, 150 MHz) of chalcone **3**

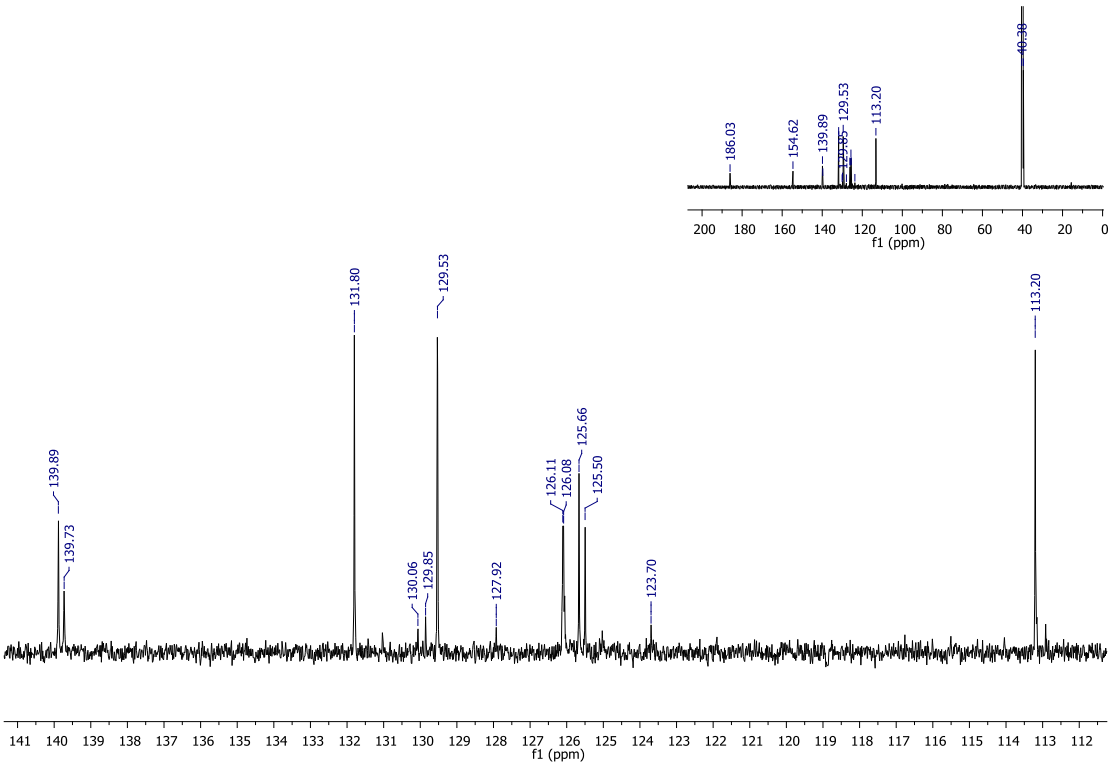

Figure S.7. UV-vis spectrum of chalcone **3** from HPLC-DAD experiment

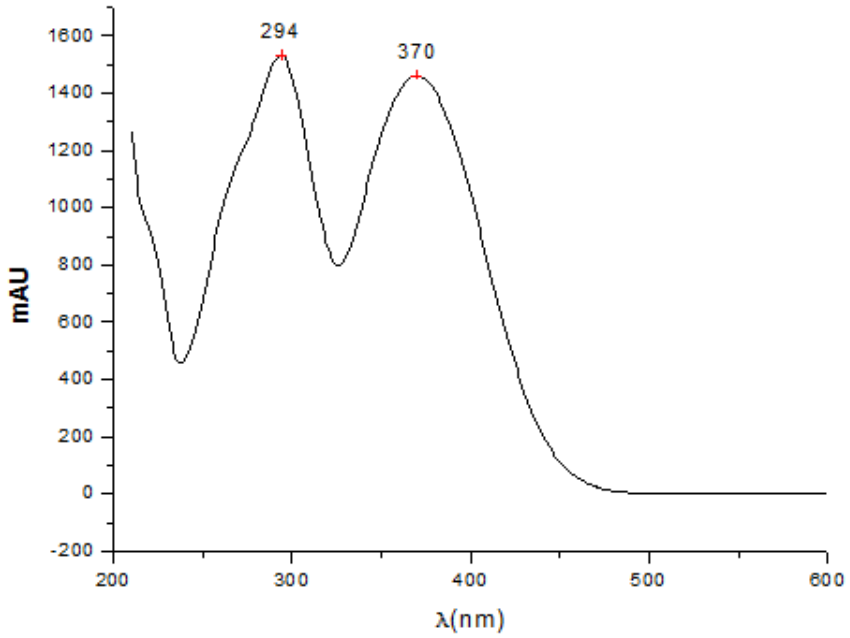

Figure S.8. HPLC-DAD chromatogram of chalcone **3**, MeOH:H_2O (3:1)

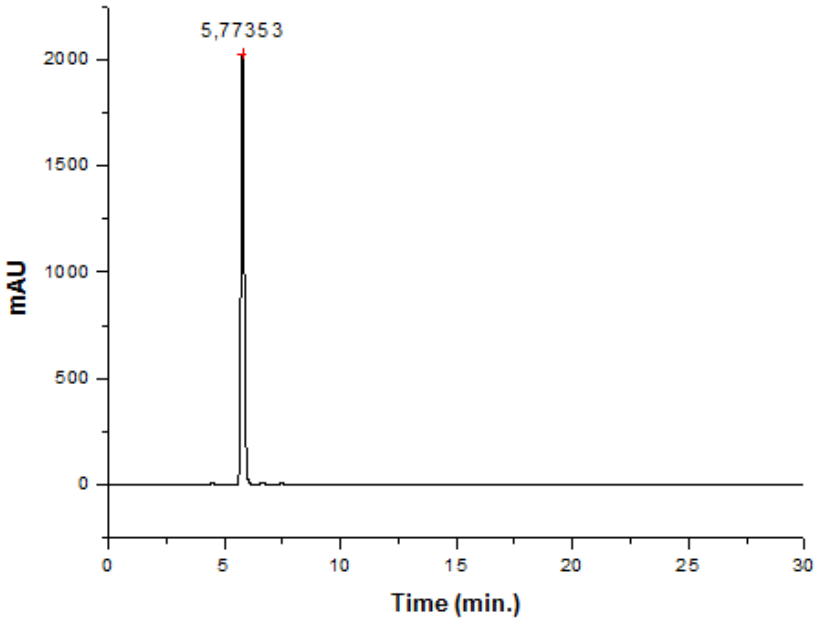

Figure S.9. ^{1}H NMR spectrum (DMSO-d_6, 600 MHz) of chalcone **4**

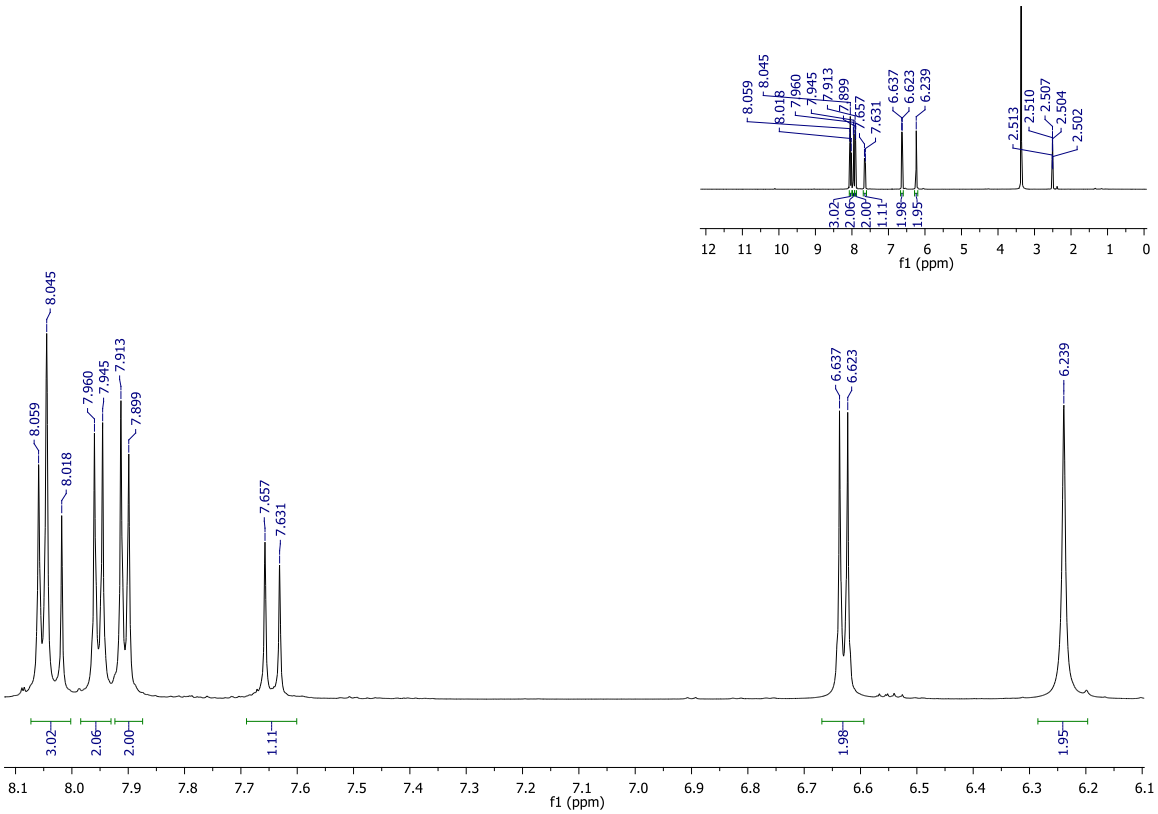

Figure S.10. ^{13}C NMR spectrum (DMSO-d_6, 150 MHz) of chalcone **4**

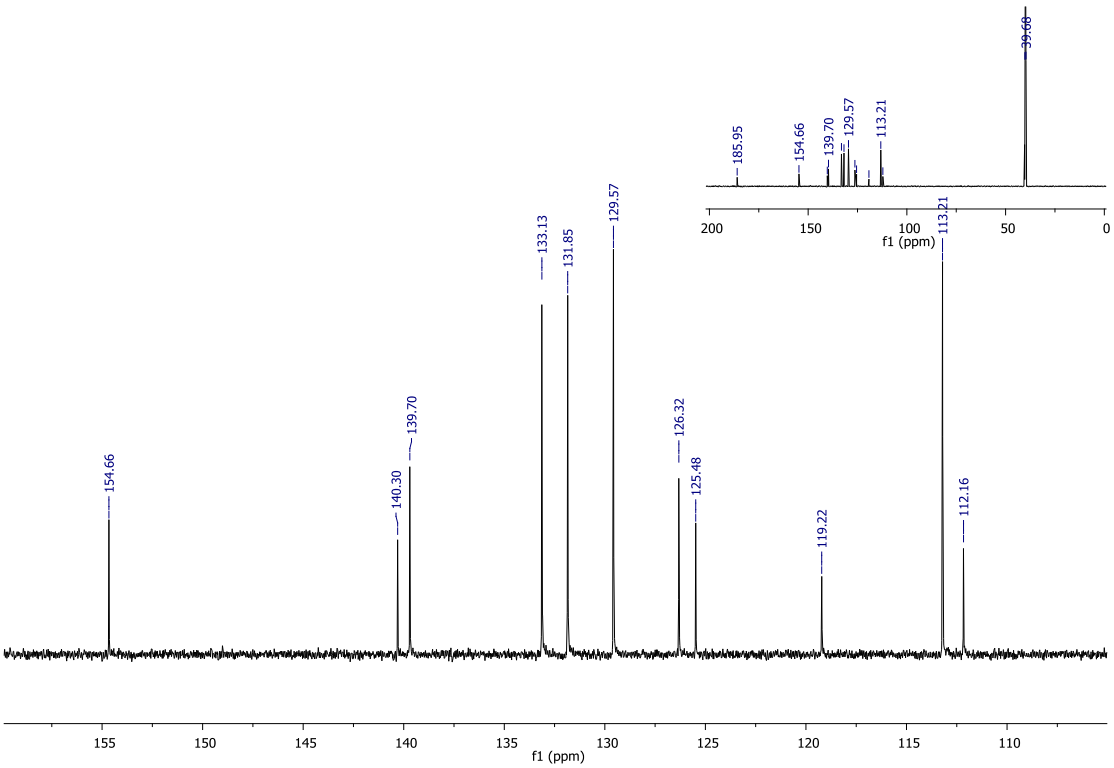

Figure S.11. UV-vis spectrum of chalcone **4** from HPLC-DAD experiment

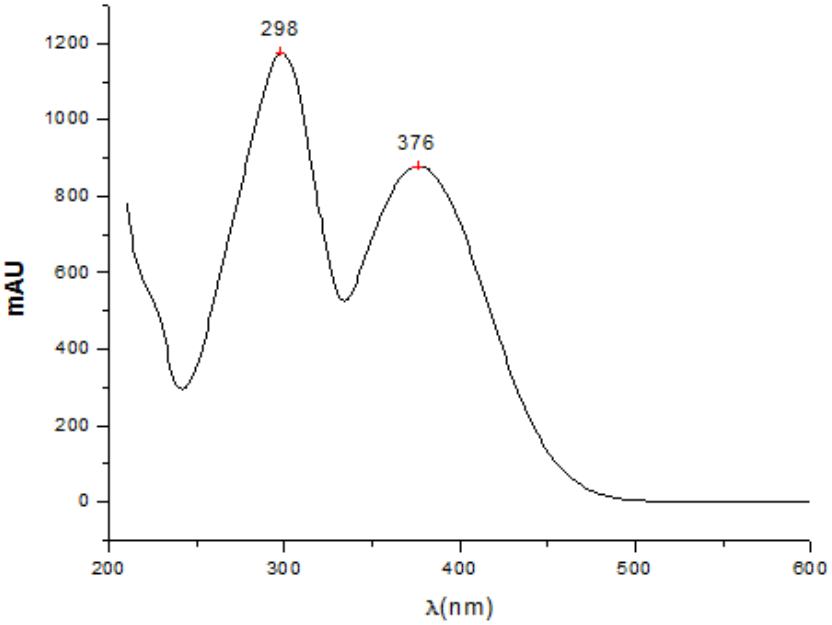

Figure S.12. HPLC-DAD spectrum of chalcone **4**, MeOH:H_2O (3:1)

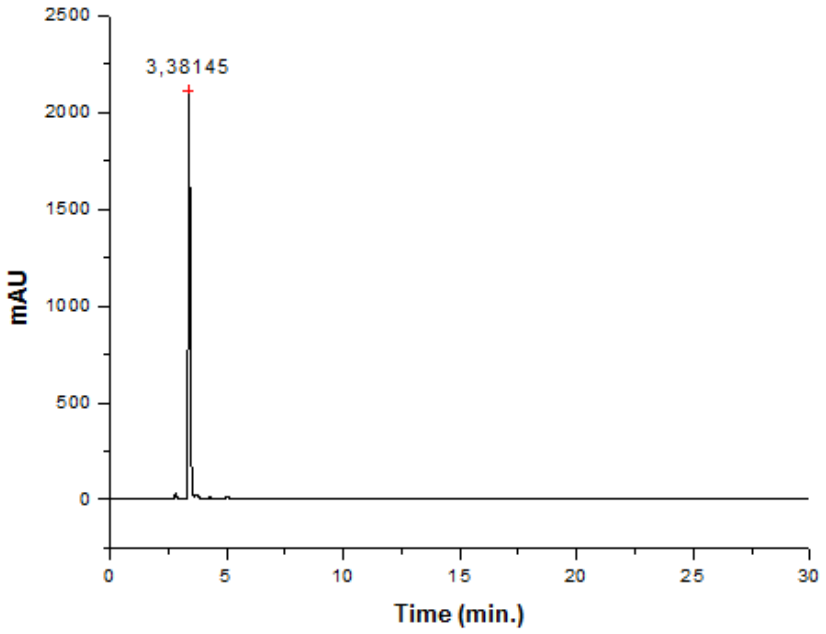

Figure S.13. UV-vis spectrum of chalcone **5** from HPLC-DAD experiment

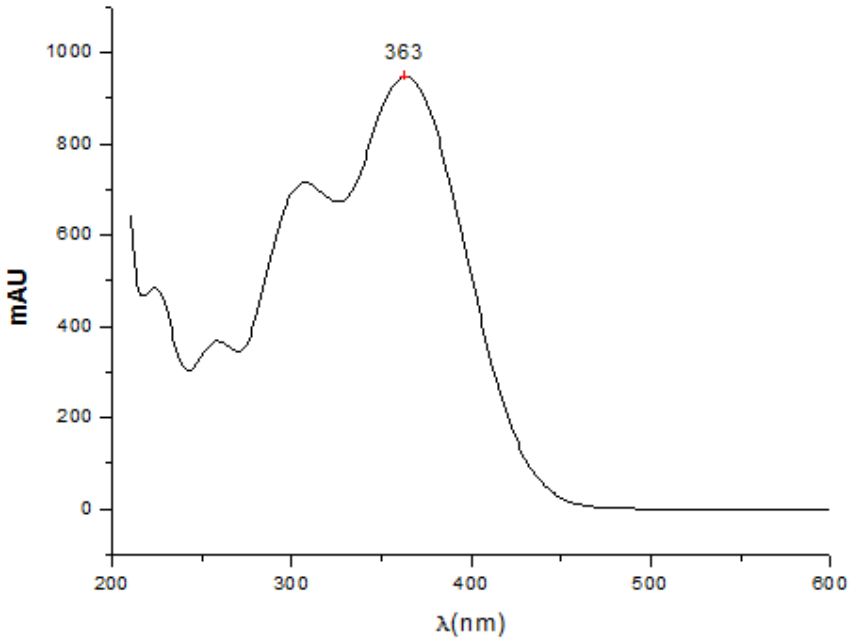

Figure S.14. HPLC-DAD chromatogram of chalcone **5**, MeOH:H_2O (3:1)

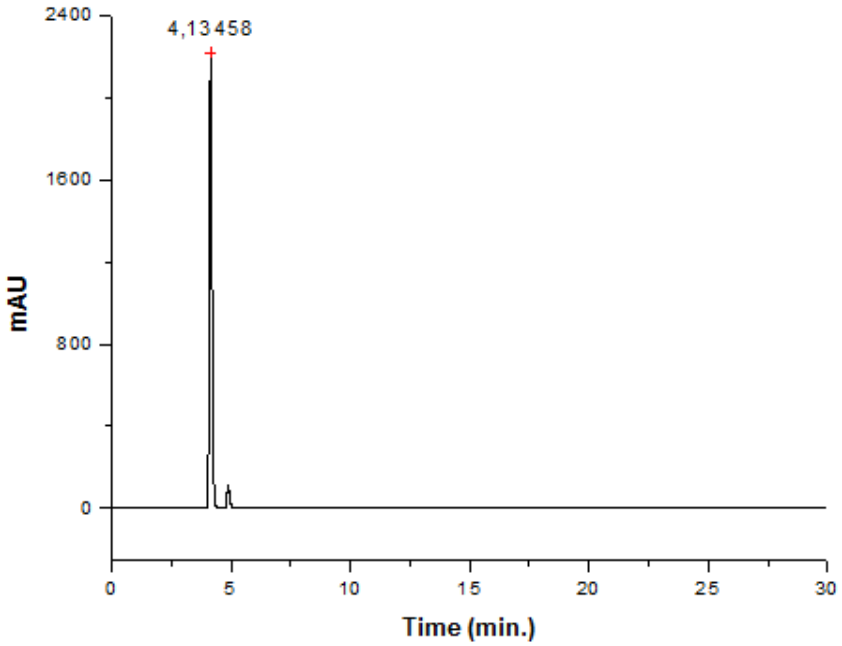

Figure S.15. UV-vis spectrum of chalcone **6** from HPLC-DAD experiment

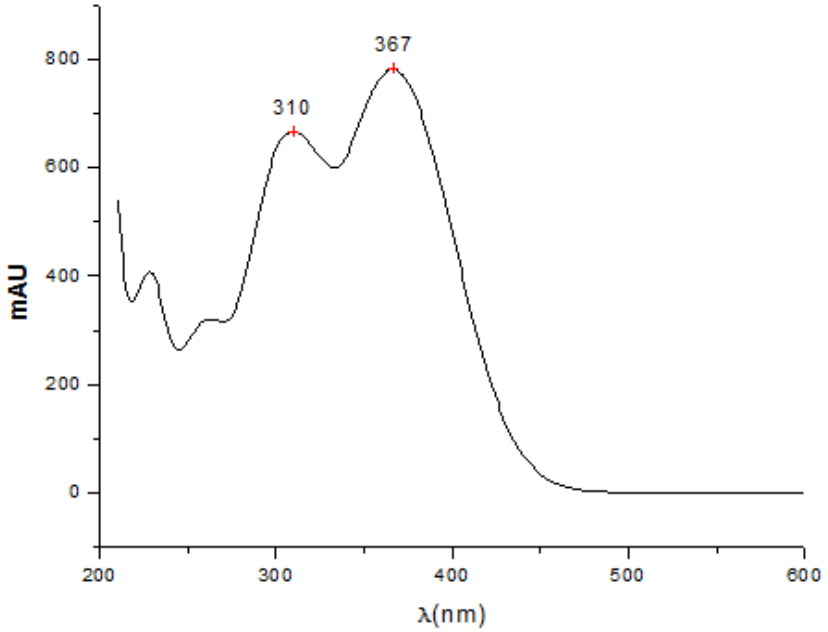

Figure S.16. HPLC-DAD chromatogram of chalcone **6**, MeOH:H_2O (3:1)

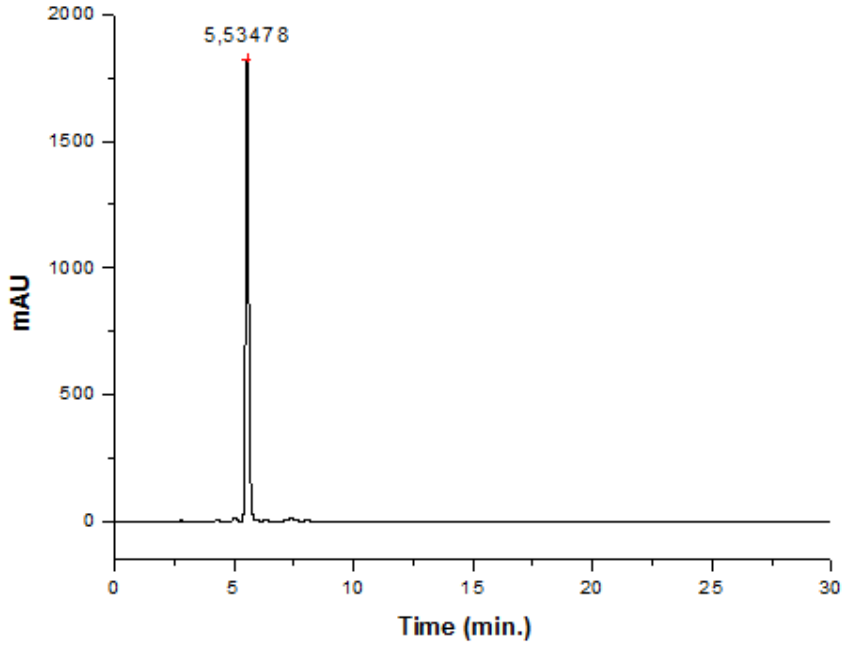

Figure S.17. ^{1}H NMR spectrum (DMSO-d_6, 600 MHz) of chalcone **7**

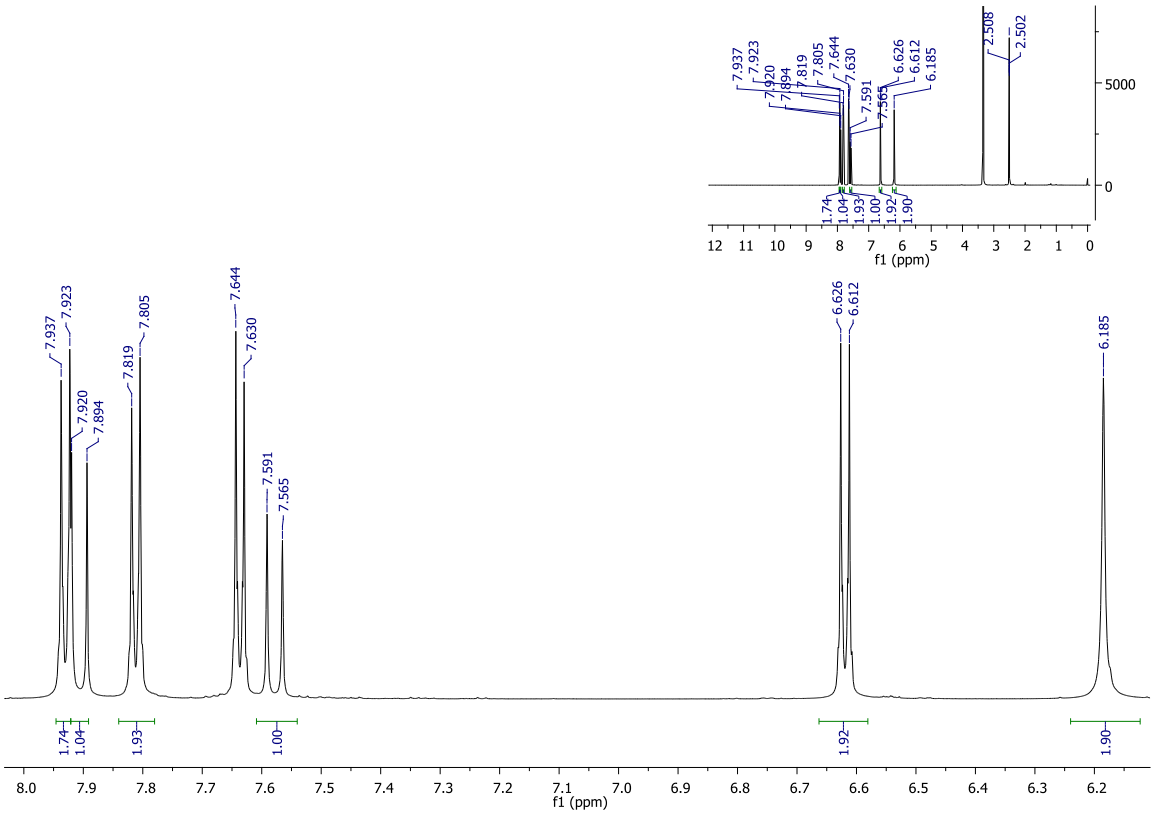

Figure S.18. ^{13}C NMR spectrum (DMSO-d_6, 150 MHz) of chalcone **7**

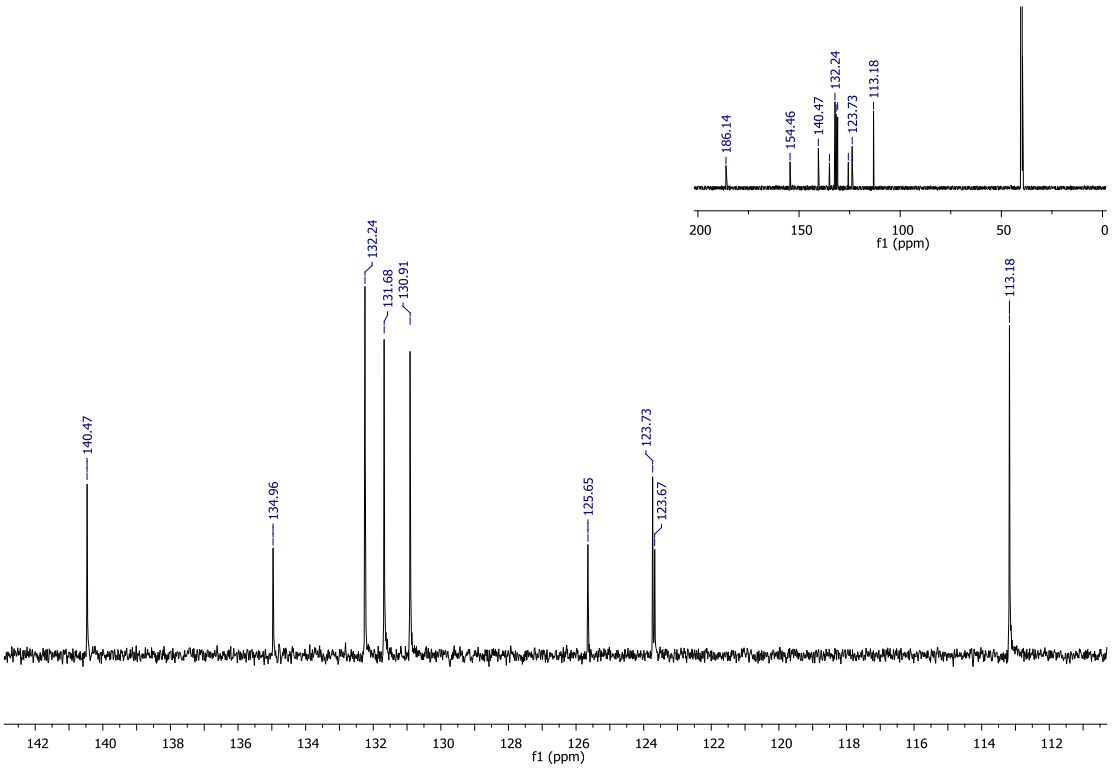

Figure S.19. UV-vis spectrum of chalcone **7** from HPLC-DAD experiment

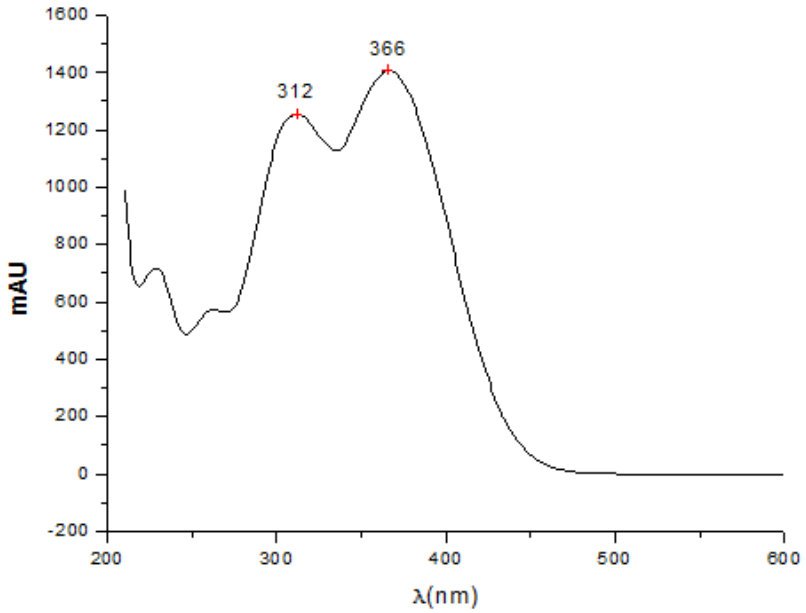

Figure S.20. HPLC-DAD chromatogram of chalcone **7**, MeOH:H_2O (3:1)

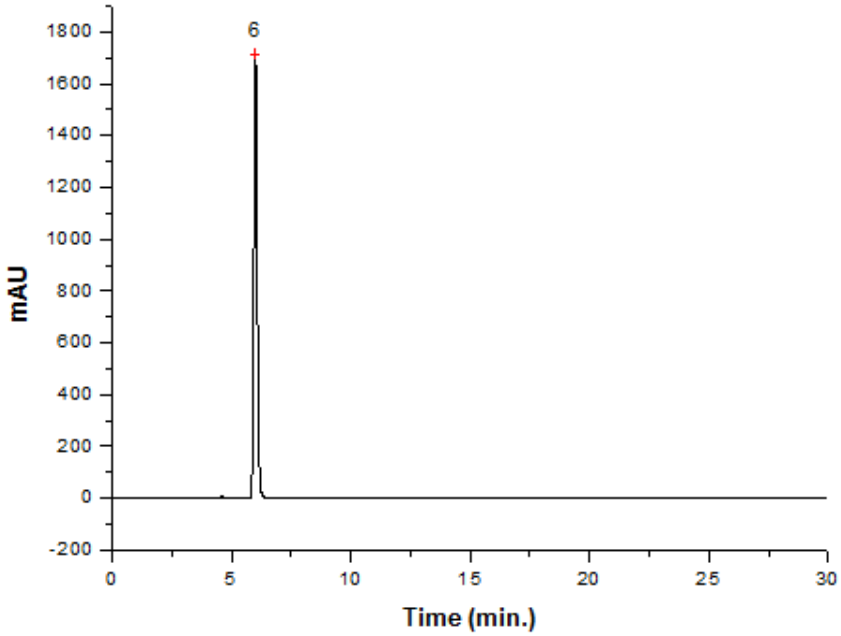

Figure S.21. ^{1}H NMR spectrum (DMSO-d_6, 600 MHz) of chalcone **8**

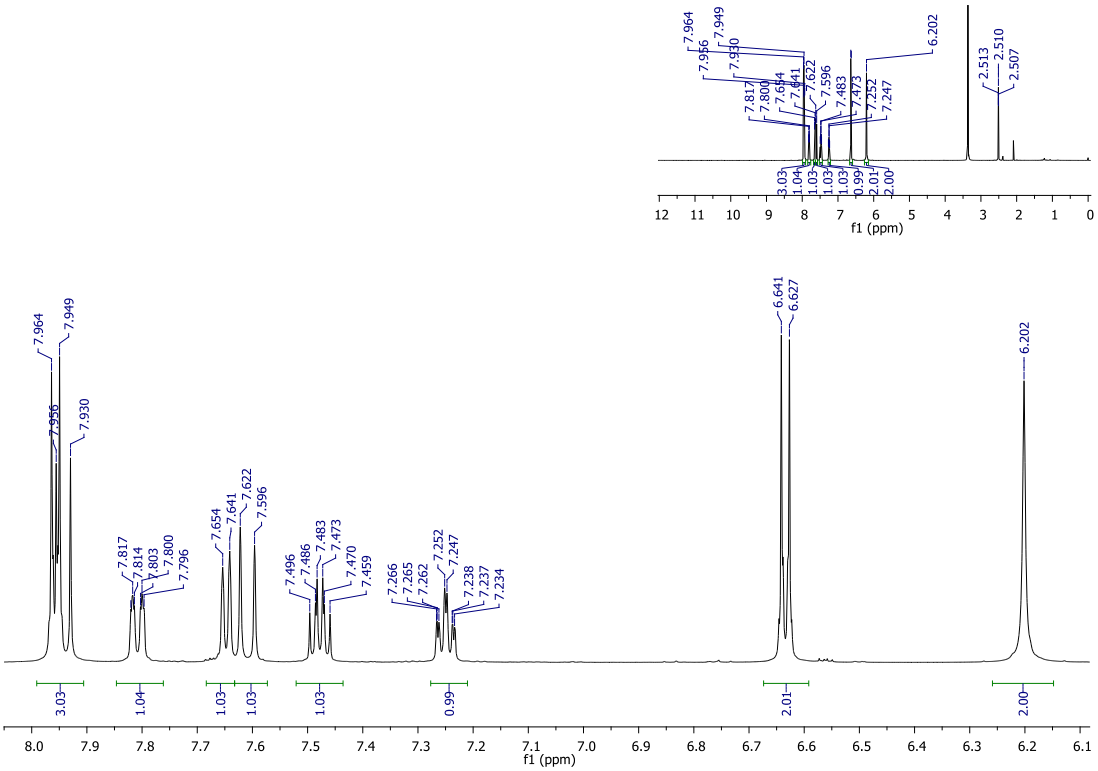

Figure S.22. ^{13}C NMR spectrum (DMSO-d_6, 150 MHz) of chalcone **8**

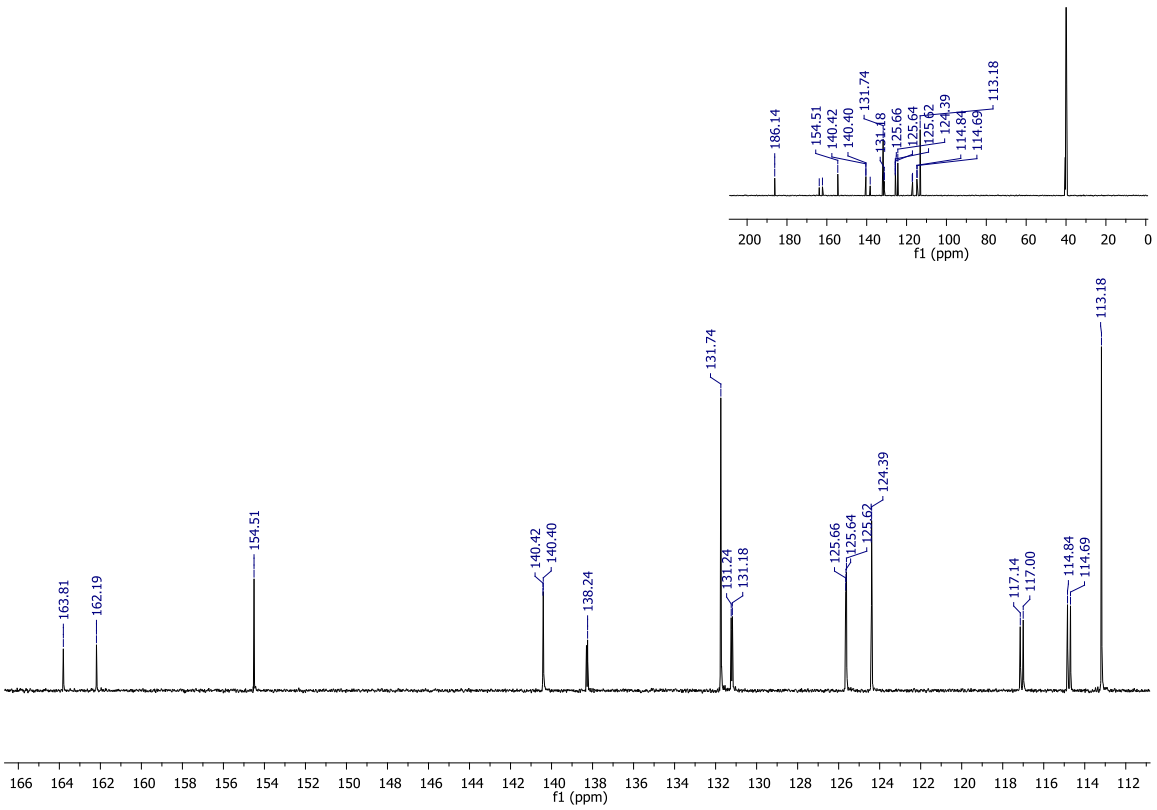

Figure S.23. UV-vis spectrum of chalcone **8** from HPLC-DAD experiment

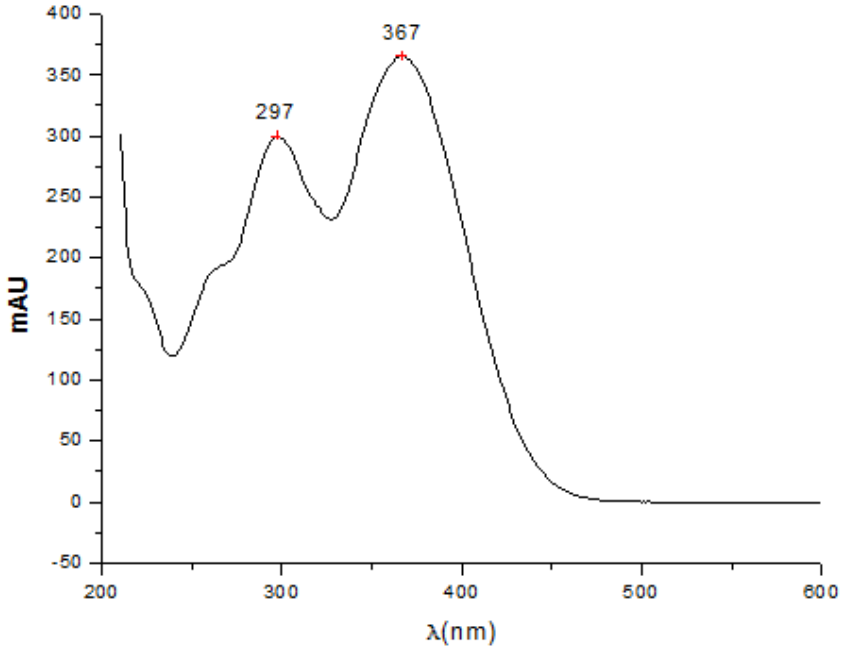

Figure S.24. HPLC-DAD chromatogram of chalcone **8**, MeOH:H_2O (3:1)

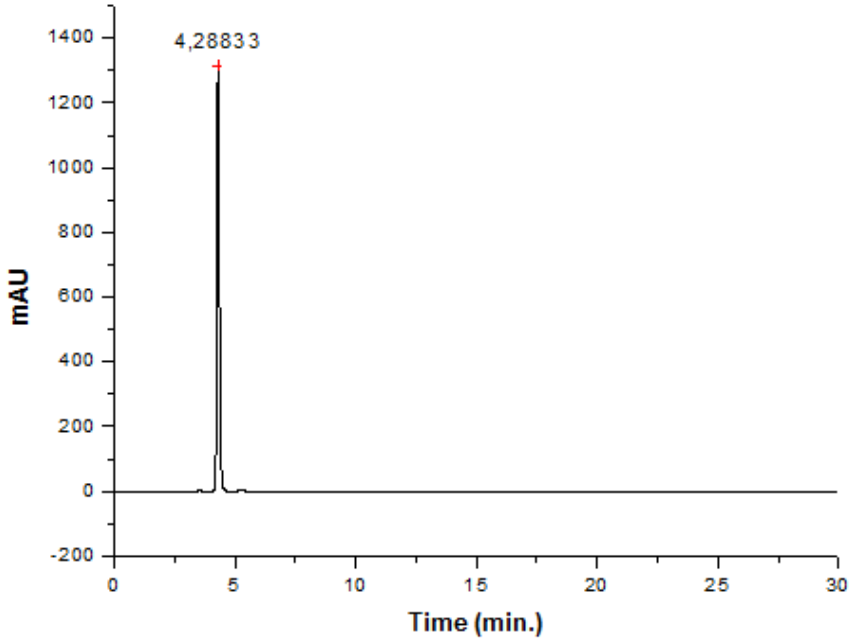

Figure S.25. ^{1}H NMR spectrum (DMSO-d_6, 600 MHz) of chalcone **9**

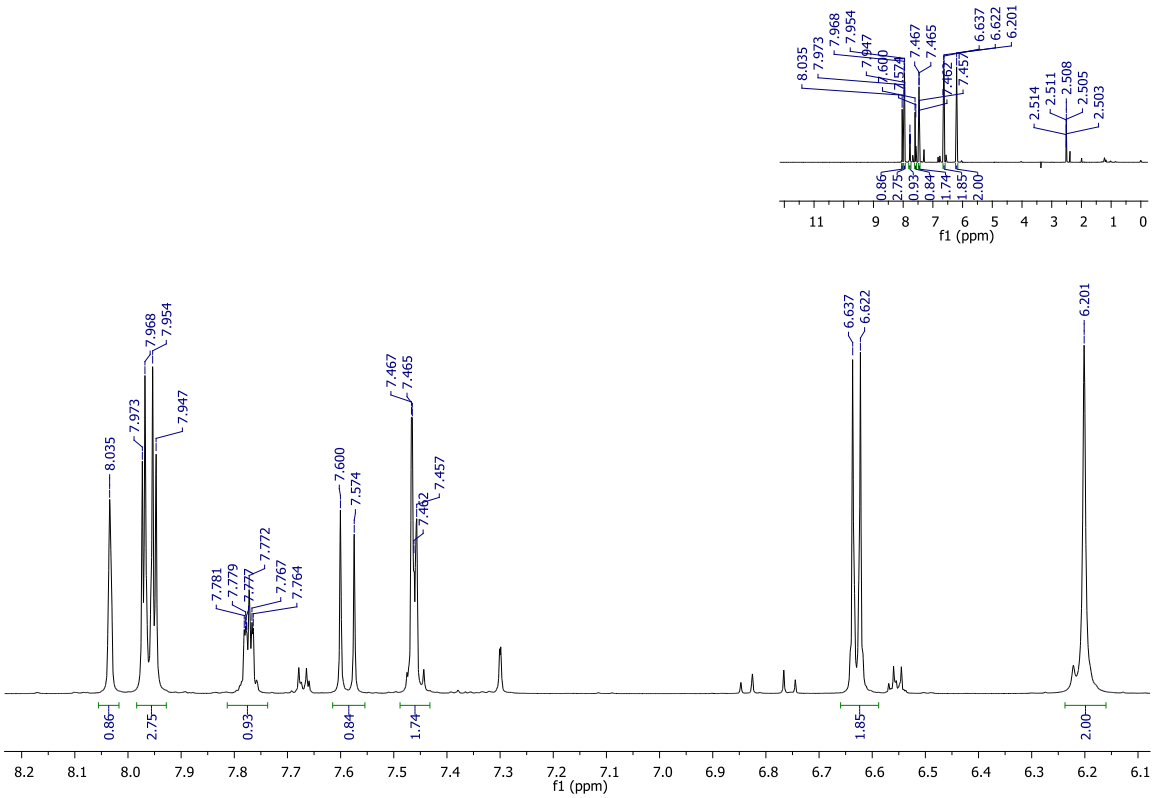

Figure S.26. ^{13}C NMR spectrum (DMSO-d_6, 150 MHz) of chalcone **9**

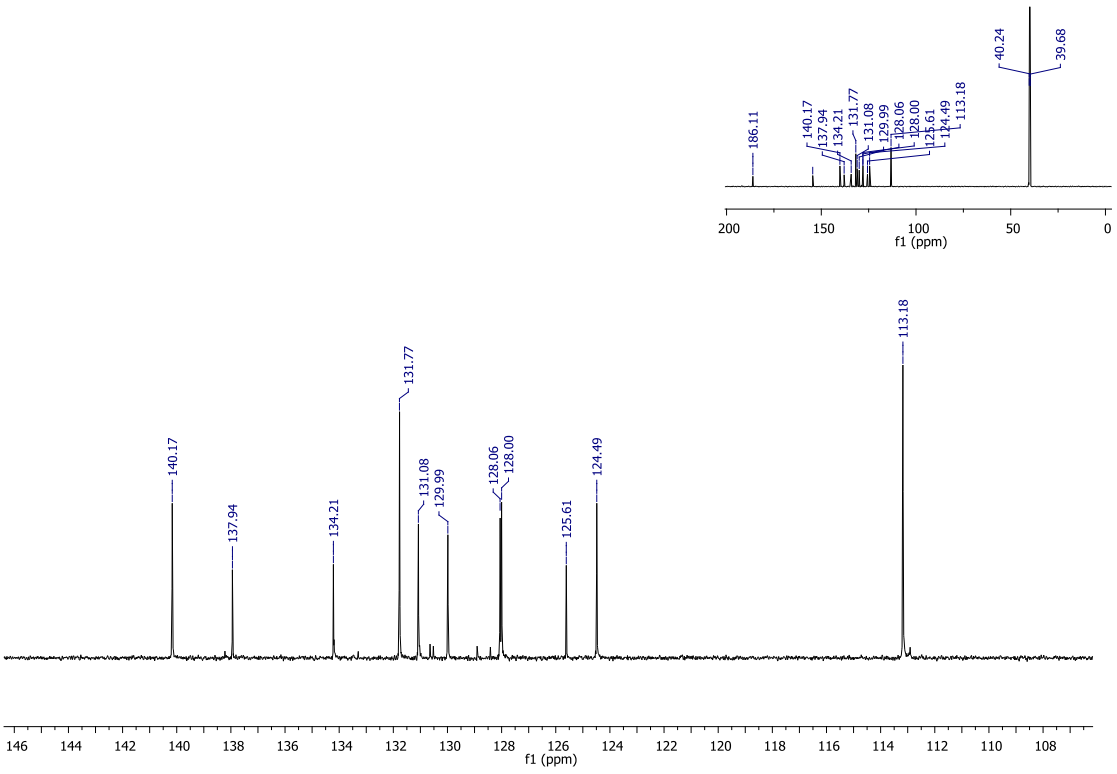

Figure S.27. UV-vis spectrum of chalcone **9** from HPLC-DAD experiment

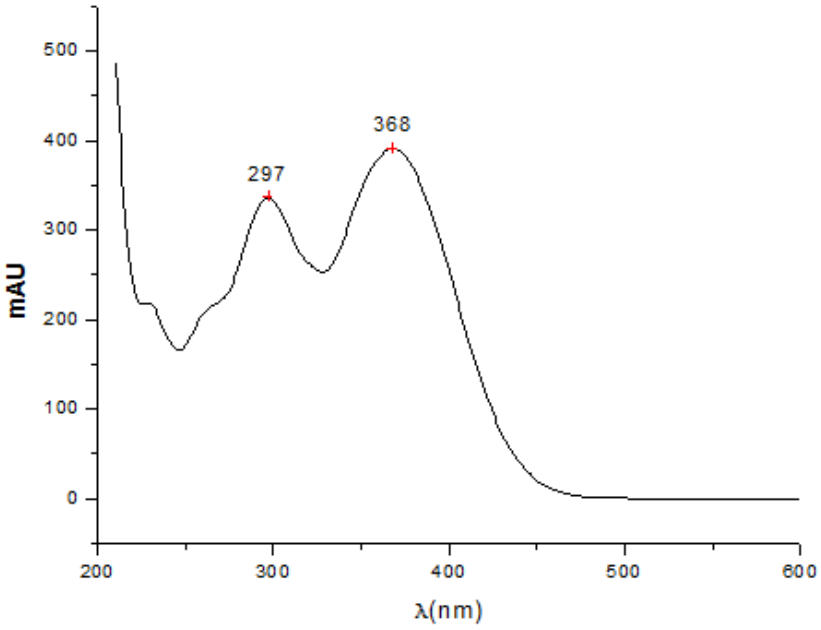

Figure S.28. HPLC-DAD chromatogram of chalcone **9**, MeOH:H_2O (3:1)

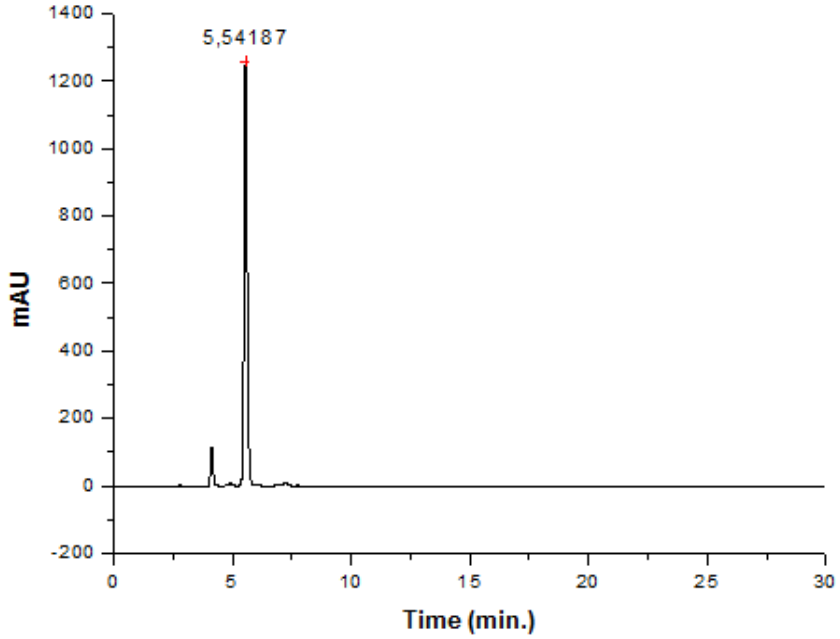

Figure S.29. ^{1}H NMR spectrum (DMSO-d_6, 600 MHz) of chalcone **10**

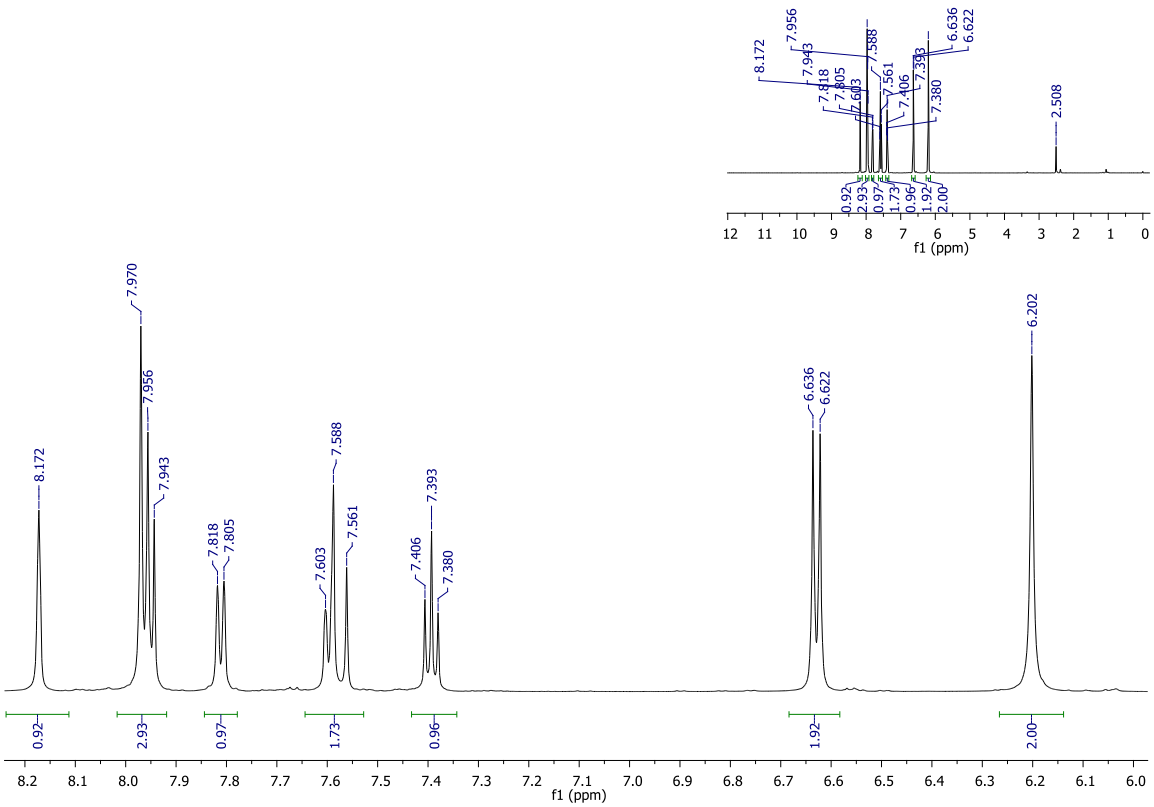

Figure S.30. ^{13}C NMR spectrum (DMSO-d_6, 150 MHz) of chalcone **10**

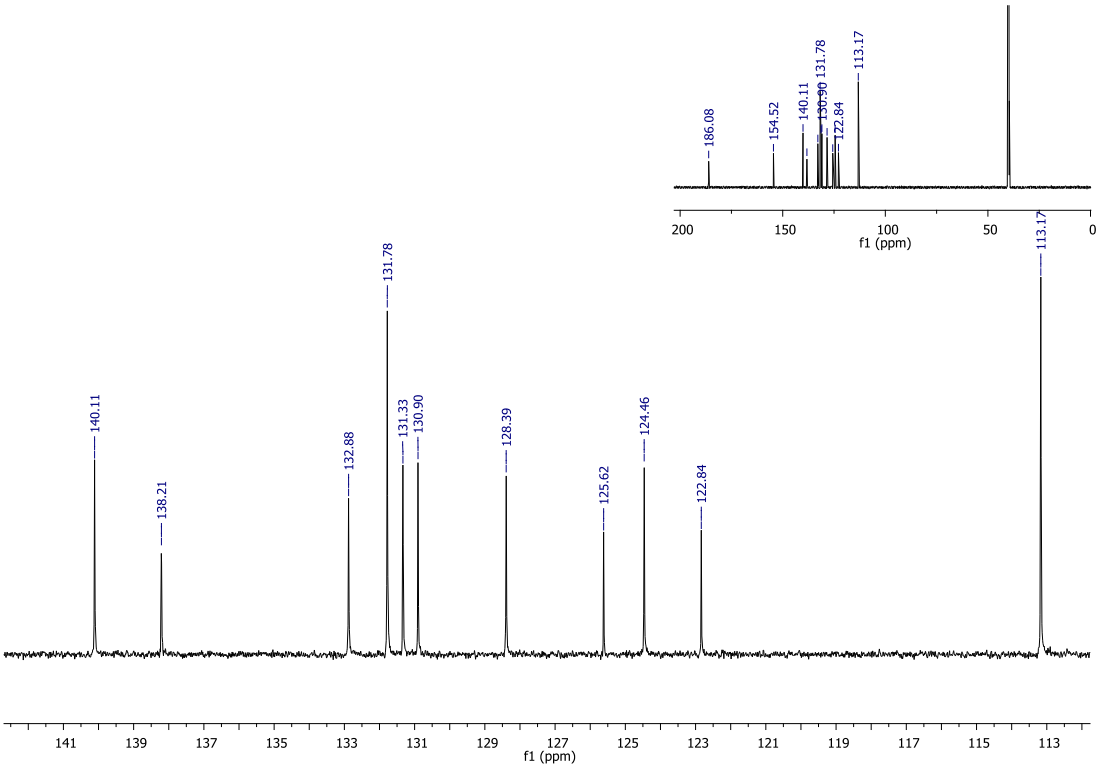

Figure S.31. UV-vis spectrum of chalcone **10** from HPLC-DAD experiment

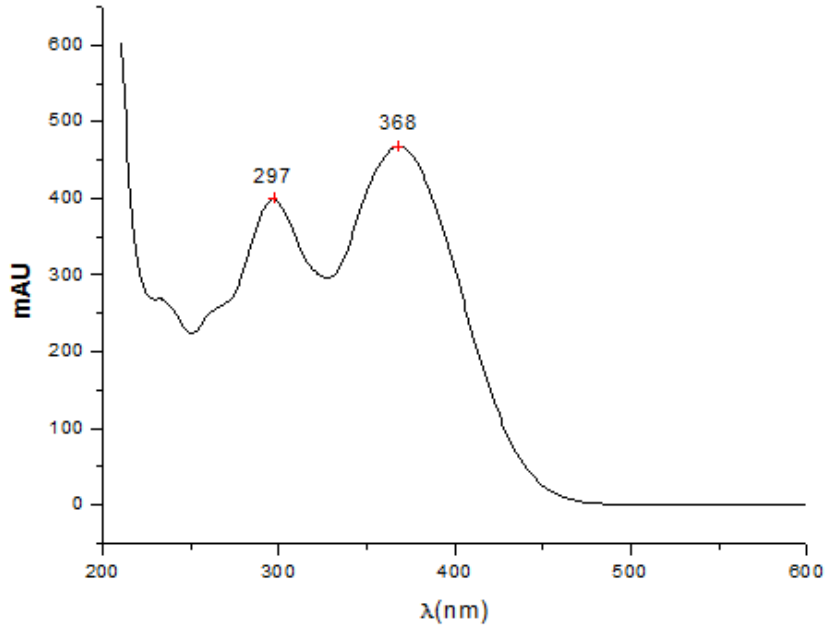

Figure S.32. HPLC-DAD chromatogram of chalcone **10**, MeOH:H_2O (3:1)

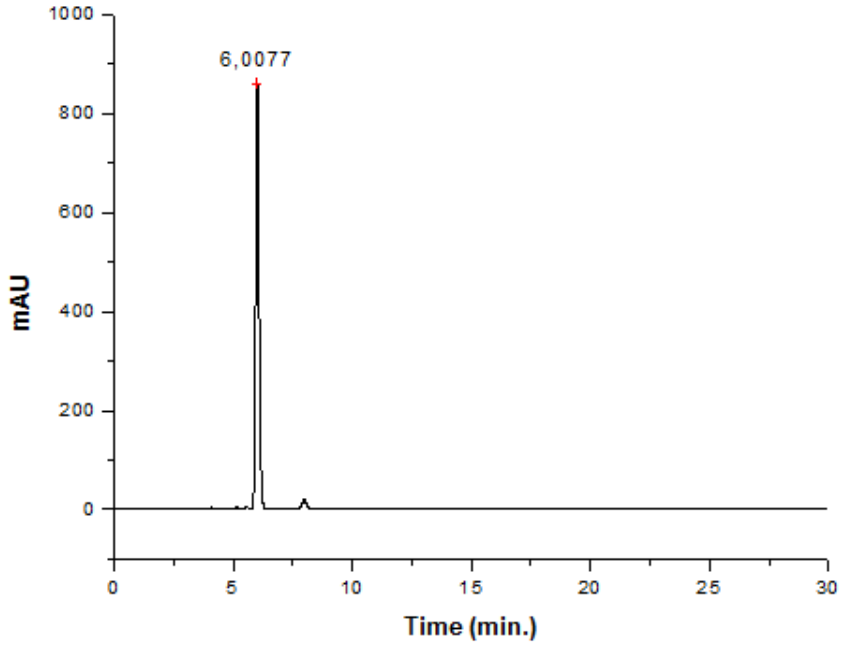

Figure S.33. ^{1}H NMR spectrum (DMSO-d_6, 600 MHz) of chalcone **11**

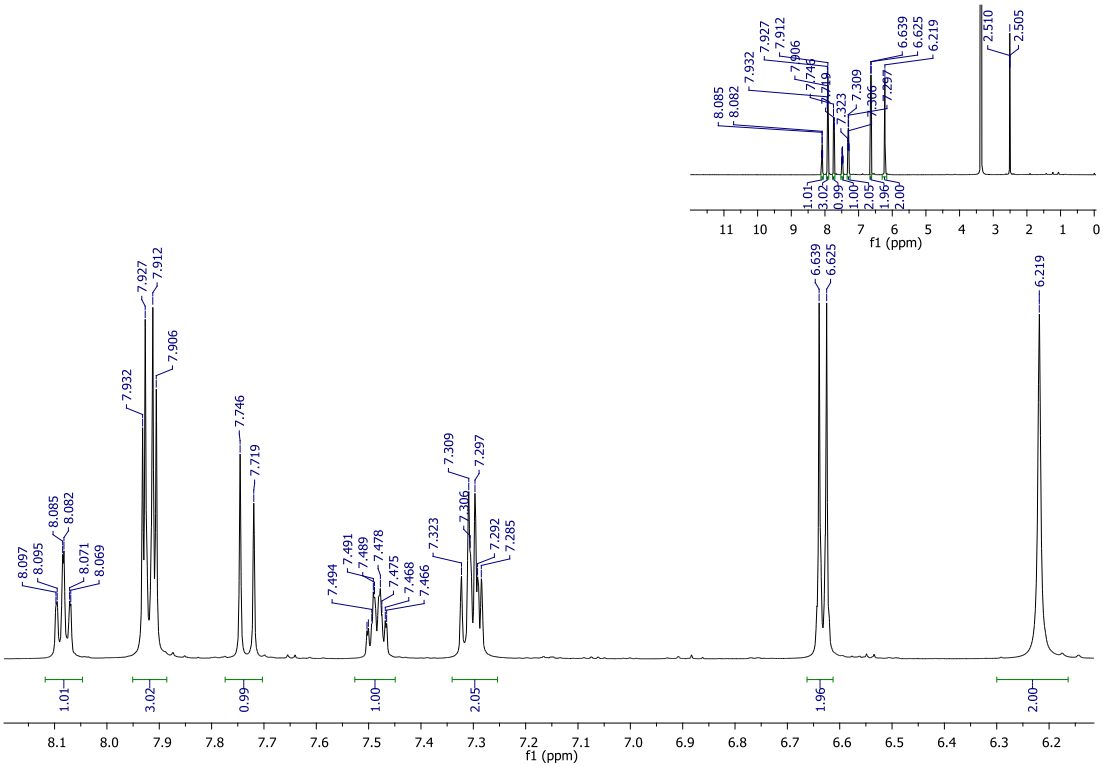

Figure S.34. ^{13}C NMR spectrum (DMSO-d_6, 150 MHz) of chalcone **11**

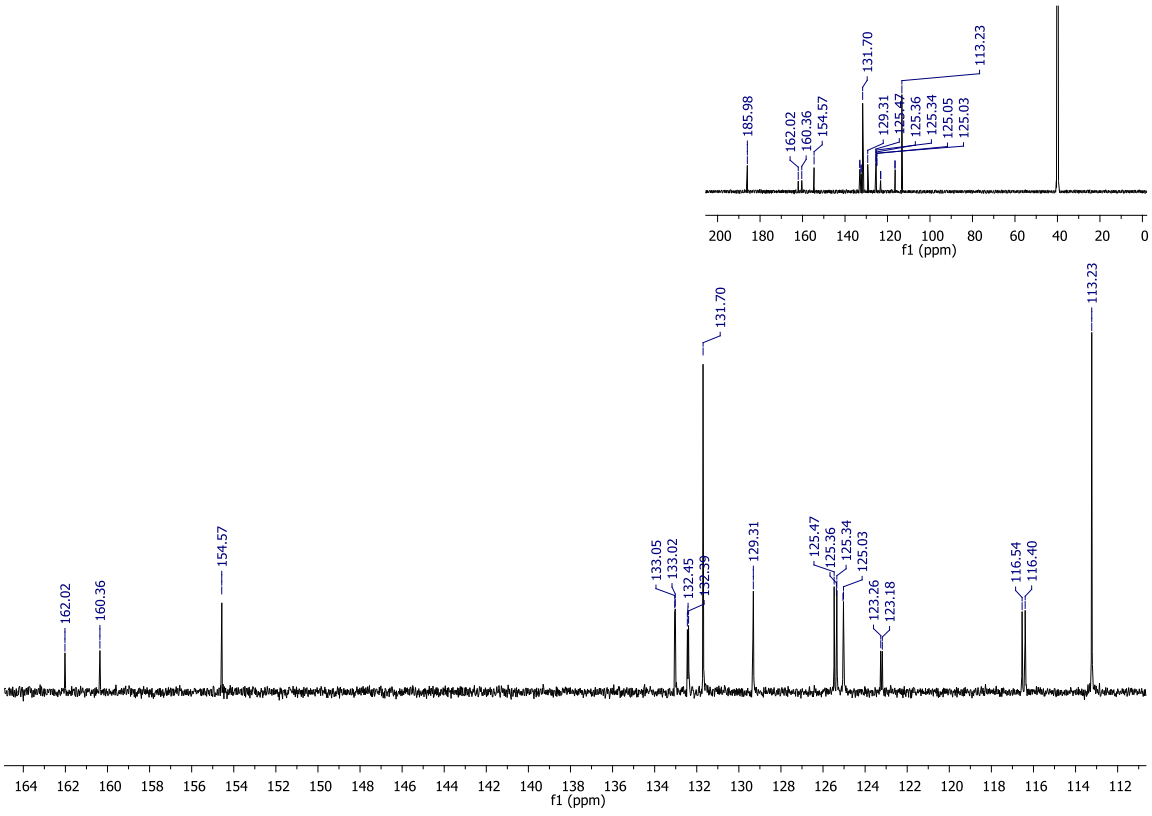

Figure S.35. UV-vis spectrum of chalcone **11** from HPLC-DAD experiment

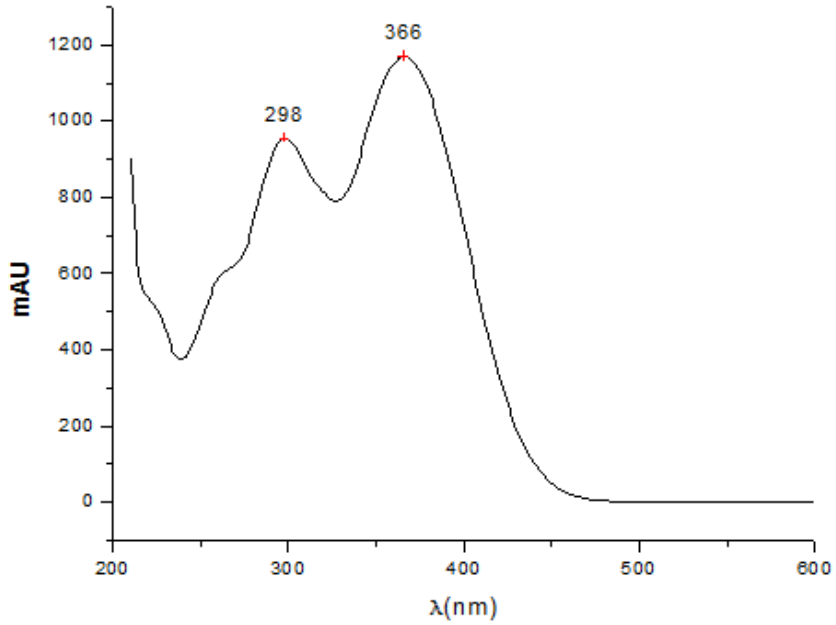

Figure S.36. HPLC-DAD chromatogram of chalcone **11**, MeOH:H_2O (3:1)

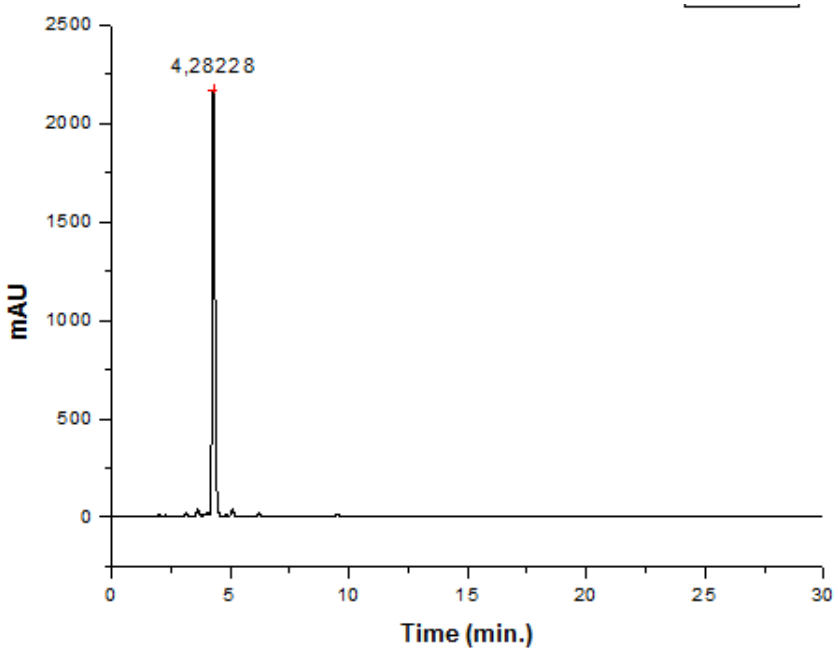

Figure S.37. ^{1}H NMR spectrum (DMSO-d_6, 600 MHz) of chalcone **12**

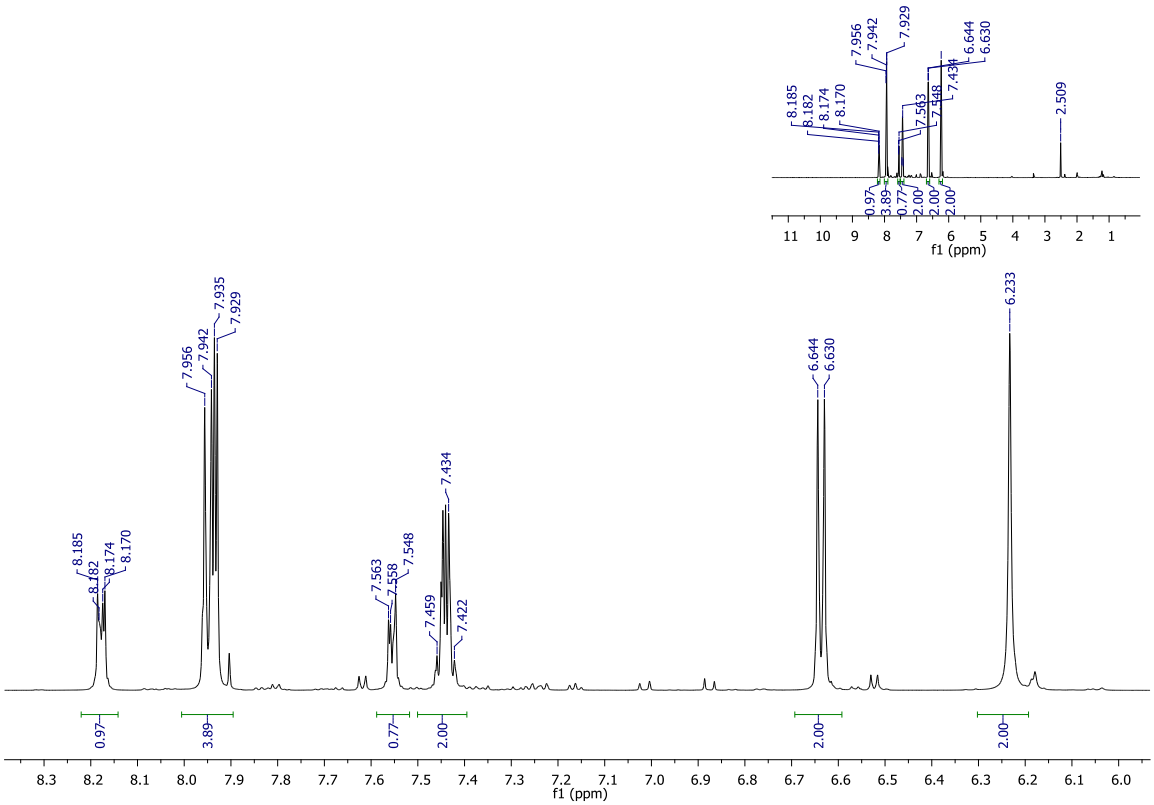

Figure S.38. ^{13}C NMR spectrum (DMSO-d_6, 150 MHz) of chalcone **12**

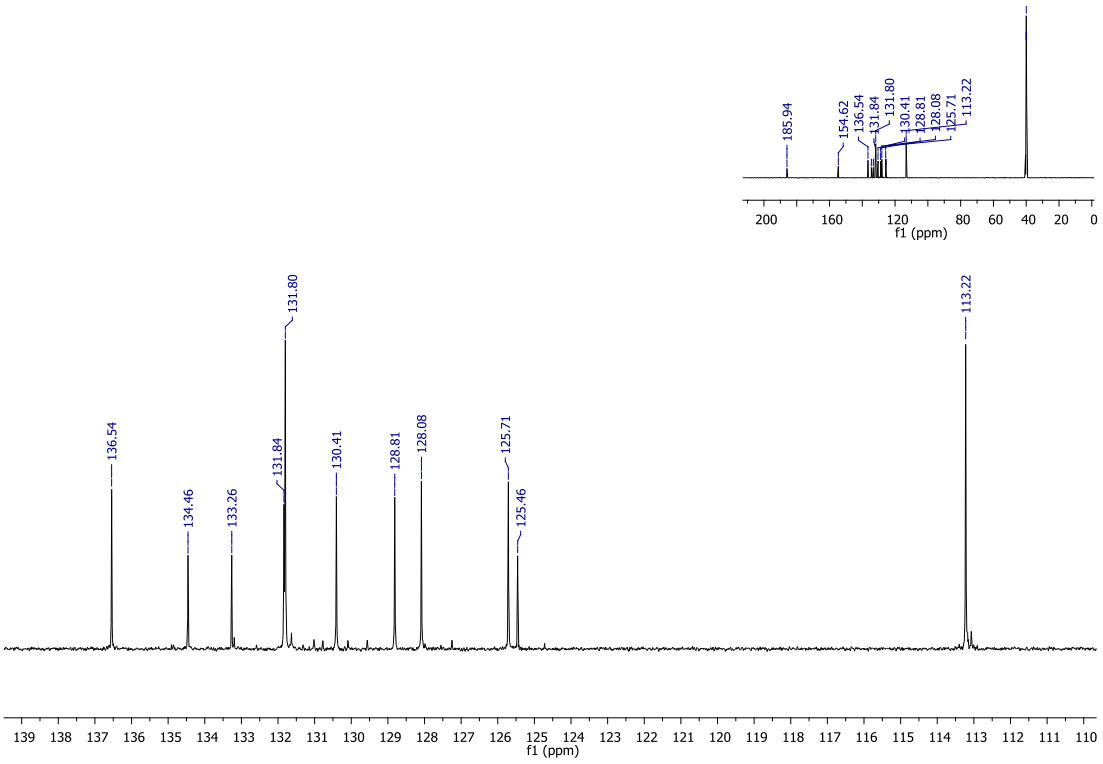

Figure S.39. UV-vis spectrum of chalcone **12** from HPLC-DAD experiment

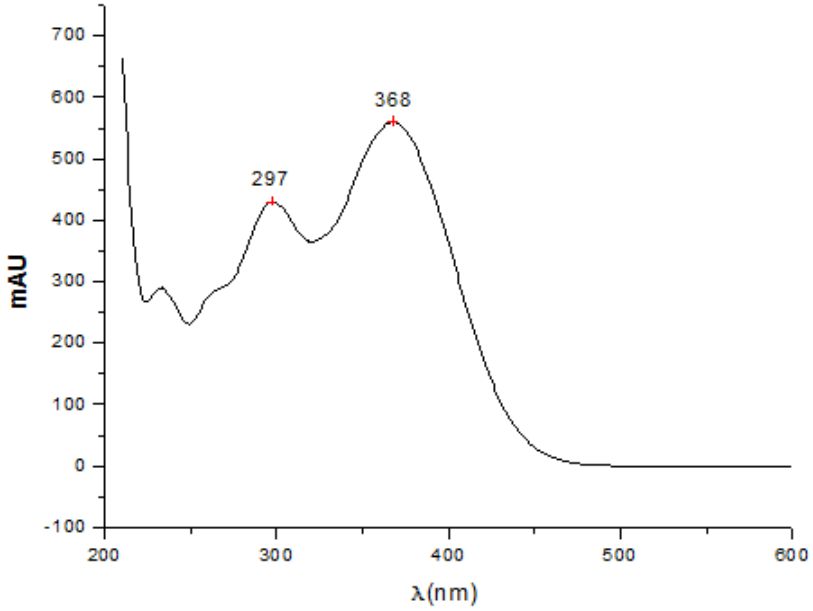

Figure S.40. HPLC-DAD chromatogram of chalcone **12**, MeOH:H_2O (3:1)

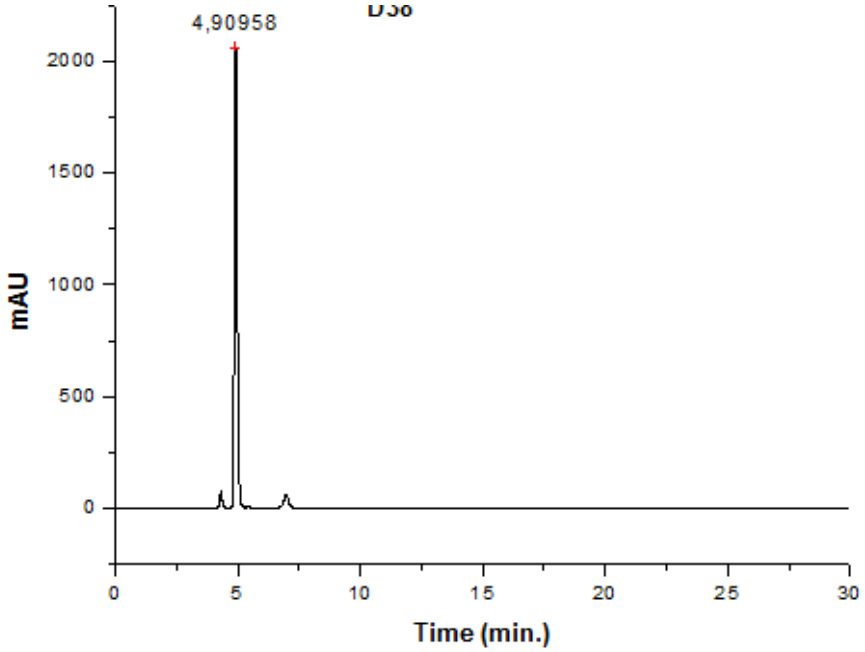

Figure S.41. UV-vis spectrum of chalcone **13** from HPLC-DAD experiment

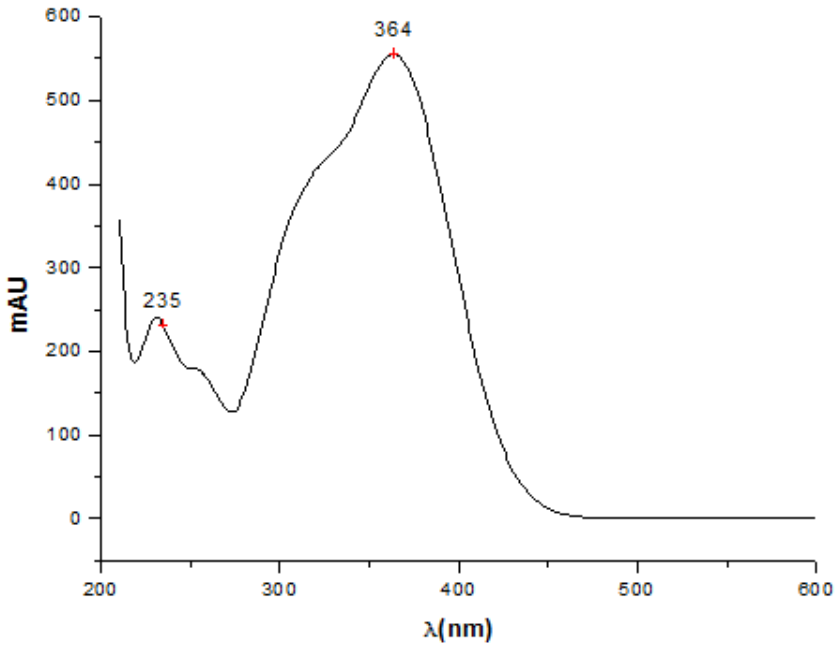

Figure S.42. HPLC-DAD chromatogram of chalcone **13**, MeOH:H_2O (3:1)

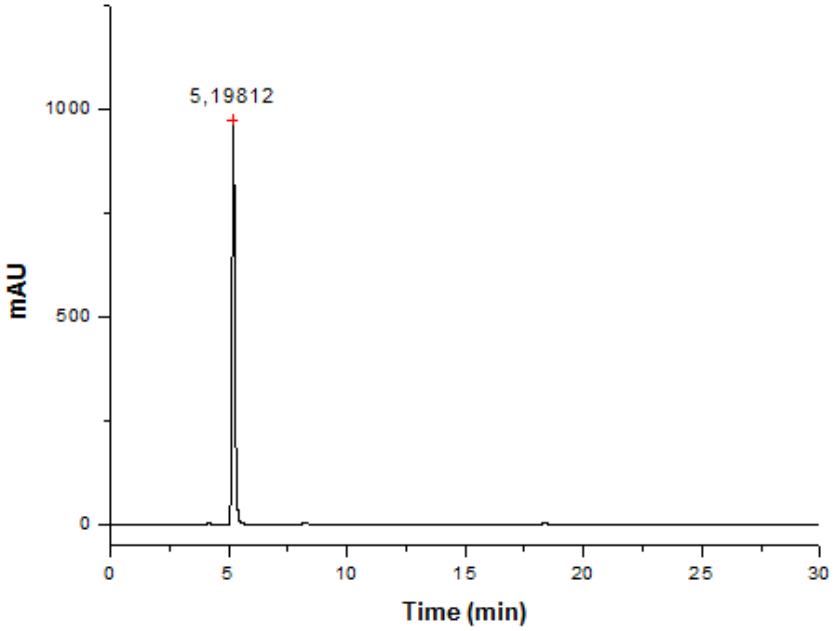

Figure S.43. UV-vis spectrum of chalcone **14** from HPLC-DAD experiment

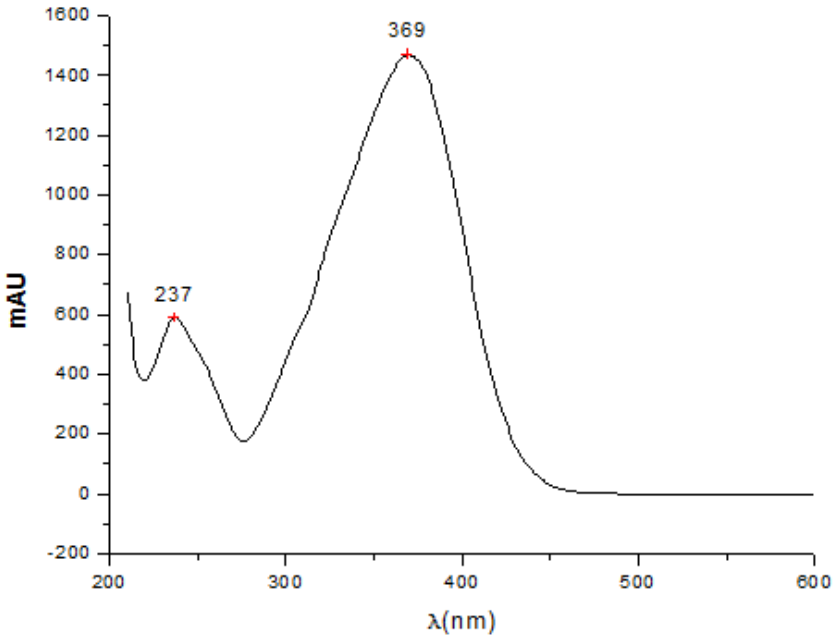

Figure S.44. HPLC-DAD chromatogram of chalcone **14**, MeOH:H_2O (3:1)

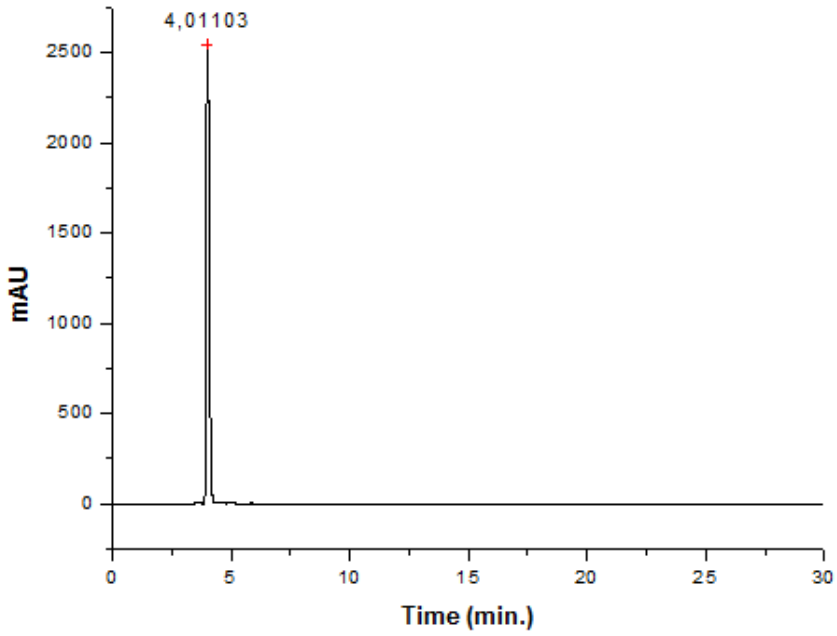

Figure S.45. UV-vis spectrum of chalcone **15** from HPLC-DAD experiment

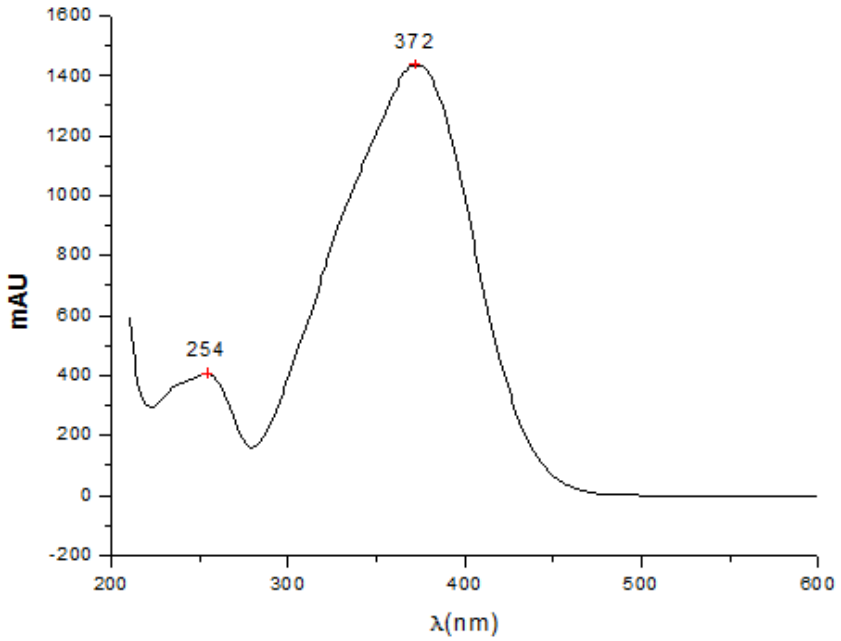

Figure S.46. HPLC-DAD chromatogram of chalcone **15**, MeOH:H_2O (3:1)

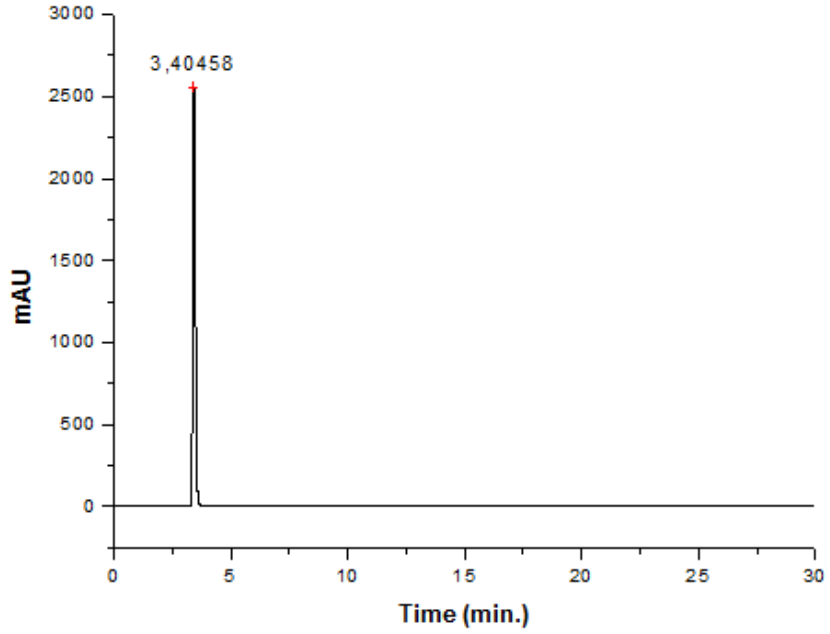

Figure S.47. UV-vis spectrum of chalcone **16** from HPLC-DAD experiment

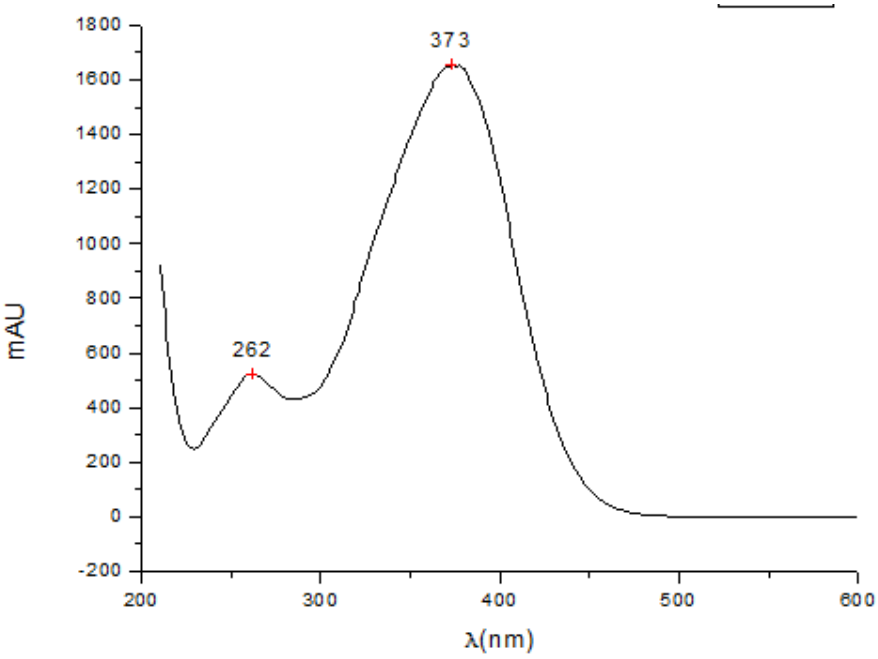

Figure S.48. HPLC-DAD chromatogram of chalcone **16**, MeOH:H_2O (3:1)

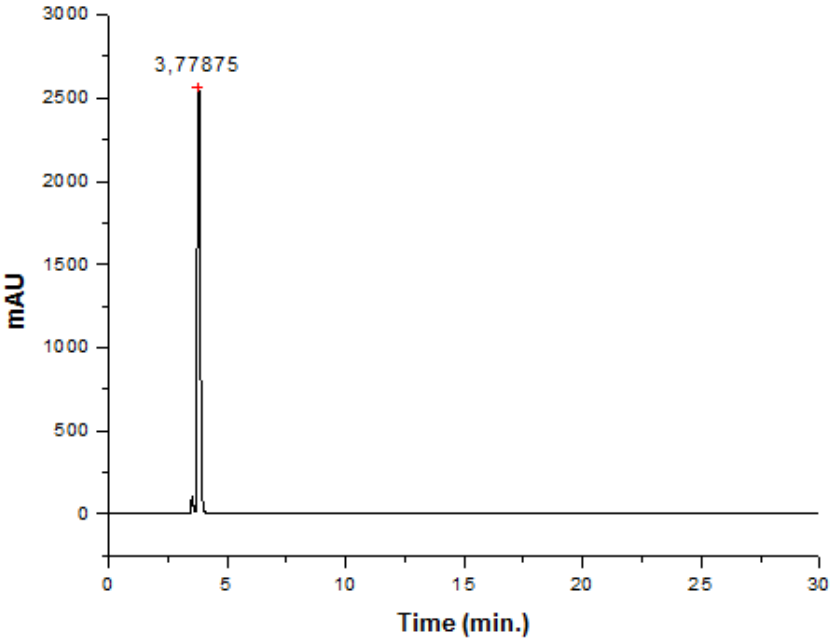

Figure S.49. ^{1}H NMR spectrum (DMSO-d_6, 600 MHz) of chalcone **17**

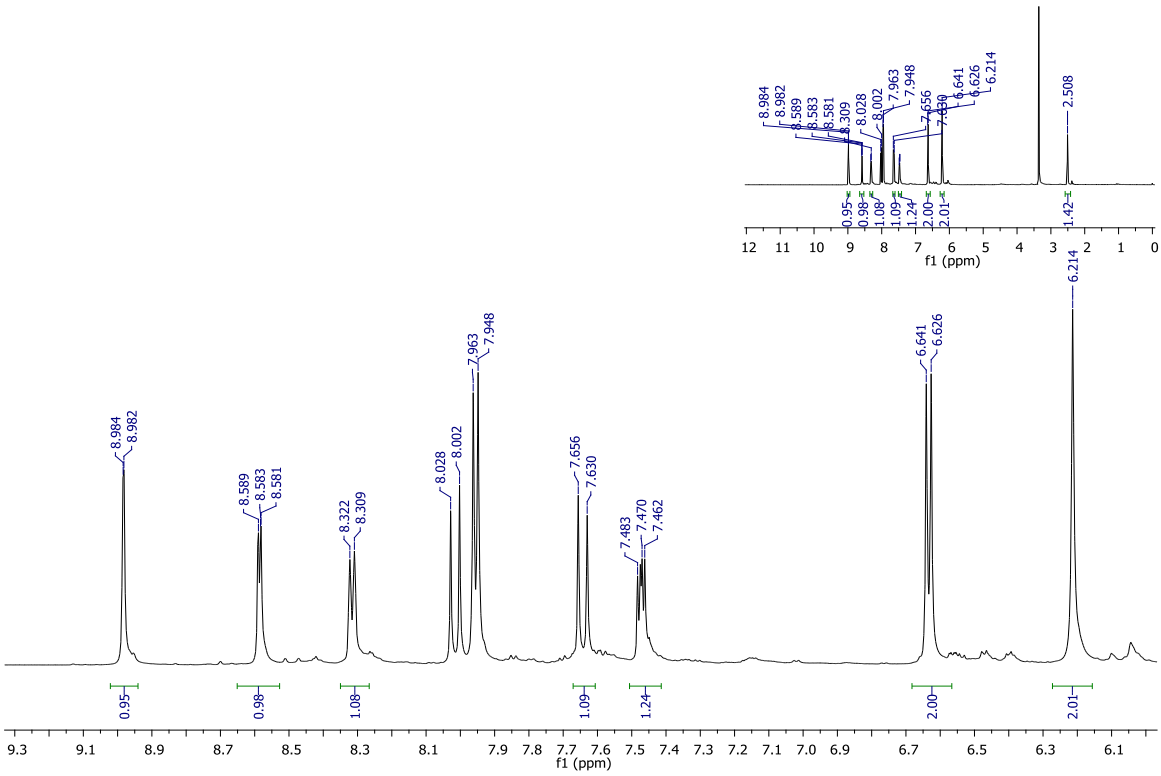

Figure S.50. ^{13}C NMR spectrum (DMSO-d_6, 150 MHz) of chalcone **17**

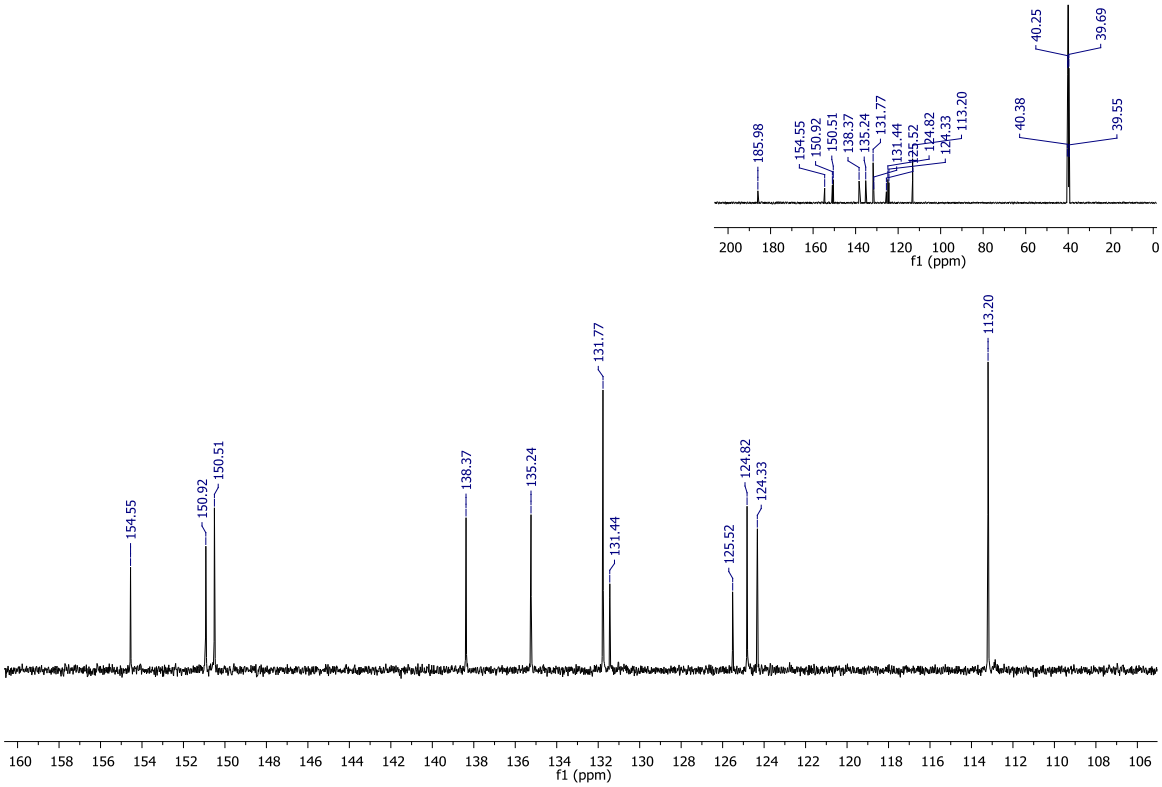

Figure S.51. UV-vis spectrum of chalcone **17** from HPLC-DAD experiment

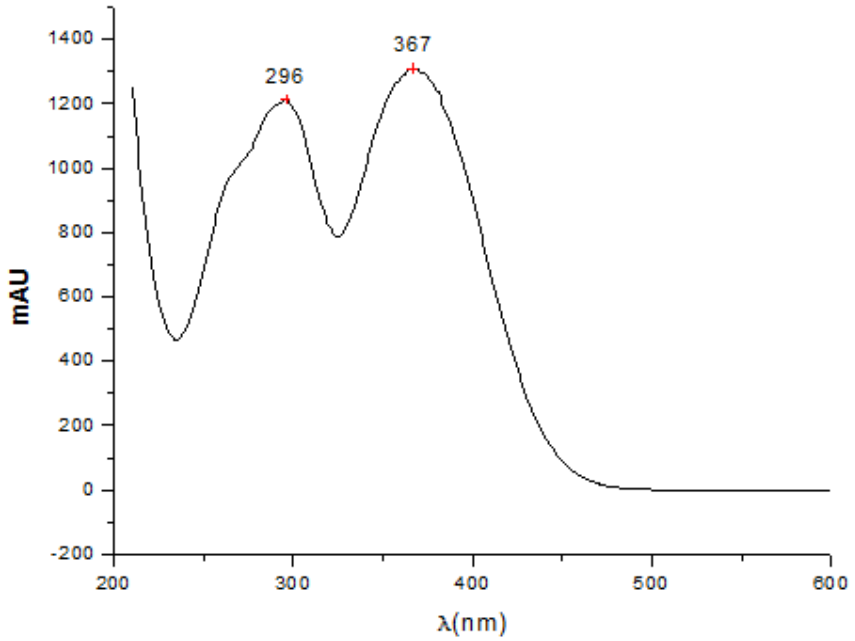

Figure S.52. HPLC-DAD chromatogram of chalcone **17**, MeOH:H_2O (3:1)

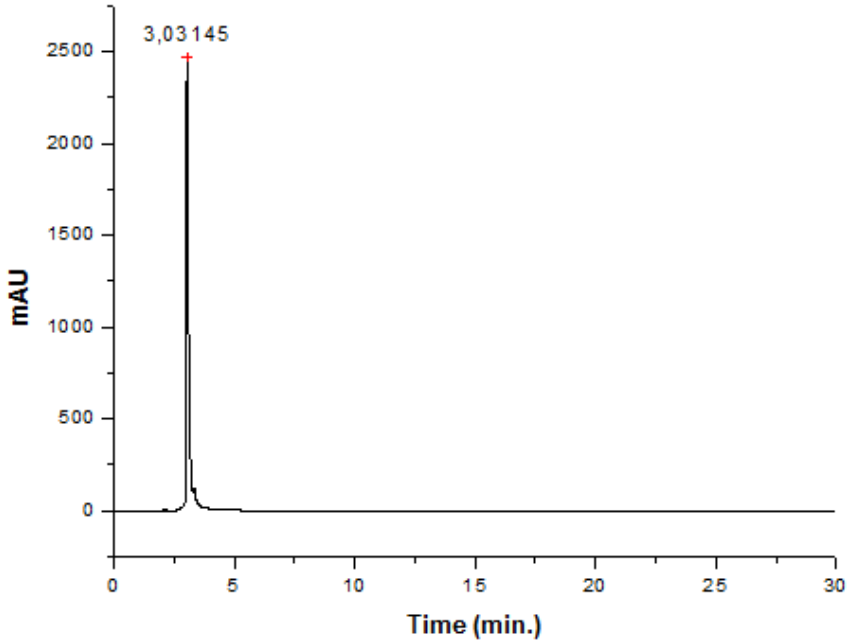

Figure S.53. ^{1}H NMR spectrum (DMSO-d_6, 600 MHz) of chalcone **18**

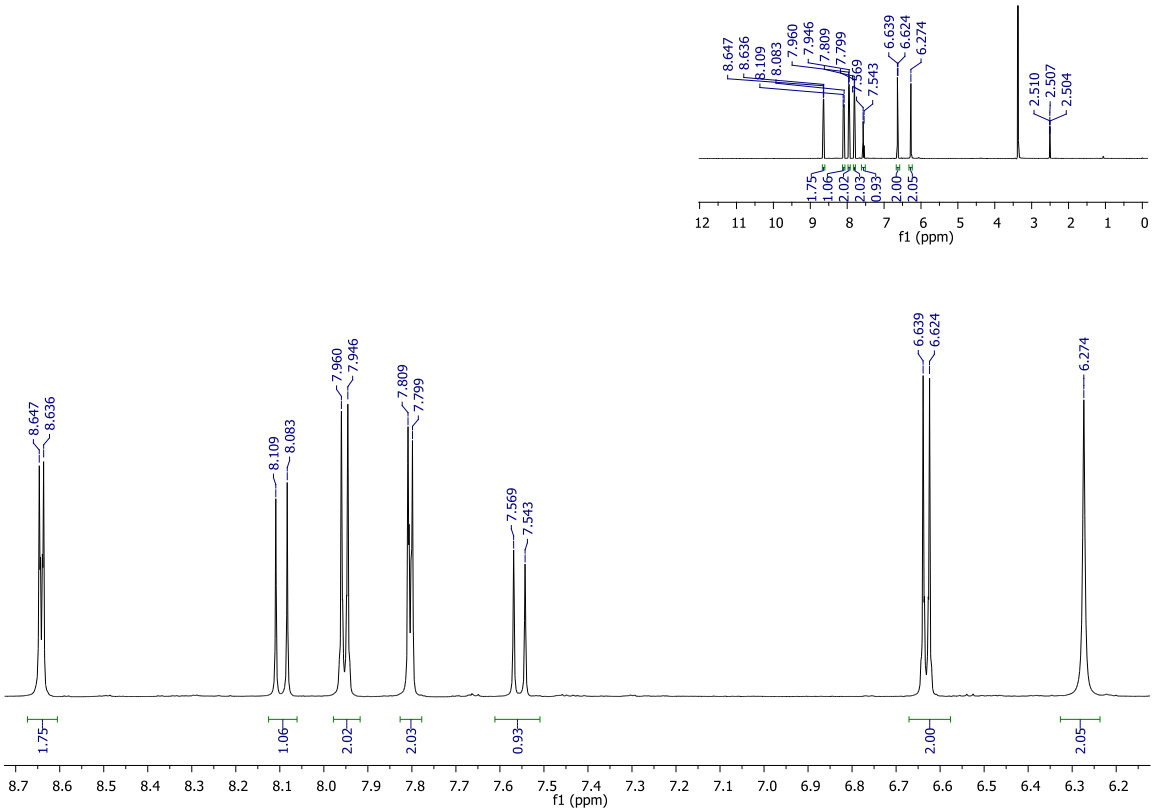

Figure S.54. ^{13}C NMR spectrum (DMSO-d_6, 150 MHz) of chalcone **18**

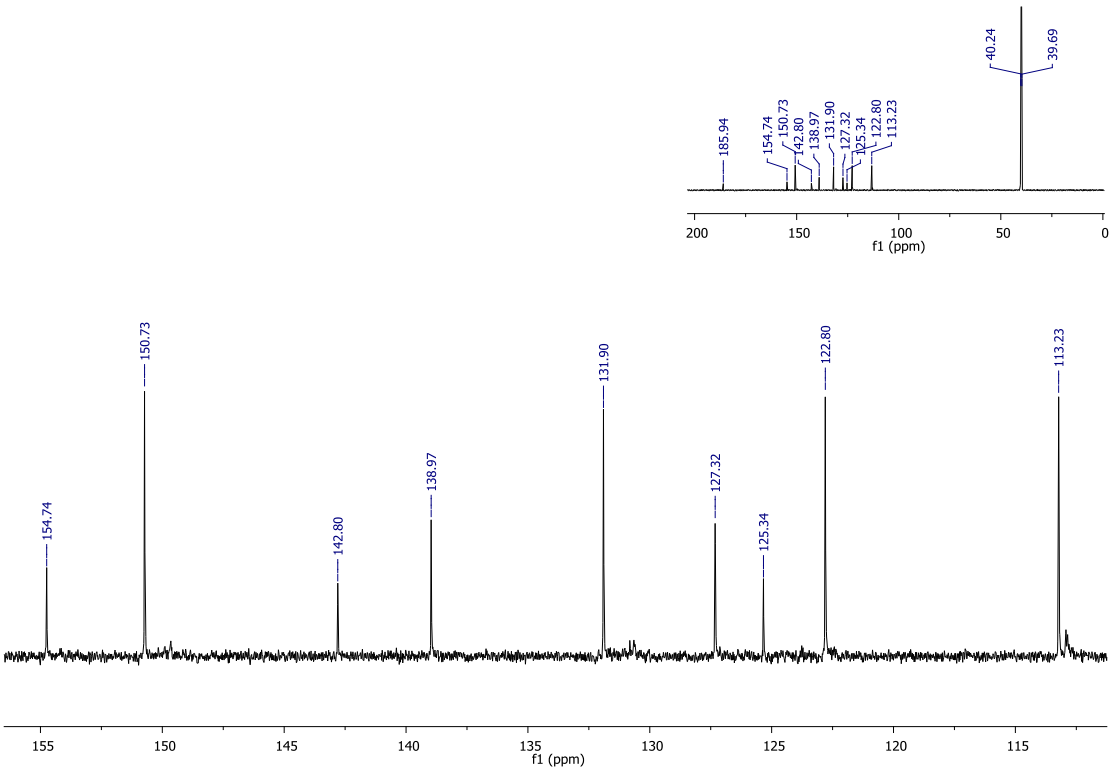

Figure S.55. UV-vis spectrum of chalcone **18** from HPLC-DAD experiment

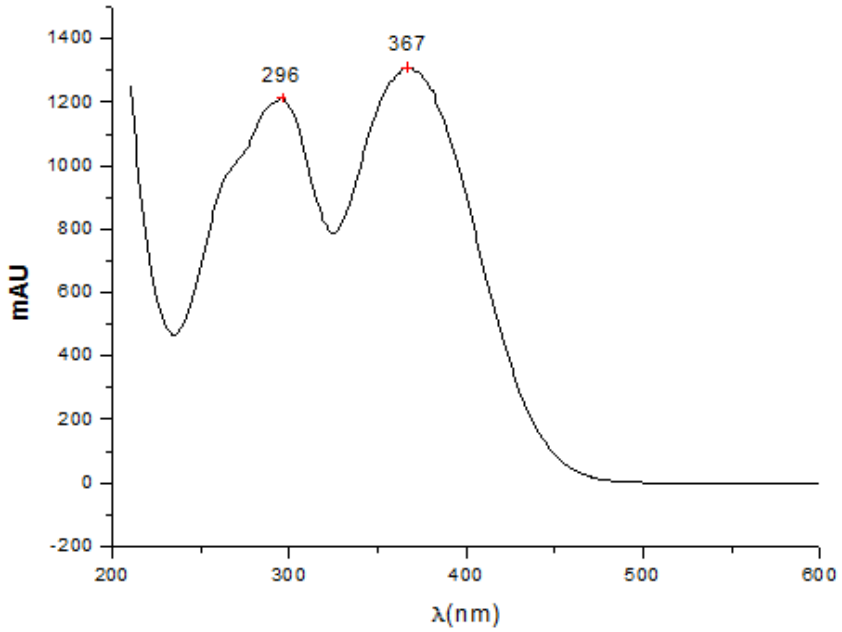

Figure S.56. HPLC-DAD chromatogram of chalcone **18**, MeOH:H_2O (3:1)

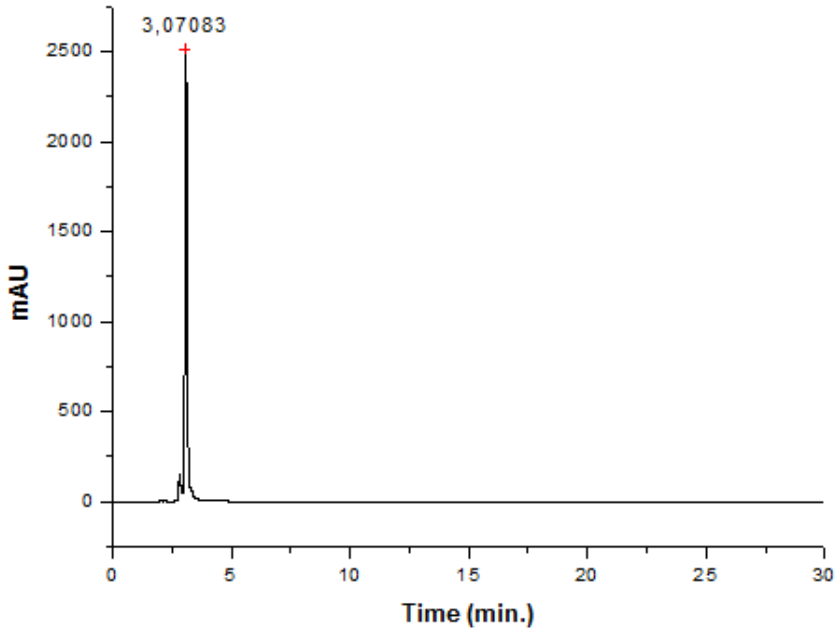

Figure S.57. UV-vis spectrum of chalcone **19** from HPLC-DAD experiment

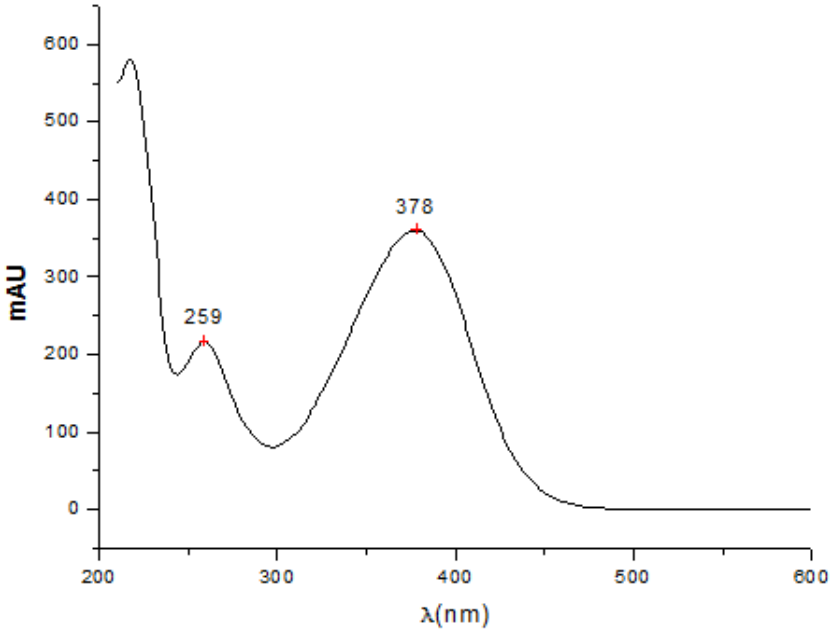

Figure S.58. HPLC-DAD chromatogram of chalcone **19**, MeOH:H_2O (3:1)

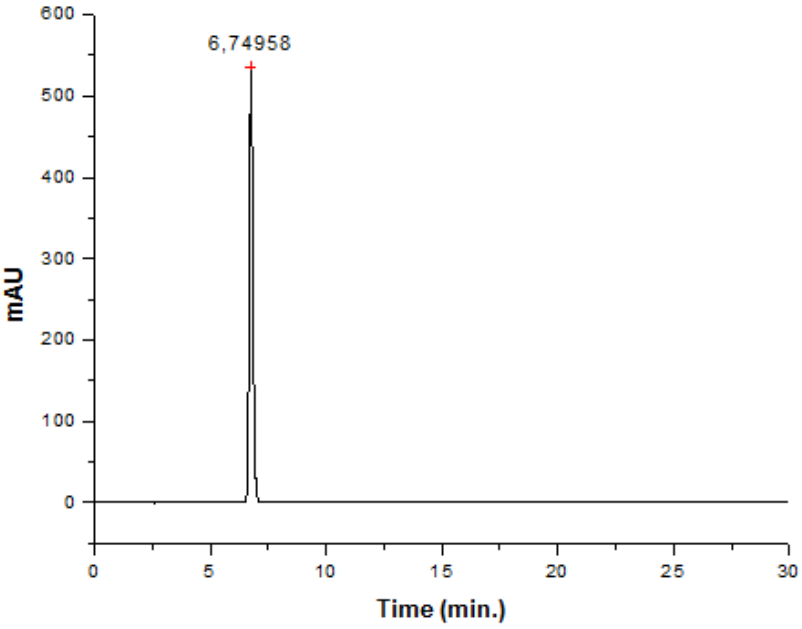

Figure S.59. ^{1}H NMR spectrum (DMSO-d_6, 600 MHz) of chalcone **20**

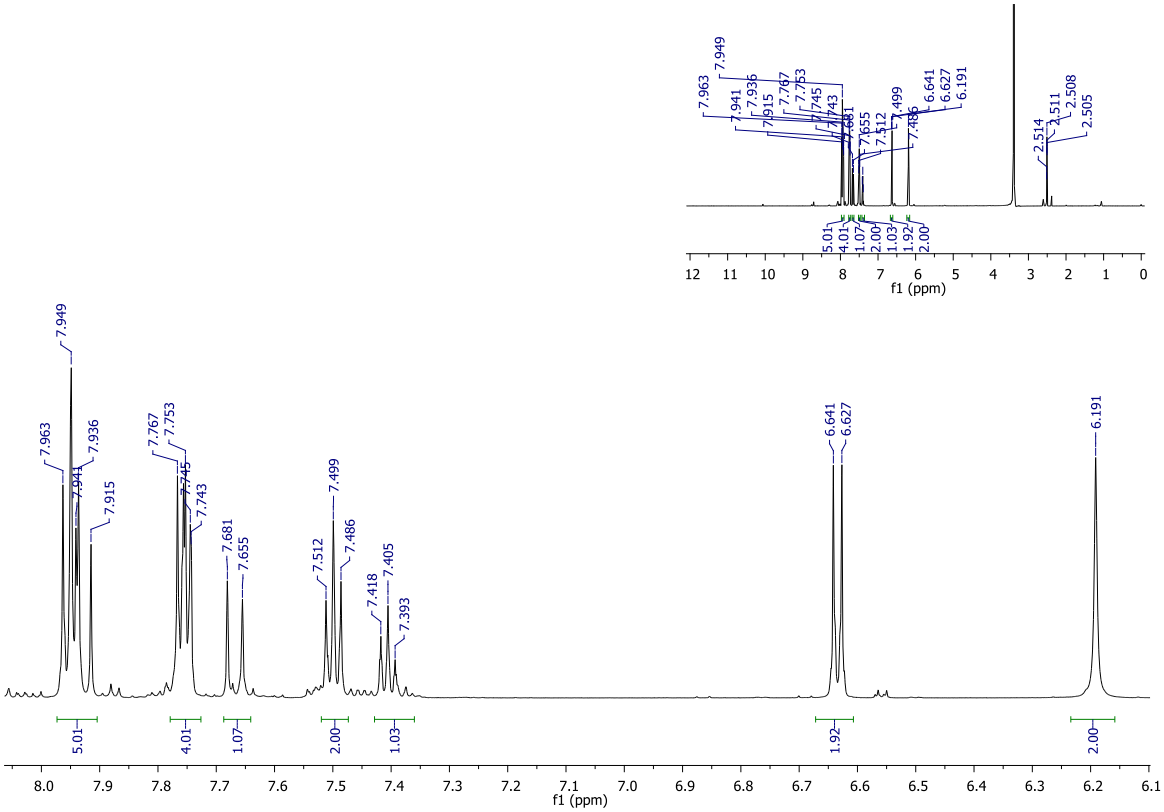

Figure S.60. ^{13}C NMR spectrum (DMSO-d_6, 150 MHz) of chalcone **20**

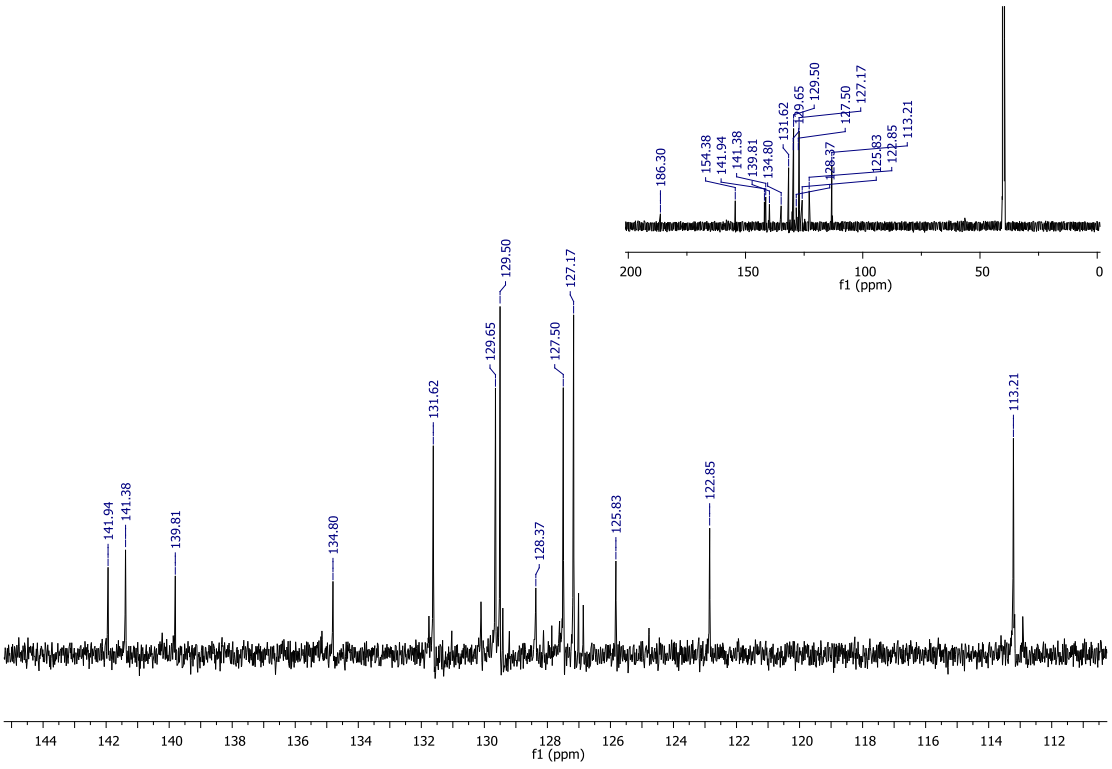

Figure S.61. UV-vis spectrum of chalcone **20** from HPLC-DAD experiment

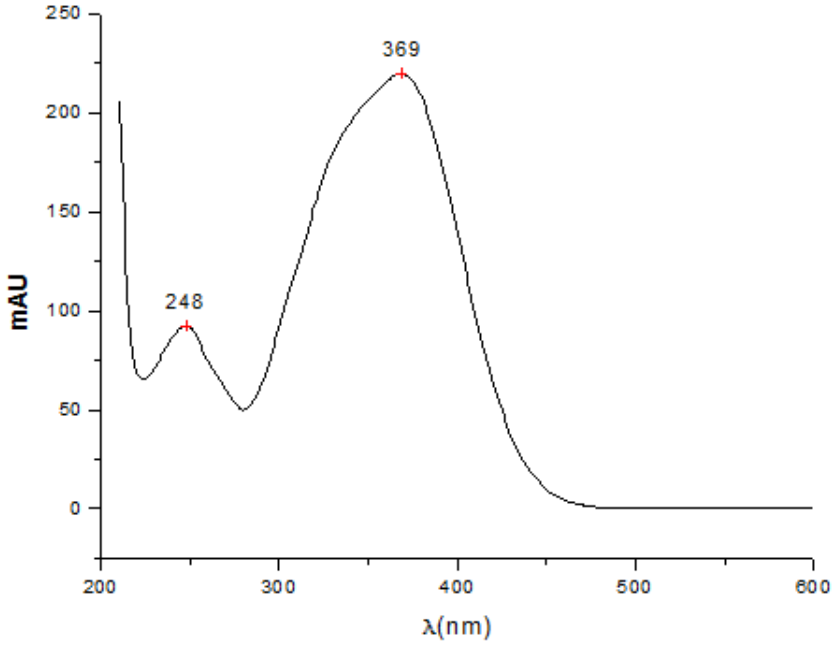

Figure S.62. HPLC-DAD chromatogram of chalcone **20**, MeOH:H_2O (3:1)

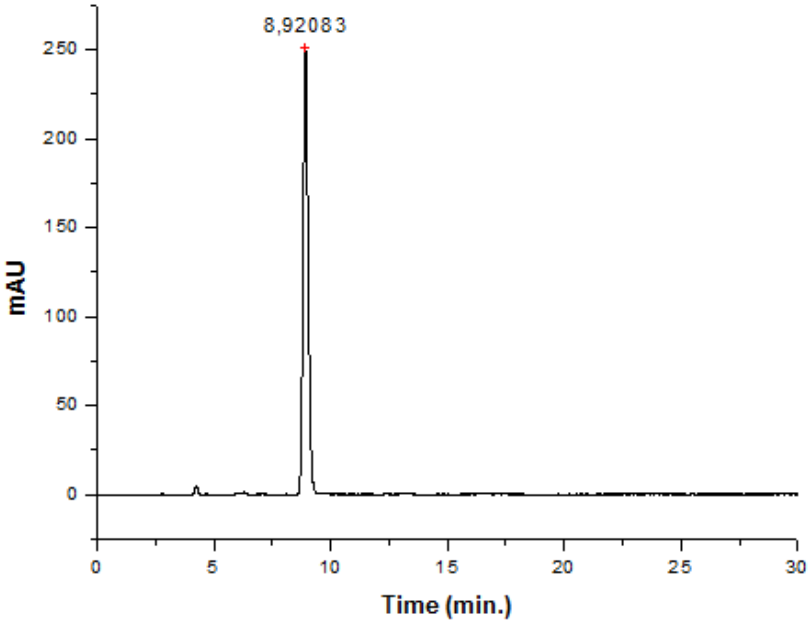

Supplemental Data References

1. Santos MB, Pinhanelli VC, Garcia MAR, Silva G, Baek SJ, França SC, Fachin AL, Marins M, Regasini LO. Antiproliferative and pro-apoptotic activities of 2′- and 4′-aminochalcones against tumor canine cells. Eur J M Chem. 2017;138:884–889.

2. Nazir S, Ansari FL, Hussain T, Mazhar K, Muazzam AG, Qasmi Z-H, Makhmoor T, Noureen H, Mirza B. Brine shrimp lethality assay 'an effective prescreen': Microwave-assisted synthesis, BSL toxicity and 3DQSAR studies-based designing, docking and antitumor evaluation of potent chalcones. Pharmaceutical Biology. 2013;51(9):1091–1103.

3. Jardim GAM, Guimarães TT, Pinto M do CFR, Cavalcanti BC, de Farias KM, Pessoa C, Gatto CC, Nair DK, Namboothiri INN, da Silva Júnior EN. Naphthoquinone-based chalcone hybrids and derivatives: synthesis and potent activity against cancer cell lines. MedChemComm. 2015;6(1):120–130.

4. Chintakrindi AS, Gohil DJ, Kothari ST, Chowdhary AS, Kanyalkar MA. Design, synthesis and evaluation of chalcones as H1N1 Neuraminidase inhibitors. Medicinal Chemistry Research. 2018;27(4):1013–1025.

5. Thirumurthy K, Thirunarayanan G. A facile designed highly moderate craspedia flowerlike sulphated Bi 2 O 3 -fly ash catalyst: Green synthetic strategy for (6 H -pyrido[3,2-b]carbazol-4-yl)aniline derivatives in water. Arabian Journal of Chemistry. 2018;11(4):443–452.

6. Blickenstaff RT, Hanson WR, Reddy S, Witt R. Potential radioprotective agents--VI. Chalcones, benzophenones, acid hydrazides, nitro amines and chloro compounds. Radioprotection of murine intestinal stem cells. Bioorganic & Medicinal Chemistry. 1995;3(7):917–922.

7. Yi F, Peng Y, Song G, Li J. Solid phase synthesis of aminochalcones. Journal of Chemical Research. 2005;2005(5):311–312.

8. Chu W-C, Bai P-Y, Yang Z-Q, Cui D-Y, Hua Y-G, Yang Y, Yang Q-Q, Zhang E, Qin S. Synthesis and antibacterial evaluation of novel cationic chalcone derivatives possessing broad spectrum antibacterial activity. European Journal of Medicinal Chemistry. 2018;143:905–921.

9. Mai CW, Yaeghoobi M, Abd-Rahman N, Kang YB, Pichika MR. Chalcones with electron-withdrawing and electron-donating substituents: Anticancer activity against TRAIL resistant cancer cells, structure–activity relationship analysis and regulation of apoptotic proteins. Eur J Med Chem. 2014;77:378–387.

10. Selvam P, Babu KV, Nanjundan S. Synthesis, characterization and photocrosslinking properties of polyacrylamides having bromo substituted pendant cinnamoyl moieties. European Polymer Journal. 2005;41(1):35–45.

11. Gan X, Wang Y, Hu D, Song B. Design, Synthesis, and Antiviral Activity of Novel Chalcone Derivatives Containing a Purine Moiety. Chinese Journal of Chemistry. 2017;35(5):665–672.

12. Prasad YR, Rani VJ, Rao AS. In vitro Antioxidant Activity and Scavenging Effects of Some Synthesized 4'-Aminochalcones. Asian Journal of Chemistry. 2013;25(1):52–58.

13. Amir M, Ali S, K S. Synthesis and biological evaluation of some new pyrazoline derivative as anti-inflammatory agents. Indian Journal of Chemistry. 2016;55B:478–485.

14. Atla SR, Sistla R, Yejella RP. Study of the Ant-Tumor Activity of Synthetic Pyrido [2,3-*d*] Pyrimidines, Pyrimidines and Corresponding Chalcone Derivatives. 2018;9(9):3804–3814.

Capítulo III

3. Capítulo III - Manuscrito

Bioorganic Chemistry

Synthesis of new antiproliferative agents and HDAC-inhibitors against breast cancer cells

Mariana Bastos dos Santos[1]; Jéssica Gislaine[2]; Aline Renata Pavan[3]; Bruna V. Jardim Perassi[2]; Jean Leandro dos Santos[3]; Débora Aparecida Pires de Campos Zuccari[2]; Luis Octavio Regasini[1*].

[1] *Department of Chemistry and Environmental Sciences, Institute of Biosciences, Humanities and Exact Sciences (IBILCE), São Paulo State University (UNESP), São José do Rio Preto, São Paulo, Brazil;*

[2] *Department of Molecular Biology, Medicine College of São José do Rio Preto (FAMERP), São José do Rio Preto, São Paulo, Brazil;*

[3] *Department of Drugs and Pharmaceutics, School of Pharmaceutical Sciences, São Paulo State University (UNESP), Araraquara, São Paulo, Brazil;*

***Correspondence to:** luis.regasini@unesp.br (L.O.R.); Tel.: 55-17-3221-2362.

ABSTRACT

Breast cancer is the most incident cancer among women, and the treatment to the Triple Negative Breast Cancer (TNBC) subtype has demonstrated the highest recurrence rates, due to the lack of targeted therapy. HDAC inhibitors have been studied as one approach to the treatment to TNBC disease, in association with others cytotoxic agents, including tamoxifen. Herein we described the synthesis of new chalcone-HDAC-inhibitors hybrids (**23a** and **23b**) and analogues (**25**, **27a**–**27c**) as antiproliferative agents against breast cancer cells. Hybrids **23a** and **23b** were synthesized after four steps strategy with14 and 22 % yield. Compounds were tested against HDAC 1, 2, 4, 6 and 11 at 10 μmol L^{-1}. Hybrid **23a** was the most potent hybrid with IC_{50} value of 3.6 μmol L^{-1} against HDAC2. Analogue **27c** was the most potent compound against HDAC2 with IC_{50} value of 0.15 μmol L^{-1}, it was as potent as suberanilohydroxamic acid (SAHA). The most potent inhibitors had their antiproliferative activity evaluated against breast cancer cells. Compound **27c** IC_{50} was 9.10 ± 2.5 and 10.51 ± 1.0 μmol L^{-1} against MCF-7 and MDA-MB-231 respectively. Docking studies with HDAC2 demonstrated the hybrid **23a** and sulfonamide **27c** aligns near to the co-crystallized compound **20Y**, interacting with the same aminoacids (Gly 145, Asp154, Phe155, Phe210). In summary, we found one new analogue (**27c**) as potent as the HDAC inhibitor SAHA and with antiproliferative activity against breast cancer cells, the new hybrid **23a** had selective inhibitory activity against HDAC from class I, and it was active against breast cancer cells. Further studies will allow us to understand the action of the **23a** and **27c** analogue on the induced type of death.

Keywords: breast cancer, hybrids, chalcone, HDAC-inhibitor

3.1.Introduction

Among women cancers, breast cancer is the most diagnosed one and it was responsible for 626 thousands death worldwide in 2018 [1]. Breast cancer is classified in three major subtypes (ER, HER2 and TNBC) according to the presence of membrane receptors as well as in four development stages (I-IV), treatment has been addressed according to the subtype of disease and development stage [2,3]. ER disease subtype is the most common, representing 70 % of all cases. In contrast, the TNBC stage I disease represents 15 % of the breast cancer subtypes, and has the lowest 5-year specific survival rate among the subtypes, 85 %. TNBC stage IV disease has the lowest overall survival, of 1 year, whereas ER and HER2 overall survival of 5 years. [2,4]. TNBC treatment is characterized by the lack of targeted therapy due to its lack of ER, PR and HER2 membrane receptors [2,5,6].

Histone Deacetylase (HDAC) proteins are divided into four classes isoforms in humans [7]. These proteins are overexpressed in cancers, including breast cancer [8]. Mainly class I HDAC proteins overexpression have been reported in breast cancer [9,10], and HDAC 2 overexpression has been correlated to poor prognosis, aggressiveness and metastasis potential on breast cancer [11]. In this context, the development of HDAC inhibitors has been studied as cancers epigenetic treatment approach [12]. Terranova-Barberio and co-authors demonstrated that HDAC inhibitor decreased *in vivo* TNBC tumors and increased the survival of mices [13].

Chalcones ability to induce apoptosis in cancer cells, including breast cancer cells such as ER (MCF-7) and TNBC (MDA-MB-231) have been reported [14–18]. In our previous study we found chalcones upregulated the pro-apoptotic p53 wild type protein on MCF-7 breast cancer cells, as well as inhibited cells viability even in breast cancer cells acidic condition [14]. Due to these chalcones pro-apoptotic actions against breast cancer cells and the HDAC inhibitors action on TNBC in association with others cytotoxic compounds [19-21], we used the hybridization, an useful medicinal chemistry tool, to design new hybrids of chalcones and HDAC inhibitors [22,23]. We evaluated their action on breast cancer cells, and in HDAC inhibition in comparison with their parental compounds.

We synthesized chalcone-HDAC-inhibitor hybrids and sulfonamide derivatives. Their activity was screened against five HDAC isoforms at 10 μmol L^{-1}, the most potent compounds had their IC_{50} determined against HDAC2. The inhibitors had their cytotoxicity

evaluated against breast cancer cells, including ER (MCF-7 line) and TNBC (MDA-MB-231 line). We also evaluated the interaction with HDAC 2 protein using *in silico* experiments by Maestro® Software. Additionally, we studied *in silico* pharmacokinetics properties of compounds.

3.2.Results and Discussion

2.1. Chemistry

We designed the hybrids (Scheme 1) based on chalcone skeleton and in two HDAC inhibitors [8,24]: *i)* chalcone skeleton: chalcones have been reported as antiproleferative and pro-apoptotic agents against breast cancer cells [25], as well as acting on cancer targets such as, p53 pro-apoptotic protein upregulation [14], accordingly, we used chalcone scaffold, as one hybrid subunit; *ii)* zinc binding domain (ZBD): groups that coordinates with the zinc ion of HDAC proteins in HDAC inhibitors, we used benzamide which is already present in some HDAC inhibitor drugs such as entinostat, benzamide usually is more stable than hydroxamic acids [26]; *iii)* linker domain: to connect the chalcone scaffold to the ZBD, we used sulfonamide and hydrofobic cyclic structure similar to the drug belinostat.

Scheme 1. Design of chalcone-HDAC inhibitor hybrids

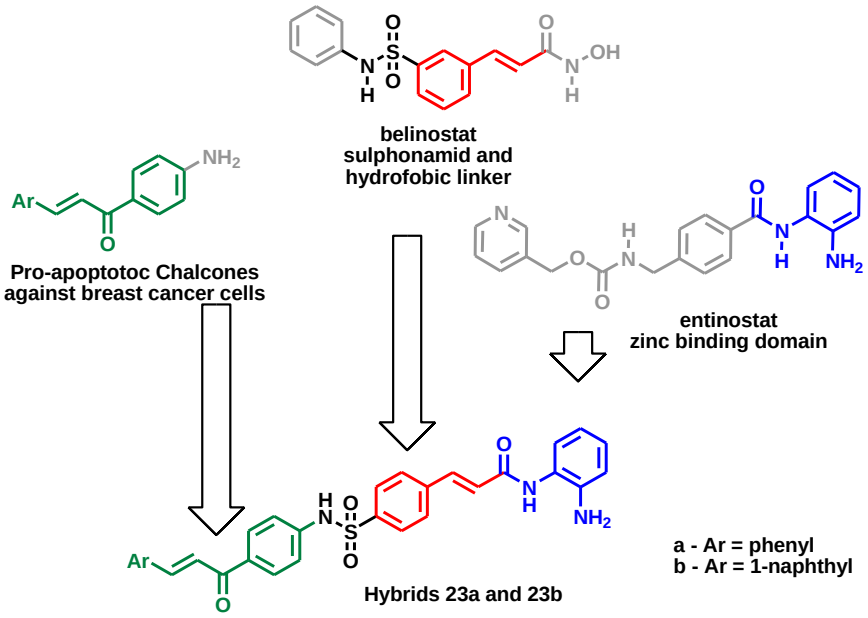

Synthesis of hybrids **23a** and **23b** was performed in four steps (Scheme 2). Chalcones **1** and **19** were obtained from Claisen-Schmidt aldol reaction, using protocols previous by our work [16]. Compound **21** was obtained from cinnamic acid chlorosulfonation in 61 % yield. From the nucleophilic substitution between chalcones with **21**, sulfonamides **22a** and **22b** were synthesized in 30 and 7.6 % yield, respectively. Benzamides **23a** and **23b** were obtained in 14 and 22 % yield from the coupling reaction between carboxilic acids **22a** and **22b** with *o*-phenylenediamine (OPD) using EDAC and HOBt.

Scheme 2. Synthesis of chalcone-HDAC inhibitors hybrids **23a** and **23b**

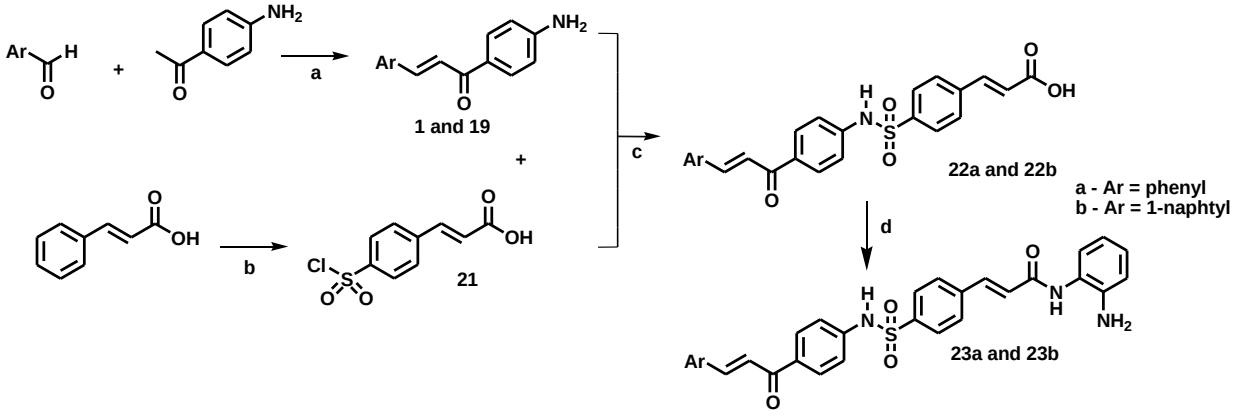

a) NaOH, EtOH [27]; **b)** $HClO_3S$ [28]; **c)** DCM, pyridine [29]; **d)** OPD, EDAC, HOBt, DMF [30].

Structures of hybrids **23a** and **23b** were confirmed by ^{1}H and ^{13}C NMR spectral data analyses. ^{1}H NMR demonstrated four doublets with coupling constants (*J*) of 8.0 Hz each corresponded to the *ortho*-coupling of the pairs of aromatic hydrogens [31]. Four doublets with *J* of 16.0 Hz were attributed to olefinic hydrogens. Two doublet of doublets of doublets with chemical shifts (δ_H) of 6.66 and 6.97 ppm, and two doublet of doublets in $\delta_H \approx 6.85$ and 7.37 ppm were assigned to the benzamide ring hydrogens. Two singlets at $\delta_H \approx 1.3$ and 9.05 ppm were ascribed to amine and amide hydrogens [30].

Hybrids ^{13}C NMR spectra demonstrated two signals in downfield region, at δ_C of 163.0 and 188 ppm, which were ascribed to the carbonyl carbons of α,β-unsatured amide and α,β-unsatured ketone, respectively [30].

We synthesized analogues of hybrids, sulfonamides, to derive structural features related to HDAC inhibition and antiproliferative activity. Synthesis of these compounds is

illustrated on Scheme 3. Intermediates **24a** and **24b** were obtained in 82 and 76 % yields. Analogue **25** was obtained from **24a** coupling with OPD in 21 % yield. Esthers **26a** and **26b** were obtained from Fischer sterification of **24** in 80 and 87 % yield, respectively. From the esthers nucleophilic substitution reactions with hydroxilamine, analogues **27a**–**27c** were obtained in 50, 11 and 83 % yield, respectively.

Scheme 3. Synthesis of analogues **25**, **27a–27c**

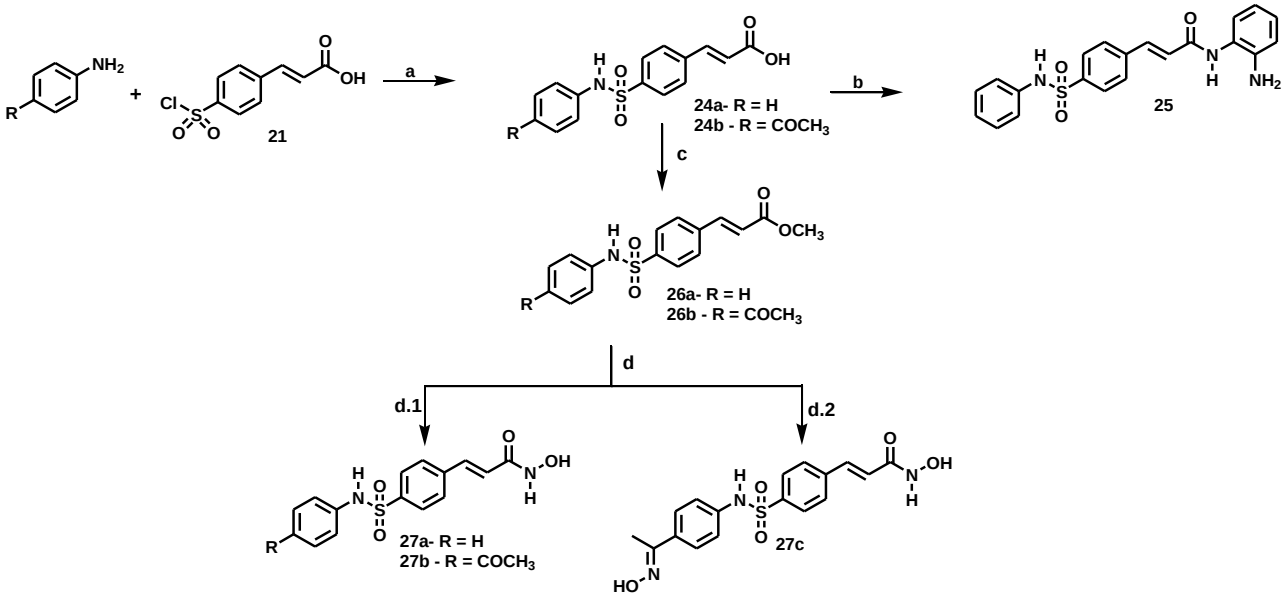

a) DCM, pyridine[29,32]; b) OPD, EDAC, HOBt, DMF [30]; c) MeOH/H_2SO_4, [32]; d) $NH_2OH.HCl$, MeOH, NaOH [33].

Compounds **25**, **27a**–**27c** had their structure confirmed by ^{1}H and ^{13}C NMR spectra analyses. Compounds **27a** and **27b** demonstrated signals at δ_H 9.1 and 10.9 ppm, which were ascribed to the OH and NH hydrogens of hydroxamic acid funtionality. Carbonyl carbon of hydroxamic acid resonance at δ_C 162.5 ppm [33]. ^{13}C NMR spectrum of compound **27c** demonstrated two signals in downfield region: $\delta_C \approx 162.5$ and 152.8 ppm, ascribed to hydroxamic and oxyme carbonyl carbon [34]. Compounds NMR spectra are presented on Supplementary Material.

2.2. Biological Activity

2.2.1. Inhibition of HDAC

HDAC inhibitory activity of compounds was screened at 10 μmol L^{-1} in duplicate and the most potent ones were selected to IC_{50} determination. Compounds were screened

against four HDAC zinc dependent class: HDAC1 and HDAC 2 (class I), HDAC4 (class IIA), HDAC6 (class IIB) and HDAC11 (class IV) (Table 1).

Table 1. Percentages of HDAC inibition at 10 μmol L^{-1}

Compound	Class I		Class IIA	Class IIB	Class IV
	HDAC1	HDAC2	HDAC4	HDAC6	HDAC11
22a	nt	9 [l,m]	nt	nt	nt
22b	nt	13 [j,k,l]	nt	nt	nt
23a	82 ± 0.0 [b]	63 ± 0.0 [d]	10 ± 0.7 [l]	36 ± 0.0 [l]	0.0± 0.0 [n]
23b	28 ± 2.8 [f,g]	19 ± 2.8 [h,i,j]	2 ± 1.4 [m,n]	13 ± 4.2 [k,l]	0.0± 0.0 [n]
25	72 ± 0.7 [c]	63 ± 1.4 [d]	6 ± 0.7 [l,m,n]	24 ± 3.5 [g,h,i]	0.0 ± 0.0 [n]
27a	100 ± 0.0 [a]	100 ± 0.0 [a]	81 ± 0.0 [b]	100 ± 0.0 [a]	25 ± 0.7 [g,h]
27b	100 ± 0.0 [a]	99 ± 0.7 [a]	69 ± 0.0 [c,d]	100 ± 0.0 [a]	17 ± 2.1 [i,j,k]
27c	100 ± 0.0 [a]	100 ± 0.0 [a]	87 ± 0.7 [b]	100 ± 0.0 [a]	26 ± 0.7 [f,g]
Entinostat	nt	100 ± 0.0 [a]	nt	nt	nt
***TSA**	nt	nt	72 ± 0.0 [c]	nt	31 ± 0.7 [e,f]
SAHA	100 ± 0.0 [a]	nt	nt	100 ± 0.0 [a]	nt

nt = not tested; *TSA = tricostatin A

[a–n] Different letters indicate statistically different values according to Anova multiple comparisons test followed by Tuckey post test, $p < 0.05$

Hybrid **23a** was more active against all HDAC than hybrid **23b**, probably due to the hindrance of the bulky naphtyl ring in comparison to phenyl. Among hybrid analogues, compound **27c** was the most potent one against five HDAC enzymes. This compound exhibits oxyme group, oxymes have been reported as HDAC inhibitors [35], and α-oxyme amide have been reported as HDAC isoform selective inhibitors [36], we found **27c** was not selective.

Carboxilic acids, such as valproic acid, have been reported as weak HDAC inhibitors [37], thus we assayed acids **22a** and **22b** against HDAC2. Comparisons among carboxilic acids **22a** and **22b** with the benzamides **23a** and **23b** demonstrate the relevance of strong quelatogenic moiety to HDAC inhibition.

Hybrid **23a** was more potent against HDAC1 and 2 than against HDAC from class II and IV, indicating this compound may be selective, this characteristic is intrinsic to some benzamides [26,38].

The comparison of HDAC inhibition between compounds **23a** and analogue **25** indicates the chalcone subunit maintain similar activity against HDAC2. Against HDAC1,

23a is more potent than **25**, indicating that chalcone subunit confered higher potency. These results confirm the hybridization efficacy.

Comparisons among analogues **25**, **27a**–**27c** indicated that hydroxamic acids leads to more potent compounds (**27a**–**27c**) than the benzamide (**25**). However, **25** is selective to HDAC 1 and 2 in comparison to **27a**–**27c**.

Bouchain and coauthors [39] demonstrated the compound **27a** was active against HDAC1 (IC_{50} = 0.2 μmol L^{-1}), and it was cytotoxic against human colon cancer cells (HCT-116 line, IC_{50} = 3 μmol L^{-1}).

HDAC2 is one of the HDAC most overexpressed in breast cancer, and this is correlated with aggressive features and metastic potential in breast cancer [40, 11]. Therefore, IC_{50} of the most potent hybrid, **23a**, and its analogue, **27c**, were evaluated against HDAC2. We selected **25** to measure IC_{50} against HDAC2 to evaluate its activity in comparison with **23a** (Table 2), because **25** may be considered a direct precursor subunit of **23a**.

Table 2. IC_{50} of selected compounds against HDAC2

Compound	IC_{50} (μmol L^{-1})
23a	3.6
25	3.7
27c	0.15
SAHA	0.14

IC_{50} values of compounds **23a** and **25** were similar, suggesting that against HDAC2, the chalcone subunit did not decrease the activity in the HDAC inhibitor proposed scaffold, whereas **25** corresponds to the subunit of the proposed hybrid without the chalcone subunit. However both were less potent than the HDAC inhibitor SAHA. On the other hand, the oxyme analogue **27c** had similar potency to SAHA against HDAC2, and **27c** was more potent than **23a** and **25**.

Lauffer and coauthors [41] described the activity of the benzamid drug entinostat against HDAC2, with IC_{50} value of 0.45 μmol L^{-1}, in comparison with the benzamids **23a** and **25** IC_{50} results, entinostat would be more potent.

2.2.2. Antiproliferative Activity

The most potent HDAC inhibitor hybrid, **23a**, and all analogues were evaluated regarding their antiproliferative activity against ER (MCF-7), and TNBC breast cancer cells (MDA-MB-231) (Table 3).

Table 3. Compounds IC_{50} (μmol L^{-1}) values against breast cancer cells

Compound	MCF-7 (ER)	MDA-MB-231 (TNBC)
1*	> 100 [a]	60.3 ± 2.9 [c]
22a	69.8 ± 12 [c]	85.9 ± 3.0 [b]
23a	19.5 ± 3.4 [d,e]	30.4 ± 8.8 [d]
25	19.9 ± 1.0 [d,e]	4.60 ± 0.2 [f,g,h]
27a	7.45 ± 0.8 [e,f,g,h]	3.04 ± 0.7 [g,h]
27b	16.1 ± 1.2 [e,f,g]	17.0 ± 4.9 [e,f]
27c	9.10 ± 2.5 [e,f,g,h]	10.5 ± 1.0 [e,f,g,h]
Doxorubicin*	0.61 ± 0.2 [h]	1.03 ± 0.3 [h]

*Antiproliferative activity was described in our previous work [14]

[a–h] Different letters indicate statistically different values according to Anova multiple comparisons test followed by Tuckey post test, $p < 0.05$ [42].

Hybrid **23a** was more active than carboxilic acid analogue, **22a**, against both cell lines, confirming the importance of the benzamide subunit as ZBD on antiproliferative activity against breast cancer cells.

Moreover, analogue **25** which bears sulfonamide and the benzamide in the ZBD, and chalcone **1**, may be considered direct precursor subunits of hybrid **23a**. Therefore evaluating **23a** antiproliferative activities in comparison to its precursors, **23a** was more active than chalcone **1** against both cell lines [14] highlighting the importance of hybridization. However, **23a** had similar activity than **25** against MCF-7, and against TNBC cells (MDA-MB-231) it was less active than **25**.

Analogues **25**, **27a**–**27c** were similarly active against both cell lines, only **25** was more active against MDA-MB-231 than against MCF-7 cells. Analogue **25** has been already reported as an active compound against ovarian cancer cells (OVCAR-3) with IC_{50} of 68 μmol L^{-1} [43].

2.3. Docking Study

In order to understand the inhibitory activity of compounds against HDAC 2, we performed docking studies using Maestro softwares. Protein structure was obtained from Protein Data Bank (PDB) data base under the PDB code 4LY1 for HDAC2. Calculation of docking positions was made by OPLS3 method [44]. We ranked the best position of each compound using docking score (also known as GlydeScore) function (Table 4) [45,46].

The docking method validation was done by the re-docking of the crystallized ligand, **20Y** on HDAC2 and the Root Mean Square Deviation (RMSD) value obtained was 0.46. RMSD values up to 2.0 Å are considered as a reproducible model of the crystal structure [47,48].

Table 4. Docking score of compounds against HDAC2

	HDAC 2 (PDB - 4LY1)
Compound	**Docking Score**
22a	-5.298
22b	-4.684
23a	-11.730
23b	-11.826
25	-10.296
27a	-8.220
27b	-8.079
27c	-8.735
entinostat	-10.544
MGCD-0103	-11.772
SAHA	-7.370
20Y	-12.192

The best positions ranked were evaluated regarding the aminoacids involved in HDAC2 -compound interaction, including comparisons to inhibitor **20Y** (Table 5). In order to access the list of interactions of the docking poses, we used the Discovery Studio Software®. From this software, interactions images are reported on Figure 1. Interactions of the crystallized **20Y** with HDAC2 (4LY1) was reported in the studies of Lauffer [41], and the list of interactions of **20Y**, **23a**, **23b**, **25** and **27c** with HDAC2 is demonstrated on Table 5. Interactions of only **20Y** with HDAC2 in the crystal structure are not demonstrated on Table 5.

Figure 1. Interactions of compounds **23a**, **23b**, **25** and **27c** with HDAC2

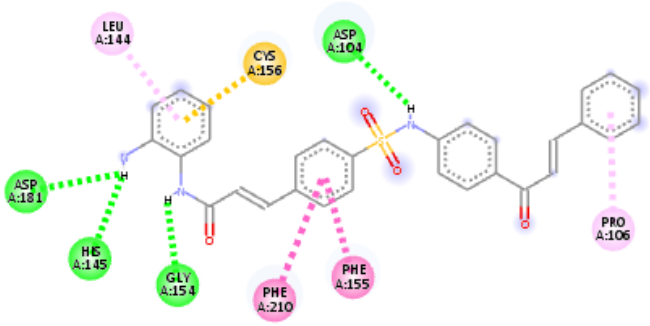

a) 23a

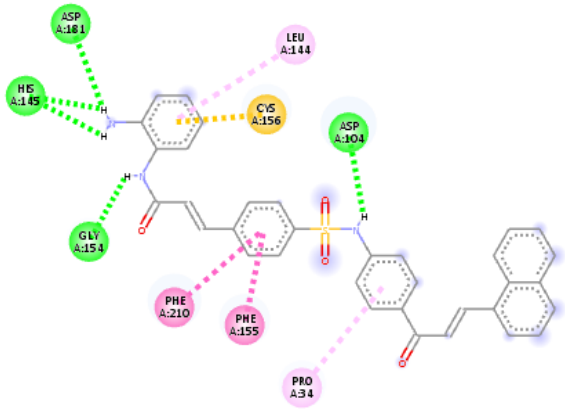

b) 23b

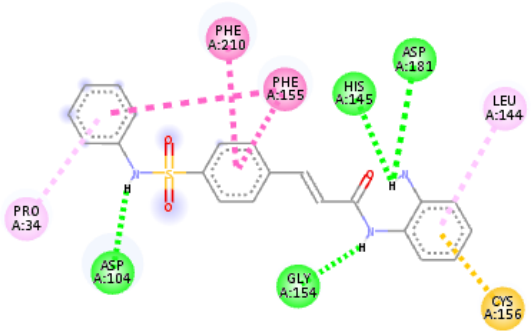

c) 25

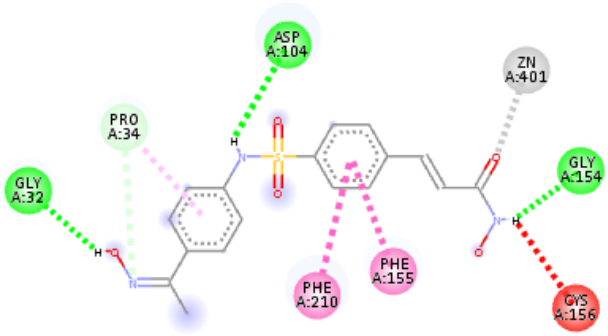

d) 27c

Table 5. Aminoacids interactions of the docking assays

Amino acid	**20Y (Crystal)**	**23a**	**23b**	**25**	**27c**
	Interactions				
His145	H bond*	H bond*	H bond**	H bond*	-
Gly154	H bond*	H bond*	H bond*	H bond*	H bond*
Asp181	H bond*	H bond*	H bond*	H bond*	-
His183	H bond*	-	-	-	-
Tyr308	H bond*	-	-	-	-
Gly32				H bond*	H bond*
Asp104	-	H bond*	H bond*	H bond*	H bond*
Leu144	Hydrophobic	π-alkyl	π-alkyl	π-alkyl	-
Phe155	Hydrophobic	π-π stacked	π-π stacked	π-π stacked**	π-π stacked
Cys156	Hydrophobic	π-sulfur	π-sulfur	π-sulfur	-
Phe210	Hydrophobic	π-π stacked	π-π stacked	π-π stacked	π-π stacked
Pro 34	-	-	π-alkyl	π-alkyl	π-alkyl
Pro106	-	π-alkyl	-	-	-

*H bond - hydrogen bond; ** two interactions

Compounds **23a** and **23b** interacted with 9 aminoacid residues in the binding site, performing 4 hydrogen bonds. Seven of these aminoacids, His145, Gly154, Asp181, Leu144, Cys156, Phe155, Phe210, represent residues that also interacted with **20Y** in the crystal structure reported by Lauffer and coauthors [41]. Chalcone subunit of the hybrid **23a** is outside of the HDAC2 binding site, however, the second phenyl ring from the chalcone subunit of **23a**, which corresponds to the chalcone ring B, interacts with aromatic ring of Pro106 residue, on the rim of HDAC2 binding pocket.

Compounds **23a**, **23b**, **25** and **27c** were superposed with **20Y** in the HDAC2 binding site (Figure 2). Hybrids and their analogues demonstrated chelatogenic benzamide groups are superposed to the inhibitor **20Y** and near to the zinc cofactor, indicating very closely similar HDAC2 interaction to **20Y** mainly in the zinc coordination.

Figure 2. Images of Hybrids **23a**, **23b** and analogues (**25** and **27c**) superposed with **20Y** (cyan)

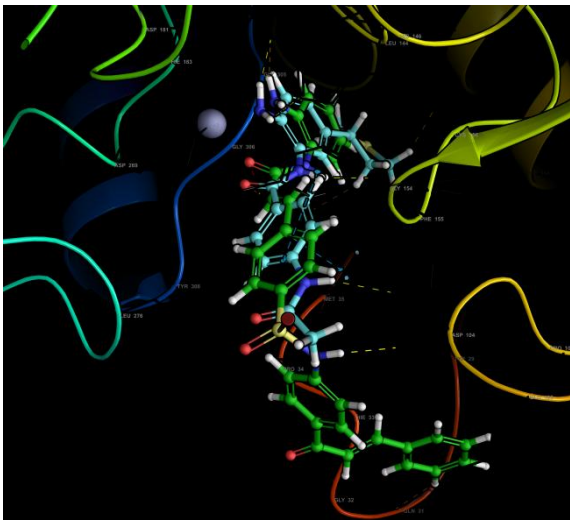

23a

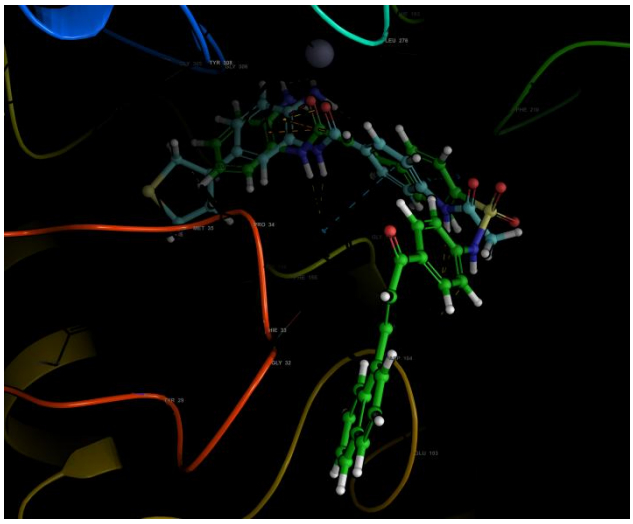

23b

.

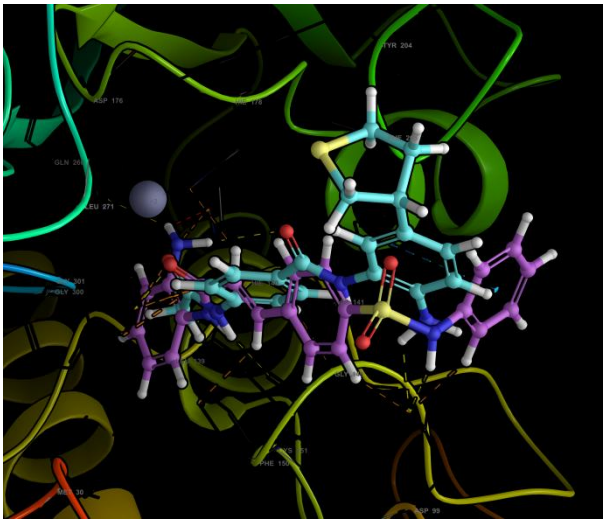

25

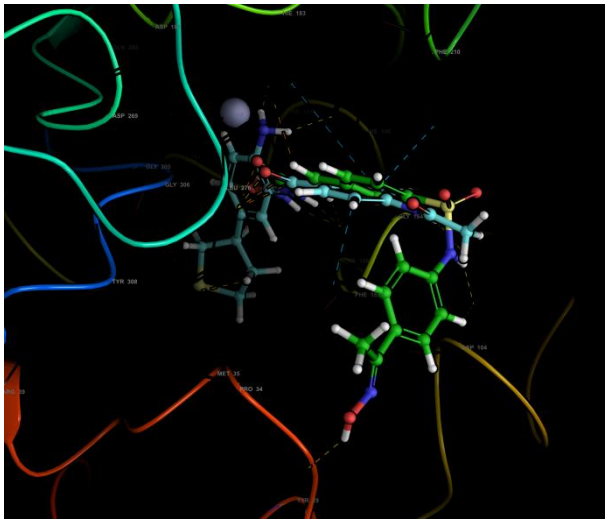

27c

2.4. *In silico* prediction of Pharmacokinetics of Hybrids

Compounds physicochemical properties to achieve the appropriated pharmacokinetics, may be delineated. Pharmacokinetics properties approach in early research phases is recommended to enable successful in drug development [49]. Lipinski developed some recomendations about physicochemical properties of compounds (Lipinski's rule of five), aiming to predict good pharmacokinetics [50]. The rule of five suggests compounds structure should have: *i*) less than 5 hydrogen bonds donors (HBD); *ii*) less than 10 hydrogen bond acceptors (HBA); *iii*) molecular weight (MW) less than 500

g/mol; *iv*) maximum lipophilicity (milog *P*) of 5; *v*) not violate more than one of the previous rules [51].

Veber and coauthors proposed criteria for appropriated biovaibility based on 1100 drug candidates structures: a) rotatable bond (NROBT) ≤ 10; b) topological polar surface area (TPSA) ≤ 140 $Å^2$ [52].

Pharmacokinetics and bioavaibility features were predicted by Molinspiration Tools for Chemoinformatics available online (Table 6) [53]. Additionally the percentage of human intestinal absorption (HIA), was measured by PreAdmet tools available online [54,55]. Hybrids (**23a**, **23b**) respected the physicochemical boundaries delineated by Veber, however they did not respected the Lipinski boundaries indicating they may have restrictions to oral bioavailability based on Lipinski's Violations, MW > 500 and *mi*logP > 5. On the other hand, analogues (**25**, **27a**–**27c**) respected Lipinski and Veber boundaries.

Table 6. Parameters of Lipinki's and Veber's Rules

Cpd	HIA	TPSA ($Å^2$)	*mi*log *P*	MW	HBD	HBA	Lipinski's Violations	NROBT	Veber's Violation
22a	96.85	100.54	4.55	433.49	2	6	0	8	0
22b	96.84	100.54	5.53	483.55	2	6	1	8	0
23a	95.59	118.36	5.54	523.61	4	7	2	9	0
23b	96.79	118.36	6.52	573.67	4	7	2	9	0
25	93.55	101.29	3.67	393.47	4	6	0	6	0
27a	89.94	95.50	2.22	318.35	3	6	0	5	0
27b	90.32	112.57	2.12	360.39	3	7	0	6	0
27c	84.36	128.09	2.18	375.41	4	8	0	6	0

Cpd = compound

Human intestinal absorption (HIA) is a relevant process in compounds pharmakinetics determination. Yee and coauthors [56] classified compounds according to their percentage of HIA in poorly absorbed (0–20%), moderately absorbed (20–70%) and well absorbed (70–100%), as demonstrated in Table 6, all synthesized compounds will be well absorbed.

3.3.Materials and Methods

3.1. Chemistry

Reagents and solvents were purchased from Merck®. Reactions were monitored by thin-layer chromatography (TLC - aluminum plates with fluorescent indicator Supelco®). Structure of compounds were confirmed by ^{1}H and ^{13}C NMR spectral data analyses, obtained in Bruker Avance III (14 T and 9.4 T) equipments using dimethyl sulfoxide (DMSO-d_6) and acetone- d_6. NMR spectra values were represented as chemical shifts (δ in ppm), coupling constants (J) and multiplicities: s, singlet; d, dublet; dd, doublet of doublets; ddd, doublet of doublet of doublets; and m = multiplet. Melting points (m.p.) were measured using Tecnopon PFM-II apparatus. Mass spectrum was obtained in UHR TOF - Bruker in configuration ESI-IT in negative ionization mode.

3.1.1. Preparation of Hybrids 23a and 23b

Synthetic route to hybrids **23a** and **23b** was stablished using a four step strategy (Scheme 1). Chalcones **1** and **19** were prepared (step a) according to the previous reported studies by our group [14].

3.1.1.1. Compound 21

Compound **21** was synthesized by cinnamic acid chlorosulfonation reaction (Scheme 2, step b). 55 mL of chlorosulfonic acid was stirred with 81 mmol of cinnamic acid at 15 ºC for 3 h at room temperature for 3 days [28]. The mixture was poured in crude ice and the white solid precipitated was filtered and washed with water, dried at room temperature, and recrystallized using ethyl acetate. White crystals (61 %). **^{1}H NMR (600 MHz, DMSO-d_6) δ (mult., J)**: 7.66 (d, J = 8.3 Hz, H-3 and H-5), 7.62 (d, J = 8.3 Hz, H-2 and H-6), 7.57 (d, J = 16.0 Hz, H-7), 6.53 (d, J = 16.0 Hz, H-8). **^{13}C NMR (150 MHz, DMSO-d_6) δ:** 168.0 (C-9), 149.8 (C-7), 143.8 (C-4), 134.8 (C-1), 128.3 (C-3 and C-5), 126.5 (C-2 and C-6), 120.1 (C-8).

3.1.1.2. Carboxylic acids 22a and 22b

Compound **22a** was synthesized from the reaction between **21** and chalcone **1** according to the procedure described by Chao and coauthors [29]. Chalcone **1** (6.5 mmol) was solubilized in 65 mL of pyridine, with **21** (6.5 mmol) suspended in 80 mL dichloromethane (DCM), and stirred at 40 °C for 18 h. The mixture was evaporated and the residue was

precipitated in HCl solution (6 mol/L), filtered and washed with water. Crude product was purified over silica column chromatography, using chloroform and methanol. Light yellow solid (30 %), m.p = 269–271 °C. **^{1}H NMR (600 MHz, DMSO-d_6) δ (mult., J):** 8.07 (d, J = 8.9 Hz, H-3' and H-5'), 7.89 (d, J = 15.5 Hz, H-9'), 7.89 (d, J = 8.9 and 7.8 Hz, H-12' and H-14'), 7.86 (d, J = 7.7 Hz, H-3 and H-5), 7.85 (d, J = 8.9 Hz, H-11' and H-15'), 7.69 (d, J = 15.6 Hz, H-8'), 7.60 (d, J = 16.1 Hz, H-7), 7.45 – 7.46 (m, H-13') 7.45 (d, J = 7.0 Hz, H-2 and H-6), 7.27 (d, J = 8.8 Hz, H-2' and H-6'), 6.65 (d, J = 16.1 Hz, H-8). **^{13}C (151 MHz, DMSO-d_6) δ:** 188.0 (C-7'), 167.6 (C-9), 144.0 (C-7), 142.8 (C-1') 142.2 (C-9'), 140.5 (C-4), 139.3 (C-1), 135.2 (C-10'), 133.1 (C-13'), 131.0 (C-4'), 130.8 (C-3' and C-5'), 129.5 (C-12' and C-14'), 129.4 (C-3 and C-5), 129.3 (C-2 and C-6), 127.7 (C-11' and C-15'), 123.1 (C-8'), 122.3 (C-8), 118.6 (C-2' and C-6').

Compound **22b** was synthesized from the reaction between **21** and chalcone **19** under similarly conditions to **22a** synthesis. Crude **22b** was purified by preparative Thin Layer Chromatography using chloroform and methanol as solvents. Light yellow solid (8 %), m.p. = 270–272 °C. **^{1}H NMR (600 MHz, DMSO-d_6) δ_H (mult J):** 8.49 (d, J = 15.3 Hz, H-9'), 8.26 (d, J = 8.3 Hz, H-11'), 8.20 (d, J = 7.2 Hz, H-8'), 8.06 (d, J = 7.9 Hz, H-3 and H-5), 8.05 (d, J = 7.2 Hz, H-17'), 8.02 (d, J = 7.6 Hz, H-12'), 7.93 (d, J = 15.3 Hz, H-8'), 7.85 (m, H-3', H-5' and H-16'), 7.65 (ddd, J = 8.4, 6.8 and 1.4 Hz, H-15'), 7.61 (d, J = 8.0 Hz, H-2 and H-6), 7.59 (d, J = 16.1 Hz, H-7), 7.22 (d, J = 8.6 Hz, H-2' and H-6'), 6.63 (d, J = 16.0 Hz, H-8). **^{13}C NMR (150 MHz, DMSO-d_6) δ:** 187.6 (C-7'), 167.7 (C-9), 142.3 (C-7), 139.4 (C-9'), 133.8 (C-1'), 131.9 (C-4), 131.6 (C-1), 131.1 (C-10'), 130.8 (C-3' and C-5'), 130.5 (C-10'), 129.3 (C-3 and C-5), 127.7 (C-2 and C-6), 127.6 (C-2' and C-6'), 127.4 (C-18'), 126.8 (C-14'), 126.2 (C-13'), 126.0 (C-16'), 125.6 (C-15'), 125.0 (C-12'), 123.5 (C-17'), 122.9 (C-11'), 118.9 (C-8'), 118.7 (C-8).

3.1.1.3. Hybrids 23a and 23b

Compound **23a** was prepared by the reaction of **22a** with *o*-phenylenediamine (OPD) according to the procedures described by Kortelainen and coauthors [30] with minor modifications. 0.95 mmol of **22a** was solubilized in 23 mL of THF and was stirred with 2.4 mmol of *N*-(3-dimethylaminopropyl)-*N*'-ethylcarbodiimide hydrocloride (EDAC) at 0 °C for 40 min. In this mixture 2.19 mmol of OPD was added, followed by the addition of triethylamine (TEA, 2.4 mmol), and it was stirred at room temperature for 24 h. The

mixture was dried, solubilized in dichloromethane, washed with sodium bicarbonate (1 mol/L), HCl (1 mol/L) and water. The residue was dried at room temperature. Crude product was purified by preparative Thin Layer Chromatography using chloroform and acetone as solvents. Light yellow solid (14 % yield), m.p. = 126–128 °C. **^{1}H NMR (600 MHz, acetone-d_6) δ (mult., J):** 9.05 (s, NH), 8.09 (d, J = 8.7 Hz, H-3 and H-5), 7.95 (d, J = 8.4 Hz, H-11' and H- 15'), 7.85 (d, J = 15.6 Hz, H-9'), 7.87 – 7.77 (m, H-2, H-6, H-3' and H-5'), 7.75 (d, J = 15.6 Hz, H-8'), 7.65 (d, J = 15.7 Hz, H-7), 7.49 – 7.43 (m, H-12' – H-14'), 7.41 (d, J = 8.7 Hz, H-2' and H-6'), 7.37 (dd, J = 7.9 and 1.3 Hz, H-6''), 7.08 (d, J = 15.7 Hz, H-8), 6.97 (ddd, J = 8.0, 7.8 and 1.3 Hz, H-4''), 6.66 (ddd, J = 7.9, 7.8 and 1.2 Hz H-5''), 6.85 (dd, J = 8.0 and 1.2 Hz, H-3''), 1.30 (s, NH2). **^{13}C (150 MHz, acetone-d_6) δ:** 187.5 (C-7'), 163.0 (C-9), 143.5 (C-1'), 141.9 (C- 7), 139.7 (C-2''), 138.2 (C-4), 135.2 (C-1), 133.3 (C-10'), 130.4 (C-13'), 130.1 (C-3' and C-5'), 128.9 (C-12' and C-14'), 128.6 (C-3 and C-5), 128.3 (C-2 and C-6), 127.7 (C-11', C-15' and C-4'), 126.2 (C-4''), 125.2 (C-1''), 124.8 (C-6''), 124.3 (C-8'), 121.7 (C-5''), 118.9 (C-2' and C-6'), 117.3 (C-8), 116.9 (C-3'').

Synthesis of **23b** was carried out by the coupling of **22b** with OPD in a similar procedure described to **23a** synthesis and purification. Yellow solid (22 %), m.p. = 102–106 °C. **^{1}H NMR (600 MHz, DMSO-d_6) δ_H (mult. J):** 9.48 (s, N<u>H</u>), 8.52 (d, J = 15.4 Hz, H-9'), 8.27 (d, J = 8.3 Hz, H-11'), 8.21 (d, J = 7.2 Hz, H-13'), 8.13 (d, J = 8.8 Hz, H-3 and H-5), 8.07 (d, J = 8.2 Hz, H-17'), 8.02 (d, J = 7.6 Hz, H-12'), 7.95 (d, J = 15.5 Hz, H-8'), 7.93 (d, J = 9.1 Hz, H-2 and H-6), 7.82 (d, J = 8.5 Hz, H-3' and H-5'), 7.66 (ddd, J = 8.4, 6.8, 1.4 Hz, H-14'), 7.63 (d, J = 7.5 Hz, H-14'), 7.60 (d, J = 7.8 Hz, H-16'), 7.58 (d, J = 15.8 Hz, H-7), 7.34 (m, H-6''), 7.32 (d, J = 8.8 Hz, H-2' and H-6'), 7.00 (d, J = 15.8 Hz, H-8), 6.93 (ddd, J = 8.0, 7.8 and 1.2, H-4''), 6.76 (dd, J = 8.0, 1.3 Hz, H-3''), 6.56 (ddd, J = 8.2, 7.8 and 1.3, H-5''), 1.24 (s, N<u>H$_2$</u>). **^{13}C NMR (150 MHz, DMSO-d_6) δ:** 187.9 (C-7'), 163.4 (C-9), 142.8 (C-2''), 142.1 (C-7), 140.0 (C-1'), 139.9 (C-4), 138.0 (C-19'), 133.8 (C-18'), 131.8 (C-14'), 131.6 (C-13'), 131.3 (C-4'), 130.8 (C-3' and C-5'), 129.3 (C-16'), 128.9 (C-3 and C-5), 127.9 (C-2 and C-6), 127.7 (C-15'), 126.8 (C-12'), 126.4 (C-4''), 126.2 (C-2' and C-6'), 126.1 (C-17'), 125.2 (C-11'), 124.9 (C-1''), 123.7 (C-6''), 123.5 (C-8'), 118.7 (C-8), 116.7 (C-5''), 116.5 (C-3'').

3.1.2. Preparation of analogues 25, 27a–27c

These analogues were prepared from chemical strategy from two or three steps (Scheme 2).

3.1.2.1. Carboxylic acids 24a and 24b

Compound **24a** was obtained from the nucleophic substitution reactin between aniline and **21** (Scheme 3, step a) 4.0 mmol of aniline was solubilized in piridine, and 4.0 mmol of **21** suspenden in DCM was added in the reaction and stirred for 3 h at 40 °C. The mixture was evaporated and the residue was precipitated in HCl solution (6 mol/L), filtered and washed with water. Crude product was recrystallized on ethanol. Light pink solid (82 %) **^{1}H NMR (600 MHz, DMSO-d_6) δ (mult., J):** 10.38 (s, NH), 7.85 (d, J = 8.4 Hz, H-3 and H-5), 7.75 (d, J = 8.4 Hz, H-2 and H-6), 7.59 (d, J = 16.0 Hz, H-7), 7.24 (dd, J = 7.8 and 7,9 Hz. H-3' and H-5'), 7,10 (d, J = 7.9 Hz, H-2' and H-6'), 7.04 (dd, J = 7.3 and 7.3 Hz, H-4'), 6.64 (d, J = 16.0 Hz, H-8). **^{13}C NMR (150 MHz, DMSO-d_6) δ:** 167.6 (C-9), 142.3 (C-7), 140.7 (C-1'), 138.9 (C-4), 137.9 (C-1), 129.7 (C-3' and C-5'), 129.3 (C-3 and C-5), 127.6 (C-2 and C-6), 124.7 (C-4'), 122.9 (C-8), 120.6 (C-2' and C-6').

Compound **24b** was obtained from the nucleophilic substitution reaction between 4-aminoacetophenone and **21** in similar conditions to obtaintion of **24a**. Light pink solid (76 %), m.p. = 286–289 °C. **^{1}H NMR (400 MHz, DMSO-d_6) δ (mult., J):** 10.96 (s, NH), 7.87 (d, J = 8.4 Hz, H-3 and H-5), 7.86 (d, J = 8.0 Hz, H-3' and H-5'), 7.84 (d, J = 8.4 Hz, H-2 and H-6), 7.59 (d, J = 16.0 Hz, H-7), 7.23 (d, J = 8.7 Hz, H-2' and H-6'), 6.63 (d, J = 16.0 Hz, H-8), 2.47 (s, CH_3-8'). **^{13}C NMR (150 MHz, DMSO-d_6) δ:** 197.0 (C-7'), 167.6 (C-9), 142.5 (C-7), 142.2 (C-1'), 140.4 (C-4), 139.3 (C-1), 132.6 (C-4'), 130.4 (C-3' and C-5'), 129.5 (C-3 and C-5), 127.7 (C-2 and C-6), 123.1 (C-8), 118.5 (C-2' and C-6'), 26.9 (C-8').

3.1.2.2. Analogue 25

Compound **25** was prepared by the coupling of **24a** with OPD (Scheme3, step d). 0.95 mmol of **24a** was solubilized in 23 mL of THF and was stirred with 2.4 mmol of EDAC at 0 °C for 40 min. In this mixture 2.19 mmol of OPD was added, followed by the addition of 2.4 mmol TEA, and it was stirred at room temperature for 24 h. The mixture was dried, solubilized in DCM, washed with sodium bicarbonate (1 mol/L), HCl (1 mol/L) and water. The residue was dried at room temperature. Crude product was purified by preparative

Thin Layer Chromatography using chloroform and methanol. Light yellow solid (21 %). **^{1}H NMR (600 MHz, acetone-d_6) δ (mult., *J*):** 9.06 (s, NHCO), 7.83 (d, *J* = 8.3 Hz, H-3 e H-5), 7.77 (d, *J* = 8.3 Hz, H-2 e H-6), 7.65 (d, *J* = 15.6 Hz, H-7), 7.37 (d, *J* = 7.6 Hz, H-6''), 7.23 (d, *J* = 7.6, H-2' e H-6'), 7.26 (dd, *J* = 7.6 e 7.3, H-3' e H-5'), 7.10 – 7.04 (m, H-4'), 7.07 (d, *J* = 15.7 Hz, H-8), 6.98 (dd, *J* = 7.7 e 7.3 Hz, H-4''), 6.85 (d, *J* = 7,7 Hz, H-3''), 6.66 (dd, *J* = 7.6 e 7.3 Hz, H-5''). **^{13}C NMR (150 MHz, acetone-d_6) δ:** 163.1 (C-9), 141.9 (C-7), 140.4 (C-2''), 139.5 (C-4), 138.3 (C-1), 137.8 (C-1'), 129.1 (C-3' e C-5'), 128.2 (C-4''), 128.1 (C-3 e C-5), 127.7 (C-2 e C-6), 126.2 (C-1''), 125.1 (C-6''), 124.8 (C-5''), 124.6 (C-8), 121.0 (C-2' e C-6'), 117.3 (C-4'), 116.9 (C-3'').

3.1.2.3. Esthers 26a and 26b

Compound **26a** was obtained from the sterification of **24a**. 18 mmol of compound **24a** was solubilized in 180 mL of methanol and 9 mL of sulfuric acid for 36 h [32]. The mixture was dried, the precipitate was washed with cold water and dried at room temperature. Light pink crystals (80 %) **^{1}H NMR (600 MHz, DMSO-d_6) δ (mult., *J*):** 10.4 (s, NH), 7.89 (d, *J* = 8.5 Hz, H-3 and H-5), 7.76 (d, *J* = 8.5 Hz, H-2 and H-6), 7.67 (d, *J* = 16.1 Hz, H-7), 7.24 (dd, *J* = 9.0 and 8,6 Hz, H-3' and H-5'), 7.10 (dd, *J* = 8.6, 1.0 Hz, H-2' and H-6'), 7.03 (dd, *J* = 9.0 and 1.7 Hz, H-4'), 6.76 (d, *J* = 16.1 Hz, H-8), 3.73 (s, OCH_3). **^{13}C NMR (150 MHz, DMSO-d_6) δ:** 166.7 (C-9), 143.0 (C-7), 140.9 (C-1'), 138.6 (C-4), 137.9 (C-1), 129.7 (C-3' and C-5'), 129.4 (C-3 and C-5), 127.6 (C-2 and C-6), 124.8 (C-4'), 121.4 (C-8), 120.6 (C-2' and C-6'), 52.2 (OCH_3).

Compound **26b** was obtained from the sterification with methanol of **24b**. The reaction procedures were similar to synthesis of **26a**. Light pink solid (87 %), m.p. = 230–233 °C. **^{1}H NMR (400 MHz, DMSO-d_6) δ (mult., *J*):** 10.99 (s, NH), 7.91 (d, *J* = 8.5 Hz, H-3 and H-5), 7.85 (d, *J* = 8.6 Hz, H-3' and H-5'), 7.84 (d, *J* = 8.8 Hz, H-2 and H-6), 7.66 (d, *J* = 16.1 Hz, H- 7), 7.23 (d, *J* = 8.8 Hz, H-2' and H-6'), 6.75 (d, *J* = 16.1 Hz, H-8), 3.72 (s, O$\underline{C}H_3$), 2.46 (s, $C\underline{H}_3$-8'). **^{13}C NMR (150 MHz, DMSO-d_6) δ:** 197.1 (C-7'), 166.7 (C-9), 142.8 (C-7), 142.4 (C-1'), 140.6 (C-4), 139.0 (C-1), 132.6 (C-4'), 130.4 (C-3' and C-5'), 129.6 (C-3 and C-5), 127.7 (C-2 and C-6), 121.6 (C-8), 118.5 (C-2' and C-6'), 52.2 (O$\underline{C}H_3$), 26.9 (C-8').

3.1.2.4. Analogues 27a – 27c

Compound **27a** was obtained from the nuclephilic substitution reaction of **26a** with hydroxilamine [33]. 1.5 mmol of hydroxylamine hydrocloride was stirred in 20 mL solution of sodium hydroxide in anhydrous methanol at 0 °C and inert atmosphere during 20 minutes. **26a** (0.5mmol) was added and the reaction was maintained in these conditions during 4 h. After conversion, the mixture was acidified to pH 7 with HCl solution. The precipitate was filtered and washed with water, washed with cold ethyl ether and dried. Yellow solid (50 %), m.p. = 142–145 °C. **^{1}H NMR (600 MHz, DMSO-d_6) δ (mult., J):** 10. 9 (s, NHS), 10.4 (s, NH), 9.18 (s, OH), 7.76 (d, J = 8.5 Hz, H-3 and H-5), 7.72 (d, J = 8.5 Hz, H-2 and H-6), 7.46 (d, J = 15.8 Hz, H-7), 7.23 (dd, J = 7.8 and 7.7 Hz, H-3' and H-5'), 7.09 (d, J = 7.6 Hz, H-2' and H-6'), 7.03 (m, H-4'), 6.55 (d, J = 15.8 Hz, H-8). **^{13}C NMR (150 MHz, DMSO-d_6) δ:** 162.5 (C-9), 140.1 (C-7), 139.5 (C-1'), 138.0 (C-4), 137.0 (C-1), 129.7 (C-3 and C-5), 128.6 (C-3' and C-5'), 127.8 (C-2 and C-6), 124.7 (C-4'), 122.7 (C-7), 120.6 (C-2' and C-6').

Compound **27b** was obtained from nuclephilic substitution reaction of **26b** with hydroxilamine [33]. Reactions conditions were similar to synthesis of **27a**. Light yellow solid (11 %), m.p. = 183–185 °C. **^{1}H NMR (400 MHz, DMSO-d_6) δ (mult., J):** 11.12 (s, NHS), 10.92 (br s, NHO), 9.18 (br s, OH), 7.84 (d, J = 7.1 Hz, H-2/H-3 and H-5/H-6), 7.74 (d, J = 8.3 Hz, H-3' and H-5'), 7.46 (d, J = 15.6 Hz, H-7), 7.21 (d, J = 8.4 Hz, H-2' and H-6'), 6.55 (d, J = 15.6 Hz, H-8), 2.46 (s, C$\underline{H}_3$-8'). **^{13}C NMR (150 MHz, DMSO-d_6) δ:** 197.0 (C-7'), 162.5 (C-9), 142.6 (C-7), 139.9 (C-1'), 136.9 (C-4), 132.5 (C-1''), 130.3 (C-3' and C-5'), 128.8 (C-3 and C-5), 127.8 (C-2 and C-6), 122.9 (C-8), 118.5 (C-2' and C-6'), 26.9 (C-8').

Compound **27c** was obtained from nuclephilic substitution and addition reactions of **26a** with hydroxilamine [33]. 5 mmol of hydroxylamine hydrocloride was stirred in 20 mL solution of sodium hydroxide in anhydrous methanol at 0 °C and inert atmosphere during 20 minutes. **26a** (0.5mmol) was added and the reaction was maintained in these conditions during 4 h. After conversion, the mixture was acidified to pH 7 with HCl solution. The precipitate was filtered and washed with water. Yellow solid (83 %), m.p. = 166–169 °C. **^{1}H NMR (600 MHz; DMSO-d_6) δ (mult., J):** 11.00 (s, =NO$\underline{H}$), 7.76 (d, J = 8.4 Hz, H-3/H-5), 7.67 (d, J = 8.4, H-2/H-6), 7.44 (d, J = 15.8, H-7); 7.44 (d, J = 8.7, H-3'/H-5'), 7.02

(d J = 8.7, H-2'/H-6'), 6.52 (d, J = 15.8 Hz, H-8), 2.04 (s, 8'-C$\underline{H}_3$). **^{13}C NMR (150 MHz; DMSO-d_6) δ:** 162.6 (C-9), 152.8 (C-7'), 142.1 (C-4), 141.6 (C-1'), 138.7 (C-1), 131.1 (C-4'), 128.4 (C-2 and C-6), 127.6 (C-3 and C-5), 126.7 (C-3' and C-5'), 122.2 (C-8), 120.1 (C-2' and C-6'), 11.8 (C-8').

3.2. Biological Evaluation

3.2.1. HDAC Proteins Inhibition

HDAC proteins inhibition assays were performed with HDAC1, 2, 4, 6, 11, in BPS Bioscience enterprise (http://bpsbioscience.com/) under the following studies number: SPSU/190503 and SPSU/190528 by fluorogenic assays. Compounds were solubilized in DMSO, and assayed at DMSO final concentration of 10 %. Enzymatic reactions were performed in duplicates at 37 °C during 30 minutes, these reactions.were conducted in a 50 μL mixture containing HDAC assay buffer, 5 μg BSA, specific HDAC substrates, HDAC enzyme and respective compounds [57].

Human HDAC enzymes catalog numbers, and the mass used in assays were: HDAC1 - 50051, 7.8 ng; HDAC2 - 50052, 15 ng; HDAC4 - 50004, 0.3 ng; HDAC6 - 50006, 20 ng and HDAC11 - 50011, 60 ng. Substrates to HDAC1, 2 and 6 was 10 μmol L^{-1} of a fluorogenic, acetylated peptide BPS substrate 3 (catalog number 50037). And substrates to HDAC4 and 11 was 2 μmol L^{-1} fluorogenic, acetylated peptide substrate for class 2a (catalog number 50040).

After enzymatic reations, 50 μL of 2 × HDAC Developer was add to the wells for the HDAC enzymes and the plate was incubated at room temperature for 15 minutes. Fluorescence intensity was measured at excitation of 360 nm and emission of 460 nm in Tecan Infinite M100 microplate reader.

3.2.2. Antiproliferative Assays

Breast cancer cells from American Type Culture Collection (ATCC) MCF-7 (HTB-22) and MDA-MB-231 (HBT-26) were cultivated in Dubelcco Eagle Media (DMEM, Gibco) high glucose supplemented with 10 % fetal bovine sorum (FBS, LGC), penicillin-streptomycin (100 μg/mL, Merck) at 37 °C in humidified atmosphere. The antiproliferative activity of compounds was evaluated using MTT assay [14,58]. MCF-7 and MDA-MB-231 cells were seeded in a 96 well plate at concentrations of 1.0×10^4 and 2.5×10^4 cells per well, respectively, cultivated during 24 h, and treated with compounds during 48 h.

Compounds concentration varied from 1.25 to 80 μmol L^{-1}. After treatment with compounds, the cultured media was removed, the cells were washed with PBS solution, and incubated with MTT solution (1 mg/mL) during 40 min. MTT solution was replaced by dimethylsulfoxide (DMSO) to solubilization of formazan crystals. Absorbance was measured in 562 nm in Thermoplate TP reader. Concentration-response curves were ploted to determination of the IC_{50} values.

3.3. Docking Studies

Compounds had their molecular modeling calculations assayed on HDAC2 crystal structure obtained from Protein Data Bank (PDB), under the ID number 4LY1, with resolution of 1.57 Å.

Protein structure was imported to Maestro® software and prepared as the following steps: *i*) water molecules removal; *ii*) hydrogen atoms addition; *iii*) filling of missing aminoacids lateral chains; *iv*) protein energy minimization using OPLS3 force field. The protein interaction box (grid) was defined in the active site of HDAC proteins based on the place of the co-crystallized ligand, with dimensions of 10Å × 10Å × 10Å. HDAC inhibitors structures (compounds **23a**, **23b**, **25**, **27a**–**27c**), and ligand reference compounds (**20Y**) were prepared using Ligand Preparation function (LigPrep) to minimize the force field energy OPLS3 of the ionization states at pH 7 ± 2 [59]. Docking simulation was carried out using the prepared structures in Glide software using OPLS3 method [42]. In order to validate the procedure, compound **20Y** was re-docked on HDAC2 (4LY1), and the *Root Mean Square Deviation* (RMSD) value was obtained [47].

3.4. Pharmacokinetics *in silico* predictions of hybrids

Investigations about the pharmacokinetics of compounds were performed by *in silico* methods using Molinspiration and PreADMET, online softwares [53,55]. Values of log $P_{o/w}$, MW, HBA, HBD and NROTB were calculated and they evaluated according to the Lipinski's and Veber's pharmacokinetics parameters.

3.4.Conclusion

Two new hybrids with benzamide group as ZBD, and four analogues were synthesized and evaluated against HDAC proteins isoforms from different classes (I, IIA, IIB and IV). Hybrid **23a** was the most potent hybrid, with IC_{50} value of 3.6 μmol L^{-1}

against HDAC2. We found the analogue **27c** was active against HDAC1, 2, 4 and 6, and it was a potent inhibitor of HDAC2, with IC_{50}value similar to SAHA.

Antiproliferative assays demonstrated **23a** was more active than the chalcone precursor against breast cancer cells (MCF-7 and MDA-MB-231), and that the analogue **27c** also demonstrated antiproliferative activity against these cells.

Docking studies with HDAC2 protein structure demonstrated that hybrids and analogues aligns near to the co-crystallized compound **20Y**, and interacts with similar aminoacids.

3.5.References

[1] F. Bray, J. Ferlay, I. Soerjomataram, R.L. Siegel, L.A. Torre, A. Jemal, Global cancer statistics 2018: GLOBOCAN estimates of incidence and mortality worldwide for 36 cancers in 185 countries, CA-Cancer J. Clin. 68 (2018) 394–424. doi:10.3322/caac.21492.

[2] A.G. Waks, E.P. Winer, Breast Cancer Treatment: A Review, JAMA. 321 (2019) 288. doi:10.1001/jama.2018.19323.

[3] M. Chavez-MacGregor, E.A. Mittendorf, C.A. Clarke, D.Y. Lichtensztajn, K.K. Hunt, S.H. Giordano, Incorporating Tumor Characteristics to the American Joint Committee on Cancer Breast Cancer Staging System, Oncologist. 22 (2017) 1292–1300. doi:10.1634/theoncologist.2017-0116.

[4] J.N. Mills, A.C. Rutkovsky, A. Giordano, Mechanisms of resistance in estrogen receptor positive breast cancer: overcoming resistance to tamoxifen/aromatase inhibitors, Curr. Opin. Pharmacol. 41 (2018) 59–65. doi:10.1016/j.coph.2018.04.009.

[5] C. Yam, S.A. Mani, S.L. Moulder, Targeting the Molecular Subtypes of Triple Negative Breast Cancer: Understanding the Diversity to Progress the Field, Oncologist. 22 (2017) 1086–1093. doi:10.1634/theoncologist.2017-0095.

[6] A. Dalmases, I. Gonzalez-Navarrete, S. Menendez, O. Arpí, J.M. Coromines, S. Servitja, I. Tusquets, C. Chamizo, R. Rincón, L. Espinosa, A. Bigas, P. Eroles, J. Furriol, A. Lluch, A. Rovira, J. Albanell, F. Rojo, Deficiency in p53 is required for doxorubicin induced transcriptional activation of NF-кB target genes in human breast cancer, Oncotarget. 5 (2014). doi:10.18632/oncotarget.1556.

[7] K.J. Falkenberg, R.W. Johnstone, Histone deacetylases and their inhibitors in cancer, neurological diseases and immune disorders, Nat. Rev. Drug Discov. 13 (2014) 673–691. doi:10.1038/nrd4360.

[8] M. Haberland, R.L. Montgomery, E.N. Olson, The many roles of histone deacetylases in development and physiology: implications for disease and therapy, Nat. Rev. Genet. 10 (2009) 32–42. doi:10.1038/nrg2485.

[9] K. Ververis, T.C. Karagiannis, An atlas of histone deacetylase expression in breast cancer: fluorescence methodology for comparative semi-quantitative analysis, Am. J. Transl. Res. 4 (2012) 24–43.

[10] B.M. Müller, L. Jana, A. Kasajima, A. Lehmann, J. Prinzler, J. Budczies, K.-J. Winzer, M. Dietel, W. Weichert, C. Denkert, Differential expression of histone deacetylases HDAC1, 2 and 3 in human breast cancer - overexpression of HDAC2 and HDAC3 is associated with clinicopathological indicators of disease progression, BMC Cancer. 13 (2013) 215. doi:10.1186/1471-2407-13-215.

[11] H. Zhao, Z. Yu, L. Zhao, M. He, J. Ren, H. Wu, Q. Chen, W. Yao, M. Wei, HDAC2 overexpression is a poor prognostic factor of breast cancer patients with increased multidrug resistance-associated protein expression who received anthracyclines therapy, JPN J. Clin. Oncol. 46 (2016) 893–902. doi:10.1093/jjco/hyw096.

[12] E. Ceccacci, S. Minucci, Inhibition of histone deacetylases in cancer therapy: lessons from leukaemia, Brit. J. Cancer. 114 (2016) 605–611. doi:10.1038/bjc.2016.36.

[13] M. Terranova-Barberio, S. Thomas, N. Ali, N. Pawlowska, J. Park, G. Krings, M.D. Rosenblum, A. Budillon, P.N. Munster, HDAC inhibition potentiates immunotherapy in triple negative breast cancer, Oncotarget. 8 (2017). doi:10.18632/oncotarget.23169.

[14] M.B. dos Santos, D. Bertholin Anselmo, J.G. de Oliveira, B.V. Jardim-Perassi, D. Alves Monteiro, G. Silva, E. Gomes, A. Lucia Fachin, M. Marins, D.A.P. de Campos Zuccari, L. Octavio Regasini, Antiproliferative activity and p53 upregulation effects of chalcones on human breast cancer cells, J. Enzym. Inhib. Med. Ch. 34 (2019) 1093–1099. doi:10.1080/14756366.2019.1615485.

[15] G. Silva, M. Marins, N. Chaichanasak, Y. Yoon, A.L. Fachin, V.C. Pinhanelli, L.O. Regasini, M.B. dos Santos, G.M. Ayusso, B. de C. Marques, W.W. Wu, J.-N. Phue, R.-F. Shen, S.J. Baek, Trans-chalcone increases p53 activity via DNAJB1/HSP40 induction and CRM1 inhibition, PLOS ONE. 13 (2018) e0202263. doi:10.1371/journal.pone.0202263.

[16] S. Iftikhar, S. Khan, A. Bilal, S. Manzoor, M. Abdullah, A.-H. Emwas, S. Sioud, X. Gao, G.A. Chotana, A. Faisal, R.S.Z. Saleem, Synthesis and evaluation of modified chalcone based p53 stabilizing agents, Bioorg. Med. Chem. Lett. 27 (2017) 4101–4106. doi:10.1016/j.bmcl.2017.07.042.

[17] D.D. Jandial, C.A. Blair, S. Zhang, L.S. Krill, Y.-B. Zhang, X. Zi, Molecular targeted approaches to cancer therapy and prevention using chalcones, Curr. Cancer Drug Tar. 14 (2014) 181–200.

[18] Y. Zhang, B. Srinivasan, C. Xing, J. Lü, A new chalcone derivative (E)-3-(4-methoxyphenyl)-2-methyl-1-(3,4,5-trimethoxyphenyl)prop-2-en-1-one suppresses prostate cancer involving p53-mediated cell cycle arrests and apoptosis, Anticancer Res. 32 (2012) 3689–3698.

[19] A. Sulaiman, B. Sulaiman, L. Khouri, S. McGarry, C. Nessim, A. Arnaout, X. Li, C. Addison, J. Dimitroulakos, L. Wang, Both bulk and cancer stem cell subpopulations in triple-negative breast cancer are susceptible to Wnt, HDAC, and ERα coinhibition, FEBS Lett. 590 (2016) 4606–4616. doi:10.1002/1873-3468.12496.

[20] N. Garmpis, C. Damaskos, A. Garmpi, E. Kalampokas, T. Kalampokas, E. Spartalis, A. Daskalopoulou, S. Valsami, M. Kontos, A. Nonni, K. Kontzoglou, D. Perrea, N. Nikiteas D. Dimitroulis Histone Deacetylases as New Therapeutic Targets in Triple-negative Breast Cancer: Progress and Promises, Cancer Genom. Proteom. 14 (2017). doi:10.21873/cgp.20041.

[21] C. Damaskos, S. Valsami, M. Kontos, E. Spartalis, T. Kalampokas, E. Kalampokas, A. Athanasiou, D. Moris, A. Daskalopoulou, S. Davakis, G. Tsourouflis, K. Kontzoglou, D. Perrea, N. Nikiteas, D. Dimitroulis, Histone Deacetylase Inhibitors: An Attractive Therapeutic Strategy Against Breast Cancer, Anticancer Res. 37 (2017) 35–46. doi:10.21873/anticanres.11286.

[22] H.A. Abou-Zied, B.G.M. Youssif, M.F.A. Mohamed, A.M. Hayallah, M. Abdel-Aziz, EGFR inhibitors and apoptotic inducers: Design, synthesis, anticancer activity and docking studies of novel xanthine derivatives carrying chalcone moiety as hybrid molecules, Bioor. Chem. 89 (2019) 102997. doi:10.1016/j.bioorg.2019.102997.

[22] S.-Y. Seo, Multi-targeted hybrids based on HDAC inhibitors for anti-cancer drug discovery, Arch. Pharm. Res. 35 (2012) 197–200. doi:10.1007/s12272-012-0221-9.

[24] M. Mottamal, S. Zheng, T. Huang, G. Wang, Histone Deacetylase Inhibitors in Clinical Studies as Templates for New Anticancer Agents, Molecules. 20 (2015) 3898–3941. doi:10.3390/molecules20033898.

[25] V.Raja. Solomon, H. Lee, Anti-breast cancer activity of heteroaryl chalcone derivatives, Biomedicine & Pharmacotherapy. 66 (2012) 213–220. doi:10.1016/j.biopha.2011.11.013.

[26] C.J. Chou, D. Herman, J.M. Gottesfeld, Pimelic Diphenylamide 106 Is a Slow, Tight-binding Inhibitor of Class I Histone Deacetylases, J. Biol. Chem. 283 (2008) 35402–35409. doi:10.1074/jbc.M807045200.

[27]. S.M., . H.P.S., . S.D.G., . N.S.H.N.M., Synthesis and Characterization of Some Chalcone Derivatives, Trends Appl. Sci. Res. 2 (2007) 52–56. doi:10.3923/tasr.2007.52.56.

[28] J.P. Parker, H. Nimir, D.M. Griffith, B. Duff, A.J. Chubb, M.P. Brennan, M.P. Morgan, D.A. Egan, C.J. Marmion, A novel platinum complex of the histone deacetylase inhibitor belinostat: Rational design, development and in vitro cytotoxicity, J. Inorg. Biochem. 124 (2013) 70–77. doi:10.1016/j.jinorgbio.2013.03.011.

[29] N.S. Chao, L. Shagan, B. Dina, A. Aike, B. Isa, Synthesis and Tyrosinase Activity of Novel Chalcone Derivatives, Chemical Journal of Chinese Universities. 35 (2014) 1204–1211.

[30] M. Kortelainen, A. Suhonen, A. Hamza, I. Pápai, E. Nauha, S. Yliniemelä-Sipari, M. Nissinen, P.M. Pihko, Folding Patterns in a Family of Oligoamide Foldamers, Chem. Eur. J. 21 (2015) 9493–9504. doi:10.1002/chem.201406521.

[31] T.R. Hoye, H. Zhao, A Method for Easily Determining Coupling Constant Values: An Addendum to "A Practical Guide to First-Order Multiplet Analysis in 1 H NMR Spectroscopy," J. Org. Chem. 67 (2002) 4014–4016. doi:10.1021/jo001139v.

[32] P.W. Finn, M. Bandara, C. Butcher, A. Finn, R. Hollinshead, N. Khan, N. Law, S. Murthy, R. Romero, C. Watkins, V. Andrianov, R.M. Bokaldere, K. Dikovska, V. Gailite, E. Loza, I. Piskunova, I. Starchenkov, M. Vorona, I. Kalvinsh, Novel Sulfonamide Derivatives as Inhibitors of Histone Deacetylase, Helv. Chim. Acta. 88 (2005) 1630–1657. doi:10.1002/hlca.200590129.

[33] E. Adiguzel, F. Yilmaz, M. Emirik, M. Ozil, Synthesis and characterization of two new hydroxamic acids derivatives and their metal complexes. An investigation on the keto/enol, E/Z and hydroxamate/hydroximate forms, J. Mol. Struct. 1127 (2017) 403–412. doi:10.1016/j.molstruc.2016.07.081.

[34] G.E. Hawkes, K. Herwig, J.D. Roberts, Nuclear magnetic resonance spectroscopy. Use of carbon-13 spectra to establish configurations of oximes, J. Org. Chem. 39 (1974) 1017–1028. doi:10.1021/jo00922a001.

[35] G. Giannini, M. Marzi, R. Pezzi, T. Brunetti, G. Battistuzzi, M.D. Marzo, W. Cabri, L. Vesci, C. Pisano, N-Hydroxy-(4-oxime)-cinnamide: A versatile scaffold for the synthesis of novel histone deacetilase (HDAC) inhibitors, Bioorg. Med. Chem. Lett. 19 (2009) 2346–2349. doi:10.1016/j.bmcl.2009.02.029.

[36] C.B. Botta, W. Cabri, E. Cini, L. De Cesare, C. Fattorusso, G. Giannini, M. Persico, A. Petrella, F. Rondinelli, M. Rodriquez, A. Russo, M. Taddei, Oxime Amides as a Novel Zinc Binding Group in Histone Deacetylase Inhibitors: Synthesis, Biological Activity, and Computational Evaluation, J. Med. Chem. 54 (2011) 2165–2182. doi:10.1021/jm101373a.

[37] M. Gottlicher, Valproic acid defines a novel class of HDAC inhibitors inducing differentiation of transformed cells, EMBO J. 20 (2001) 6969–6978. doi:10.1093/emboj/20.24.6969.

[38] T. Eckschlager, J. Plch, M. Stiborova, J. Hrabeta, Histone Deacetylase Inhibitors as Anticancer Drugs, Int. J. Mol. Sci. 18 (2017) 1414. doi:10.3390/ijms18071414.

[39] G. Bouchain, D. Delorme, Novel hydroxamate and anilide derivatives as potent histone deacetylase inhibitors: synthesis and antiproliferative evaluation, Curr. Med. Chem. 10 (2003) 2359–2372.

[40] W. Shan, Y. Jiang, H. Yu, Q. Huang, L. Liu, X. Guo, L. Li, Q. Mi, K. Zhang, Z. Yang, HDAC2 overexpression correlates with aggressive clinicopathological features and DNA-damage response pathway of breast cancer, Am. J. Cancer Res. 7 (2017) 1213–1226.

[41] B.E.L. Lauffer, R. Mintzer, R. Fong, S. Mukund, C. Tam, I. Zilberleyb, B. Flicke, A. Ritscher, G. Fedorowicz, R. Vallero, D.F. Ortwine, J. Gunzner, Z. Modrusan, L. Neumann, C.M. Koth, P.J. Lupardus, J.S. Kaminker, C.E. Heise, P. Steiner, Histone Deacetylase (HDAC) Inhibitor Kinetic Rate Constants Correlate with Cellular Histone Acetylation but Not Transcription and Cell Viability, J. Biol. Chem. 288 (2013) 26926–26943. doi:10.1074/jbc.M113.490706.

[42] H.W. Thompson, R. Mera, C. Prasad, The Analysis of Variance (ANOVA), Nutr. Neurosci. 2 (1999) 43–55. doi:10.1080/1028415X.1999.11747262.

[43] V.K. Jain, A.V. Chavan, S.S. Mahajan, Design, Synthesis and in vitro cytotoxicity studies of novel sulfonamides, Der Pharmacia Sinica. 6 (2015) 28–35.

[44] E. Harder, W. Damm, J. Maple, C. Wu, M. Reboul, J.Y. Xiang, L. Wang, D. Lupyan, M.K. Dahlgren, J.L. Knight, J.W. Kaus, D.S. Cerutti, G. Krilov, W.L. Jorgensen, R. Abel, R.A. Friesner, OPLS3: A Force Field Providing Broad Coverage of Drug-like Small Molecules and Proteins, J. Chem. Theory Comput. 12 (2016) 281–296. doi:10.1021/acs.jctc.5b00864.

[45] R.A. Friesner, J.L. Banks, R.B. Murphy, T.A. Halgren, J.J. Klicic, D.T. Mainz, M.P. Repasky, E.H. Knoll, M. Shelley, J.K. Perry, D.E. Shaw, P. Francis, P.S. Shenkin, Glide: A New Approach for Rapid, Accurate Docking and Scoring. 1. Method and Assessment of Docking Accuracy, J. Med. Chem. 47 (2004) 1739–1749. doi:10.1021/jm0306430.

[46] T.A. Halgren, R.B. Murphy, R.A. Friesner, H.S. Beard, L.L. Frye, W.T. Pollard, J.L. Banks, Glide: A New Approach for Rapid, Accurate Docking and Scoring. 2. Enrichment Factors in Database Screening, J. Med. Chem. 47 (2004) 1750–1759. doi:10.1021/jm030644s.

[47] J. Kirchmair, P. Markt, S. Distinto, G. Wolber, T. Langer, Evaluation of the performance of 3D virtual screening protocols: RMSD comparisons, enrichment assessments, and decoy selection—What can we learn from earlier mistakes?, J. Comp. Aid. Mol. Des. 22 (2008) 213–228. doi:10.1007/s10822-007-9163-6.

[48] J.M. Kalita, S.K. Ghosh, S. Sahu, M. Dutta, A Statistical Analysis to Find Out an Appropriate Docking Method, Asian J. Pharm. Clin. Res. 8 (2015) 158–160.

[49] T. Tuntland, B. Ethell, T. Kosaka, F. Blasco, R.X. Zang, M. Jain, T. Gould, K. Hoffmaster, Implementation of pharmacokinetic and pharmacodynamic strategies in early research phases of drug discovery and development at Novartis Institute of Biomedical Research, Front. Pharmacol. 5 (2014). doi:10.3389/fphar.2014.00174.

[50] C.A. Lipinski, Lead- and drug-like compounds: the rule-of-five revolution, Drug Discov. Today Technol. 1 (2004) 337–341. doi:10.1016/j.ddtec.2004.11.007.

[51] C.A. Lipinski, F. Lombardo, B.W. Dominy, P.J. Feeney, Experimental and computational approaches to estimate solubility and permeability in drug discovery and development settings, Adv. Drug Deliver. Rev. 23 (1997) 3–25. doi:10.1016/S0169-409X(96)00423-1.

[52] D.F. Veber, S.R. Johnson, H.-Y. Cheng, B.R. Smith, K.W. Ward, K.D. Kopple, Molecular Properties That Influence the Oral Bioavailability of Drug Candidates, J. Med. Chem. 45 (2002) 2615–2623. doi:10.1021/jm020017n.

[53] Molinspiration Chemoinformatics. Available online: http://www.molinspiration.com/ (accessed on November 9th, 2018).

[54] P. Ertl, B. Rohde, P. Selzer, Fast Calculation of Molecular Polar Surface Area as a Sum of Fragment-Based Contributions and Its Application to the Prediction of Drug Transport Properties, J. Med. Chem. 43 (2000) 3714–3717. doi:10.1021/jm000942e.

[55] PreAdmet. Available online: <https://preadmet.bmdrc.kr/adme/> (Accessed on January 2019).

[56] S. Yee, In vitro permeability across Caco-2 cells (colonic) can predict in vivo (small intestinal) absorption in man--fact or myth, Pharm. Res. 14 (1997) 763–766.

[57] Z.-Q. Ning, Z.-B. Li, M.J. Newman, S. Shan, X.-H. Wang, D.-S. Pan, J. Zhang, M. Dong, X. Du, X.-P. Lu, Chidamide (CS055/HBI-8000): a new histone deacetylase inhibitor of the benzamide class with antitumor activity and the ability to enhance immune cell-mediated tumor cell cytotoxicity, Cancer Chemother Pharmacol. 69 (2012) 901–909. doi:10.1007/s00280-011-1766-x.

[58] T. Mosmann, Rapid colorimetric assay for cellular growth and survival: Application to proliferation and cytotoxicity assays, J. Immunol. Methods. 65 (1983) 55–63. doi:10.1016/0022-1759(83)90303-4.

[59] A. Carlesso, C. Chintha, A.M. Gorman, A. Samali, L.A. Eriksson, Merits and pitfalls of conventional and covalent docking in identifying new hydroxyl aryl aldehyde like compounds as human IRE1 inhibitors, Sci. Rep-UK. 9 (2019). doi:10.1038/s41598-019-39939-z.

Supplementary Materials

Synthesis and evaluation of new antiproliferative HDAC-inhibitors against breast cancer

Mariana Bastos dos Santos[1]; Jéssica Gislaine[2]; Aline Renata Pavan[3]; Bruna V. Jardim Perassi[2]; Jean Leandro dos Santos[3]; Débora Aparecida Pires de Campos Zuccari[2]; Luis Octavio Regasini[1*].

[1] *Department of Chemistry and Environmental Sciences, Institute of Biosciences, Humanities and Exact Sciences (IBILCE), São Paulo State University (UNESP), São José do Rio Preto, São Paulo, Brazil;*

[2] *Department of Molecular Biology, Medicine College of São José do Rio Preto (FAMERP), São José do Rio Preto, São Paulo, Brazil;*

[3] *Department of Drugs and Pharmaceutics, School of Pharmaceutical Sciences, São Paulo State University (UNESP), Araraquara, São Paulo, Brazil;*

***Correspondence to:** luis.regasini@unesp.br (L.O.R.); Tel.: 55-17-3221-2362.

1. SPECTROCOPY DATA

Structure of compounds were confirmed by ^{1}H and ^{13}C NMR spectra analyses, obtained in Bruker Avance III (14 T and 9.4 T) equipments using deutered solvents, dimethyl sulfoxide and acetone. NMR spectra of compounds were represented as chemical shifts (δ in ppm), coupling constants (J), and multiplicities: s, singlet; d, dublet; dd, doublet of doublets; ddd, doublet of doublet of doublets; and m = multiplet. Melting points (m.p.) were measured using Tecnopon PFM-II apparatus. Mass spectrum of sulfonamide **27c** was obtained in UHR TOF - Bruker in configuration ESI-IT in negative ionization mode. Here we summarized ^{1}H and ^{13}C NMR spectra and MS spectra on Figures SM1–SM31. Compound **27c** HMBC and HSQC were colletected, and data interpretation are represented on Scheme 1.

Figure SM.1. ^{1}H NMR spectrum (DMSO-d_6, 600 MHz) of compound **21**

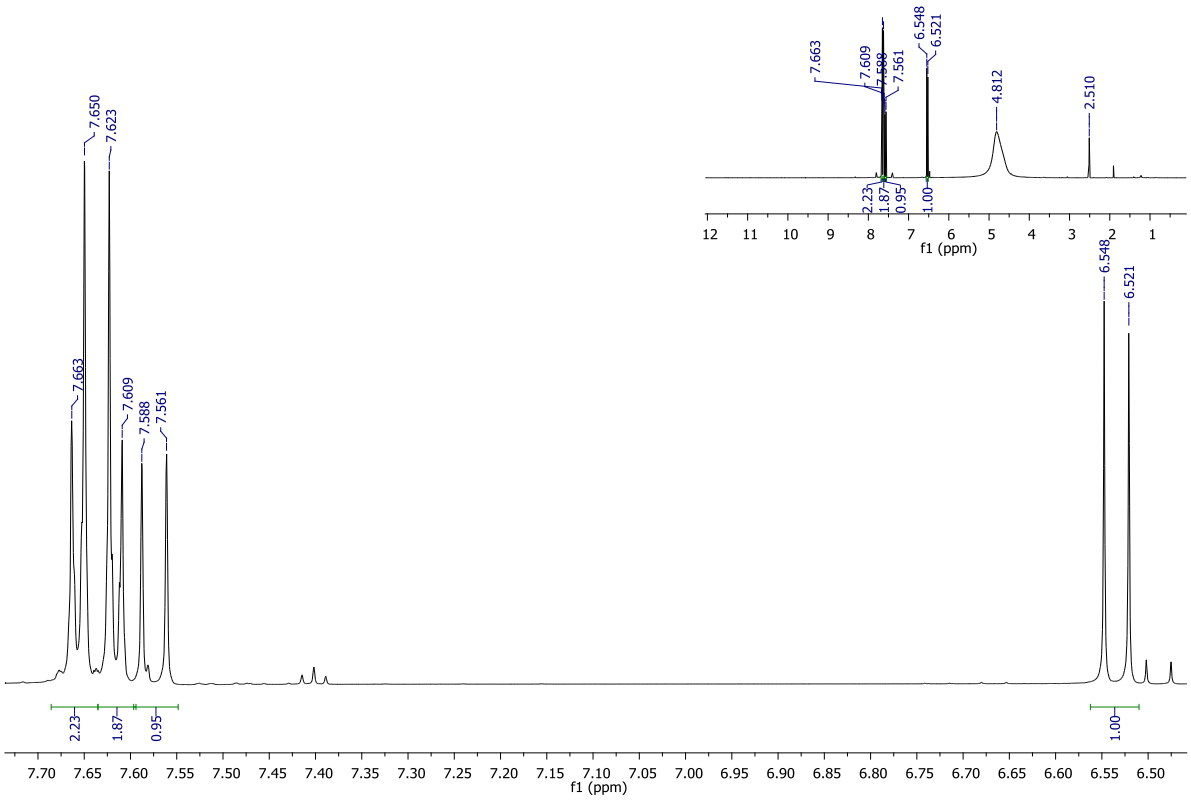

Figure SM.2. ^{13}C NMR spectrum (DMSO-d_6, 150 MHz) of compound **21**

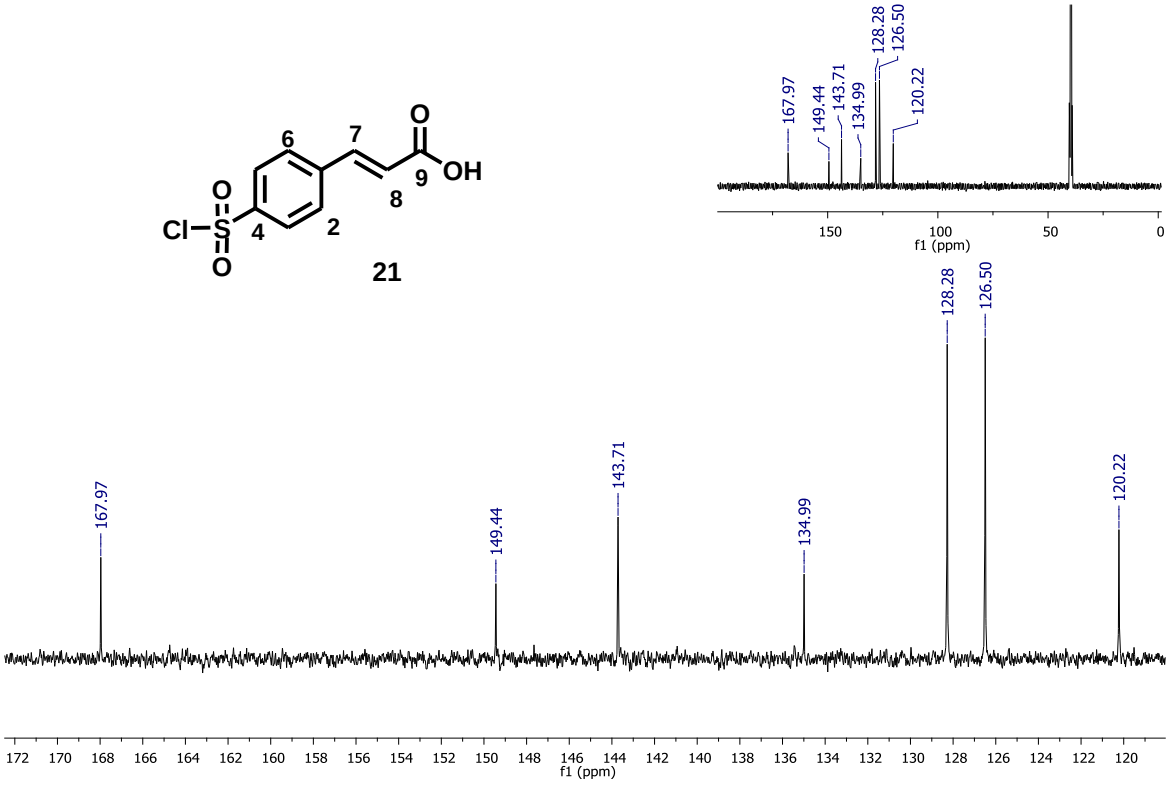

Figure SM.3. ^{1}H NMR spectrum (DMSO-d_6, 600 MHz) of compound **22a**

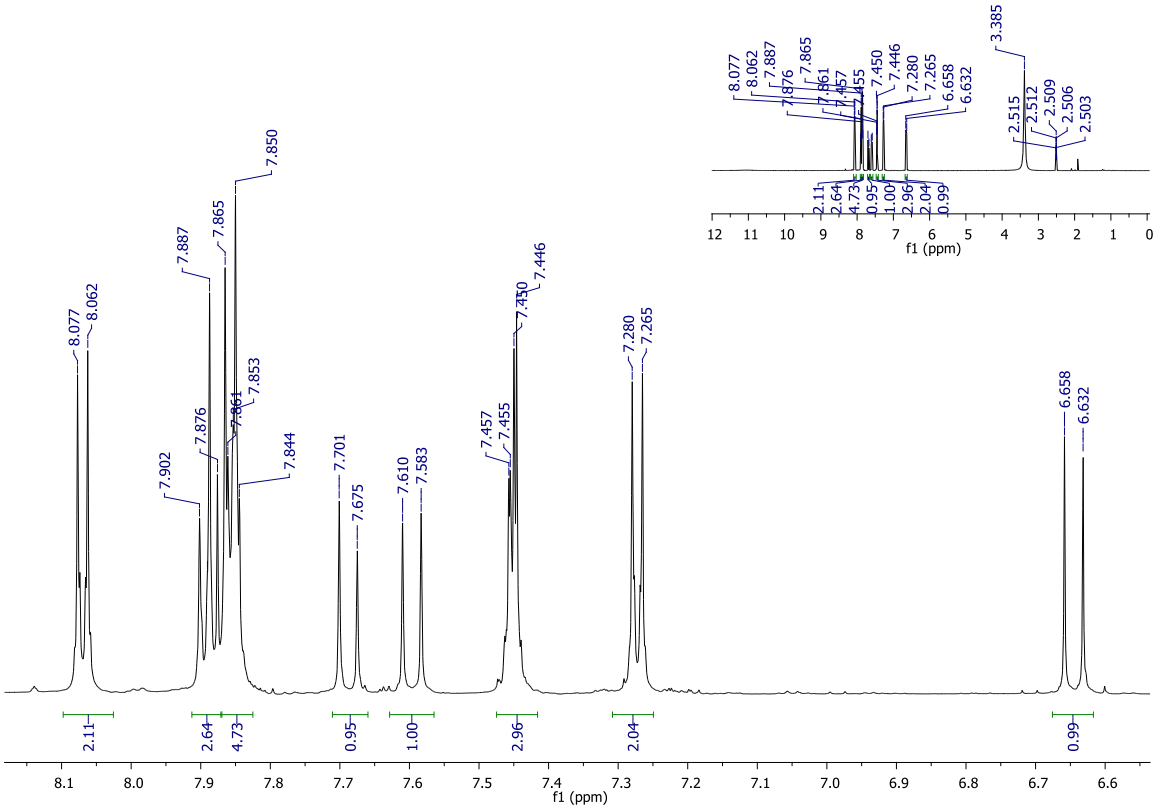

Figure SM.4. ^{13}C NMR spectrum (DMSO-d_6, 150 MHz) da substância **22a**

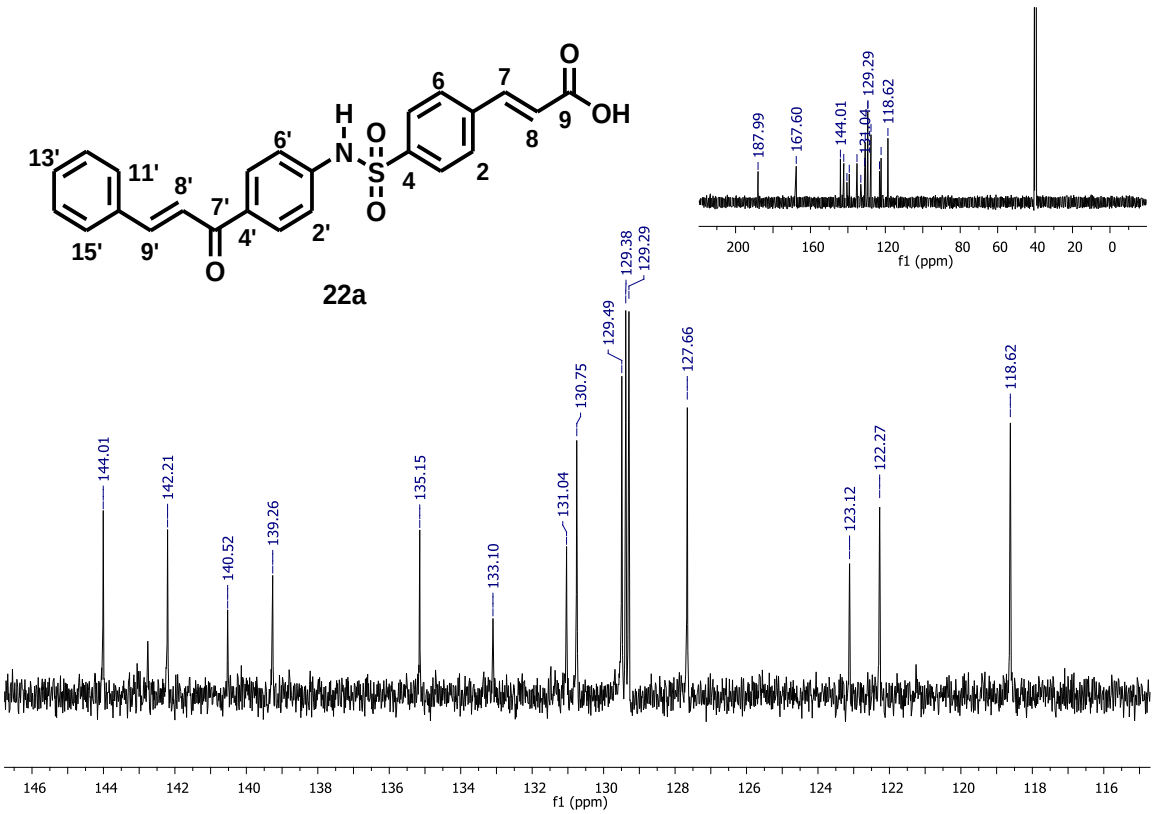

Figure SM.5. ^{1}H NMR spectrum (DMSO-d_6, 600 MHz) of compound **22b**

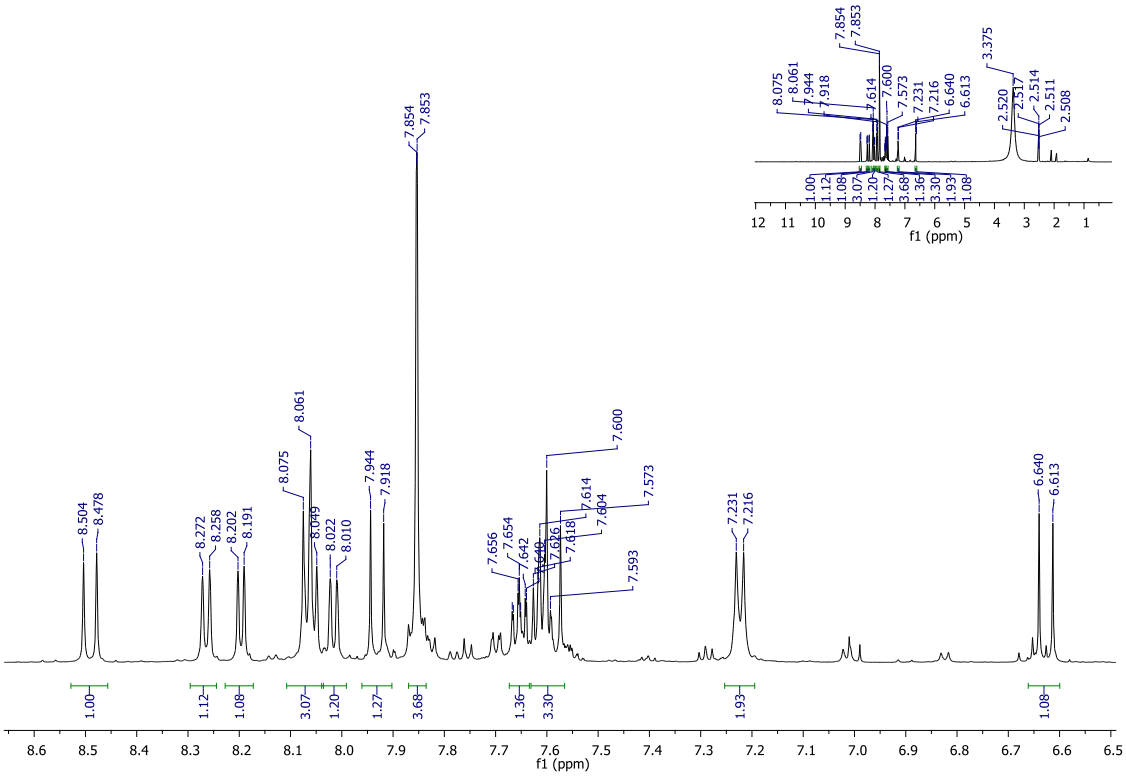

Figure SM.6. ^{13}C NMR spectrum (DMSO-d_6, 600 MHz) of compound **22b**

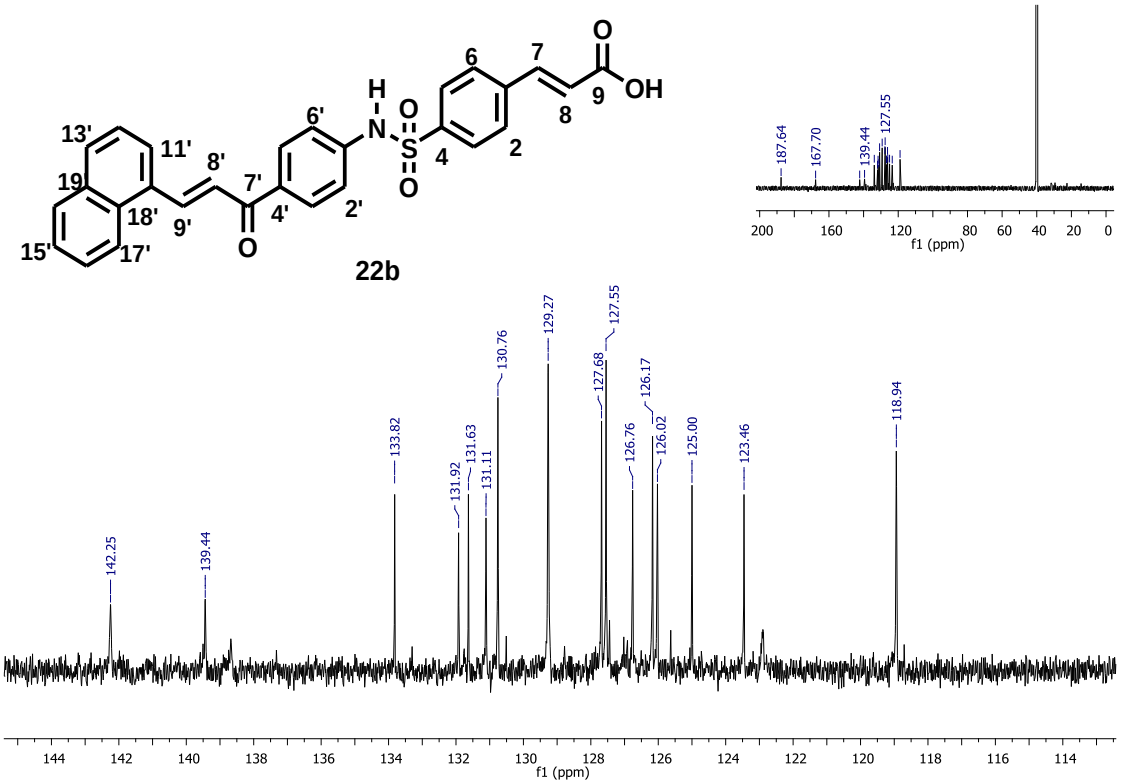

Figure SM.7. ^{1}H NMR spectrum (Acetone-d_6, 600 MHz) of compound **23a**

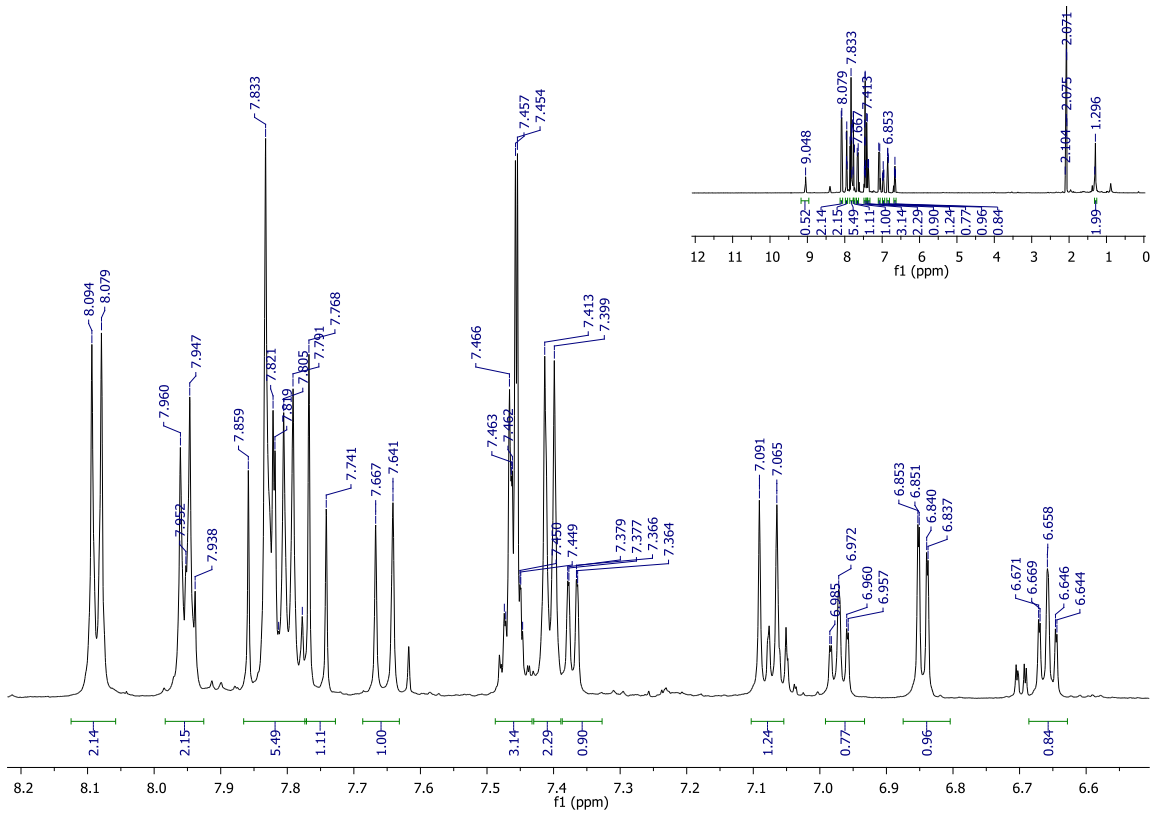

Figure SM.8. ^{13}C NMR spectrum (Acetone-d_6, 150 MHz) of compound **23a**

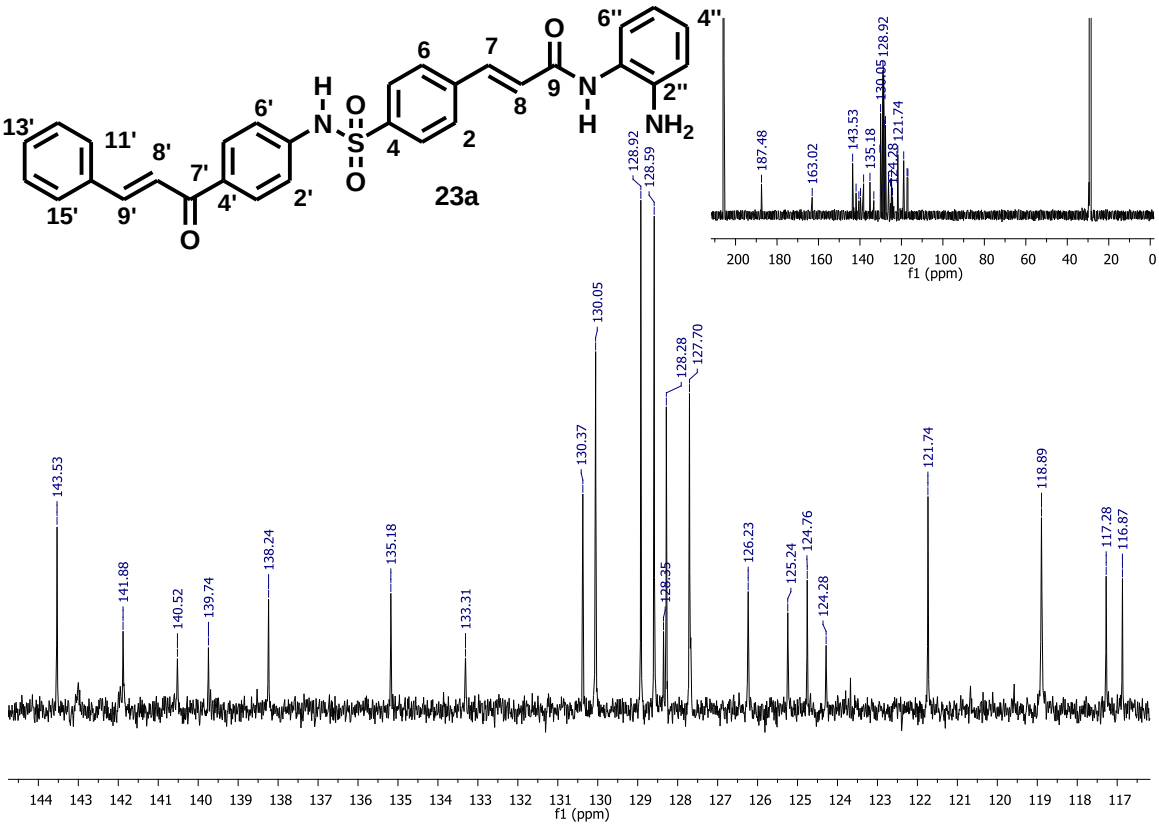

Figure SM.9. ^{1}H NMR spectrum (DMSO-d_6, 600 MHz) of compound **23b**

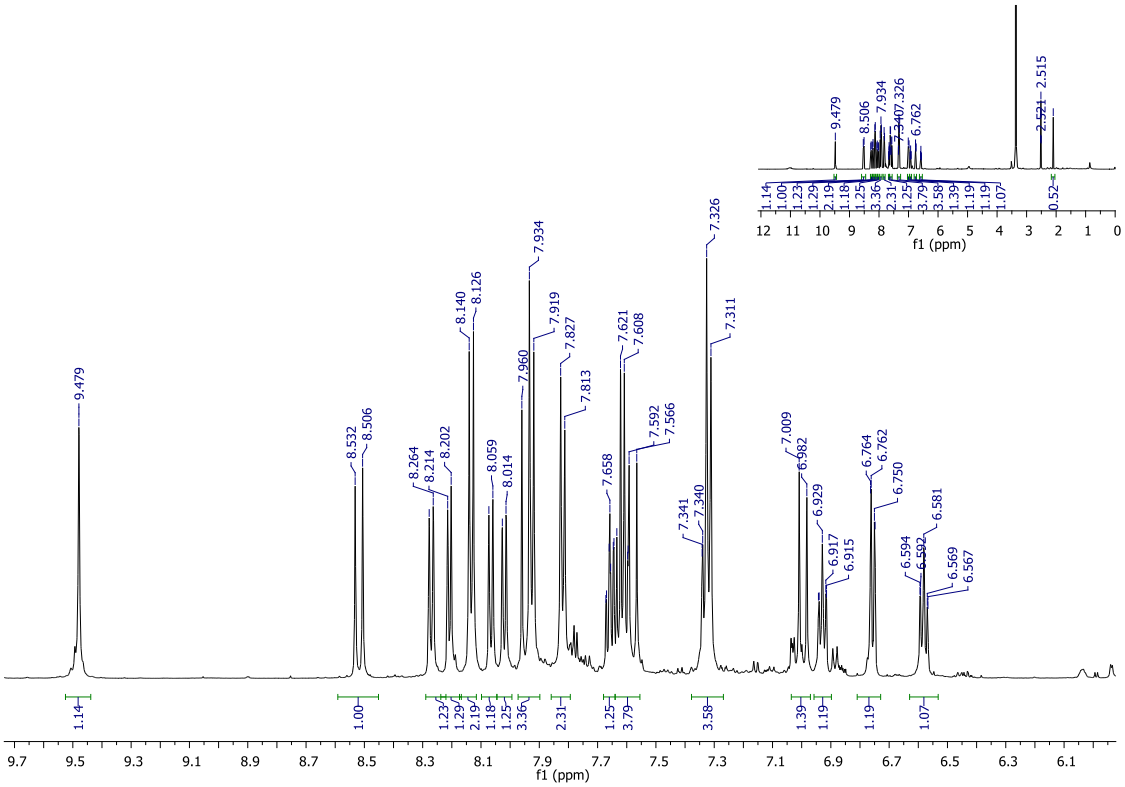

Figure SM.10. ^{13}C NMR spectrum (DMSO-d_6, 600 MHz) of compound **23b**

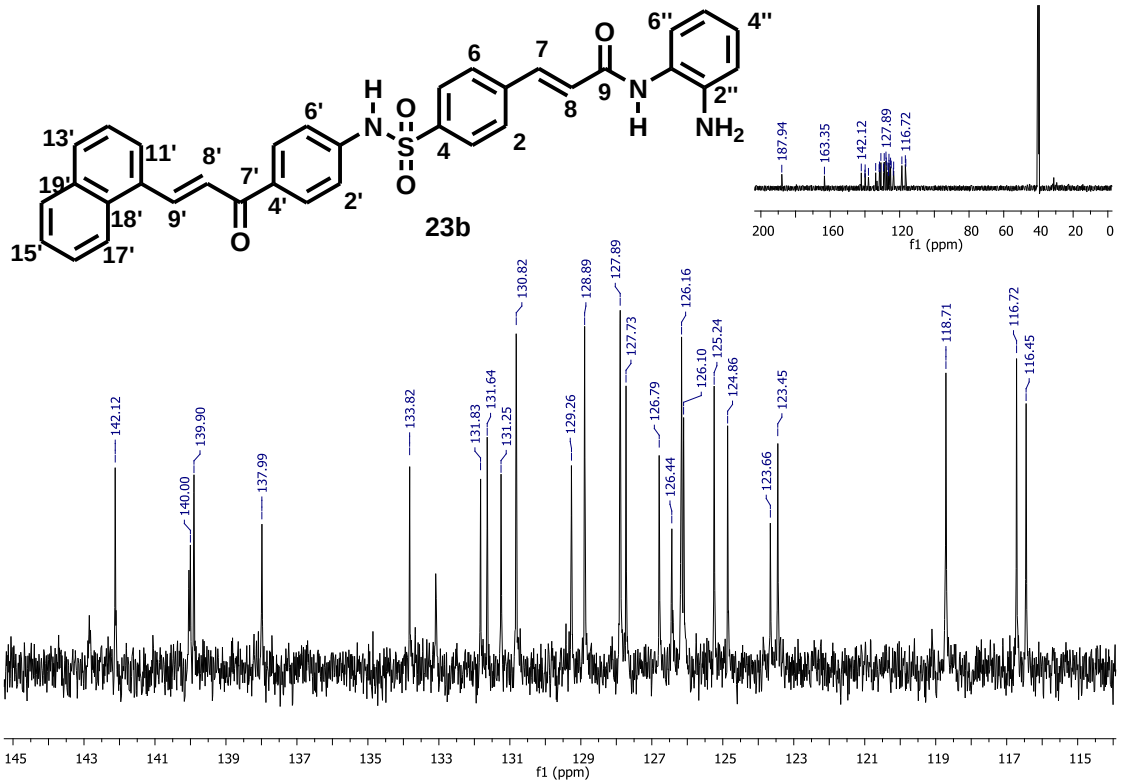

Figure SM.11. ^{1}H NMR spectrum (DMSO-d_6, 600 MHz) of compound **24a**

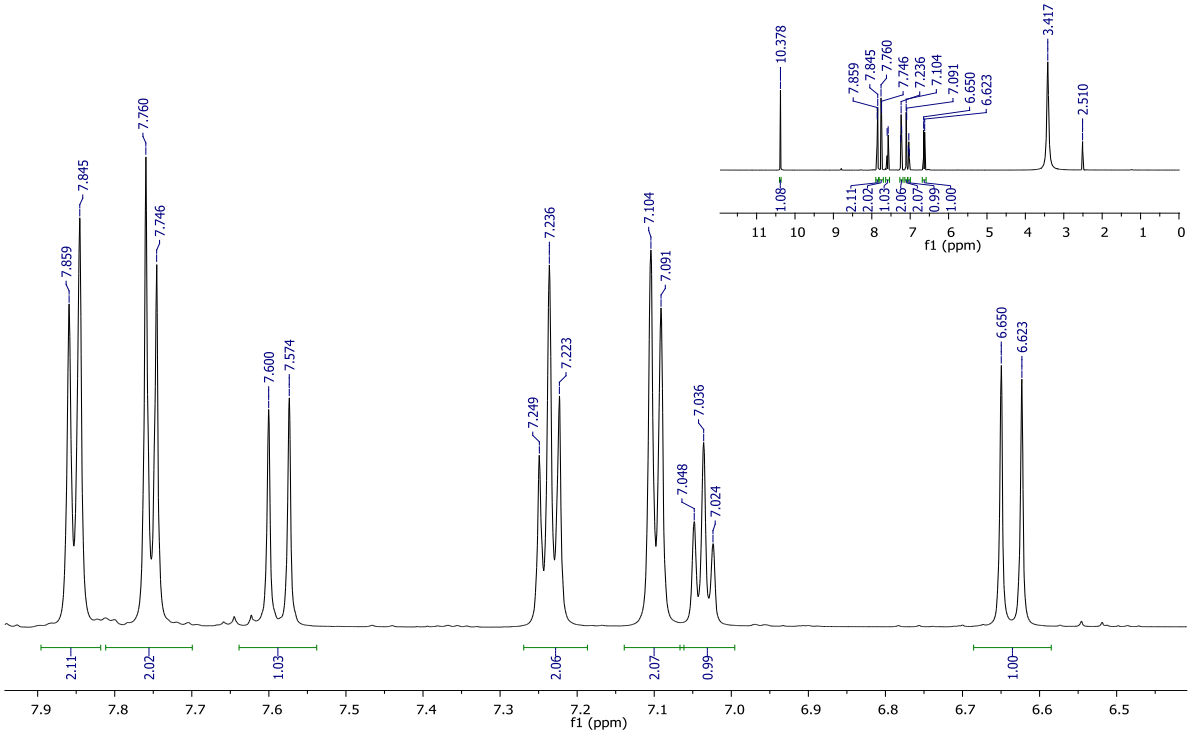

Figure SM.12. ^{13}C NMR spectrum (DMSO-d_6, 150 MHz) of compound **24a**

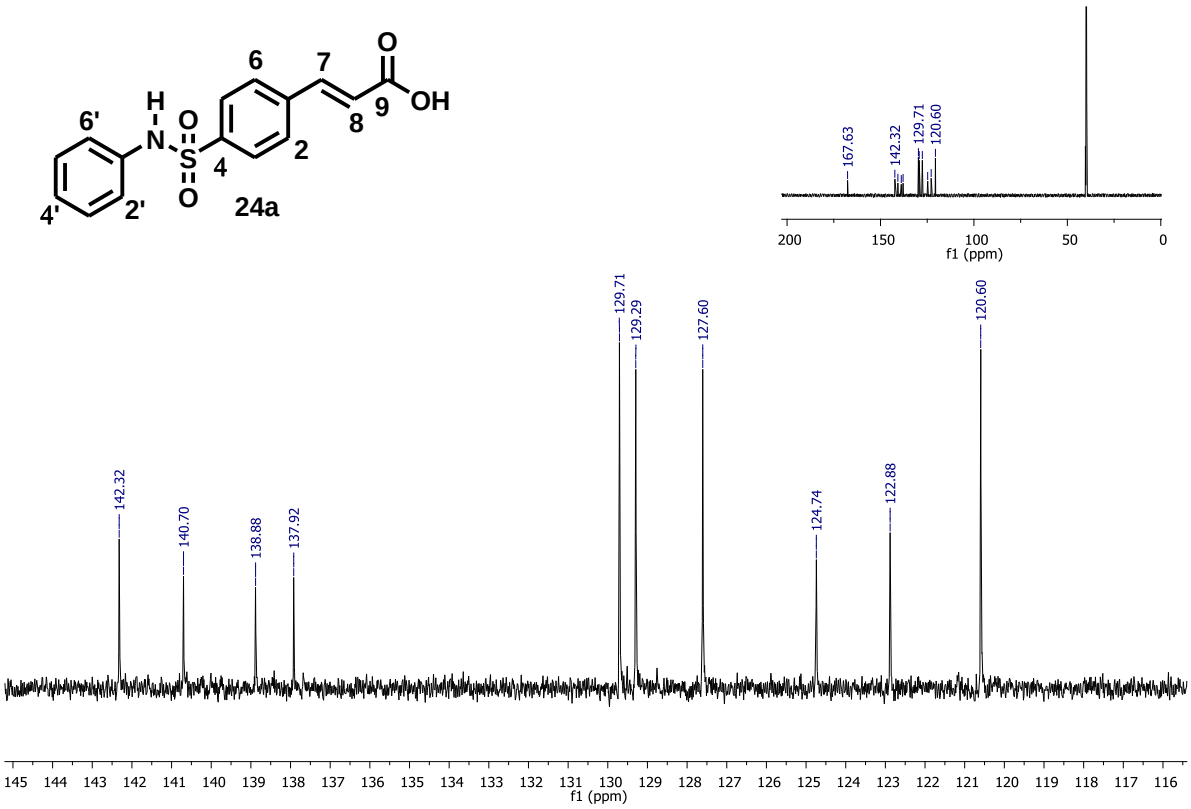

Figure SM.13. ^{1}H NMR spectrum (DMSO-d_6, 600 MHz) of compound **24b**

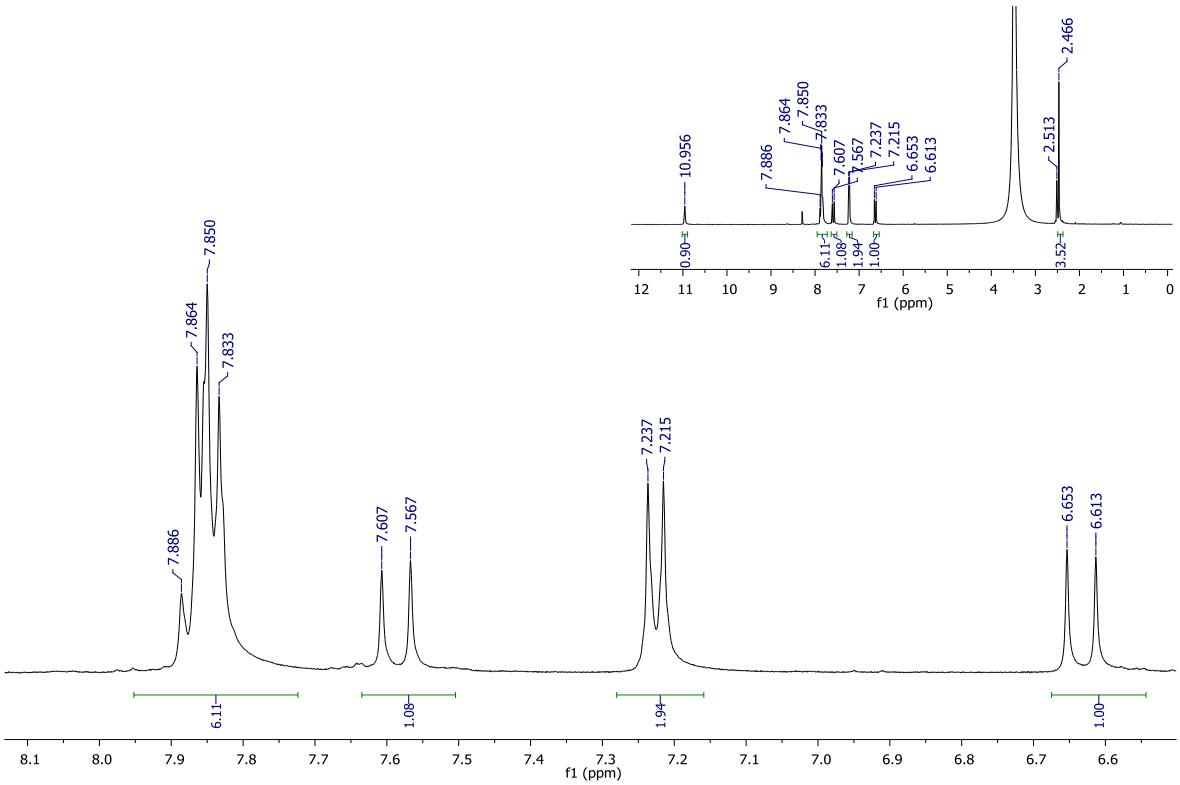

Figure SM.14. ^{13}C NMR spectrum (DMSO-d_6, 150 MHz) of compound **24b**

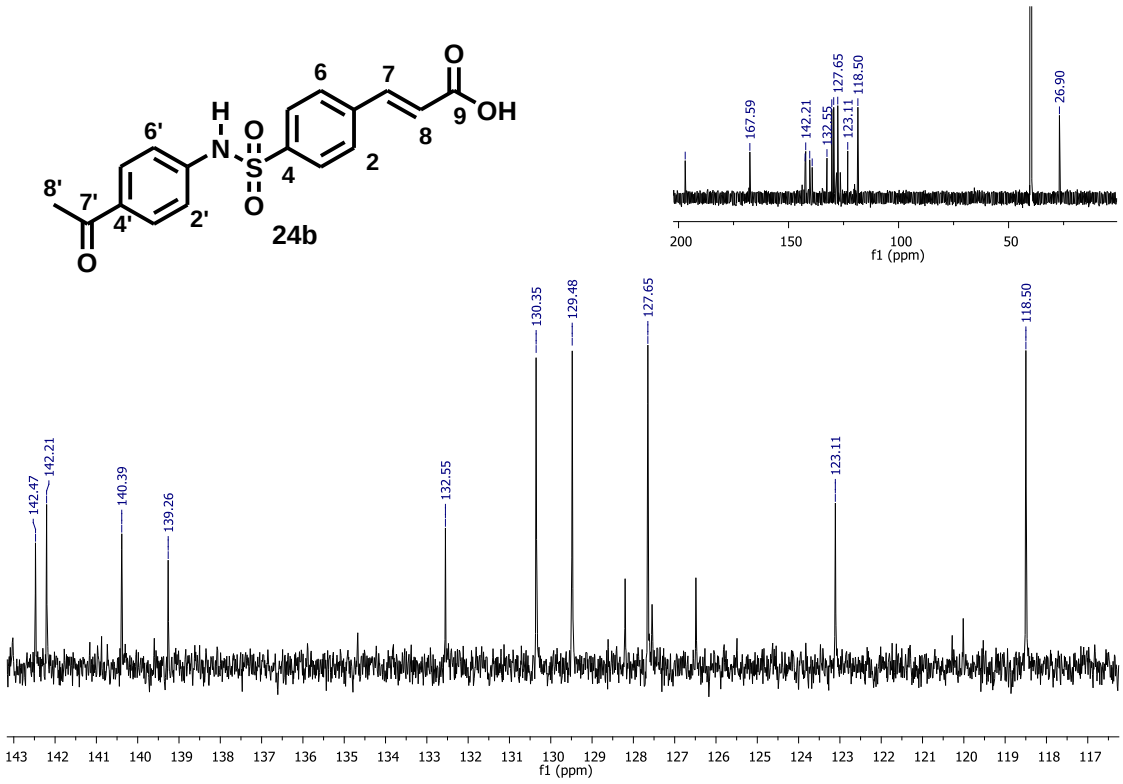

Figure SM.15. ^{1}H NMR spectrum (acetona-d_6, 600 MHz) of compound **25**

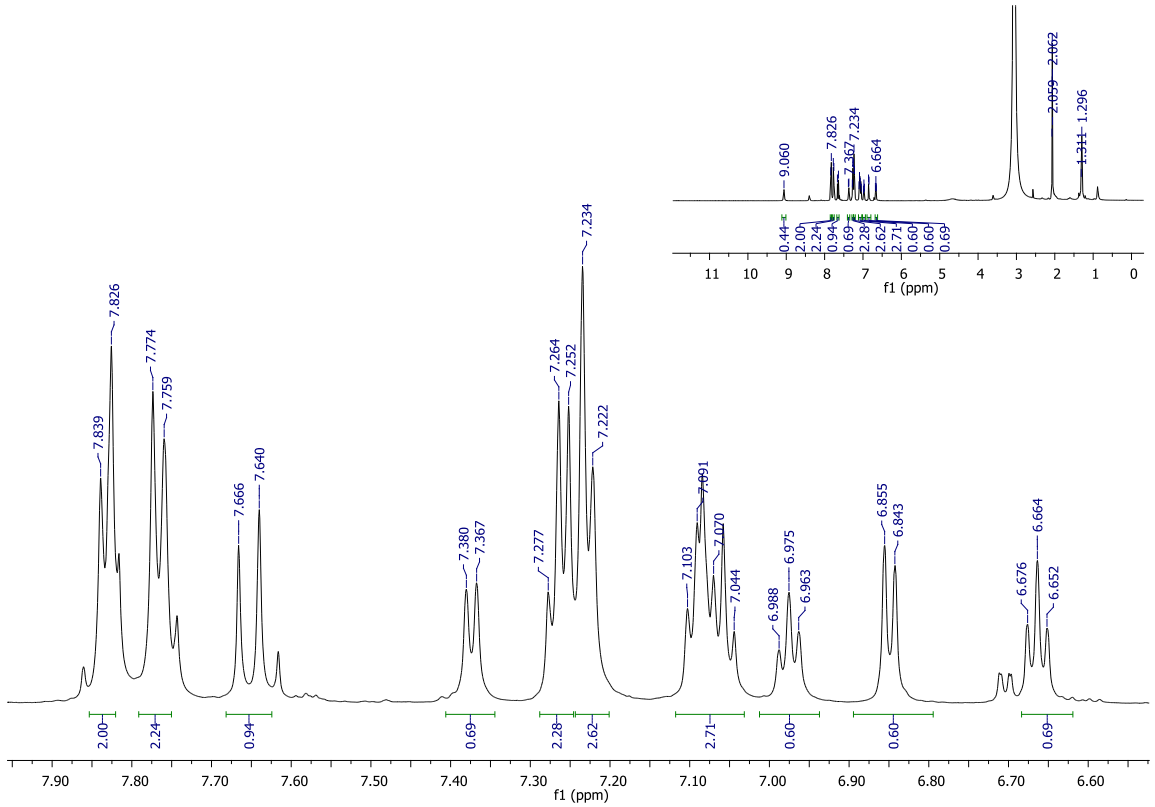

Figure SM.16. ^{13}C NMR spectrum (acetona-d_6, 150 MHz) of compound **25**

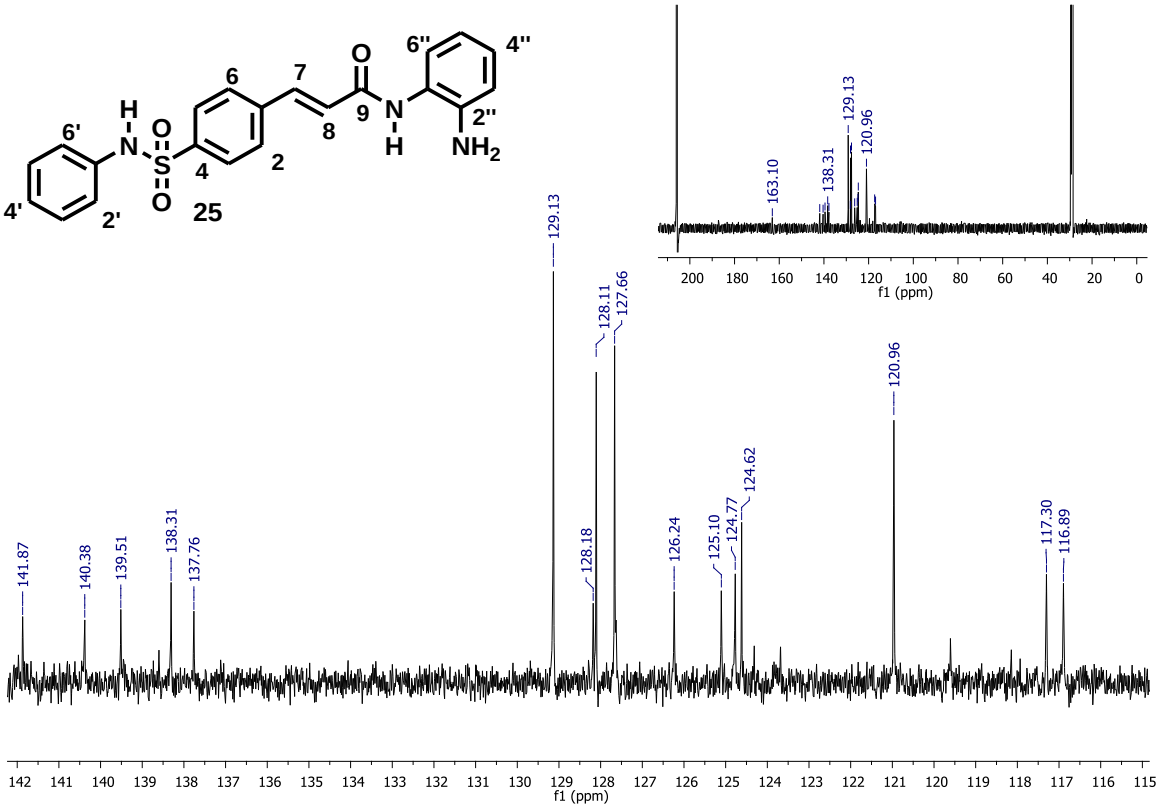

Figure SM.17. ^{1}H NMR spectrum (DMSO-d_6, 600 MHz) of compound **26a**

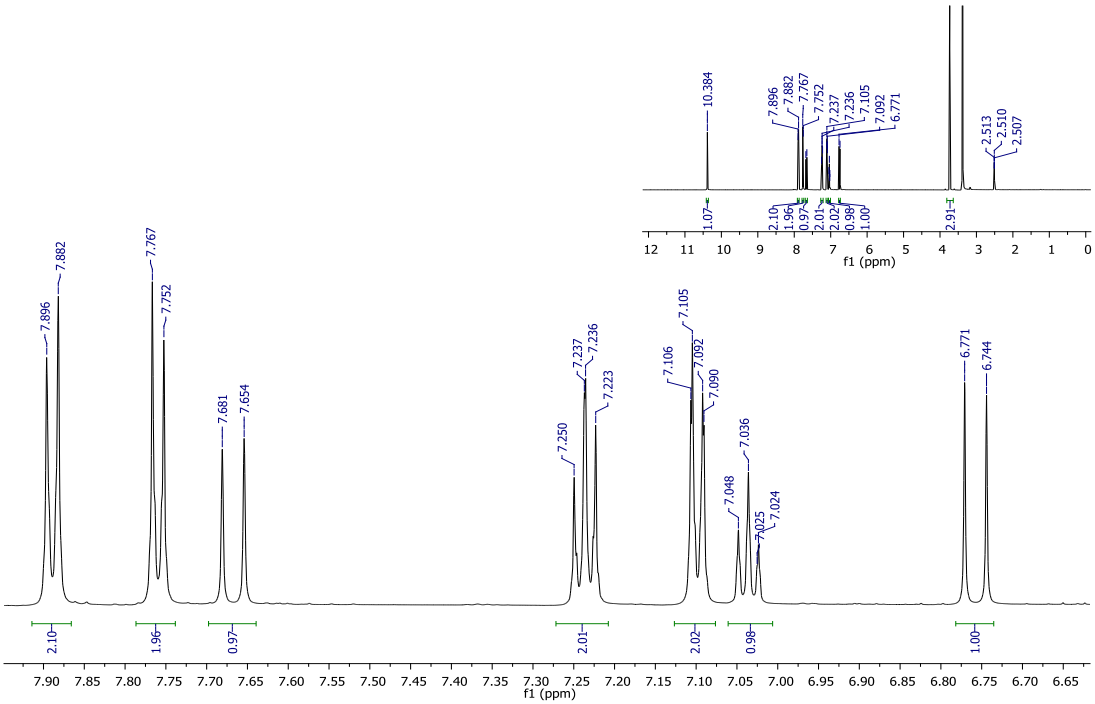

Figure SM.18. ^{13}C NMR spectrum (DMSO-d_6, 150 MHz) of compound **26a**

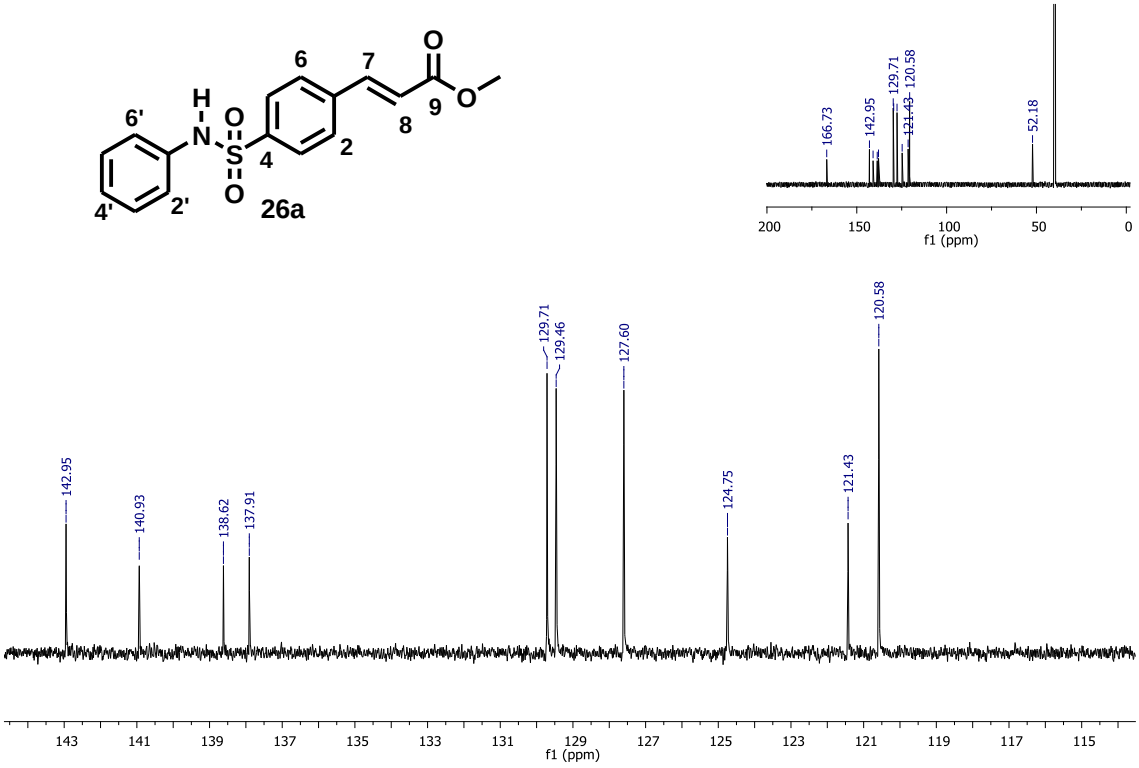

Figure SM.19. ^{1}H NMR spectrum (DMSO-d_6, 600 MHz) of compound **26b**

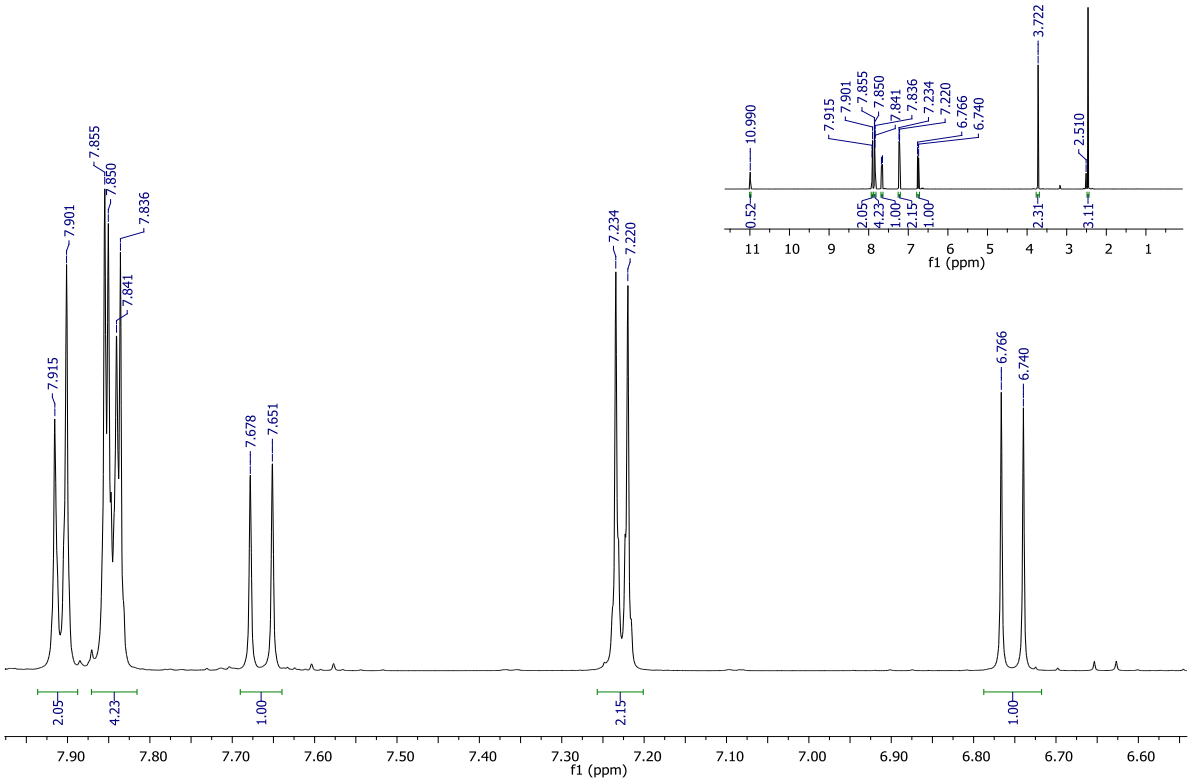

Figure SM.20. ^{13}C NMR spectrum (DMSO-d_6, 150 MHz) of compound **26b**

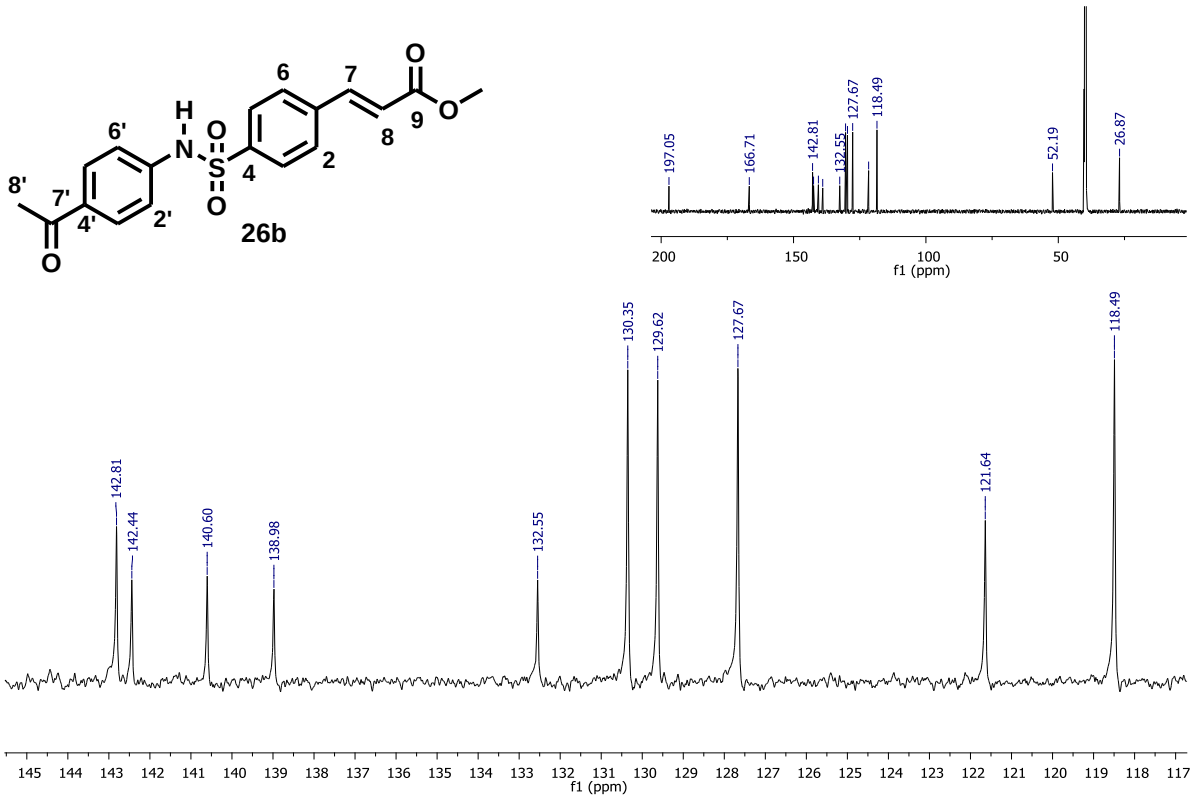

Figure SM.21. ^{1}H NMR spectrum (DMSO-d_6, 600 MHz) of compound **27a**

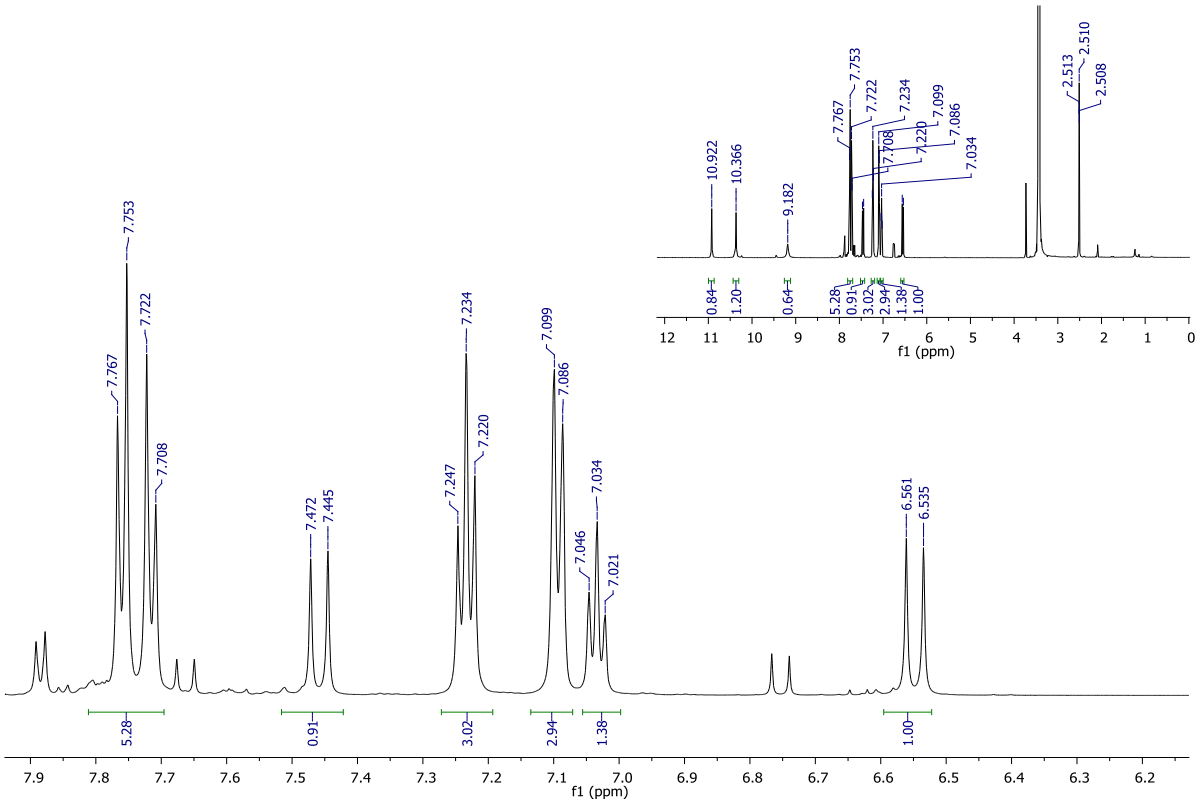

Figure SM.22. ^{13}C NMR spectrum (DMSO-d_6, 150 MHz) of compound **27a**

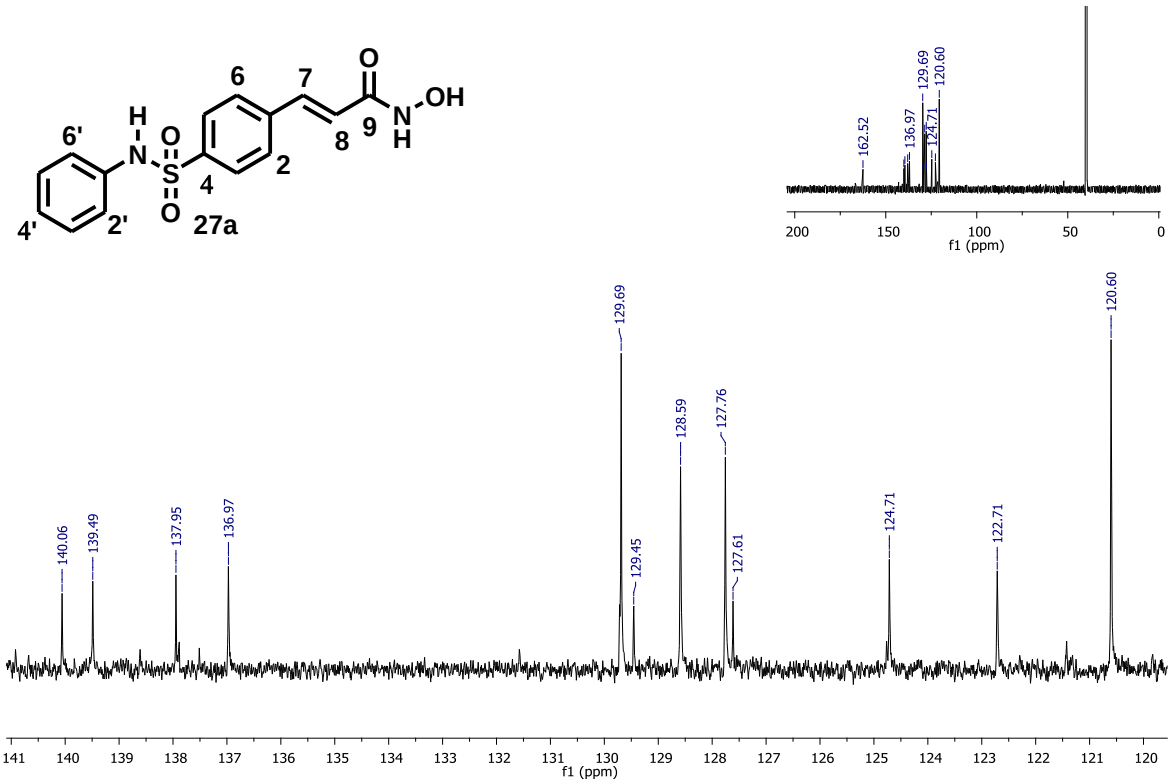

Figure SM.23. ^{1}H NMR spectrum (DMSO-d_6, 600 MHz) of compound **27b**

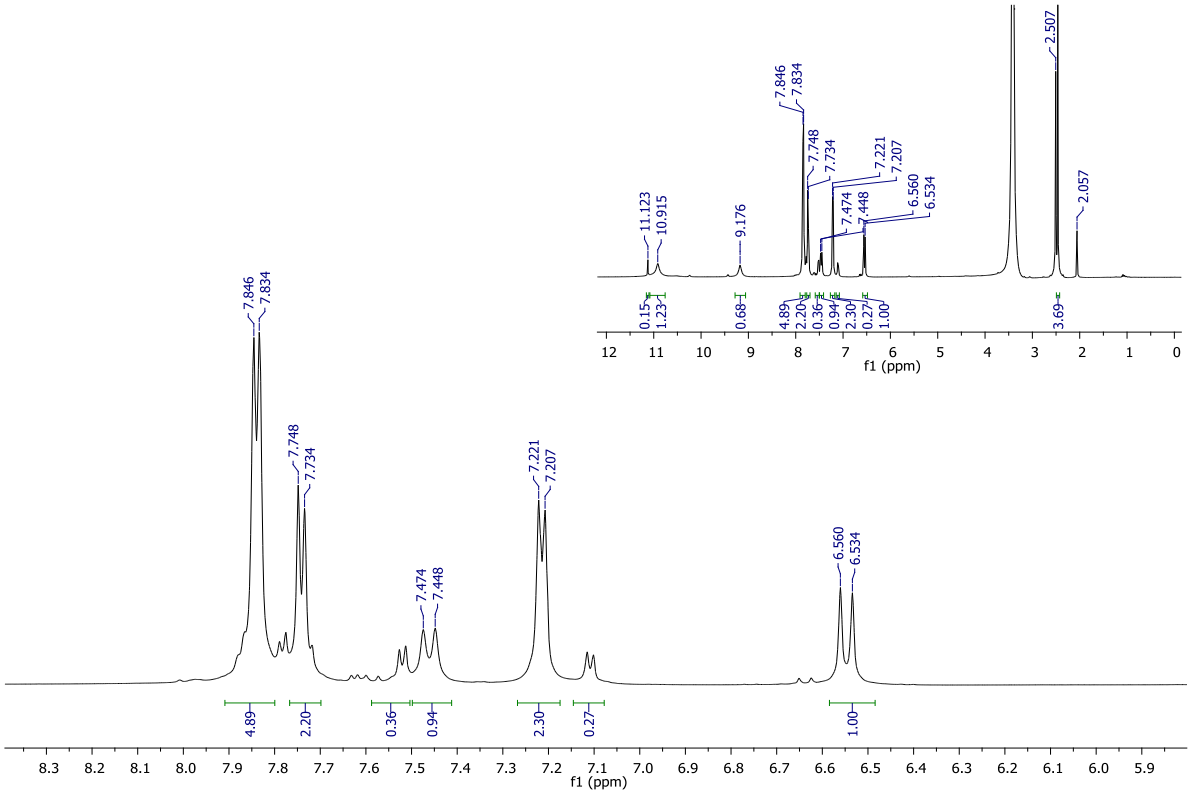

Figure SM.24. ^{13}C NMR spectrum (DMSO-d_6, 150 MHz) of compound **27b**

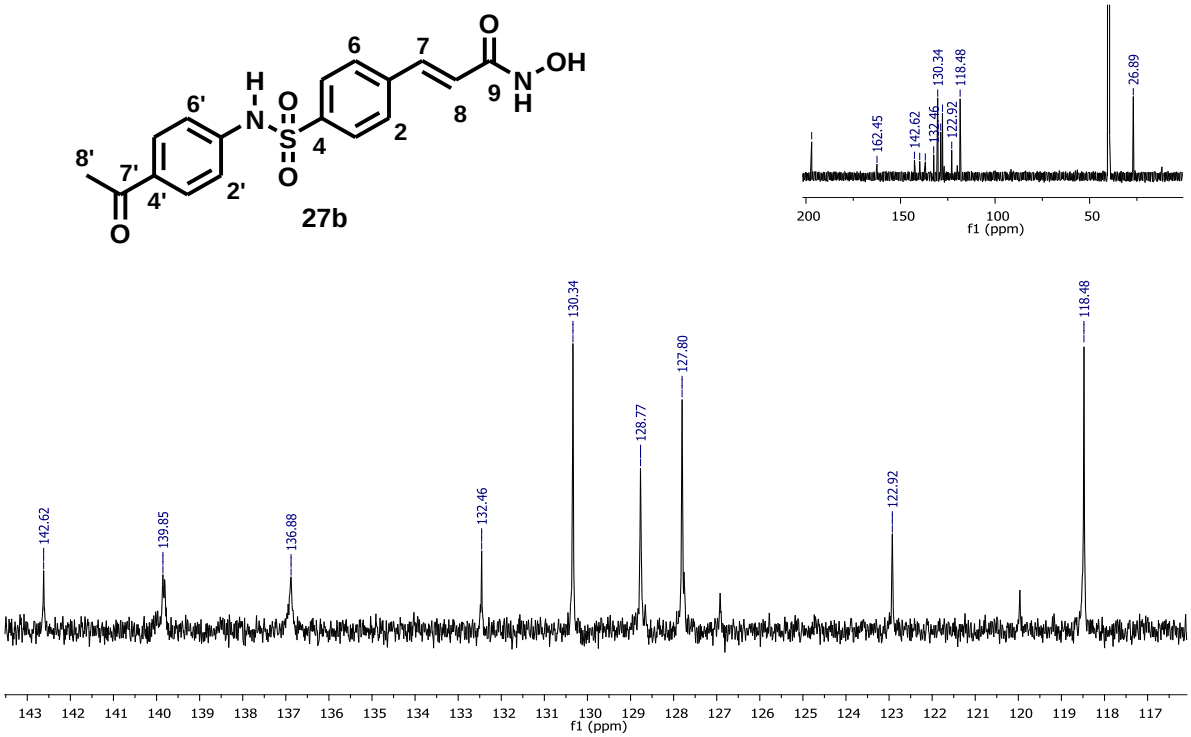

Figure SM.25. ^{1}H NMR spectrum (DMSO-d_6, 600 MHz) of compound **27c**

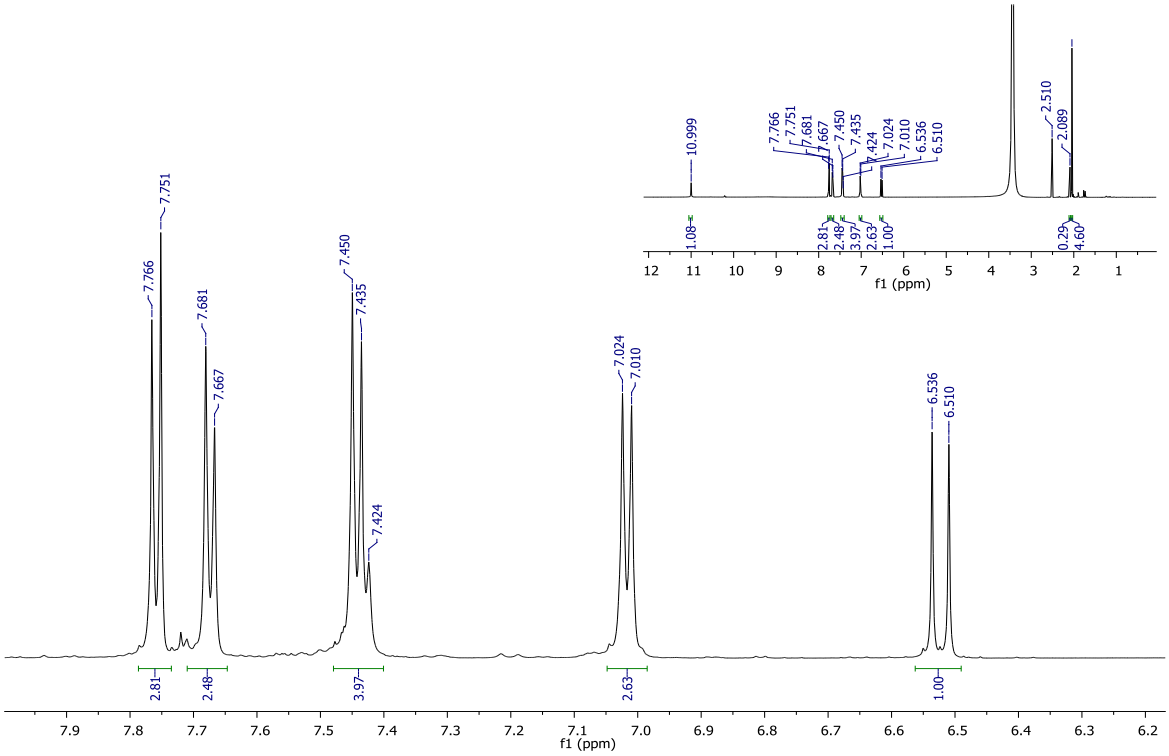

Figure SM.26. ^{13}C NMR spectrum (DMSO-d_6, 150 MHz) of compound **27c**

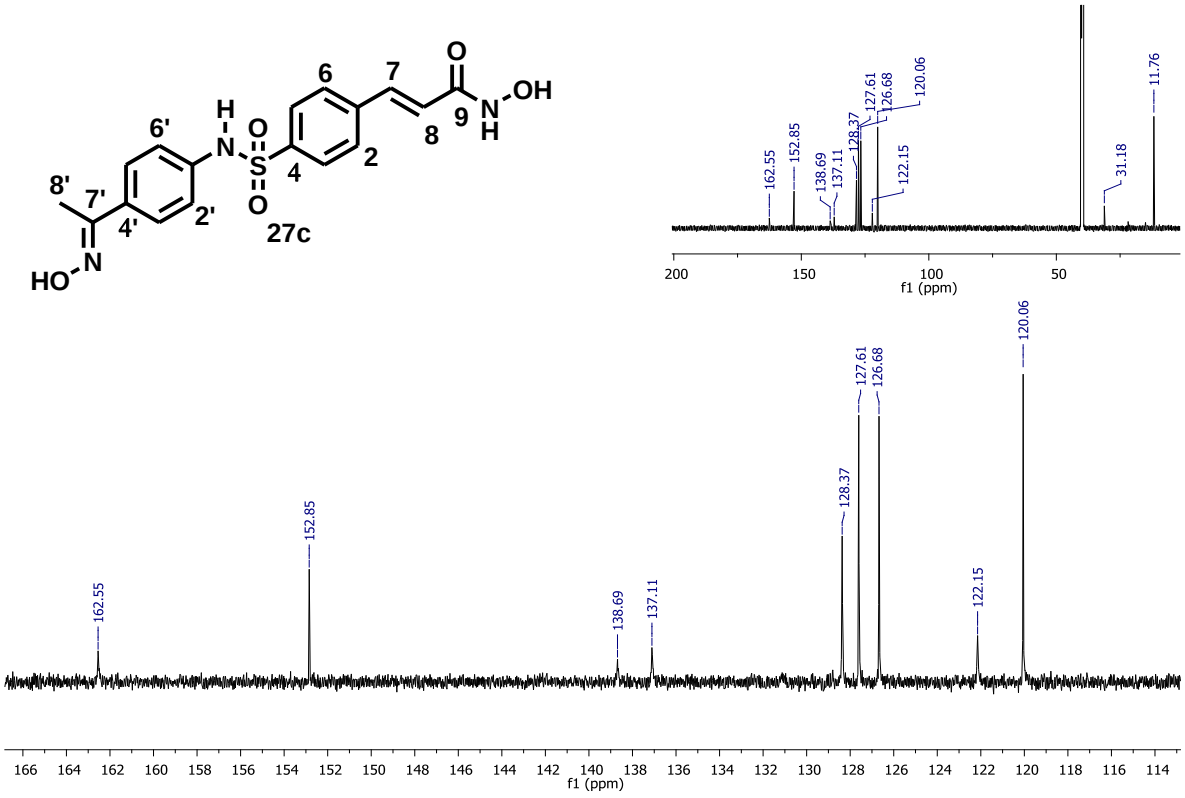

Figure SM.27. HSQC spectrum of compound **27c**

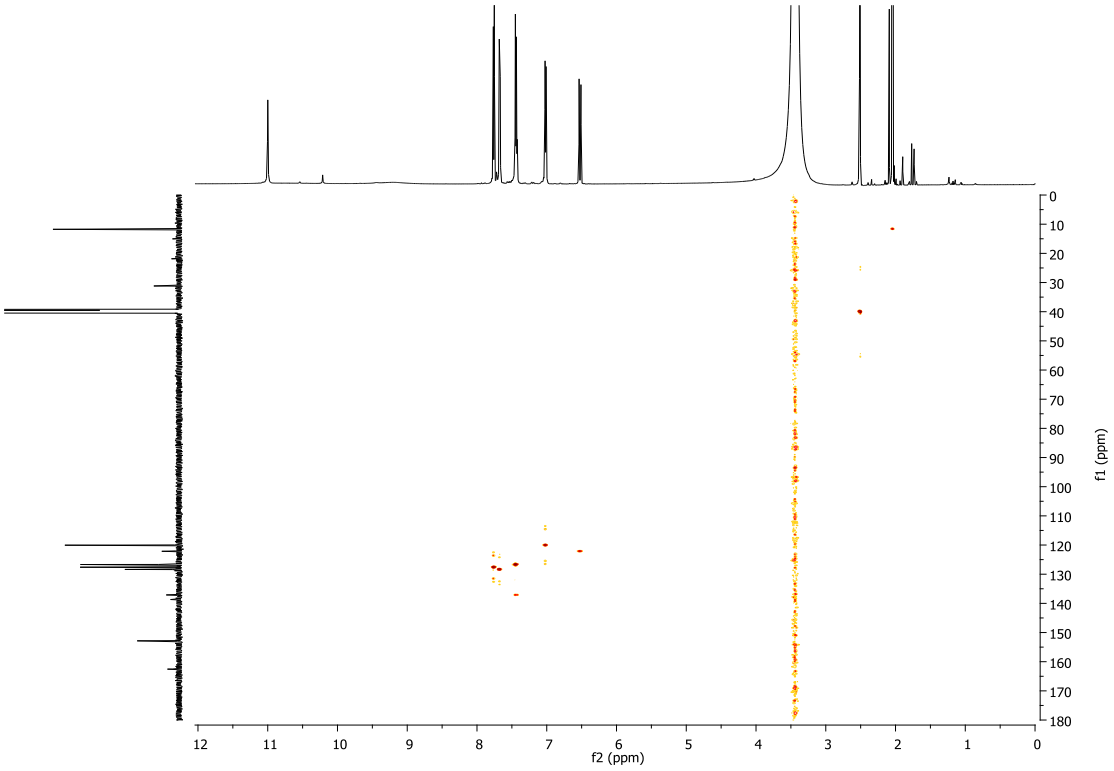

Figure SM.28. Magnification of the HSQC spectrum da of compound **27c**

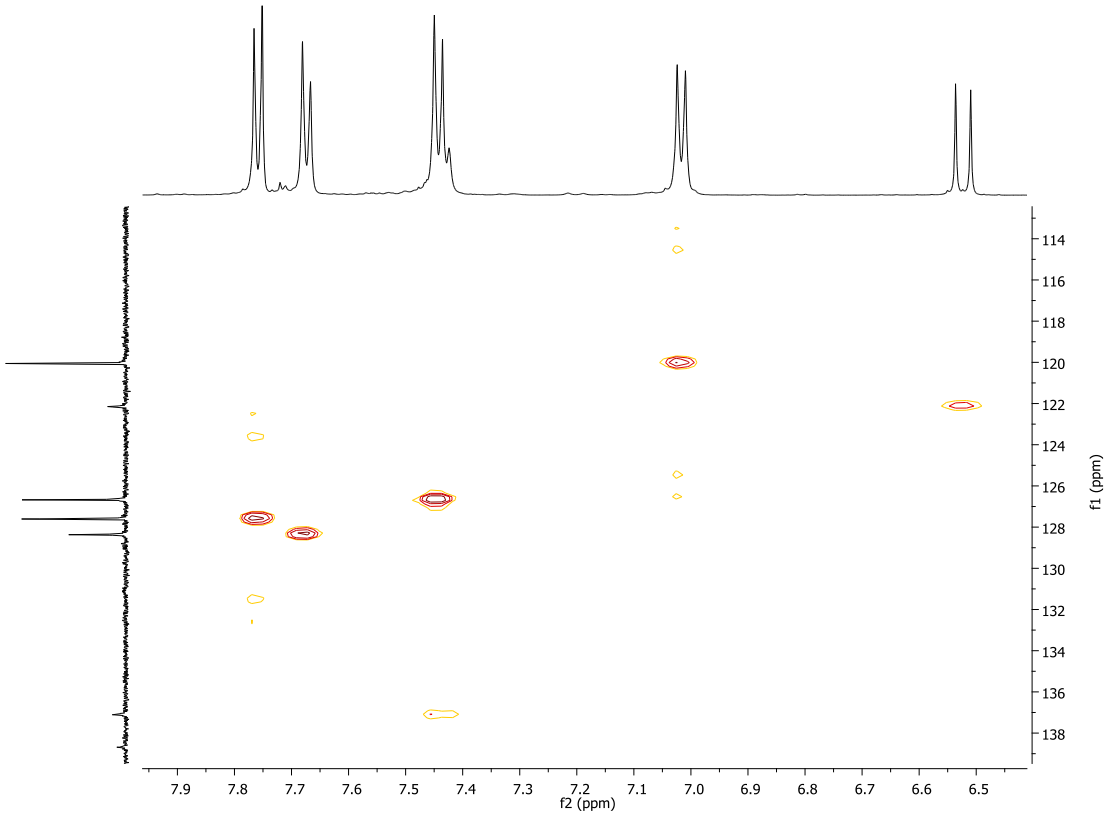

Figure SM.29. HMBC spectrum of compound **27c**

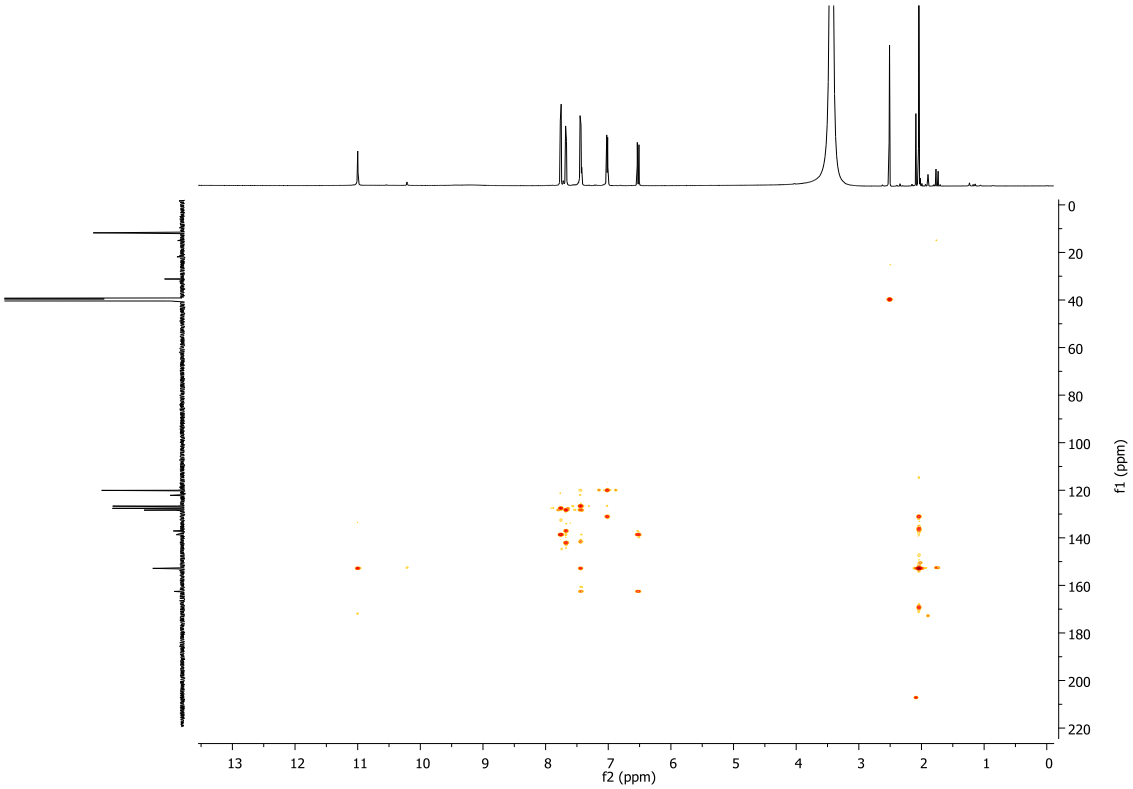

Figure SM.30. Magnification of the HMBC spectrum da of compound **27c**

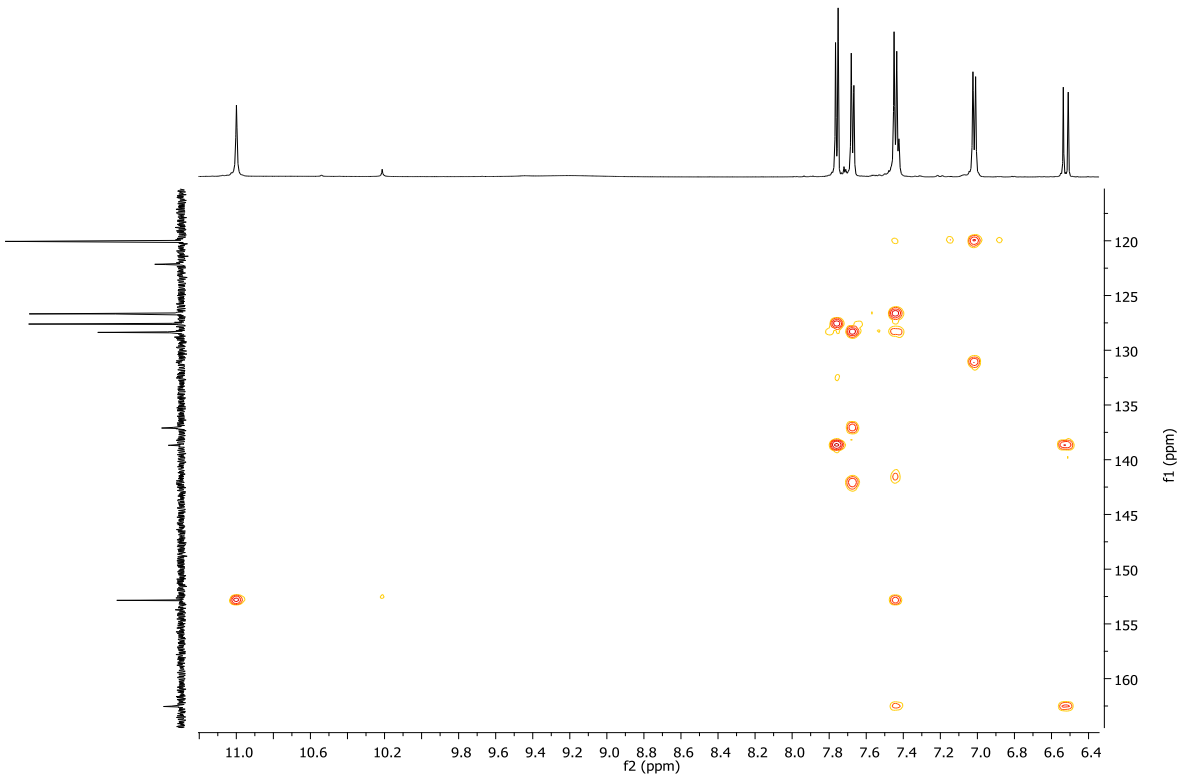

Figure SM.31. Mass spectrum of compound **27c**

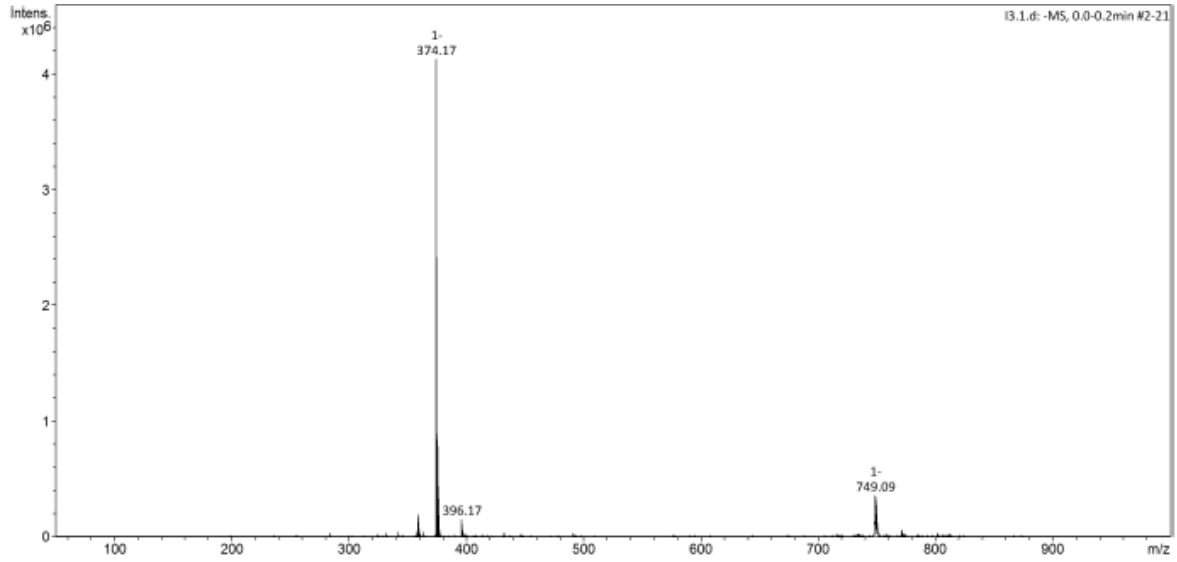

Scheme SM1. Compound **27c** NMR correlations obtained from HMBC NMR experiment J^2 (black arrows) and J^3 (green arrows) in the structure of **27c**

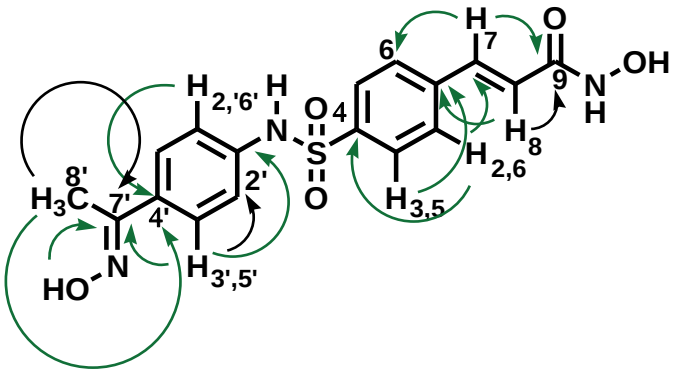

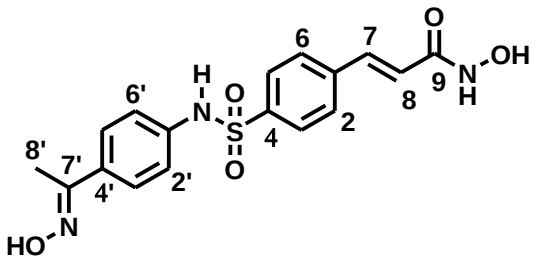

Position	δ_H; mult; J (Hz) 600 MHz; DMSO-d_6	δ_C 150 MHz; DMSO-d_6	HMBC
1	-	138.7	H-3, H-5 and H-8,
2 e 6	7.67; d; 8.4	128.4	H-7
3 e 5	7.76; d; 8.4	127.6	H-3 and H-5
4	-	*142.1	H-2 and H-6
1'	-	*141.6	H-3' and H-5'
2' e 6'	7.02; d; 8.7	120.1	H-2', H-6', H-3' and H-5'
3' e 5'	7.44; d; 8.7	126.7	H-3' and H-5'
4'	-	*131.1	H-2', H-6', H-8'
8	6.52; d; 15.8	122.2	-
7	7.44; d; 15.8	137.1	H-2 and H-6
9	-	162.6	H-7 and H-8
7'	-	152.8	H-3', H-5', =NOH, H-8'
8'	2.04; s	11.8	-
=NOH	11.0; s	-	-

*values from HMBC spectrum

Capítulo IV

4. Capítulo IV

4.1. CONCLUSÕES E PERSPECTIVAS

Foi realizada a síntese de 20 aminochalconas, as quais tiveram suas estruturas confirmadas por RMN de ^{1}H e ^{13}C. Essas substâncias foram ensaiadas à 20 μmol L^{-1} contra as linhagens de câncer de mama MCF-7 e MDA-MB-231. As substâncias **11** e **17** foram as mais ativas contra as duas linhagens com valores de CI_{50} de 13,2 ± 3,5 a 37,4 ± 5,2 μmol L^{-1}. Além disso, demonstraram ser capazes de manter a atividade antiproliferativa contra essas células mesmo em condição de acidose. Essas chalconas induziram a morte celular por apoptose, e superexpressaram a proteína pró-apoptótica p53 na linhagem MCF-7.

Foram planejados e sintetizados dois novos híbridos chalcona-inibidor de HDAC, e quatro análogos com rendimentos variando de 14 a 83 %. Essas substâncias foram avaliadas contra 5 isoformas de HDAC (HDAC1, 2, 4, 6 e 11) a 10 μmol L^{-1}. O híbrido **23a** e seu análogo **27c** exibiram CI_{50} de 3,6 e 0,15 μmol L^{-1} contra HDAC2. As substâncias **23a** e **27c** tiveram a atividade antiproliferativa contra células de câncer de mama (MCF-7 e MDA-MB-231) avaliada e exibiram valores de CI_{50} que variaram de 9,10 ± 2,5 μmol L^{-1} a 10,51 ± 1,0 μmol L^{-1}, sendo que **23a** demonstrou ser mais ativo do que sua chalcona precursora contra as duas linhagens. Estudos de modelagem molecular demonstraram que os híbridos e o análogo **27c** posicionam-se próximos ao inibidor co-cristalizado **20Y**.

O presente trabalho conduziu a substâncias antiproliferativas e potentes inibidoras de HDAC. Estudos sobre o tipo de morte induzido pelo híbrido (**23a**) e análogos (**25**, **27a**–**27c**) em células de câncer de mama, assim como a ação dessas substâncias em linhagem de células de mama não tumorigênicas (MCF-10A) serão realizados.